The dynamics of hepatic lipid metabolism in humans: understanding their role in fatty liver disease

---

A thesis submitted for the degree of Doctor of Philosophy



Pippa Jane Gunn

Green Templeton College · Radcliffe Department of Medicine · University of Oxford

Michaelmas 2018

Memorandum

The work in this thesis is the original work of the author and experiments were carried out at the Oxford Centre for Diabetes, Endocrinology and Metabolism; work done by anyone else or at different institutions is clearly stated. Supervision was carried out Professor Leanne Hodson, Dr. Charlotte Green and Professor Fredrik Karpe and funding was provided by the Medical Research Council.

The Sugar Overfeeding Study presented in Chapter 6 (section 6.2.3) was funded by the British Heart Foundation as part of Professor Leanne Hodson's Senior Fellowship in Basic Science. This study was undertaken with the help of Louise Dennis, Rachel Craven-Todd and the CIU research nurses. Dr. Pam Dyson provided dietary advice and support and Mr. Thomas Cornfield, Dr. Sion Parry and Dr. Fredrik Rosqvist helped with sample analysis.

The dimethyl sulfoxide work presented in Chapter 3 (section 3.3.1) was part of a larger set of experiments carried out by Dr. Nikolaos Nikolaou, which has now been published (Nikolaou *et al.*, 2016). In addition, the comparison of culturing sera in HepG2 and Huh7 cells in Chapter 3 (section 3.3.3) has been published (Gunn *et al.*, 2017) and some of the work discussing *in vitro* models for the study of hepatic FA metabolism in Chapter 1 (section 1.2.2) has been included in a larger review (Green *et al.*, 2018).

I hereby state that no part of this thesis has been submitted for any degree at this or any other university.

Acknowledgements

Firstly, I would like to thank my supervisors, Leanne and Charlotte; I couldn't have asked for more support throughout my DPhil. I'm so grateful for all the ideas, guidance, encouragement and opportunities you've given me; it's been a privilege to work with two people who I admire on both a personal and professional level. Thanks also for the laughs, the foodie chats and, of course, the ginger crunch!

Many thanks also to Camilla - it's been such a pleasure to collaborate with you. Your willingness to answer questions, offer advice, provide cells and carry out analysis has been invaluable; thanks to both you and Tomas for your hard work and perseverance on creating the DGAT2 knockout cell line.

I'm also grateful to those who have helped with my experiments and analysis in any way, big or small. Thanks to Tom, Matt H, Cat, Elspeth, Anne, Amy, Sion and Carlo, it's been great to work with you. Thank you to Matt N and Senthil for your help with the Oxford Biobank data and to Val especially, but also Francesca and Dan, at the TDI for your assistance with the IN Cell Analyzer; also to the CIU nurses, Pam, Sion, Tom and Fredrik R for your work on SOS.

I would also like to mention those who have made life in (and out) of the lab a bit more fun: thanks to Nick, Claire, Suan and Antje. Shahana, thank you for looking out for me during the mounting pressure of the last few months, and Katia, thanks for sitting next to me at our first induction and for all the good times (mostly wine, food and exercise-related) we've had since.

I also don't believe that I would have had the opportunity to undertake this DPhil if it hadn't been for experience gained earlier in my research career, so thank you to Sigi, Bernadette and Debra for boosting both my CV and my self-belief.

I'm also incredibly thankful for my wonderful family, you have faithfully loved and supported me in every season of life. I am so blessed to have you and I don't know where I would be without you.

And finally, but most fundamentally, for getting me here and for getting me through:

All glory to him, who is able, through his mighty power at work within us, to accomplish infinitely more than we might ask or think.

Ephesians 3:20

Abstract

Non-alcoholic fatty liver disease (NAFLD) has become increasingly prevalent. It is associated with changes in hepatic and whole-body fatty acid (FA) metabolism, with the first stage of the disease, steatosis, characterised by excess triacylglycerol (TAG) storage with a specific (macrovesicular) lipid droplet (LD) pattern; the final step in TAG synthesis is catalysed by diacylglycerol acyltransferase (DGAT). Although the pathogenesis of NAFLD is known to include both genetic and lifestyle factors, the sequence of events that precedes lipid accumulation in the liver remains unclear.

Human hepatoma cell lines (HepG2 and Huh7 cells) were optimised for use as models of hepatic FA metabolism. Use of human serum in the cell media resulted in reduced *de novo* lipogenesis (DNL) and improved levels of FA oxidation and secretion in both cell lines; Huh7 cells were used for subsequent experiments. To create a macrovesicular LD pattern, low (glucose only) and high (glucose and fructose) levels of sugar were added to the media in combination with low and high concentrations of FAs. The addition of high fat high sugar (HFHS) media to Huh7 cells caused accumulation of large LDs in a more macrovesicular pattern, which was similar to steatotic primary hepatocytes.

Low and high sugar and fat treatments were used on CRISPR-modified Huh7 cells with *DGAT2* knocked out; changes in these cells included a reduction in TAG secretion, DNL and glucose uptake from the media. In the HFHS treatment, *DGAT2* knockout was associated with signs of oxidative stress and inflammation, suggesting an interaction between substrate availability and DGAT2 function. Recruitment of controls and people carrying a *DGAT2* mutation who took part in a sugar overfeeding intervention demonstrated that a change in DGAT2 function may impact systemic glucose disposal, evident by increased carbohydrate oxidation and a resistance to metabolic changes caused by sugar overfeeding.

Overall, I developed physiologically-relevant models of hepatocellular metabolism and steatosis. Investigations using these models in parallel with human participants identified altered DGAT2 function as having a potential role in NAFLD.

Table of contents

CHAPTER 1: GENERAL INTRODUCTION
1.1 HEPATIC FATTY ACID METABOLISM....1
1.1.1 Biochemistry of fatty acids and triacylglycerol....1
1.1.2 Sources of hepatic fatty acids....3
1.1.2.1 Adipose-derived non-esterified fatty acids....3
1.1.2.2 Dietary fatty acids....3
1.1.2.3 *De novo* lipogenesis....4
1.1.3 Metabolism and storage of hepatic fatty acids....8
1.1.3.1 Elongation and desaturation of fatty acids....8
1.1.3.2 Triacylglycerol synthesis....11
1.1.3.3 Triacylglycerol storage....11
1.1.4 Fates of hepatic fatty acids....14
1.1.4.1 Fatty acid oxidation....14
1.1.4.2 Lipoprotein secretion....16
1.2 MODELS FOR STUDYING HEPATIC FATTY ACID METABOLISM....17
1.2.1 Investigating hepatic fatty acid metabolism using stable isotope tracers....18
1.2.2 *In vitro* models of hepatic fatty acid metabolism....20
1.3 THE ROLE OF DGAT ENZYMES IN HEPATIC FATTY ACID METABOLISM....24
1.3.1 The DGAT enzymes....24
1.3.1.1. The interaction between DGAT enzymes and hepatic triacylglycerol synthesis and storage....25
1.3.1.2 The interaction between DGAT enzymes and sources of hepatic fatty acids....26
1.3.1.3 The interaction between DGAT enzymes and the fates of hepatic fatty acids....27
1.3.1.4 The effect of DGAT enzymes on whole-body metabolism....28
1.4 NON-ALCOHOLIC FATTY LIVER DISEASE....31
1.4.1 Natural history and prevalence....31
1.4.2 Pathogenesis....33
1.4.2.1 Systemic fatty acid metabolism and insulin resistance....33
1.4.2.2 Changes in hepatic insulin signalling and fatty acid metabolism in NAFLD....34
1.4.2.3 The effect of genetics and lipid droplet pattern....36
1.5 DIETARY MACRONUTRIENTS AND HEPATIC FATTY ACID METABOLISM....38
1.5.1 Dietary sugars....39

Table of contents

1.5.1.1 Theory for the impact of sugar intake on liver fat accumulation 40
1.5.1.2 Experimental evidence for the impact of sugar intake on liver fat accumulation 40
1.5.2 Dietary fat 43
1.5.2.1 The impact of dietary fat intake on liver fat accumulation 43
1.5.2.2 The impact of *n*-3 PUFA on liver fat accumulation and NAFLD pathogenesis. 44
1.6 CONCLUDING REMARKS 45
CHAPTER 2: MATERIALS AND METHODS
2.1 MATERIALS 46
2.2 METHODS 46
2.2.1 Cell culture procedures 46
2.2.1.1 Routine cell culture 46
2.2.1.2 Passaging of cells 46
2.2.1.3 Seeding cells for treatment 47
2.2.1.4 Freezing down and storage of cells in liquid nitrogen 47
2.2.1.5 Bringing up cells from storage in liquid nitrogen 48
2.2.1.6 Treatment of cells with fatty acids 48
2.2.1.7 Determination of cell viability using MTT 48
2.2.2 Biochemical analysis 49
2.2.2.1 3-hydroxybutyrate concentration measurement 49
2.2.2.2 Cholesterol concentration measurement 50
2.2.2.3 Fructose concentration measurement 50
2.2.2.4 Glucose concentration measurement 51
2.2.2.5 Lactate concentration measurement 51
2.2.2.6 Triacylglycerol concentration measurement 51
2.2.2.7 Urea concentration measurement 52
2.2.3 Quantitative reverse-transcription PCR 52
2.2.3.1 RNA extraction 52
2.2.3.2 Reverse transcription 54
2.3.3.3 Quantitative PCR 54
2.3.3.4 Determination of reference genes 56

2.2.4 Protein extraction and Western blotting 56
2.2.4.1 Protein extraction and quantification 56
2.2.4.2 Gel electrophoresis and Western blotting 57
2.2.5 Lipid extraction and gas chromatography-mass spectrometry 59
2.2.5.1 Lipid extraction 59
2.2.5.2 Gas chromatography 61
2.2.5.3 Stable isotope tracers and gas chromatography-mass spectrometry 61
2.2.6 Imaging and analysis of samples using the IN Cell 6000 Analyzer 63
2.2.6.1 Preparation of cells for IN Cell analysis 63
2.2.6.2 Image acquisition and analysis using the IN Cell Analyzer 6000 63
2.2.7 Determination of oxidative stress 64
2.2.7.1 ROS-Glo™ H_2O_2 Assay 64
2.2.7.2 2′,7′-Dichlorofluorescin diacetate fluorescence 65
2.2.8 Lipoprotein separation and lipid content calculation 65
2.2.9 Biochemical assays 67
2.2.9.1 Glycogen assay 67
2.2.9.2 Acetate Assay 68
2.2.10 Enzyme-linked immunosorbent assays (ELISAs) 68
2.2.10.1 ApoB ELISA 69
2.2.10.2 IL-8 ELISA 69
2.2.10.3 Phospho-Akt (ser473) ELISA 70
2.2.11 Statistics 70

CHAPTER 3: OPTIMISATION OF EXISTING *IN VITRO* MODELS OF HEPATIC FATTY ACID METABOLISM

3.1 INTRODUCTION 76
3.2 METHODS 78
3.2.1 DMSO experiments 78
3.2.2 Glucose experiments 78
3.2.3 Serum experiments 78
3.2.4 Analytical techniques 79
3.3 RESULTS 80

3.3.1 The effect of DMSO on metabolic phenotype and function in HepG2 cells.....80

3.3.1.1 The effect of DMSO on the metabolic phenotype of HepG2 cells.....80

3.3.1.2 The effect of DMSO on liver function and endoplasmic reticulum stress markers in HepG2 cells.....83

3.3.2 The effect of glucose concentration on Huh7 and HepG2 function and metabolism 85

3.3.2.1 The effect of media glucose concentration on the metabolic phenotype of HepG2 and Huh7 cells.....85

3.3.2.2 The effect of media glucose concentration on liver function and ER stress markers in HepG2 and Huh7 cells.....89

3.3.3 The effect of human serum and foetal bovine serum on HepG2 and Huh7 function and metabolism 91

3.3.3.1 The effect of culturing sera on storage and synthesis of TAG in HepG2 and Huh7 cells.....91

3.3.3.2 The effect of culturing sera on FA composition in TAG and PL fractions in HepG2 and Huh7 cells 93

3.3.3.3 The effect of culturing sera on TAG and FA disposal in HepG2 and Huh7 cells 97

3.3.3.4 The effect of culturing sera on insulin and insulin-like growth factor-1 signalling in HepG2 and Huh7 cells.....98

3.4 DISCUSSION.....101

3.5 SUMMARY 107

CHAPTER 4: DEVELOPMENT OF A NEW *IN VITRO* MODEL OF HEPATIC LIPID DROPLET PATTERN AND FATTY ACID METABOLISM

4.1 INTRODUCTION 108

4.2 METHODS.....111

4.2.1 Experimental treatments.....111

4.2.1.1 Single *vs.* repeated FA dose experiments.....111

4.2.1.2 FA concentration experiments.....111

4.2.1.3 Cell viability experiments 112

4.2.1.4 Steatosis induction experiments 112

4.2.1.5 Glucose and fructose disappearance experiments.....113

4.2.2 Analytical techniques.....113

4.3 RESULTS.....114

4.3.1 Optimisation of steatosis treatment protocol....114
4.3.1.1 The effect of single or repeated FA doses on TAG accumulation....114
4.3.1.2 The effect of media FA concentration on FA metabolism and lipid droplet accumulation....114
4.3.1.3 The effect of media monosaccharide and FA concentration on cell viability...117
4.3.2 Development of an *in vitro* model of macrovesicular steatosis....119
4.3.2.1 The effect of media composition on lipid droplet size....119
4.3.2.2 The effect of media composition on FA synthesis and storage....122
4.3.2.3 The effect of media composition on FA composition, elongation and desaturation....122
4.3.2.4 The effect of media composition on lipoprotein secretion....127
4.3.2.5 The effect of media composition on FA oxidation and oxidative stress....129
4.3.2.6 The effect of media composition on glucose metabolism....129
4.3.2.7 The effect of media monosaccharide and FA concentration on glucose and fructose disappearance....129
4.4 DISCUSSION....132
4.5 SUMMARY....140
CHAPTER 5: INVESTIGATING THE INTERACTION BETWEEN DGAT2 ACTIVITY AND SUBSTRATE AVAILABILITY *IN VITRO*
5.1 INTRODUCTION....141
5.2 METHODS....144
5.2.1 CRISPR-Cas9 modification of Huh7 cells....144
5.2.1.1 Design of targeting components for the CRISPR/Cas9 system and transfection of Huh7 cells....145
5.2.2 siRNA knockdown of DGAT2....148
5.2.2.1 Optimisation with siGLO Green Transfection Indicator....148
5.2.2.2 DGAT2 knockdown....149
5.2.3 Analytical techniques....149
5.3 RESULTS....150
5.3.1 Creation of a DGAT2 knockout cell line....150
5.3.2 Optimisation of siRNA knockdown in Huh7 cells....150
5.3.3 Investigating the effects of *DGAT2* knockout on FA storage and metabolism in the presence of different nutritional substrates in Huh7 cells....155

5.3.3.1 The effect of DGAT2 knockout on intracellular lipid accumulation in Huh7 cells 155

5.3.3.2 The effect of DGAT2 knockout on FA synthesis in Huh7 cells.....157

5.3.3.3 The effect of DGAT2 knockout on exogenous FA storage in Huh7 cells 161

5.3.3.4 The effect of DGAT2 knockout on FA composition, elongation and desaturation in Huh7 cells 166

5.3.3.5 The effect of DGAT2 knockout on lipid droplet pattern in Huh7 cells 167

5.3.3.6 The effect of DGAT2 knockout on lipid secretion in Huh7 cells.....170

5.3.3.7 The effect of DGAT2 knockout on FA composition secreted from Huh7 cells 172

5.3.3.8 The effect of DGAT2 knockout on FA oxidation, oxidative stress and inflammation in Huh7 cells 177

5.3.3.9 The effect of DGAT2 knockout on glucose metabolism in Huh7 cells 178

5.4 DISCUSSION.....180

5.5 SUMMARY 191

CHAPTER 6: INVESTIGATING THE INTERACTION BETWEEN DGAT2 MUTATIONS AND SUGAR OVERFEEDING IN HUMANS

6.1 INTRODUCTION 192

6.2 METHODS.....195

6.2.1 Identification of DGAT2 mutations and participant characteristics in the Oxford Biobank cohort 195

6.2.2 DNA sequencing of Huh7 cells 195

6.2.2.1 Primer design for *DGAT2* Exon 6 & 7 196

6.2.2.2 DNA extraction of Huh7 cells.....196

6.2.2.3 Polymerase chain reaction.....197

6.2.2.4 Agarose gel electrophoresis 197

6.2.2.5 PCR product cleanup 198

6.2.3 Dietary intervention and postprandial study days.....198

6.2.3.1 Subjects.....198

6.2.3.2 Dietary intervention 199

6.2.3.3 Determination of liver fat and body composition.....200

6.2.3.4 Postprandial study day.....200

6.2.3.5 Analytical methods 201

Table of contents

6.2.3.6 $^{13}CO_2$ enrichment analysis....202
6.2.3.7 Calculations and statistical analysis....203
6.3 RESULTS....204
6.3.1 Identifying DGAT2 variants from the Oxford Biobank....204
6.3.2 Sequencing exon 6 and 7 of *DGAT2* in Huh7 cells....206
6.3.3 Sugar overfeeding intervention and postprandial study days....206
6.3.3.1 Subject recruitment and observational data....206
6.3.3.2 Baseline characteristics and dietary adherence....210
6.3.3.3 The effect of sugar overfeeding on anthropometry and fasting plasma biochemistry....213
6.3.3.4 The effect of sugar overfeeding on postprandial substrate appearance and hormonal response to a mixed meal....213
6.3.3.5 The effect of sugar overfeeding on postprandial hepatic fatty acid synthesis and metabolism and substrate utilisation in response to a mixed test meal....216
6.4 DISCUSSION....221
6.5 SUMMARY....227
CHAPTER 7: GENERAL DISCUSSION AND FUTURE DIRECTIONS
7.1 GENERAL DISCUSSION AND FUTURE DIRECTIONS....228
7.1.1 Improving and developing *in vitro* hepatocyte models....228
7.1.2 Investigating the role of DGAT2 function in fatty acid metabolism....230
APPENDIX A: CHAPTER 2 SUPPLEMENTARY MATERIAL....233
APPENDIX B: CHAPTER 3 SUPPLEMENTARY MATERIAL....237
APPENDIX C: CHAPTER 4 SUPPLEMENTARY MATERIAL....243
C.1 Isolation of primary hepatocytes....243
APPENDIX D: CHAPTER 5 SUPPLEMENTARY MATERIAL....250
APPENDIX E: CHAPTER 6 SUPPLEMENTARY MATERIAL....257
REFERENCE LIST....260

List of tables and figures

CHAPTER 1: GENERAL INTRODUCTION

Figure 1.1-1. The primary sources and fates of hepatic fatty acids....2

Figure 1.1.2-1. Glycolysis and fructolysis provide substrate for *de novo* fatty acid synthesis...7

Figure 1.1.3-1. Fatty acid metabolism *via* elongation and desaturation....10

Figure 1.1.3-2. Synthesis of triacylglycerol....12

Figure 1.4.1-1. The natural history of non-alcoholic fatty liver disease....33

CHAPTER 2: MATERIALS AND METHODS

Table 2.1-1. Materials and suppliers used....71

CHAPTER 3: OPTIMISATION OF EXISTING *IN VITRO* MODELS OF HEPATIC FATTY ACID METABOLISM

Table 3.3.1-1. The effect of dimethyl sulfoxide on differentiation, tumour and fatty acid metabolism gene expression in HepG2 cells....81

Figure 3.3.1-1. The effect of dimethyl sulfoxide on metabolic parameters in HepG2 cells.....82

Figure 3.3.1-2. The effect of dimethyl sulfoxide on endoplasmic reticulum stress markers in HepG2 cells....84

Figure 3.3.2-1. The effect of media glucose concentration on glucose metabolism and cell function in HepG2 and Huh7 cells....86

Table 3.3.2-1. The effect of glucose concentration on differentiation, tumour and fatty acid metabolism gene expression in Huh7 and HepG2 cells....87

Figure 3.3.2-2. The effect of media glucose concentration on FA metabolism in HepG2 and Huh7 cells....88

Figure 3.3.2-3. The effect of glucose on amino acid catabolism and endoplasmic reticulum stress markers in HepG2 and and Huh7 cells....90

Figure 3.3.3-1. Storage and synthesis of triacylglycerol in HepG2 and Huh7 cells....91

Table 3.3.3-1. mRNA expression of lipid metabolism genes in Huh7 and HepG2 cells....92

Figure 3.3.3-2. Metabolism and composition of triacylglycerol and phospholipid fractions in Huh7 and HepG2 cells....95

Table 3.3.3-2. Fatty acid composition of triacylglycerol in Huh7 and HepG2 cells cultured with HS or FBS....96

Table 3.3.3-3. Fatty acid composition of phospholipids in Huh7 and HepG2 cells cultured with HS or FBS....96

Figure 3.3.3-3. Secretion of triacylglycerol and fatty acid oxidation in Huh7 and HepG2 cells....99

Figure 3.3.3-4. Insulin and insulin-like growth factor-1 signalling in Huh7 and HepG2 cells....100

CHAPTER 4: DEVELOPMENT OF A NEW *IN VITRO* MODEL OF HEPATIC LIPID DROPLET PATTERN AND FATTY ACID METABOLISM

Figure 4.3.1-1. The effect of changing media daily on uptake of fatty acids and intracellular triacylglycerol levels in HepG2 cells.....115

Figure 4.3.1-2. The effect of fructose and fatty acids on metabolic parameters in Huh7 cells.....116

Table 4.3.1-1. The effect of fructose and fatty acids on gene expression in Huh7 cells.....118

Figure 4.3.1-3. The effect of fructose and fatty acids on cell viability determined by MTT assay in Huh7 cells.....118

Figure 4.3.2-1. The effect of media composition on lipid droplet characteristics in Huh7 cells.....120

Table 4.3.2-1. The effect of media composition on gene expression in Huh7 cells.....121

Figure 4.3.2-2. The effect of media composition on fatty acid synthesis and storage in Huh7 cells.....123

Table 4.3.2-2. The effect of media composition on fatty acid composition of triacylglycerol in Huh7 cells.....124

Table 4.3.2-3. The effect of media composition on fatty acid composition of phospholipids in Huh7 cells.....125

Figure 4.3.2-3. The effect of media composition on fatty acid metabolism in Huh7 cells.....126

Figure 4.3.2-4. The effect of media composition on lipoprotein secretion.....128

Figure 4.3.2-5. The effect of media composition on fatty acid oxidation and oxidative stress in Huh7 cells.....130

Figure 4.3.2-6. The effect of media composition on glucose metabolism in Huh7 cells.....131

Figure 4.3.2-7. Disappearance of glucose and fructose in Huh7 cells.....131

CHAPTER 5: INVESTIGATING THE INTERACTION BETWEEN DGAT2 ACTIVITY AND SUBSTRATE AVAILABILITY *IN VITRO*

Figure 5.3.1-1. Targeting strategy for diacylglycerol acyltransferase 2 deletion *via* CRISPR-Cas9 mediated non-homologous end joining.....151

Figure 5.3.1-2. Light microscopy images of knockout and wildtype Huh7 cells.....152

Figure 5.3.2-1. siGLO Green fluorescence in Huh7 cells as a marker of transfection efficiency.....152

Figure 5.3.2-2. Preliminary results investigating the efficiency and effect of *DGAT2* knockdown in Huh7 cells.....154

Figure 5.3.2-3. siGLO green fluorescence in Huh7 cells as a marker of transfection efficiency.....155

List of tables and figures

Figure 5.3.3-1. The effect of media composition on lipid storage in Huh7 cells with wildtype or knockout of the *DGAT2* gene.....156

Table 5.3.3-1. The effect of media composition on gene expression in Huh7 cells with wildtype or knockout of the *DGAT2*.....158

Table 5.3.3-2. The effect of media composition on fatty acids remaining in the media after 24 hours on Huh7 cells with wildtype or knockout of the *DGAT2* gene.....159

Figure 5.3.3-2. The effect of media composition on *de novo* lipogenesis in Huh7 cells with wildtype or knockout of the *DGAT2* gene.....160

Figure 5.3.3-3. The effect of media composition on exogenous fatty acid storage and partitioning in Huh7 cells with wildtype or knockout of the *DGAT2* gene.....162

Table 5.3.3-3. The effect of media composition on fatty acid composition of triacylglycerol in Huh7 cells with wildtype or knockout of the *DGAT2* gene.....164

Table 5.3.3-4. The effect of media composition on fatty acid composition of phospholipids in Huh7 cells with wildtype or knockout of the *DGAT2* gene.....165

Figure 5.3.3-4. The effect of media composition on fatty acid desaturation and elongation in Huh7 cells with wildtype or knockout of the *DGAT2* gene.....168

Figure 5.3.3-5. The effect of media composition on lipid droplet characteristics in Huh7 cells with wildtype or knockout of the *DGAT2* gene.....169

Figure 5.3.3-6. The effect of media composition on lipoprotein secretion in Huh7 cells with wildtype or knockout of the *DGAT2* gene.....171

Table 5.3.3-5. The effect of media composition on fatty acid composition of triacylglycerol secreted in the media of Huh7 cells with wildtype or knockout of the *DGAT2* gene.....173

Table 5.3.3-6. The effect of media composition on fatty acid composition of phospholipids secreted in the media of Huh7 cells with wildtype or knockout of the *DGAT2* gene.....174

Figure 5.3.3-7. The effect of media composition on exogenous fatty acid secretion in Huh7 cells with wildtype or knockout of the *DGAT2* gene.....175

Figure 5.3.3-8. The effect of media composition on markers of fatty acid oxidation, oxidative stress and inflammation in Huh7 cells with wildtype or knockout of the *DGAT2* gene.....176

Figure 5.3.3-9. The effect of media composition on markers of glucose metabolism in Huh7 cells with wildtype or knockout of the *DGAT2* gene.....179

CHAPTER 6: INVESTIGATING THE INTERACTION BETWEEN DGAT2 MUTATIONS AND SUGAR OVERFEEDING IN HUMANS

Table 6.3.1-1. Fasting metabolic characteristics of carriers (A/G) compared to non-carriers (G/G) of two *DGAT2* single nucleotide polymorphisms from the Oxford Biobank.....205

Figure 6.3.2-1. Sequencing results from exon 6 and 7 of the *DGAT2* gene in Huh7 cells.....207

List of tables and figures

Table 6.3.3-1. Anthropometric and body composition characteristics of people carrying the single nucleotide polymorphisms rs151179593 and rs140793537 compared to a cluster of matched non-carriers from the Oxford Biobank.....208

Table 6.3.3-2. Fasting plasma biochemistry characteristics of people carrying the single nucleotide polymorphisms rs151179593 and rs140793537 compared to a cluster of matched non-carriers from the Oxford Biobank.....209

Table 6.3.3-3. Participant characteristics and fasting plasma biochemistry before and after a sugar overfeeding intervention in people carrying a *DGAT2* mutation and controls.....211

Table 6.3.3-4. Dietary intake before and after a sugar overfeeding intervention in people carrying a *DGAT2* mutation and controls.....212

Figure 6.3.3-1. The effect of sugar overfeeding on postprandial substrate appearance and hormonal response to a mixed meal.....215

Figure 6.3.3-2. The effect of sugar overfeeding on postprandial hepatic fatty acid and metabolism and substrate utilisation in response to a mixed meal.....219

Table 6.3.3-5. Postprandial measurements and area under the curve values before and after a sugar overfeeding intervention in people carrying a *DGAT2* mutation and controls.....220

APPENDIX A: CHAPTER 2 SUPPLEMENTARY MATERIAL

Table A.1. TaqMan® Assays used for gene expression analysis.....233

Table A.2. List of antibodies from Cell Signalling used for immunoblotting.....234

Figure A.1. The stability of reference genes in HepG2 cells.....235

Figure A.2. The stability of reference genes in Huh7 cells.....236

APPENDIX B: CHAPTER 3 SUPPLEMENTARY MATERIAL

Figure B-1. Markers of FA metabolism in HepG2 cells when grown in human serum and foetal bovine serum cells for three, seven or 14 days.....237

Figure B-2. Markers of FA metabolism in Huh7 cells when grown in human serum and foetal bovine serum cells for three, seven or 14 days.....238

Table B-1. mRNA expression of FA metabolism genes in HepG2 cells when grown in human serum and foetal bovine serum cells for three, seven or 14 days.....239

Table B-2. mRNA expression of FA metabolism genes in Huh7 cells when grown in human serum and foetal bovine serum cells for three, seven or 14 days.....240

Figure B-3. A time course of glucose uptake in HepG2 and Huh7 cells.....241

Table B-3. Fatty acid composition in foetal bovine serum and human serum.....242

APPENDIX C: CHAPTER 4 SUPPLEMENTARY MATERIAL

Table C.1. The effect of media composition on fatty acid composition of triacylglycerol in Huh7 cells.....245

Table C.2. The effect of media composition on fatty acid composition of phospholipids in Huh7 cells....246

Figure C.1. The effect of media composition on fatty acid metabolism in triacylglycerol and phospholipids of Huh7 cells....247

Figure C.2. The effect of culture time on lipid droplet accumulation in Huh7 cells....248

Figure C.3. Lipid droplet populations in whole liver tissue and isolated hepatocytes from two steatotic (25% and 30% fat) livers....248

Figure C.4. Lipid droplet population and quantification in liver histology samples using the IN Cell Analyzer 6000....249

Figure C.5. Interleukin-8 levels in the media of Huh7 cells....249

APPENDIX D: CHAPTER 5 SUPPLEMENTARY MATERIAL

Table D.1. Target sequences of the four *DGAT2*-targeting siRNA contained in Dharmafect ON-TARGETplus *DGAT2* siRNA....250

Table D.2. Target sequences of the four non-targeting siRNA contained in Dharmafect ON-TARGETplus Non-targeting Control Pool....250

Figure D.1. Preliminary results investigating the efficiency of *DGAT2* knockdown in Huh7 cells....251

Table D.3. The effect of media composition on fatty acid composition of triacylglycerol in Huh7 cells with wildtype or knockout of the *DGAT2* gene....252

Table D.4. The effect of media composition on fatty acid composition of phospholipids in Huh7 cells with wildtype or knockout of the *DGAT2* gene....253

Table D.5. The effect of media composition on fatty acid composition of triacylglycerol secreted in the media of Huh7 cells with wildtype or knockout of the *DGAT2* gene....254

Table D.6. The effect of media composition on fatty acid composition of phospholipids secreted in the media of Huh7 cells with wildtype or knockout of the *DGAT2* gene....255

Figure D.3. The effect of media composition on exogenous fatty acid secretion in Huh7 cells with wildtype or knockout of the *DGAT2* gene....256

APPENDIX E: CHAPTER 6 SUPPLEMENTARY MATERIAL

Table E.1. Primers designed for amplification of exons 6 and 7 in the *DGAT2* gene....257

Figure E.1. The effect of sugar overfeeding on fasting plasma biochemistry in participants with a mutation in the *DGAT2* gene or matched controls....258

Figure E.2. The effect of sugar overfeeding on fasting plasma biochemistry in participants with a mutation in the *DGAT2* gene or matched controls....259

Abbreviations

3-OHB	3-hydroxybutyrate
AA	Arachidonic acid
ACC	Acetyl-CoA carboxylase
ARF/COP	ADP ribosylation factor/coat protein
ASO	Antisense oligonucleotide
ATGL	Adipose triglyceride lipase
AUC	Area under the curve
CE	Cholesterol ester
CES	Carboxylesterase
ChREBP	Carbohydrate-responsive element-binding protein
CIDE	Cell death-inducing DFFA-like effector
CM	Chylomicron
CPT	Carnitine palmitoyltransferase
DAG	Diacylglycerol
DGAT	Diacylglycerol acyltransferase
DHA	Docosahexaenoic acid
DMSO	Dimethyl sulfoxide
DNL	*De novo* lipogenesis
ELOVL	Fatty acid elongase
EPA	Eicosapentaenoic acid
ER	Endoplasmic reticulum
FA	Fatty acid
FABP	Fatty acid binding protein
FADS	Fatty acid desaturase
FAS	Fatty acid synthase
FAT/CD36	Fatty acid translocase/cluster of differentiation 36
FATP	Fatty acid transport protein
FBS	Foetal bovine serum
FIT2	Fat storage-inducing transmembrane protein 2
GPAT	Glycerol-3-phosphate acyltransferase
HDL	High-density lipoprotein
HFHS	High fat high sugar

Abbreviations

HOMA-IR	Homeostatic model assessment of insulin resistance
HS	Human serum
HSL	Hormone-sensitive lipase
IR	Insulin resistance
LCPUFA	Long-chain polyunsaturated fatty acid
LD	Lipid droplet
LDL	Low-density lipoprotein
LFHS	Low fat high sugar
LFLS	Low fat low sugar
LXR	Liver X receptor
MAG	Monoacylglycerol
MGAT	Monoacylglycerol acyltransferase
MUFA	Monounsaturated fatty acid
NAFLD	Non-alcoholic fatty liver disease
NASH	Non-alcoholic steatohepatitis
NEFA	Non-esterified fatty acid
PL	Phospholipid
PLIN	Perilipin
PNPLA	Patatin-like phospholipase domain-containing protein
PPAR	Peroxisome proliferator-activated receptor
PUFA	Polyunsaturated fatty acid
RER	Resting energy expenditure
ROS	Reactive oxygen species
RQ	Respiratory quotient
SCD	Stearoyl-CoA desaturase
SFA	Saturated fatty acid
SREBP	Sterol regulatory element-binding protein
SSB	Sugar-sweetened beverage
TAG	Triacylglycerol
TCA	Tricarboxylic acid
VLDL	Very low-density lipoprotein

Chapter 1

General introduction

1.1 HEPATIC FATTY ACID METABOLISM

The liver is a key regulator in systemic metabolism. It is made up of four cells types: liver endothelial cells, Kupffer cells, stellate cells and hepatocytes (Kmiec, 2001). The liver sinusoidal cells are composed of endothelial and Kupffer cells and are located adjacent to blood vessels; Kupffer cells are specialised immune cells that regulate the immune response of the liver (Knolle & Gerken, 2000). Stellate cells and hepatocytes are both involved in nutrient metabolism, with hepatocytes making up around 80% of liver tissue (Kmiec, 2001). The liver is connected to the gut by the hepatic portal vein, which supplies the majority of the liver's blood supply; it is therefore an important organ in regulating and metabolising nutritional substrates (*e.g.* glucose, Tappy & Le, 2010). The liver is also involved in lipid, and specifically fatty acid (FA), metabolism, where it is involved in storage, synthesis and distribution of FAs in its regulation of whole-body metabolism (Boberg *et al.*, 1972; Nguyen *et al.*, 2008) (Figure 1.1-1).

1.1.1 Biochemistry of fatty acids and triacylglycerol

Fatty acids are hydrocarbon chains that, when esterified to a glycerol backbone, create mono, di, or triacylglycerol (MAG, DAG and TAG, respectively): TAG is an inert molecule that most fat is stored as in the human body. FAs are also required for phospholipid (PL) synthesis and are therefore an integral constituent of organelle and cell membranes, as well as having roles as signalling molecules and transcription factor ligands. FAs are classified by their chain length and degree of saturation: most FAs are between 12 and 24 carbons in length, and these carbons can be saturated with hydrogen atoms (two hydrogen atoms per carbon atom), or

unsaturated, with either one (monounsaturated) or several (polyunsaturated) carbons forming a double bond with an adjacent carbon in the presence of a single hydrogen. If unsaturated, the location of the first unsaturated carbon in a FA chain is denoted by its distance from the *n*-terminus, or methyl end, either as an *n* or omega number (Kihara, 2012).

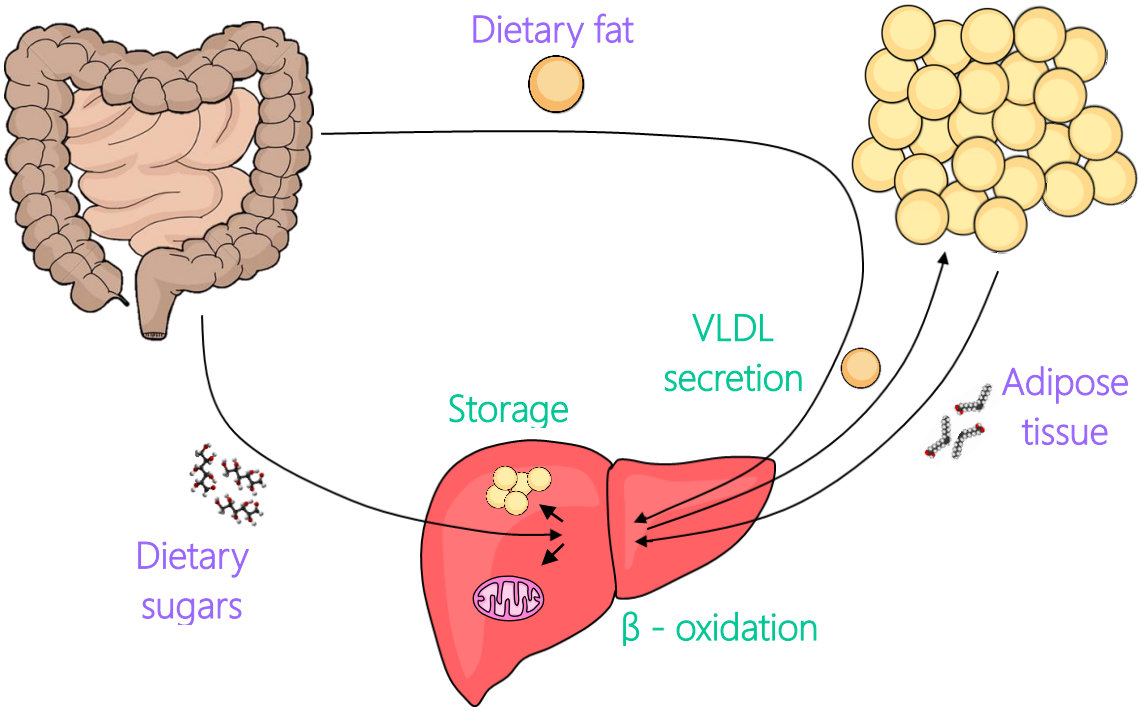


Figure 1.1-1. The primary sources (purple) and fates (green) of hepatic fatty acids (FAs). Dietary fat is incorporated into chylomicrons in the gut in the form of triacylglycerol (TAG) before entering the circulation to deliver FAs to tissues, where they are liberated by lipoprotein lipase, before being taken up by the liver as chylomicron remnants. Adipose tissue releases non-esterified fatty acids into the circulation which are taken up by the liver *via* the hepatic artery. Dietary sugars absorbed into the circulation at the small intestine can be used to form FAs by *de novo* lipogenesis (DNL). FAs in the liver can be used to synthesise TAG, which is incorporated into very low-density lipoprotein (VLDL) particles for delivery of fat to peripheral tissues. FAs can be oxidised, primarily *via* β-oxidation, for energy production in the liver. FAs partitioned into storage in the liver are esterified to make TAG and stored within lipid droplets.

1.1.2 Sources of hepatic fatty acids

1.1.2.1 Adipose-derived non-esterified fatty acids

Fat is primarily stored as TAG within lipid droplets (LDs) of adipocytes, which represent the largest energy store in the body; lipolysis of stored TAG yields non-esterified FA (NEFA). This process is under the control of insulin: in the fasting state, low ambient insulin levels allow adipose triglyceride lipase (ATGL), hormone sensitive lipase (HSL) and monoacylglycerol lipase to hydrolyse an ester bond, liberating fatty acids from their glycerol backbones in sequence (Zechner *et al.*, 2012). Once released into the circulation, FAs are bound to albumin (known as NEFA or free fatty acids; FFA) and upon reaching the hepatic artery, membrane-bound fatty acid transport proteins (FATPs) and fatty acid translocase/cluster of differentiation 36 (FAT/CD36) facilitate their entry into hepatocytes (Mashek, 2013). The amount of FAs taken up into the liver is proportional to the concentration in the circulation (Hagenfeldt *et al.*, 1972), with adipose-derived FAs accounting for the largest proportion of hepatic FAs (Donnelly *et al.*, 2005). In order to be utilised within hepatocytes in downstream metabolism, FAs are acetylated to fatty acyl-CoAs by fatty acyl-CoA synthetases (Mashek, 2013).

1.1.2.2 Dietary fatty acids

Dietary fat is predominantly comprised of TAG, which accounts for approximately 95% of fat consumed. However, due to its hydrophobicity, TAG must be hydrolysed before absorption: in the proximal half of the small intestine, pancreatic lipase hydrolyses dietary TAG to form two FAs and MAG. Once within the enterocyte, either *via* the glycerol-3-

phosphate acyltransferase (GPAT) or monoacylglycerol (MAG) pathway, TAG molecules are formed and chylomicrons (CMs) are synthesised at the endoplasmic reticulum (ER) (Yen *et al.*, 2015). CMs are comprised of a core of TAG and cholesterol esters (CE), which are surrounded by apolipoproteins (apo)B48 and apoAIV and PLs. Mature CMs exit the enterocyte *via* the basolateral membrane and are absorbed into the lymphatic system before entering the blood stream. Once in the circulation, CMs deliver about 80% of FAs to peripheral tissues *via* the action of lipoprotein lipase and apoCII and apoE are transferred from high-density lipoproteins (HDLs) (Feingold & Grunfeld, 2000). At the liver, the chylomicron remnant is recognised by the low-density lipoprotein (LDL) receptor due to its apoE protein and is taken up into liver, before hepatic lysosomes release FAs (Feingold & Grunfeld, 2000).

1.1.2.3 De novo lipogenesis

Monosaccharides, along with other non-lipid precursors, can contribute to hepatic fat *via* their conversion to lipids through *de novo* lipogenesis (DNL). Glucose and fructose both enter the liver through glucose transporters: GLUT2 is the primary transporter expressed on hepatocyte membranes, although several others are present at lower levels (Debosch *et al.*, 2014; Karim *et al.*, 2012). Although GLUT2 is not directly insulin-mediated, in the postprandial state, where insulin stimulates glucose disposal *via* glycogenesis and lipogenesis, glucose uptake into the liver is indirectly stimulated (Honka *et al.*, 2018; Petersen *et al.*, 2017). Fructose metabolism is not insulin-stimulated; the first step in fructose metabolism is its

phosphorylation by fructokinase, which has a low K_m and high V_{max}, facilitating rapid fructose clearance from the portal vein (Adelman *et al.*, 1967; Tappy & Le, 2010).

Once within the hepatocyte, glucose can be stored as glycogen through glycogenesis, or undergo glycolysis. Pyruvate, the product of glycolysis, has several fates: in the absence of oxygen, it is converted to lactate; it can be used for energy production *via* the tricarboxylic acid (TCA) cycle; or used as a substrate for DNL (Li *et al.*, 2015b). Once it has undergone a three-step reaction to produce glycerol-3-phosphate, fructose shares a similar fate to glucose (Figure 1.1.2-1). However, since fructose lacks the regulative influence of insulin, which controls glycolysis at the level of glucokinase and phosphofructokinase 1, its metabolism and entry into subsequent pathways is thought to be largely unregulated (Sanders & Griffin, 2016; Tappy & Le, 2010). The production of acetyl-CoA from pyruvate by pyruvate dehydrogenase provides the substrate required for DNL.

Acetyl-CoA carboxylase (ACC) and fatty acid synthase (FAS) perform the subsequent steps to produce malonyl-CoA and a fatty acyl-CoA, respectively (Sanders & Griffin, 2016). FAS is a multi-enzyme protein, which requires donation of seven malonyl-CoA molecules through a cycling process of decarboxylative condensation in order to form the final product of DNL, palmitate (C16:0) (Nguyen *et al.*, 2008; Sanders & Griffin, 2016). Malonyl-CoA also performs a regulatory function in FA metabolism, since it inhibits FA oxidation by interacting with carnitine palmitoyl transferase-1 (CPT-1, see section 1.1.4.1; Foster, 2012). Both FAS and ACC are controlled allosterically and by phosphorylation and dephosphorylation; important regulators are substrates (*e.g.* glutamate, citrate) and insulin, which stimulate activity, and

activity of the cAMP and AMP-activated protein kinase (AMPK) axis and fatty acyl-CoAs, which inhibit activity (Nguyen *et al.*, 2008; Sanders & Griffin, 2016).

These enzymes are also transcriptionally regulated, primarily by sterol regulatory element-binding protein (SREBP)-1c and carbohydrate-responsive element-binding protein (ChREBP). SREBP-1c exists in a membrane-bound, inactive form at the ER in association with SREBP cleavage-activating protein (SCAP) and insulin-induced gene (INSIG); under certain conditions, SCAP dissociates from INSIG and the SREBP1-c-SCAP complex moves to the Golgi apparatus. Here, two proteases cleave SREBP-1c to produce a mature form that translocates to the nucleus and increases transcription of its target genes, which include *ACACA* (the gene encoding the major hepatic isoform of ACC, ACC1) and *FASN*, which encodes FAS (Shimano & Sato, 2017). ChREBP also requires translocation to the nucleus, which is facilitated by glycolytic by-products and results in increased transcription of genes possessing the carbohydrate response element, including *ACACA* and *FASN* (Filhoulaud *et al.*, 2013). Both transcription factors are stimulated by insulin *via* activation of liver X receptor (LXR), which upregulates transcription (Sanders & Griffin, 2016), and inhibited by unsaturated FAs (Hannah *et al.*, 2001; Postic *et al.*, 2007). SREBP1-c is also directly stimulated by insulin through nuclear SREBP-1c stabilisation and transcriptionally regulated by glucagon/cAMP (Nguyen *et al.*, 2008).

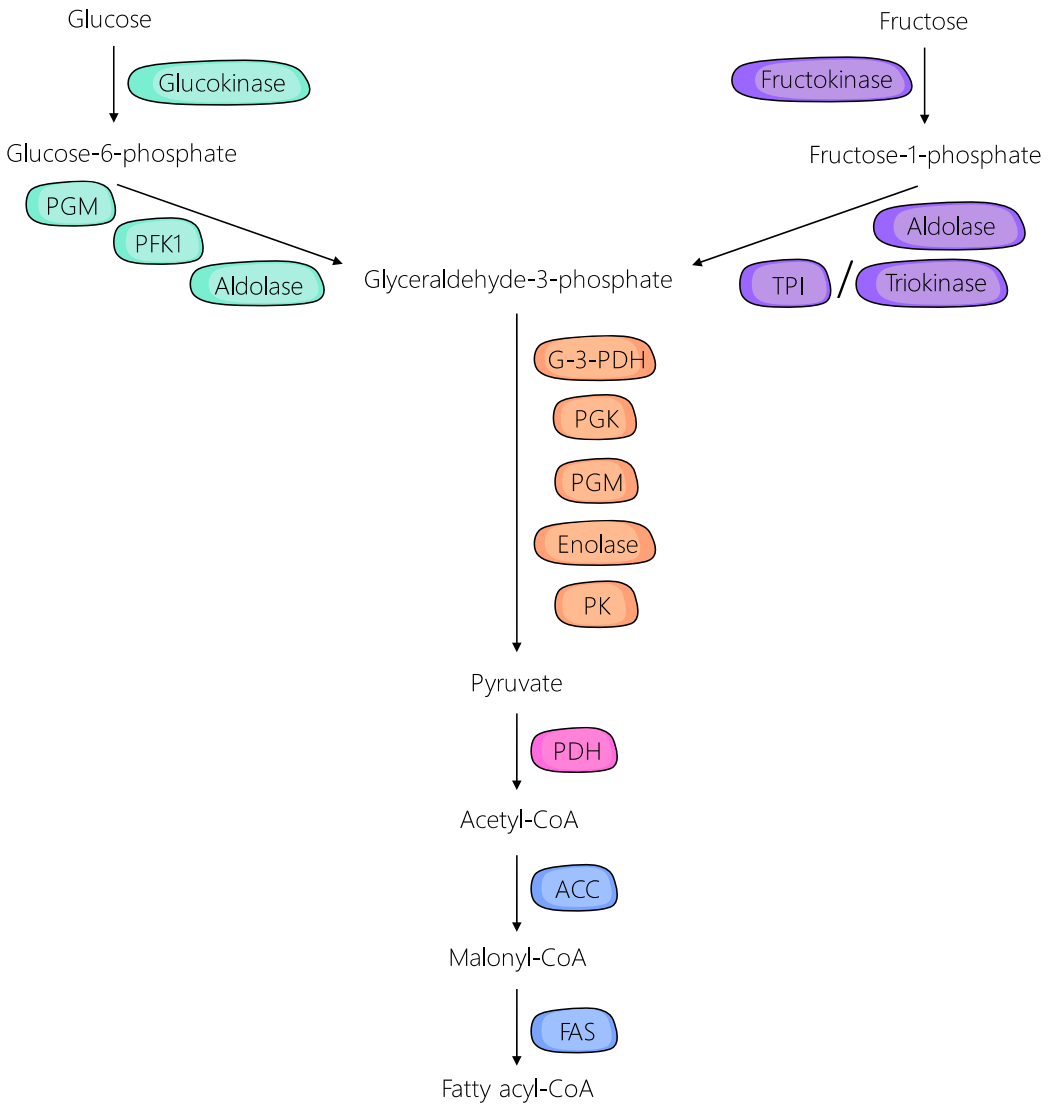


Figure 1.1.2-1. Glycolysis and fructolysis provide substrate for *de novo* fatty acid synthesis. The first half of glycolysis is an ATP consuming process that results in glyceraldehyde-3-phosphate (G-3-P) production (green enzymes; PGM, phosphoglucomutase; PFK1, phosphofructokinase 1). Insulin controls this stage of glycolysis through regulation of glucokinase and PFK1; however, fructolysis can also produce G-3-P from fructose, without the control of insulin (purple enzymes; TPI, triose phosphate isomerase). The second half of glycolysis is ATP generating, and results in pyruvate production (orange enzymes; G-3-PDH, G-3-P dehydrogenase; PGK, phosphoglycerokinase; PGM, phosphoglyceromutase; PK, pyruvate kinase). Decarboxylation of pyruvate by pyruvate dehydrogenase (PDH) results in acetyl-CoA formation, which can enter the citric acid cycle, ketogenesis, or, when present in excess, *de novo* lipogenesis. Acetyl-CoA carboxylase (ACC) first converts acetyl-CoA to malonyl-CoA, before fatty acid synthase (FAS), an enzyme complex consisting of six reactions, produces a 16-carbon saturated fatty acyl-CoA (palmitate). Adapted from Sanders & Griffin, 2015.

1.1.2 Metabolism and storage of hepatic fatty acids

1.1.3.1 Elongation and desaturation of fatty acids

As described in section 1.1.1, FAs exist with different chain lengths and degrees of desaturation. Both dietary and DNL-derived FAs can undergo elongation and desaturation; however, humans do not possess the necessary enzymes to produce linoleate (C18:2*n*-6) and α-linolenate (C18:3*n*-3), which therefore constitute essential FAs that must be obtained from the diet (Sassa & Kihara, 2014). Elongation takes place at the ER by FA elongase (ELOVL) enzymes. Seven members of the ELOVL family have been identified in mammals, five of which have a known role in hepatic FA metabolism (Jakobsson *et al.*, 2006; Sassa & Kihara, 2014). Of note, ELOVL6 represents an important enzyme in DNL as it elongates palmitate (C16:0), while ELOVL2 and ELOVL5 are key in PUFA metabolism: *n*-3 and *n*-6 FAs compete as substrates for these enzymes. Desaturase enzymes are responsible for adding double bonds to FA chains, with stearoyl-CoA desaturase (SCD)-1, producing a double bond in the SFAs palmitate and stearate, and FA desaturase (FADS)1 & 2 adding double bonds into *n*-3 and *n*-6 PUFAs (Sassa & Kihara, 2014; Figure 1.1.3-1).

These pathways of elongation and desaturation are important in producing FA chains that will be partitioned into storage or as membrane components, ligands and signalling molecules. In humans, the most common SFAs are palmitate (C16:0) and stearate (C18:0) (Hodson *et al.*, 2008). Although SFAs are needed for essential biological processes such as signal transduction (Legrand & Rioux, 2010), there is also evidence that they may be deleterious to human health. Specifically, they have been found to upregulate lipogenesis (Lin

et al., 2005), stimulate inflammatory pathways (Staiger *et al.*, 2006), contribute to ceramide biosynthesis (Andrieu-Abadie *et al.*, 2001) and impair insulin signalling (Kennedy *et al.*, 2009); however, despite plausible mechanistic evidence, the impact of SFAs on human health is mixed (Clifton & Keogh, 2017; de Souza *et al.*, 2015). Regulation of palmitate occurs secondary to DNL; its metabolism through elongation and desaturation are also regulated alongside palmitate synthesis by SREBP-1c (Chong *et al.*, 2008; Ricoult *et al.*, 2016).

There is also evidence that PUFAs have a role of in human health; these effects may occur due to their incorporation into membranes, eicosanoid production and gene regulation (Shaikh & Edidin, 2008). Long-chain PUFAs (LCPUFAs) include the *n*-3-derived eicosapentaenoic acid (EPA) and docosahexaenoic acid (DHA) and the *n*-6-derived arachidonic acid (AA). These FAs may modulate diseases including cardiovascular disease, depression and non-alcoholic fatty liver disease (NAFLD; see section 1.5.2.2) (Marventano *et al.*, 2015). There is some evidence, although not conclusive, that AA may be detrimental to health, primarily due to the eicosanoids derived from long-chain PUFAs, with those from *n*-6 PUFAs thought to be more pro-inflammatory (Simopoulos, 2016). Due to their interaction with LXR and peroxisome proliferator-activated receptors (PPARs), PUFAs suppress DNL and stimulate β-oxidation (Shaikh & Edidin, 2008). Although the amount and ratio of PUFAs is largely determined by dietary intake, there have been several reports of genetic variants in FADS enzymes resulting in altered FA composition and disease risk (Huang *et al.*, 2017), indicating that changes in FA metbabolism may have a causative role in disease.

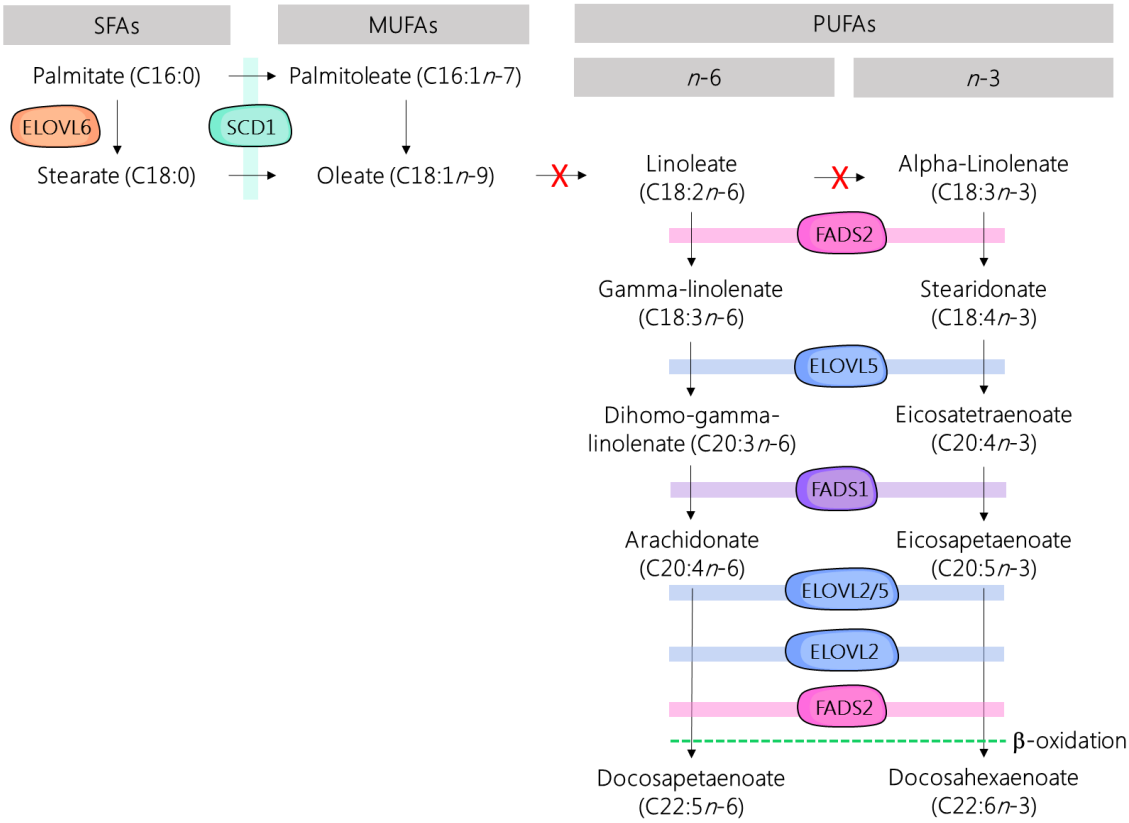


Figure 1.1.3-1. Fatty acid metabolism *via* elongation and desaturation. Palmitate can be obtained from the diet or *de novo* lipogenesis and may be desaturated by stearoyl-CoA desaturase (SCD)1 immediately to form palmitoleate, or first be elongated to stearate by fatty acid elongase (ELOVL)6 to form stearate, before desaturation to oleate. Humans do not possess the necessary enzymes to synthesise linoleate from oleate, or α-linolenate from linoleate (red crosses). Linoleate and α-linolenate are therefore essential *n*-6 and *n*-3 FAs, respectively, which must be obtained from the diet. Both essential FAs compete for fatty acid desaturase (FADS) and ELOVL enzymes to form long-chain polyunsaturated FAs (PUFAs). To form docosapetaenoate and docosahexaenoate their precursors lose two carbons by undergoing one cycle of acetyl-CoA removal *via* peroxisomal β-oxidation. SFA, saturated fatty acid; MUFA monounsaturated fatty acid.

1.1.3.2 Triacylglycerol synthesis

Like the enterocyte, the hepatocyte can esterify fatty acyl-CoAs to form TAG *via* the GPAT or MAG pathway (Figure 1.1.3-2). In the canonical GPAT pathway, a fatty acyl-CoA is joined to glycerol-3-phosphate to form lysophosphatidic acid. A further addition of a fatty acyl-CoA, catalysed by sn-1-acyl-glycerol-3-phosphate acyltransferase, forms phosphatidic acid (PA). The phosphate group is then removed by PA phosphatase (also known as lipin), to form DAG (Coleman & Lee, 2004). This pathway is stimulated in energy excess and inhibited in energy depletion, through phosphorylation and dephosphorylation of GPAT; GPAT is also a target of SREBP-1c, which allows coordination of FA synthesis through DNL and TAG synthesis (Nguyen *et al.*, 2008). The MAG pathway of TAG synthesis is usually used during hydrolysis and re-esterification of TAG, where a preformed MAG molecule has a fatty acyl-CoA added by MAG acyltransferase to form DAG, with both pathways having the final fatty acyl-CoA added to DAG by DAG acyltransferase (DGAT) (Yen *et al.*, 2015).

1.1.3.3 Triacylglycerol storage

Within the hepatocyte, TAG is stored primarily in LDs, which, apart from TAG, contain CE and are surrounded by a PL monolayer and LD-associated proteins. They form an essential store of lipids required for energy generation and membrane synthesis, as well as storage of vitamins and signalling molecules and management of cell stress (Welte & Gould, 2017). Although LDs can be found in the ER lumen, as primordial VLDL particles (see section 1.1.4.2) and within the nucleus, cytosolic LDs are the most studied. Understanding of how LDs form is in its infancy: the current hypothesis is that neutral lipids accumulate between

the membranes of the ER, initially forming a lens, before a budding LD is formed, which eventually buds off into the cytoplasm (Mashek *et al.*, 2015; Walther *et al.*, 2017). However, whether LDs are truly distinct organelles, or whether they, to some extent, always remain connected to the ER is not known.

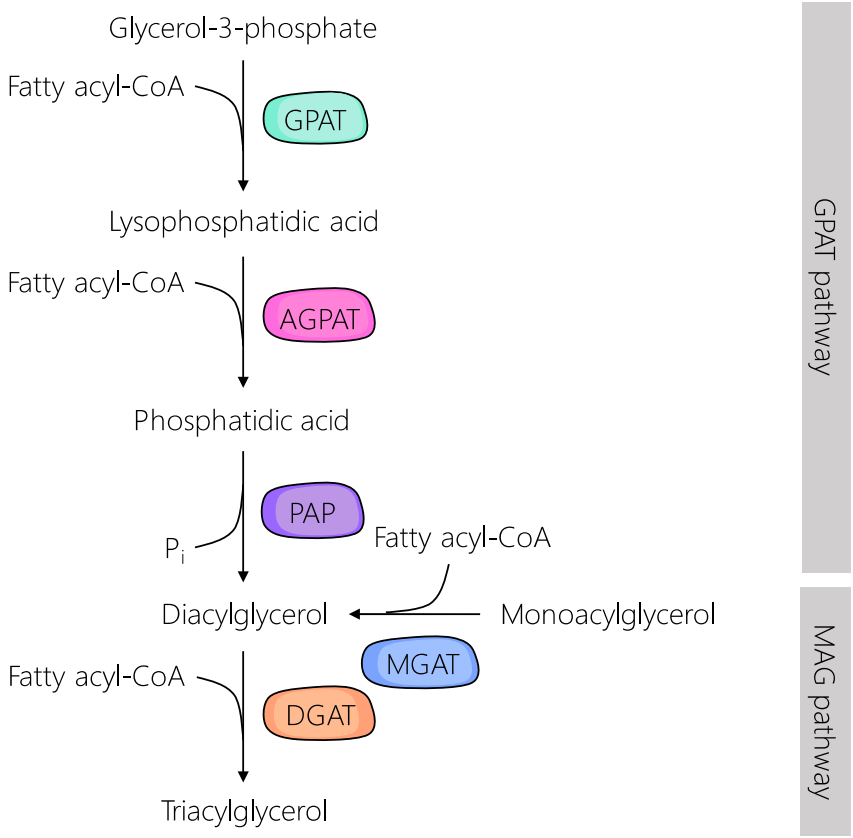


Figure 1.1.3-2. Synthesis of triacylglycerol. Fatty acyl-CoAs are added to a glycerol backbone to form triacylglycerol either *via* the glycerol-3-phosphate acyltransferase (GPAT) or monoacylglycerol (MAG) pathway. Both pathways share the final step of a fatty acyl-CoA addition *via* diacylglycerol acyltransferase (DGAT). AGPAT, sn-1-acyl-glycerol-3-phosphate acyltransferase; PAP, phosphatidic acid phosphatase (also known as lipin); MGAT, monoacylglycerol acyltransferase. Adapted from Yen *et al.*, 2015 (Yen *et al.*, 2015).

Cytosolic LDs vary in size: they can range from 0.3 to 10 μm in diameter, and may be even larger in disease states (Gluchowski *et al.*, 2017a). How LD sizes vary to such an extent is still under investigation. ER structure itself and the size at which LDs bud off from the ER may determine their eventual size: two ER-associated proteins, seipin and fat storage-inducing transmembrane protein (FIT)2 are key determinants of LD growth at the ER. Seipin is thought to regulate LD generation, determine LD protein composition and anchor budding LDs (Cartwright & Goodman, 2012; Walther *et al.*, 2017), while FIT2 is believed to control partitioning of TAG synthesised at the LD to different pools (Goh & Silver, 2013). As TAG-synthesising enzymes, the DGAT enzymes are also involved in LD growth at the ER, which is discussed further in section 1.2.

There is also evidence that LDs continue to expand within the cytosol, through LD fusion and lipid exchange, as well as through *in situ* lipid synthesis (Walther *et al.*, 2017). Fusion of LDs can occur through changes in the biophysical properties of PL membrane: when PLs are lost, the surface tension of LDs is lowered and coalescence of LDs is promoted (Gluchowski *et al.*, 2017a). In addition, LD growth can occur by lipids being transferred from one LD to another, which is facilitated by cell death-inducing DFFA-like effector (CIDE) proteins, particularly CIDEC (Walther *et al.*, 2017). Evidence of TAG synthesis occurring at LDs for direct incorporation is based on the presence of the TAG-synthesising enzymes, DGAT2 and GPAT4, being found on the surface of cytosolic LDs; these proteins are likely transferred through reconnection of LDs to the ER via the ADP ribosylation factor/coat protein (ARF/COP)-I (Wilfling *et al.*, 2013).

Also important in LD dynamics are the perilipin (PLIN) family of proteins. Five members of the PLIN family have now been discovered with different tissue distributions: PLINs 1, 2, 3 and 5 are expressed in the liver (Kimmel & Sztalryd, 2016). The PLIN family of LD proteins appear to have roles in LD stabilisation, as well as be markers of, if not have a role in, different LD distributions in hepatocytes. While PLIN3 is expressed most highly in the presence of small LDs, as they mature, there is increasing expression of PLIN5, PLIN2 and finally PLIN1 (Pawella *et al.*, 2014). PLINs are also important in allowing lipases to access cytosolic LDs, and as such, have an impact on oxidation and secretion of hepatic FAs (Itabe *et al.*, 2017).

1.1.4 Fates of hepatic fatty acids

1.1.4.1 Fatty acid oxidation

Hepatic FA oxidation can be used to meet the energy needs of the liver directly, and other tissues indirectly, the latter by the production of ketone bodies. There may be direct shuttling of fatty acyl-CoAs to oxidative organelles upon entry to the hepatocyte, otherwise lipolysis of FAs from LDs will be required (Gibbons *et al.*, 2000). ATGL is the predominant lipase that directs mobilised FA toward oxidation, while PLIN5 may facilitate oxidation by promoting LD-mitochondria interactions (Kimmel & Sztalryd, 2016; Mashek *et al.*, 2015). The predominant oxidative pathway in the liver is β-oxidation in the mitochondria; however, β-oxidation can also occur in peroxisomes and ω-oxidation in the ER.

The first step in mitochondrial β-oxidation is transformation of a fatty acyl-CoA to acyl carnitine by CPT-1 (Houten *et al.*, 2016). Acyl carnitine can then be moved to the inner

mitochondrial membrane, where CPT-2 reverses the action of CPT-1, producing fatty acyl-CoA. Carbons are removed two at a time to generate acetyl-CoA through a cycling process involving dehydrogenation, hydration, dehydrogenation and acylation (Houten *et al.*, 2016; Sassa & Kihara, 2014). Acetyl-CoA then enters the TCA cycle and electron transport chain for ATP production, or ketogenesis, within the mitochondria. Ketogenesis produces acetoacetate, acetone and 3-hydroxybutyrate (3-OHB); plasma 3-OHB is a commonly used as a surrogate marker of hepatic FA oxidation (Ontko, 1972). The primary regulator of β-oxidation is the transcription factor PPAR-α, the action of which is upregulated by FAs and glucagon, and suppressed *via* insulin (Pawlak *et al.*, 2015).

Apart from mitochondria, peroxisomes can also carry out β-oxidation. Peroxisomal oxidation is primarily used for long and very long-chain FA oxidation and is essential in producing some long-chain FA species (*e.g.* DHA, see Figure 1.1.3-1) (Poirier *et al.*, 2006; Sandalio *et al.*, 2013). However, due to the lack of a TCA cycle in peroxisomes, FAs will not undergo complete oxidation, but will be shortened to a medium-chain FA before entering the mitochondria for further oxidation cycles. As a result, the acetyl-CoA produced can either be transformed to acetyl-carnitine and enter the mitochondria for further metabolism, or it can be converted to acetate; free acetate can therefore be used as a marker of peroxisomal β-oxidation (Leighton *et al.*, 1989; Sandalio *et al.*, 2013). In addition, rather than the initial dehydrogenation step in mitochondrial β-oxidation, in peroxisomes, this is an oxidation reaction, which results in the formation of hydrogen peroxide (H_2O_2), a reactive oxygen species (ROS) (Schrader *et al.*, 2015). ROS can also be produced during ω-oxidation at the

ER, which occurs during insufficient β-oxidation and FA overload and requires CYP enzyme action (Wanders *et al.*, 2011).

1.1.4.2 Lipoprotein secretion

Part of the liver's role in systemic lipid metabolism is to assemble and secrete VLDL particles, which distribute fat to peripheral tissues *via* the action of lipoprotein lipase. As VLDL particles are hydrolysed and lipid taken up into tissues, VLDL particles first become intermediate-density, and then low-density, lipoprotein particles, before being returned to the liver and taken up by the LDL-receptor (Feingold & Grunfeld, 2000). Compared to other lipoproteins, VLDL particles have a larger lipid core, consisting of TAG and CEs; they are also associated with apolipoprotein (apo) particles, primarily apoB100 (Feingold & Grunfeld, 2000). The formation of VLDL begins with a nascent apoB100 particle passing from the rough ER to the smooth ER, where the addition of lipids *via* microsomal triglyceride transfer protein (MTP) forms a primordial VLDL particle. This particle can then be further lipidated by the lipids contained within LDs; if insufficient lipid is transferred to a primordial VLDL particle, it will undergo degradation (Ohsaki *et al.*, 2008).

The exact sources and mechanism by which this lipidation occurs is not known, although CIDEB, abhydrolase domain containing 5 and carboxylesterase (CES)1, which are all involved in TAG lipolysis, have been proposed to have a role in directing FAs towards VLDL assembly (Tiwari & Siddiqi, 2012), while PLIN2 appears to have an inhibitory role, likely by blocking lipase action (Carr & Ahima, 2016). There is also evidence of a specific process that FAs have to go through before they can be incorporated into VLDL, which involves the

esterification of FA to TAG, before lipolysis to FA for lipidation of VLDL and finally re-eseterification of excess FAs (Gibbons *et al.*, 1992; Gibbons *et al.*, 2000); whether specific LD pools contribute differently to VLDL assembly is not known (*i.e.* luminal *vs.* cytosolic). Nonetheless, once the VLDL particle is sufficiently lipidated, it undergoes vesicle-mediated transfer to the Golgi apparatus before migrating to the sinusoidal membrane for release into the circulation (Tiwari & Siddiqi, 2012).

1.2 MODELS FOR STUDYING HEPATIC FATTY ACID METABOLISM

The inaccessibility of the liver in humans makes studying hepatocellular FA metabolism challenging. As a result, a number of alternative models are employed, which have recently been reviewed (Green *et al.*, 2018). Although rodents are often used as an *in vivo* model and offer important insight into systemic FA metabolism (Bergen & Mersmann, 2005), particular caution should be used when interpreting results in relation to diet and hepatic metabolism. The use of genetically manipulated and high fat diet-fed models has led to conflicting results (Lai *et al.*, 2014); in addition, rodents naturally have a higher reliance on carbohydrate intake and DNL and exhibit differences in nutrient absorption compared to humans (Hiramine & Tanabe, 2011; McLaren *et al.*, 2018; Stone *et al.*, 2004). A number of recent reviews have examined the current animal models available, their utility and areas for development (Lau, Zhang & Yu, 2017; Van Herck, Vonghia & Francque, 2017; Jahn *et al.*, 2018); as a result, neither *in vitro* nor whole-body rodent models are considered further in this section.

1.2.1 Investigating hepatic fatty acid metabolism using stable isotope tracers

Isotopes are chemically identical forms of elements, which have a different mass due to a different number of neutrons: non-radioactive isotopes are termed stable. Since common elements exist predominantly with a particular isotope (*e.g.* ^{1}H and ^{12}C), addition of stable isotopes (*e.g.* ^{2}H and ^{13}C), which naturally exist at very low levels (<1%), to the element pool allows stable isotopes to be differentiated and 'traced' *via* mass spectrometry (Umpleby, 2015). Use of stable isotope tracers allows aspects of hepatic FA metabolism to be measured that wouldn't normally be possible, particularly, rates of DNL and the contribution of different sources of FA to liver fat content. This is done by enriching different FA pools with different isotopes and measuring appearance in secreted VLDL-TAG particles, which are representative of liver TAG content (Donnelly *et al.*, 2005).

Commonly, the systemic NEFA pool, which is predominantly derived from subcutaneous adipose tissue lipolysis, is enriched with a stable isotope-labelled FA, such as [$^{13}C/^{2}H$]palmitate. This is complexed to albumin and infused intravenously; incorporation into the plasma NEFA pool for hepatic uptake allows tracing into esterification (VLDL-TAG) or oxidation (3-OHB) pathways. Dietary FA contribution is often estimated by enriching a test meal with a single FA, such as palmitate or oleate, either in FFA or TAG form, which can be absorbed and incorporated into chylomicrons at the enterocyte (Donnelly *et al.*, 2005; Green *et al.*, 2018). Finally, DNL can be measured by administering heavy water ($^{2}H_2O$) or a labelled DNL substrate (*e.g.* glucose, fructose or acetate) (Donnelly *et al.*, 2005); however, the latter method may be confounded by the fact that these substrates, or intermediates from

their metabolism (*e.g.* lactate), can upregulate DNL (Sun & Empie, 2012). In the case of heavy water, once equilibrated with the body pool, deuterium molecules may be used in the production of palmitate during DNL, which gains hydrogen atoms from acetyl-CoA, NADPH and H_2O. Since deuterium is not uniformly distributed among these pools, a maximum of 21-22 of the 31 hydrogen atoms in palmitate can be replaced by deuterium labelling in humans (Diraison *et al.*, 1997; Green *et al.*, 2018).

Stable-isotope tracers are also used for measurement of other aspects of whole-body metabolism. Intravenously infused labelled FA (such as palmitate; the tracer) can be used to measure the rate of subcutaneous adipose tissue lipolysis; once a steady state is achieved, the amount by which it's diluted by adipose-derived palmitate (unlabelled; the tracee) allows calculation of the tracer-to-tracee ratio (TTR), with a decrease in TTR representing an elevation in lipolysis (Green *et al.*, 2018; Umpleby, 2015). Use of both ^{2}H and ^{13}C palmitate also allows for measurement of FA oxidation; however, ^{13}C allows separation of hepatic and whole-body oxidation by measurement of ^{13}C in plasma 3-OHB and $^{13}CO_2$ in expired breath, respectively (Green *et al.*, 2018; Umpleby, 2015). Although tracers offer particular insight into hepatocellular metabolism in the context of the whole-body, the utility of tracers in probing FA metabolism has also been recognised in cultured cells. Similar methods using $^{2}H_2O$ and labelled precursors (*e.g.* sugars, glycerol and acetate) have been used for assessing DNL (Hirahatake *et al.*, 2011; Lee *et al.*, 1994b; Wurie *et al.*, 2012), while labelled FAs (*e.g.* palmitate and oleate) can be used to measure FA partitioning and turnover and FA oxidation *in vitro* (Gibbons *et al.*, 1992; Huynh *et al.*, 2014).

1.2.2 *In vitro* models of hepatic fatty acid metabolism

Human-derived cellular models are a rapidly developing area of research. Although primary human hepatocytes are still considered the 'gold standard' model, they exhibit inter-donor variability and begin to dedifferentiate around 48 hours after isolation in 2D culture (Green *et al.*, 2017; Green *et al.*, 2015b). Inducible pluripotent stem cell-derived hepatocytes and HepaRG cells are two more recent models that have been developed. Both show promise as models of hepatic FA metabolism (Graffmann *et al.*, 2016; Madec *et al.*, 2011; Samanez *et al.*, 2012), although research to date is limited, and certainly in the case of stem cells, the technology is still in its infancy. In addition, development of spheroid cultures facilitate cell-to-cell interactions, offer improvements in cellular function and allow extended experimental protocols in primary hepatocytes, stem cell-derived hepatocytes and hepatocyte cell lines (Bell *et al.*, 2018; Bell *et al.*, 2016; Bell *et al.*, 2017; Luckert *et al.*, 2017): further development of such technologies will no doubt improve hepatocellular models. However, simple changes to cell media have also resulted in functional improvements in two common hepatoma cell lines used in the investigation of FA metabolism.

HepG2 cells were isolated and immortalised from a hepatoblastoma of a 15-year old Caucasian male in 1979 (Aden *et al.*, 1979; Lopez-Terrada *et al.*, 2009). Huh7 cells were derived in 1982 from the hepatocarcinoma of a 57-year old Japanese male; they are potentially permissive to hepatitis C virus (HCV) infection, with Huh7.5 cells, a clonal variant of Huh7 cells, carrying a single point mutation resulting in consistently high HCV RNA replication (Bartenschlager & Pietschmann, 2005; Sainz *et al.*, 2009). As models of hepatic nutrient

metabolism, HepG2 and Huh7 cells are widely used; however they show characteristics of dedifferentiation from mature hepatocytes: although they secrete albumin, they also express tumour markers and have limited expression of CYP enzymes, hepatic transcription factors and nuclear receptors (Donato *et al.*, 2008; Godoy *et al.*, 2013; Jeon & Kim, 2011; Nikolaou *et al.*, 2016). Approaches that attempt to improve HepG2 and Huh7/7.5 cells as hepatocyte models have included use of 1% dimethyl sulfoxide (DMSO), a differentiation-inducing agent, and human serum (HS), instead of foetal bovine serum, in cell media, which have shown utility in both improving FA metabolism and differentiation markers (Choi *et al.*, 2009; Pramfalk *et al.*, 2016; Sivertsson *et al.*, 2010; Steenbergen *et al.*, 2013).

Early work in HepG2 cells using radioactive tracers showed that they are capable of taking up exogenous lipid in the form of FAs and lipoprotein remnants (Furth *et al.*, 1992; Gibbons *et al.*, 1994; Graham & Russell, 1994; Hara *et al.*, 1993). However, hepatoma cell lines are commonly grown in glucose-only media, making them highly reliant on DNL; this is associated with essential FA deficiency and enhanced elongation of DNL-derived FAs (Furth *et al.*, 1992; Gibbons *et al.*, 1994). This elevation in DNL may be a result of rapid uptake and metabolism of glucose due to an upregulation of GLUT1, which facilitates a constant uptake of glucose independently of plasma concentrations (Amann *et al.*, 2009); high intracellular glucose levels are also used for anaerobic and aerobic glycolysis in these cells (Tong *et al.*, 2009). High rates of lipogenesis and glycolysis may also be partly mediated by ChREBP, which is expressed more highly in cancer cells and upregulates both of these pathways through its

target genes (*i.e.* ACC, FAS, glucose 6-phosphatase and glucokinase regulatory protein) (Berlanga *et al.*, 2014; Tong *et al.*, 2009).

FAs can be metabolised *via* elongation and desaturation, before being partitioned towards esterification as TAG, for storage in intracellular LDs (section 1.1.3), or as PLs, for use in membrane synthesis: both HepG2 and Huh7 cells are able to metabolise FAs through these pathways (Furth *et al.*, 1992; Wu *et al.*, 2015). In addition, both cell types synthesise TAG from DNL and exogenous FAs very efficiently (Gibbons *et al.*, 1994; Green *et al.*, 2015a; Zhao *et al.*, 2016); numerous studies supplying either oleate alone or in combination with palmitate have demonstrated an increase in intracellular TAG in response to FA treatments (Chavez-Tapia *et al.*, 2012; Green *et al.*, 2015b; Kostrzewski *et al.*, 2017). Use of both DMSO and HS have resulted in alterations in lipid content: 1% DMSO reduced intracellular TAG content in cells cultured in palmitate or glucose-only media, suggesting a reduction in both exogenous and DNL-derived FA storage (Nikolaou *et al.*, 2016; Song *et al.*, 2012). In contrast, HS increased lipid accumulation in Huh7.5 cells, which was attributed to an upregulation of PPAR-α and LXR (Steenbergen *et al.*, 2013); since LXR can upregulate both exogenous FA uptake and DNL, the source of lipid in these cells was not clear.

Normally, FA partitioning and mobilisation between intracellular pools in hepatocytes is a highly dynamic process; however, HepG2 cells exhibit levels of FA mobilisation for oxidation and VLDL secretion that are lower than those in primary hepatocytes or *in vivo* (Gibbons *et al.*, 1994), attributable to very low expression of the CES enzymes, which hydrolyse CEs and

TAG (Lehner *et al.*, 1999). However, HepG2 cells are still able to oxidise FAs, with functional mitochondrial and peroxisomal β-oxidation present (Carrasco-Torres *et al.*, 2017; Vila-Brau *et al.*, 2011; Watkins *et al.*, 1991); 3-OHB was also increased as a result of DMSO addition to the media (Nikolaou *et al.*, 2016), suggesting increased FA mobilisation. Although there is limited research on the oxidative capabilities of Huh7/7.5 cells, they too show evidence of β-oxidation and ROS generation (Rasmussen *et al.*, 2011; Vila-Brau *et al.*, 2011). In addition, culturing of Huh7.5 cells in HS increased PPAR-α expression (Steenbergen *et al.*, 2013), indicating that HS may elevate the oxidative capacity of Huh7/7.5 cells.

HepG2 and Huh7 cells also secrete lipid-poor apoB-containing lipoproteins, which resemble LDL, rather than VLDL, particles (Gibbons *et al.*, 1994; Javitt, 1990; Meex *et al.*, 2011). Although HepG2 cells have limited smooth ER, demonstrating a structural deficit relevant to lipoprotein assembly (Thrift *et al.*, 1986), inhibition of the normally hyperactive MEK-ERK signalling pathway in HepG2 cells led to an increase in cytosolic and microsomal TAG and VLDL secretion (Meex *et al.*, 2011; Tsai *et al.*, 2007), indicating that low substrate supply for apoB lipidation, rather than structural insufficiency, underlies poor secretion. This is supported by evidence that supplying exogenous FAs to culture media improves lipoprotein secretion in both HepG2 and Huh7 cells (Dashti & Wolfbauer, 1987; Ellsworth *et al.*, 1986; Meex *et al.*, 2011; Wu *et al.*, 1996). Additionally, use of 1% DMSO in HepG2 cells and HS in in HepG2 and Huh7/7.5 cells improve TAG secretion and lipoprotein profiles (Nikolaou *et al.*, 2016; Pramfalk *et al.*, 2016; Steenbergen *et al.*, 2013). Overall, these cells carry out many

of the processes required for investigation of FA metabolism, which may be improved by changes to culture media.

1.3 THE ROLE OF DGAT ENZYMES IN HEPATIC FATTY ACID METABOLISM

1.3.1 The DGAT enzymes

Diacylglycerol acyltransferase is an enzyme that catalyses the final step of TAG synthesis, the addition of a third fatty acyl-CoA to diacylglycerol (section 1.1.3.2). There are two members of the DGAT family, DGAT1 and DGAT2, named according to the order in which they were described (Cases *et al.*, 1998; Cases *et al.*, 2001; Lardizabal *et al.*, 2001). Although they catalyse the same reaction, DGAT1 and 2 belong to separate gene families, with the former belonging to the membrane-bound O-acyltransferase family, a wider group of acyltransferases, and the latter to the DGAT2 family, along with monoacylglycerol and wax acyltransferases (Yen *et al.*, 2008). The enzymes share no sequence homology and it has now been established from phylogenetic and evolutionary analyses that the two DGAT isoforms have evolved separately, being distinct from one another in a number of molecular and structural aspects (Liu *et al.*, 2012).

Although both DGATs are expressed ubiquitously, *DGAT1* is more highly expressed in skeletal muscle, intestine, skin and testis and *DGAT2* in the liver and adipose tissue (Cases *et al.*, 1998). However, expression levels vary between species: for example, within the liver, humans have an approximately 4-fold higher expression of *DGAT2* than *DGAT1*, while in mice it is more than 20-fold (McLaren *et al.*, 2018). The DGAT proteins also display

differences in their topologies and cellular locations. DGAT1 is a multipass transmembrane protein found at the ER and appears to have dual topology, with both overt (cytosolic) and latent (luminal) activity (Bhatt-Wessel *et al.*, 2018). DGAT2 is also found at the ER, as well as the LD surface, and has two transmembrane domains, with the catalytic site present on the cytosolic aspect, which would be expected to result in overt enzyme activity, although evidence suggests it also has latent activity (Ganji *et al.*, 2004). The differential expression, location and topologies of the proteins suggest that they have distinct roles in TAG synthesis; this hypothesis has now been tested in a number of models.

1.3.1.1 The interaction between DGAT enzymes and hepatic triacylglycerol synthesis and storage

In agreement with DGAT catalyzing the final committed step in TAG synthesis, a number of human and rodent *in vitro* (Choi *et al.*, 2007; Li *et al.*, 2015a; Liang *et al.*, 2004; Wurie *et al.*, 2012; Yu *et al.*, 2005), as well as animal *in vivo* overexpression (Jornayvaz *et al.*, 2011; Millar *et al.*, 2006; Monetti *et al.*, 2007; Yamazaki *et al.*, 2005) and inhibitor or knockdown studies (Choi *et al.*, 2007; McLaren *et al.*, 2018; Villanueva *et al.*, 2009; Yu *et al.*, 2005), have demonstrated a reduction or increase in hepatic TAG synthesis concomitantly with lower or higher activity of either DGAT, respectively. Evidence of a reduction in other lipid species when DGAT activity is reduced, suggests a feedback or regulatory role of these enzymes in hepatocellular metabolism (Choi *et al.*, 2007; Jornayvaz *et al.*, 2011; Monetti *et al.*, 2007; Yu *et al.*, 2005). In addition, the DGAT enzymes may contribute to different LD pools and determine their size; the evidence to date suggests that due to its presence on the cytosolic

aspect of the ER and LD surface, DGAT2 contributes to cytosolic LD growth and, therefore, a population of large LDs (Becuwe *et al.*, 2018; Li *et al.*, 2015a; Wilfling *et al.*, 2013). In contrast, DGAT1 activity appears to lead to the synthesis of small cytosolic LDs, and, due to its luminal activity, ER luminal LDs (Lehner *et al.*, 2012; Wurie *et al.*, 2011).

1.3.1.2 The interaction between DGAT enzymes and sources of hepatic fatty acids

As outlined in section 1.1.1, there are three sources of hepatic FAs; dietary and NEFA contribute to the exogenous hepatic FA pool (originating outside the liver), while DNL-derived FAs make up the endogenous FA pool (synthesised within the liver). With the use of DGAT1 and DGAT2 inhibitors in HepG2 cells, Wurie *et al.* demonstrated that while DGAT1 seemed to contribute equally to incorporation of exogenous FA ([^{14}C]oleate) and endogenous FA ([^{14}C]acetate) incorporation into intracellular TAG, DGAT2 inhibition reduced [^{14}C]oleate incorporation by around 25% and reduced [^{14}C]acetate incorporation by almost 95% (Wurie *et al.*, 2012). In the same cell line, use of DGAT1 and DGAT2 inhibitors resulted in lower [^{13}C]oleic acid labelling and [^{13}C]glycerol labelling of TAG, respectively, a result confirmed *via* antisense oligonucleotide (ASO)-mediated *Dgat2* knockdown in mice (Qi *et al.*, 2012). These results suggest that DGAT2 preferentially uses DNL-derived FAs, while DGAT1 has less substrate specificity, or a preference for exogenous FAs.

This hypothesis is supported in rodent models *in vitro*, since [^{3}H]glycerol incorporation into TAG was reduced by around two thirds in primary hepatocytes isolated from *Dgat2* ASO-treated rodents, which was accompanied by downregulation of DNL genes, including *Acaca,*

Fasn, Scd and Srebf1c (Choi *et al.*, 2007; Yu *et al.*, 2014). In addition, *Dgat1*$^{-/-}$ mice were protected from exogenous FA-mediated, but not DNL-mediated, steatosis (Villanueva *et al.*, 2009). However, a recent comprehensive study of DGAT1 and 2 inhibitors in mouse hepatocytes showed that only when both enzymes were inhibited simultaneously did either exogenous or endogenous labelling reduce dramatically (Li *et al.*, 2015a). Despite this, the authors did find reduced expression of DNL-regulating genes, as well as decreased nuclear localisation of SREBP-1c, suggesting that the DNL pathway was downregulated by DGAT2 inhibition (Li *et al.*, 2015a). It has also been found that DGAT2 colocalises with other DNL-related enzymes, specifically SCD1 (Man *et al.*, 2006), adding credence to the assertion that DGAT2 and DNL are linked.

1.3.1.3 The interaction between DGAT enzymes and the fates of hepatic fatty acids

Once synthesised, hepatic TAG can be stored, with FAs used as a substrate for oxidation or VLDL synthesis. Although there is some evidence that DGAT enzymes are implicated in partitioning TAG towards pools with specific fates (Li *et al.*, 2015a), how they differ in this respect is less well-defined, since both rodent and human models present contradictory evidence. While ASO-mediated *Dgat2* knockdown *in vivo* and DGAT2 inhibition *in vitro* has been found to reduce TAG secretion (Choi *et al.*, 2007; Li *et al.*, 2015a; McLaren *et al.*, 2018; Yu *et al.*, 2014), *in vitro* and liver-specific *Dgat1* overexpression *in vivo* has also been associated with increased VLDL-TAG secretion (Liang *et al.*, 2004; Yamazaki *et al.*, 2005). In addition, manipulating both DGATs in the liver of mice has been found to have no effect (Millar *et al.*, 2006). The evidence from primary human hepatocytes is equally unclear: there

is evidence of both a reduction and no effect on TAG secretion in response to DGAT2 inhibition (Li *et al.*, 2015a; McLaren *et al.*, 2018). Specific roles of the DGAT enzymes on VLDL-TAG metabolism therefore remain to be elucidated.

The DGAT enzymes may also have an impact on FA oxidation. *In vitro* rodent models demonstrate that when DGAT2 activity is reduced by ASOs or inhibitors, oxidation rates are increased (Choi *et al.*, 2007; Li *et al.*, 2015a; McLaren *et al.*, 2018; Yu *et al.*, 2014). This finding led Li *et al.* to hypothesise that DGAT1 channelled TAG toward LDs for oxidation (Li *et al.*, 2015a); however, in primary hepatocytes isolated from *Dgat1*$^{+/+}$ or *Dgat1*$^{-/-}$ mice, there was no difference in oxidation after a chow diet, but an increase in oxidation in hepatocytes of *Dgat1*$^{-/-}$ after a high fat diet (Villanueva *et al.*, 2009). This suggests that in the absence of DGAT1, excess exogenous FAs that could not be esterified were still channelled towards oxidation. It may therefore be that the inhibition of DGAT2 and DNL, which would prevent the inhibition of β-oxidation, is the main driver of these findings, supported by DGAT2 being found at mitochondrial-associated membranes at the ER (Stone *et al.*, 2009). Nonetheless, DGAT activity, and DGAT2 particularly, appears to play a regulatory role in FA oxidation.

1.3.1.4 The effect of DGAT enzymes on whole-body metabolism

Although *in vitro* and liver-specific manipulation of the DGAT enzymes offers insight into their specific roles in hepatic FA metabolism, since DGAT enzymes are ubiquitously expressed, whole-body models are required. Whole-body and tissue-specific *Dgat1*$^{-/-}$ mice are viable and show a number of beneficial metabolic phenotypes, including obesity resistance,

increased metabolic rate, reduced production of lipotoxic intermediates and efficient glucose disposal (Chen *et al.*, 2003; Liu *et al.*, 2009; Smith *et al.*, 2000). On the basis of these findings, inhibitors were developed for treatment of metabolic disease in humans; however, treatment with DGAT1 inhibitors and loss-of-function mutations in humans result in diarrhoeal disorders (Denison *et al.*, 2014; Gluchowski *et al.*, 2017b; Haas *et al.*, 2012; Stephen *et al.*, 2016), likely due to the dependence of humans on DGAT1 action for intestinal fat absorption (Hiramine & Tanabe, 2011). In contrast to the inhibitor study (Denison *et al.*, 2014), loss-of-function mutations were also associated with hyperlipidaemia, proposed to be due to increased DGAT2 activity (Gluchowski *et al.*, 2017b; Haas *et al.*, 2012).

Divergence between human and murine phenotypes of loss-of-function models are less evident for DGAT2. Although *Dgat2*$^{-/-}$ mice are not viable, use of RNA interference and inhibitors of DGAT2 in both lean and obese mice has been shown to reduce hepatic TAG and VLDL-TAG secretion, but increase circulating glucose and insulin, the latter only reported in the lean model (McLaren *et al.*, 2018). Although these results were not replicated when DGAT2 inhibition in higher primates was investigated (McLaren *et al.*, 2018), they are similar to what is observed in humans in response to niacin (vitamin B3) treatment, which is believed to be a DGAT2 inhibitor (Ganji *et al.*, 2004). In overweight and obese patients, niacin therapy resulted in reduced plasma TAG, increased HDL-cholesterol, along with an increase in blood glucose and reduced insulin sensitivity (Blond *et al.*, 2014; Fabbrini *et al.*, 2010; Hu *et al.*, 2012). However, how much of these changes were due to changes in DGAT2 activity is not

known, since niacin is likely to have other metabolic effects (*e.g.* suppressed lipolysis in adipose tissue) (Hu *et al.*, 2012).

In addition, although plasma biochemistry results from mice to humans were recapitulated, changes in hepatic TAG content were mixed, with evidence of no change (Fabbrini *et al.*, 2010) and a reduction (Hu *et al.*, 2012) with niacin therapy. Investigation of people carrying *DGAT2* SNPs suggest that DGAT2 does play a role in liver fat content; two mutations have been investigated in Chinese (rs3060) and German (rs1944438) population, the first in association with niacin therapy (Hu *et al.*, 2012) and the second with a lifestyle intervention for weight loss (Kantartzis *et al.*, 2009). In both cases, carriers of the *DGAT2* mutation studied appeared to retain liver fat, despite favourable changes in plasma biochemistry and weight loss equivalent to those seen in non-carriers. In addition, the study by Kantartzis *et al.* reported a dissociation between the *DGAT2* mutation, liver fat and insulin resistance (Kantartzis *et al.*, 2009). These results suggest that DGAT2 is involved in regulating whole-body glucose and TAG metabolism and insulin sensitivity.

The effect of reduced DGAT2 function on fat mass and body weight in rodent models is inconclusive, with short-hairpin interference of *Dgat2* resulting in a small but non-significant trend of reduced body weight in obese mice (McLaren *et al.*, 2018). The human *DGAT2* gene is located on chromosome 11q13, which, from genetic-wide association studies, has been identified as a loci related to obesity. In response to this, a study in obese German adolescents that looked at 15 variants in the *DGAT2* gene did not find any associations with obesity

(Friedel *et al.*, 2007). However, in the study by Kantartzis *et al.* reported above, there was evidence of increased body weight at baseline in homozygous carriers of the SNP (Kantartzis *et al.*, 2009), while in a Chinese population, a rare nonsense, loss-of-function mutation in DGAT2 was found to be associated with leanness (Ning *et al.*, 2017), supporting a potential role of DGAT2 in body composition.

1.4 NON-ALCOHOLIC FATTY LIVER DISEASE

1.4.1 Natural history and prevalence

Non-alcoholic fatty liver disease describes a disease spectrum that ranges from simple steatosis to non-alcoholic steatohepatitis (NASH) and finally, cirrhosis. As the name suggests, the disease occurs in the absence of excessive alcohol intake (<20 g/day for women and <30 g/day for men), but is associated with obesity and the metabolic syndrome (Marchesini *et al.*, 2003). The first stage, steatosis, is characterised by an accumulation of LDs within the hepatocyte and is defined as such when lipid accounts for more than 5% of liver volume (Kleiner & Brunt, 2012). In NASH, while the accumulation of LDs persists, there is increasing inflammation, ballooning and fibrosis. As NASH progresses to cirrhosis, LD accumulation is reduced while fibrosis and collagen deposition increase (Figure 1.4.1-1) (Brunt *et al.*, 2015). Importantly, once the cirrhotic stage is reached, transplantation is required for treatment, without which, hepatocellular carcinoma, liver failure and death can occur. First described in 1952 (Zelman, 1952), NAFLD is now the second most common reason for liver transplantation, and is predicted to become the number one cause within the next two decades (Calzadilla Bertot & Adams, 2016).

Although NAFLD is a significant health burden, observing and tracking disease prevalence and progression is difficult, since the 'gold-standard' diagnostic tool, liver biopsy, is also prone to sampling variation and grading is subjective (reviewed by (Green *et al.*, 2018)). Based on biopsies from apparently healthy living liver donors, the prevalence of steatosis was reported as 12-18% in Europe and 27-38% in the US (Anstee *et al.*, 2013). Although imaging techniques vary in their sensitivity (ultrasound and computed tomography can detect >30% steatosis and magnetic resonance imaging and spectroscopy >3% steatosis), a recent meta-analysis based on imaging studies has put the estimated global prevalence of NAFLD at approximately 24%, a similar level to the biopsy studies (Younossi *et al.*, 2016). Two follow-up studies using repeated biopsies have reported that while approximately 50% of people with steatosis without fibrosis remained at this stage, 37-47% developed fibrosis (Ekstedt *et al.*, 2006; McPherson *et al.*, 2015). Why this divergence in non-progressive (benign) steatosis and progressive phenotypes exists remains to be completely elucidated; however, NASH is associated with elevated levels of ROS, ER stress, inflammation, and cellular injury, which eventually leads to apoptosis and fibrosis (Arab *et al.*, 2018): all of these factors can be influenced by perturbed FA metabolism.

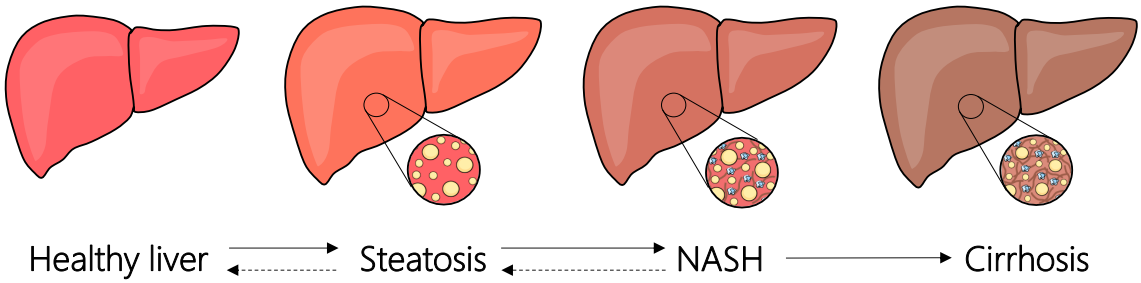


Figure 1.4.1-1. The natural history of non-alcoholic fatty liver disease (NAFLD). From a healthy liver, fat accumulation occurs; when more than 5% of the liver volume is comprised of fat, steatosis is diagnosed. In non-alcoholic steatohepatitis (NASH), infiltration of immune cells occurs and fibrosis begins to occur, which increases as the disease progresses. People with both steatosis and NASH can return to a healthy liver if hepatic fat content is reduced. From NASH, cirrhosis can develop, where increasing fibrosis becomes the histological hallmark and fat content is reduced; advanced NASH and cirrhosis can result in hepatocellular carcinoma and liver failure.

1.4.2 Pathogenesis

1.4.2.1 Systemic fatty acid metabolism and insulin resistance

The causes of steatosis are complex and multifactorial, although IR is believed to occur early in the development of NAFLD and is associated with disease progression (Anstee *et al.*, 2013). Normally, insulin signalling occurs *via* activation of the insulin receptor, which in turn activates insulin receptor substrates (IRS) 1 and 2, causing phosphorylation, and activation, of Akt. When IR occurs, failure of IRS activation has tissue-specific effects: in skeletal muscle and adipose tissue, a reduction in insulin-stimulated uptake and disposal of glucose *via* GLUT4 and muscle glycogen synthesis causes hyperglycaemia (Samuel & Shulman, 2016). In addition, lipoprotein lipase action is downregulated, causing inefficient clearance of chylomicron and lipoprotein-TAG and hyperlipidaemia, while insulin-mediated suppression of adipose tissue lipolysis during feeding is reduced, which elevates circulating NEFA

(Wilcox, 2005). If associated with obesity, adipose tissue dysfunction can also lead to the release of pro-inflammatory cytokines, increasing the risk of steatosis progression to NASH (Perla *et al.*, 2017). Together, peripheral IR creates a milieu for increased hepatic FA, with increased supply of DNL substrates and dietary and adipose-derived FA.

1.4.2.2 Changes in hepatic insulin signalling and fatty acid metabolism in NAFLD

Within the liver, there are a number of changes present in NAFLD patients. In line with an increased NEFA flux from adipose tissue, the liver appears to take up circulating FAs more efficiently: observational studies suggest that there is an upregulation of FA transporters, namely, FAT/CD36 and FABP4 and 5 in NAFLD (Bechmann *et al.*, 2010; Greco *et al.*, 2008; Westerbacka *et al.*, 2007). An increased flux of NEFA, and specifically, an increase of DAG, may cause lipotoxicity through interference with IRS activation *via* protein kinase C-ε, contributing to hepatic IR (Samuel & Shulman, 2016). Hepatic insulin signalling has three main outcomes: stimulation of the mechanistic target of rapamycin (mTOR) pathway, which upregulates lipogenesis; inactivation of forkhead box protein O1 (FoxO1), thus reducing gluconeogenesis; and activation of glycogen synthase kinase (GSK)3-β, which stimulates glycogen synthesis (Samuel & Shulman, 2016). In selective hepatic IR, while DNL continues to be stimulated by insulin, insulin-mediated regulation of gluconeogenesis and glycogen synthesis fails (Petersen *et al.*, 2017; Samuel & Shulman, 2016).

Certainly, there is an upregulation of DNL observed in NAFLD: tracer studies suggest that DNL accounts for approximately 23-25% of hepatic TAG in people with NAFLD (Donnelly *et al.*, 2005; Lambert *et al.*, 2014), compared to around 10% in those with metabolic syndrome

but low liver fat (Lambert *et al.*, 2014). Moreover, there appears to be a direct effect of impaired insulin signalling, since DNL is associated with hyperinsulinaemia (Marques-Lopes *et al.*, 2001), even when participants are matched for BMI (Schwarz *et al.*, 2003). These functional changes are associated with increased expression levels of the DNL master regulators, LXR, SREBP-1c and ChREBP (Higuchi *et al.*, 2008; Kohjima *et al.*, 2008; Lima-Cabello *et al.*, 2011). Although DNL appears to be induced as a result of IR and NAFLD development, DNL activation could also contribute towards it. Firstly, there is evidence that LXR may increase FAT/CD36 expression (Berlanga *et al.*, 2014), which would contribute to lipotoxicity-induced IR; furthermore, the interaction between DNL and FA oxidation could contribute to NAFLD progression.

DNL is known to inhibit CPT-1 and mitochondrial β-oxidation through production of malonyl-CoA; however, palmitate, the primary product of DNL can also be used in *de novo* ceramide synthesis. Apart from ceramides being thought to directly interfere with insulin signalling (Chavez & Summers, 2012), ceramide C16:0 also impedes mitochondrial function (Samuel & Shulman, 2016). This could cause excessive FA accumulation and an upregulation of microsomal FA oxidation, which would generate ROS and contribute to the inflammatory phenotype seen in NASH (Miura, 2013; Schrader *et al.*, 2015). Despite the evidence of a role of ROS in NASH development (Polimeni *et al.*, 2015; Spahis *et al.*, 2017), evidence for a change in FA oxidation during NAFLD is inconsistent (Perla *et al.*, 2017). This may be due to a dynamic response, characterised by an initial adaptation and upregulation of mitochondrial β-oxidation, before oxidative overload, and diversion of oxidation to

microsomal pathways (Koliaki *et al.*, 2015; Peng *et al.*, 2018). Indeed, CPT-1 expression has been found to be up and downregulated in NAFLD patients by around 30 and 50%, respectively (Kohjima *et al.*, 2007; Westerbacka *et al.*, 2007); it could be that a change in oxidative capacity is key to steatosis remaining benign or progressing to NASH.

Another adaptive response to increased hepatocellular TAG is an increase in VLDL-TAG secretion. Although there is evidence for an increase in VLDL-TAG secretion in NAFLD patients (Chan *et al.*, 2010; Fabbrini *et al.*, 2016), there appears to be a limit to how much VLDL-TAG secretion is possible, since a plateau in secretion has been reported beyond 10% liver fat (Fabbrini *et al.*, 2008). At a gene expression level, when steatosis accounted for more than 30% of liver volume, there was a downregulation of the genes encoding for MTP and apoB compared to people with lower levels of steatosis (Higuchi *et al.*, 2011). This change in VLDL-TAG secretion may originate from an elevation in ER stress as a result of lipid overload, impairing the ER's ability to assemble VLDL particles (Ota *et al.*, 2008); there is also evidence that ER stress increases lipoprotein uptake, ROS, and inflammatory pathways, thus further contributing to lipid accumulation and disease progression (Jo *et al.*, 2013; Sahini & Borlak, 2014). Elevation in VLDL-TAG export in response to NAFLD, may therefore represent a dynamic response depending on disease stage and phenotype.

1.4.2.3 The effect of genetics and lipid droplet pattern

Insight into the pathophysiology of NAFLD can also be gained from genetic predisposition to disease. Two genetic polymorphisms are strongly associated with the incidence and

progression of NAFLD independently of IR, the I148M variant of patatin-like phospholipase domain-containing protein 3 (*PNPLA3*) (Romeo *et al.*, 2008) and the E167K transmembrane 6 superfamily 2 (*TM6SF2*) variant (Liu *et al.*, 2014). TM6SF2 is an ER-resident protein, which may also be present at the ER-Golgi interface and cell models suggest it is involved in determining the partitioning of lipid towards intracellular LDs and VLDL particles (Mahdessian *et al.*, 2014); in humans the mutation causes a reduction in VLDL secretion (Sliz *et al.*, 2018). The mechanism of action of the *PNPLA3* mutation is more complex, although there appears to be a synergistic role in the hepatocyte of reduced PNPLA3 degradation, which maintains PNPLA3 presence on cytosolic LDs, causing perturbed FA turnover and remodelling, and activation of stellate cells (Bruschi *et al.*, 2017; Sliz *et al.*, 2018).

The action of both enzymes in LD synthesis and composition indicates the importance of these organelles in NAFLD pathogenesis. Histologically, LD pattern in liver tissue is defined as either macrovesicular (medium to large LDs with well-defined edges) or microvesicular (small, diffuse LDs with a foamy appearance) (Takahashi & Fukusato, 2014). Microvesicular steatosis is only present in around 10-15% of NAFLD and more commonly associated with lipid accumulation in other, acute disease states (Masterton *et al.*, 2011; Takahashi & Fukusato, 2014; Tandra *et al.*, 2011). Evidence of how the two patterns are implicated in NAFLD progression are limited and mixed; microvesicular steatosis has been associated with more advanced histology markers and progression to NASH (Tandra *et al.*, 2011), as well as with reduced fibrosis (Masterton *et al.*, 2011). In addition, microvesicular steatosis has been

associated with a decreased risk of IR and type 2 diabetes compared to macrovesicular steatosis (Masterton *et al.*, 2011).

Apart from these observational association studies, there is some evidence that LD protein compositions of small and large LDs is different. Pawella *et al.* tracked the expression of different PLIN proteins across several disease states and during lipid accumulation *in vitro* and found that PLIN3 and 5 were present more on smaller LDs, and PLIN1 and 2 on the largest LDs (Pawella *et al.*, 2014), although all PLIN proteins, especially PLIN1, are increased in NAFLD (Okumura, 2011; Straub *et al.*, 2008). Both PLIN1 and PLIN2 have previously been associated with NASH (Carr *et al.*, 2017; Fujii *et al.*, 2009), suggesting that a large LD pattern may contribute to NAFLD progression. Whether these proteins have a direct role in pathogenesis is not known, although since PLIN2 is known to inhibit VLDL secretion, and a reduction in *CIDEB* expression, which increases VLDL secretion, is seen in NAFLD and NASH livers (Sahini & Borlak, 2016), these mechanisms could be linked to downregulated VLDL-TAG secretion as NAFLD progresses.

1.5 DIETARY MACRONUTRIENTS AND HEPATIC FATTY ACID METABOLISM

It is apparent that liver fat accumulation often occurs in the context of obesity and metabolic syndrome, which may be associated with lifestyle factors including reduced physical activity and a poor diet; a number of dietary factors that have been implicated in the pathogenesis of NAFLD. Protein may have protective effects in liver fat accumulation (Bortolotti *et al.*, 2011), possibly by increasing energy expenditure and through the action of certain amino acids as

ligands for lipogenic transcription factors and antioxidants (de Wit *et al.*, 2012). These actions may reduce steatosis and NASH progression, although the effect of the source of protein (*i.e.* animal or plant-derived) on NAFLD pathogenesis remains unclear (Della Pepa *et al.*, 2017). In addition, intake of vitamins and other compounds with antioxidant actions may be protective in NAFLD development and progression; indeed, vitamins C, D and E have been investigated as potential NAFLD therapies (Della Pepa *et al.*, 2017; Perumpail *et al.*, 2018). However, by far the most well-researched dietary components in relation to liver fat accumulation and NAFLD are sugar and fat.

1.5.1 Dietary sugars

Free sugars are defined as all monosaccharides and disaccharides added to foods by the manufacturer, cook or consumer, plus sugars naturally present in honey, syrups and unsweetened fruit juices (SACN, 2015). Free sugars therefore encompass sucrose (composed of 50% glucose and 50% fructose), high-fructose corn syrup (HFCS; 45% glucose and 55% fructose) and honey and fruit sugars (100% fructose). As a result of increasing evidence for the detrimental effect of sugar intake on body weight and metabolic health, in 2015, the Scientific Advisory Committee on Nutrition recommended that no more than 5% of calories should be consumed as free sugars (SACN, 2015), half that suggested by the World Health Organisation (WHO, 2015). However, the latest data from the National Diet and Nutrition Survey suggests that neither target is being met by the majority of the UK population, with intakes ranging from 11 to 15% of energy intake in children and adults (NDNS, 2018). Despite

these recommendations, evidence for the effect of sugar on health, and particularly hepatic fat accumulation and NAFLD, continues to be debated.

1.5.1.1 Theory for the impact of sugar intake on liver fat accumulation

The effect of sugar intake on liver fat accumulation is primarily thought to arise from the contribution of excess fructose consumption to hepatic metabolism; there are several pathways through which fructose is hypothesised to act. Firstly, fructose has been found to upregulate lipogenic gene expression and enzyme activity (Janevski *et al.*, 2012). Although fructose can also be used as a substrate for DNL, tracer studies have shown that the amount of fructose used for this pathway is minimal (<1%) (Chong *et al.*, 2007; Sun & Empie, 2012). Nonetheless, an upregulation of this pathway also reduces β-oxidation and energy expenditure (Cox *et al.*, 2012). In addition, unlike the metabolism of glucose by glucokinase, the metabolism of fructose by fructokinase is an unregulated pathway that depletes intracellular ATP and generates uric acid; this may contribute to inflammation and oxidative stress in the development and progression of NAFLD (Jensen *et al.*, 2018; Moore *et al.*, 2014). Finally, fructose appears to increase gut permeability, allowing endotoxins to enter the circulation, which are also proposed to have a role in NAFLD pathogenesis (Thuy *et al.*, 2008).

1.5.1.2 Experimental evidence for and impact of sugar intake on liver fat accumulation

Given the theoretical basis for a role of fructose in liver fat accumulation, experimental research has also focussed heavily on the effect of fructose alone, rather than sucrose. Observationally, epidemiological data suggest increasing fructose intakes correlate with the

rise in obesity and metabolic disease (Lim *et al.*, 2010; Tappy & Le, 2010). There have also been several intervention studies that have shown fructose exposure to precede lipid accumulation in liver cell lines (Huang *et al.*, 2011; Lanaspa *et al.*, 2012) and animals fed high fructose diets (60% of energy intake) (Huang *et al.*, 2011; Koo *et al.*, 2009; Nunes *et al.*, 2014). However, more recent consumption data has revealed a reduction in sugar intake despite increasing levels of metabolic disease (Welsh *et al.*, 2011; Yang *et al.*, 2014), while not all *in vitro* models show evidence of a lipogenic role of fructose (Gnocchi *et al.*, 2014; Hirahatake *et al.*, 2011). In addition, in rats, when a high fructose diet was compared to a sucrose and starch diet (all 60% of energy intake), there were no differences in liver fat accumulation, despite increased nuclear presence of SREBP-1c and ChREBP in fructose and sucrose-fed animals (Janevski *et al.*, 2012). Thus, the effects of sucrose and fructose on fat accumulation remain unclear.

Although there is evidence that acute consumption of hypercaloric high fructose diets leads to liver fat accumulation in human intervention studies (*e.g.* Le *et al.*, 2009; Sobrecases *et al.*, 2010; Stanhope *et al.*, 2009), three recent systematic reviews and meta-analyses have concluded that there is insufficient evidence to implicate fructose as causative in liver fat accumulation when fed isocalorically (Chiavaroli *et al.*, 2015; Chiu *et al.*, 2014; Chung *et al.*, 2014). Indeed, a major confounding factor in hypercaloric diets is the resulting weight gain, making it unclear whether an elevation in liver fat is specifically attributable to fructose or more generally to overnutrition. In addition, human intervention studies predominantly use healthy, male subjects, often have unphysiological diets (*i.e.* large quantities of pure fructose)

and, in the context of habitual intake that may precede fat accumulation by years, they are short term (mostly 1-4 weeks); all meta-analyses highlighted insufficiency of good quality of research available to draw conclusions about the impact of fructose on liver fat accumulation (Chiavaroli *et al.*, 2015; Chiu *et al.*, 2014; Chung *et al.*, 2014).

In contrast to intervention studies, two meta-analyses that included only observational studies have concluded that there is a significant effect of fructose on liver fat accumulation (Asgari-Taee *et al.*, 2018; Wijarnpreecha *et al.*, 2016). Despite being reported as an effect of fructose, it was sucrose intake, in the form of sugar sweetened beverages (SSBs) that drove this association. SSB-derived fructose has been implicated in NAFLD progression: Abdelmalek *et al.* demonstrated that consumption of seven or more servings of fructose per week, which was reflected in elevated uric acid levels, was associated with significantly higher histological grades of fibrosis and lower grades of steatosis (Abdelmalek *et al.*, 2010). However, in a Finnish cohort, fructose consumption was inversely associated with NAFLD risk, likely because fructose tended to be consumed within fruits rather than SSB (Kanerva *et al.*, 2014). This suggests that fructose *per se* is not damaging and highlights the danger of implicating a single nutrient in disease pathogenesis. Rather, SSBs, which facilitate consumption of high quantities of sucrose, often in the context of excess calorie consumption and poor dietary quality, may contribute towards liver fat accumulation and NAFLD progression.

1.5.2 Dietary fat

1.5.2.1 The impact of dietary fat intake on liver fat accumulation

Dietary fats are classified based on the desaturation of the FAs they contain, with some species believed to be more beneficial to health than others (see section 1.1.3.1). However, how the contributions of SFA, MFA and PUFA may contribute to liver fat accumulation is not clear. In general, compared to low fat diets, high fat diets cause an in increase (when isocaloric) (van Herpen *et al.*, 2011; Westerbacka *et al.*, 2005) or a smaller loss (when hypocaloric) (Kirk *et al.*, 2009) in liver fat, suggesting that overall macronutrient composition is important to liver fat accumulation. Cross-sectional data suggest a deleterious association between SFA and NAFLD (Allard *et al.*, 2008), supported by experimental evidence, especially when compared to *n*-6 PUFA. In a 10-week isocaloric feeding study that adjusted the amount of dietary fat composition, higher amounts of SFA (~48% of energy from fat) caused a 6% increase in liver fat, whereas replacing SFA with *n*-6 PUFA (both contributing ~33% of energy from fat) caused a 26% reduction (Bjermo *et al.*, 2012). In a hypercaloric trial, where weight gain was controlled, consuming additional calories from *n*-6 PUFAs resulted in a 5% increase in liver fat compared to a 58% increase when excess SFAs were consumed (Rosqvist *et al.*, 2014). These differences may be attributable to SFA increasing IR and adipose tissue lipolysis and PUFA and MUFA reducing lipolysis and inhibiting DNL (Green & Hodson, 2014; Luukkonen *et al.*, 2018; Parry & Hodson, 2017).

1.5.2.2 The impact of n-3 PUFA on liver fat accumulation and NAFLD pathogenesis

The effect of PUFAs on liver fat accumulation has been further investigated through supplementation of *n*-3 PUFAs, particularly the long-chain FAs, EPA and DHA, commonly found in fish oils. Although study designs are varied and data is conflicting, two reviews have concluded that the majority of evidence suggests that *n*-3 PUFAs can reduce liver fat (de Castro & Calder, 2018; Musa-Veloso *et al.*, 2018). Beneficial effects of *n*-3 PUFA supplementation include reductions in liver fat and liver enzymes (Spadaro *et al.*, 2008; Zhu *et al.*, 2008) and improvements in insulin sensitivity (Boyraz *et al.*, 2015; Spadaro *et al.*, 2008). Along with downregulating lipogenic gene expression, there may also be benefits of *n*-3 PUFAs as a result of suppressed NFκB activity and production of anti-inflammatory eicosanoids; however, reports of improvements of NASH with *n*-3 PUFA supplementation are limited (de Castro & Calder, 2018; Tanaka *et al.*, 2008).

Further support of a beneficial effect of *n*-3 PUFAs in NAFLD is the evidence of different FA compositions in the livers of NAFLD patients. Across the TAG, PL and FFA fractions a consistent trend for reduced *n*-3 PUFA species (α-linolenate, EPA and DHA) and an increase in the *n*-3/*n*-6 ratio has been seen in steatosis compared to control livers (Araya *et al.*, 2004; Elizondo *et al.*, 2007; Puri *et al.*, 2007). Whether these changes are a marker of dietary intake or represent changes in metabolism or partitioning of these FAs, potentially due to changes in enzyme activity (see section 1.1.3.1), is not clear. Although only reported in one study, no changes were seen between NASH and steatosis (Araya *et al.*, 2004), suggesting that changes

in PUFA composition may be particularly relevant for liver fat accumulation in the early stages of NAFLD, rather than its progression to NASH.

1.6 CONCLUDING REMARKS

In conclusion, NAFLD is an increasingly prevalent disease and public health burden. Although the initial stages of the disease are characterised by excess hepatic TAG accumulation and disturbances in hepatic, and whole-body, FA metabolism, the exact pathogenesis of the disease remains to be elucidated. There is evidence that both genetic and lifestyle factors that alter hepatic FA metabolism may have an impact; however, investigating these pathways is difficult due to the inaccessibility of human livers and inconsistent translation from animal models to human disease. Therefore, the overarching aims of this thesis were to optimise a physiological, cellular model of FA metabolism and fat accumulation and, by using this model and recruiting human participants with *DGAT2* mutations, to investigate the effect of nutritional substrates and altered activity of DGAT2 on FA metabolism and the potential impact of this on NAFLD.

Chapter 2

Materials and methods

2.1 MATERIALS

All materials used are listed in Table 2.1-1.

2.2 METHODS

2.2.1 Cell culture procedures

2.2.1.1 Routine cell culture

Human hepatocellular carcinoma cells (HepG2) were a gift from Dr Karl Morten (University of Oxford). A second human hepatocellular carcinoma cell line (Huh7) were a gift from Dr Camilla Pramfalk (Karolinska Institutet). The origins of these cell lines is described in Chapter 1, section 1.2.2. Both cell lines were maintained at 37°C in 5% carbon dioxide in low-glucose (5.5 mM) Dulbecco's modified Eagle's medium (DMEM) + Glutamax™ with 10% foetal bovine serum (FBS), 1% non-essential amino acids (NEAAs) and 10,000 U/ml penicillin-streptomycin.

2.2.1.2 Passaging of cells

Both HepG2 and Huh7 cells were grown to 70-80% confluence in T75 (75 cm^2) culture flasks, at which point, maintenance media was removed and cells were washed with approximately 5 mL 1X phosphate-buffered saline (PBS). For HepG2 cells, 4 mL 1X TrypLE™ Express was added and cells were returned to the incubator for 5 minutes. After this, flasks were agitated to detach and break up cells before 11 mL complete media was added. Huh7 cells underwent the same treatment, with 2 mL 1X TrypLE™ Express and 8 mL media used. Cells were centrifuged at 1200 rpm (240 x g; HepG2) or 500 rpm (40 x g; Huh7) for 5 minutes,

supernatant was removed and cells were resuspended in 10 mL media. Cells were then seeded 1:5 in T75 flasks made up with fresh maintenance media resulting in a total volume of 15 mL. Media was replenished every 48 hours and cells were passaged every 3-4 days upon reaching 70%-80% confluence.

2.2.1.3 Seeding cells for treatment

When setting up treatment plates or flasks, cells were counted after centrifugation and resuspension in maintenance media. Cell counter slides had 20 µL cells added to two chambers and cells were counted using the Cellometer Auto T4 Bright Field Cell Counter. An average from both chambers was taken and cells were seeded at the appropriate densities. HepG2 cells were seeded at approximately 2 x 10^5 cells per mL (4 x 10^4 cells per cm^2) and Huh7 cells at 1 x 10^5 cells per mL (2 x 10^4 per cm^2) to ensure both cell lines reached confluence after three days. This difference in seeding density resulted in equivalent protein content in HepG2 and Huh7 cells after collection.

2.2.1.4 Freezing down and storage of cells in liquid nitrogen

During passaging, once dissociated from the flask and suspended in maintenance media, cells were centrifuged at 1200 rpm (240 x g; HepG2) or 500 rpm (40 x g; Huh7) for 5 minutes. Media was removed before HepG2 cells were resuspended in 90% FBS and 10% dimethyl sulfoxide (DMSO) and Huh7 cells in 70% maintenance media, 20% FBS and 10% DMSO. Approximately 1 x 10^6 cells were distributed into 1 mL cryovials and frozen at -80°C overnight in a CoolCell® Cell Freezing Container (BioCision; USA), which reduces the temperature of cells by 1°C per minute, before being transferred to liquid nitrogen for long-term storage.

2.2.1.5 Bringing up cells from storage in liquid nitrogen

Both HepG2 and Huh7 cells were thawed at 37°C in a water bath and added to 9 mL maintenance media. Cells were centrifuged at 1200 rpm (240 x g; HepG2) or 500 rpm (40 x g; Huh7) for 5 minutes and the media was removed. The pellet was then resuspended in 5 mL maintenance media and moved to a T75 flask with an additional 10 mL media. Media was changed the following day and cells were passaged at 70-80% confluence.

2.2.1.6 Treatment of cells with fatty acids

Cells were treated with a physiological mix of the FAs oleic acid, palmitic acid, linoleic acid and α-linolenic acid at a ratio of 45:30:24:1. FAs were made up in a 1000X stock (for 1000 μM) which consisted of 450, 300, 240 and 10 mM of each FA, respectively, in 100% ethanol. Bovine serum albumin was added to complete HS media at 10% (w/v) and sterile-filtered using a 0.2 μm filter. The FA stock was then added 1:100 to the BSA-containing media and the stock was heated to 70°C until clear (approximately 2 hours) and vortexed at 15 minute intervals. This 10X stock was aliquoted and frozen at -20°C before being diluted to the appropriate FA concentration on the day of treatment.

2.2.1.7 Determination of cell viability using MTT

MTT (3-(4, 5-dimethylthiazol-2-yl)-2, 5-diphenyltetrazolium bromide) is a well-established method to measure cell viability *via* a colourimetric assay. In live cells, mitochondrial dehydrogenase enzymes reduce yellow MTT to purple formazan crystals, which can then be dissolved with DMSO. The resulting absorbance can be used to determine the number of live cells present (Mosmann, 1983).

Cells were plated into a 96-well plate under normal seeding procedures. After treatment, 10 µL MTT at a concentration of 5 mg/mL was added to each well and mixed with the existing media. Cells were returned to the incubator for 3 hours before media was removed and 100 µL DMSO was added to each well, followed by 100 µL PBS. Due to cell number, the supernatant was diluted 1:2 in PBS before absorbance was measured at 630 nm on a VERSAmax Microplate Reader (Molecular Devices; CA, USA).

2.2.2 Biochemical analysis

All assays were carried out according to manufacturer's instructions and used an appropriate calibrator or standard curve for quantification, as well as quality control samples (IL Test™ SeraChem® Control Level 1 and 2 or Human Assayed Multi-sera Level 2 and 3). Assays were previously optimised for low concentrations found *in vitro* (Green *et al.*, 2015a), with lysis buffer used as a background control for intracellular cholesterol/TAG and complete media used as a background for media analysis. Assays were carried out on the ILab 600/650 (Instrumentation Laboratory, Werfen; Warrington, UK).

2.2.2.1 3-hydroxybutyrate concentration measurement

The RANBUT D-3-Hydroxybutyrate assay from Randox was used to measure 3-OHB in neat cell media and plasma. This kit oxidises 3-OHB with 3-OHB dehydrogenase; the concomitant reduction of NAD+ to NADH changes absorbance, which directly correlates to the amount of 3-OHB present in the sample. The enzyme and co-enzyme mix was reconstituted in the supplied buffer before each experiment, and standards of 500, 125 and 62.5 µmol/L were used as calibrator samples.

2.2.2.2 Cholesterol concentration measurement

For intracellular cholesterol measurement, cells were lysed in triacylglycerol (TAG) lysis buffer (1% IGEPAL® CA-630 (Nonidet P-40), 50 mM Trizma® hydrochloride and 150 mM sodium chloride) and scraped. Lysate was then pulse-sonicated at 40% amplitude before being heated to 95°C for 30 minutes and centrifuged at 15,000 x g for 10 minutes. The supernatant was removed for analysis.

The quantILab® Cholesterol assay (Instrumentation Laboratory) was used for measurement of intracellular and plasma cholesterol, which is based on an established method (Allain *et al.*, 1974). Cholesterol esters contained within the sample are first hydrolysed into cholesterol and free fatty acids via cholesterol esterase; cholesterol can then be oxidised to cholest-4-en-3-one + H_2O_2 by cholesterol oxidase. By combining $2H_2O_2$ with 4-aminoantipyrine and phenol, peroxidation occurs, producing quinoneimine, the absorbance of which can be measured at 510 nm.

2.2.2.3 Fructose concentration measurement

Fructose in neat cell media was measured using the Glucose/fructose assay from Randox. This kit first measures glucose enzymatically using hexokinase and glucose-6-phosphate dehydrogenase to produce gluconate-6-phosphate. Next, fructose-6-phosphate (F-6-P) is converted to glucose-6-phosphate (G-6-P) by phosphoglucose isomerase and the G-6-P is also converted to gluconate-6-phosphate. The NADH formed during this reaction can be measured by UV absorbance to determine the amount of total sugars:

Fructose = Total sugar – glucose.

2.2.2.4 Glucose concentration measurement

Glucose in plasma and neat cell media was measured using the quantILab® Glucose (Oxidase) assay (Instrumentation Laboratory); the Glucose (Oxidase) reagent contains the enzymes and substrates for the following reactions. Glucose oxidase converts D-Glucose to gluconic acid and H_2O_2, before H_2O_2 reacts with phenol and 4-aminoantipyrine *via* peroxidase to produce red quinoneimine. The absorbance of the red dye measured is directly proportional to the amount of glucose in the sample.

2.2.2.5 Lactate concentration measurement

The L-Lactate (LAC) assay from Randox was used to determine the lactate concentration in cell media. The method used is based on the conversion of lactate to pyruvate and H_2O_2 *via* oxidation by lactate oxidase. The reaction of H_2O_2 with 4-aminoantipyrine and N-ethyl-N-(2,hydroxyl-3-sulphpropyl)-m-toluidine generates a purple colour, which can be measured by spectrophotometry. Lactate in cell media was measured after calibration with Randox Calibration Serum level 3 and dilution of the sample 1:10 in distilled water.

2.2.2.6 Triacylglycerol concentration measurement

TAG concentrations were determined using the quantILab® Triglycerides assay from Instrumentation Laboratory. For intracellular TAG, samples were prepared as described in section 2.2.2.2; media TAG and plasma were measured neat. Glycerol standards of 50, 100, 200 and 1000 μM were used as calibrator samples before each assay was run.

First, the sample is combined with the Triglycerides reagent, which contains the enzymes and substrates for the following set of reactions. TAG is first hydrolysed to glycerol and NEFAs by lipoprotein lipase, before the glycerol is phosphorylated to glycerol-3-phosphate. Oxidation by glycerophosphate oxidise produces dihydroxyacetone phosphate and hydrogen peroxide (H_2O_2). H_2O_2 further reacts with 4-aminoantipyrine and 4-chlorophenol to produce red quinoneimine; this can be measured by absorbance at 540 nm.

2.2.2.7 Urea concentration measurement

Urea measurements in neat media were performed using the IL Urea Nitrogen Assay from quantILab® (Instrumentation Laboratory). Urea is first converted to 2NH4+ and 2HCO3- via urease. NH4 is then combined with α-oxoglutarate and NADH to form L-glutamine, NAD+ and H_2O by the action of glutamate dehydrogenase; depletion of NADH decreases absorbance, which can be used to determine urea concentration (Sampson *et al.*, 1980).

2.2.3 Quantitative reverse-transcription PCR

2.2.3.1 RNA extraction

DMSO experiments were run alongside a larger body of work for publication; RNA was therefore collected using TRI reagent® to ensure methodological continuity (Nikolaou *et al.*, 2016). TRI reagent® was added to wells and plates were frozen at -20°C before RNA extraction, which was carried out according to manufacturer's instructions. For all other experiments, the RNeasy® Plus mini kit was used, also according to manufacturer's instructions.

The RNeasy® Plus mini kit utilises the principle of selective binding and microspin technology to retain RNA longer than 200 nucleotides in a silica-based membrane. By ensuring the optimum pH and salt concentration of the silica, RNA binds to the column before undergoing a number of wash steps and finally elution of the RNA. Samples were collected in the supplied buffer RLT Plus with 1% 2-mercaptoethanol (v/v). Whilst the buffer RLT Plus contains highly denaturing guanidine-thiocyanate, which temporarily denatures RNases, 2-mercaptoethanol reduces disulfide bonds, permanently changing enzyme conformation and abolishing RNase activity. After addition of the lysis buffer, cells were scraped and RNA was frozen at -80°C.

Before extraction, samples were first defrosted to room temperature, before being heated 37°C to ensure samples were completely thawed and salts dissolved. All centrifugation was carried out at 15,000 x g for 1-2 minutes. Samples were moved into a gDNA eliminator spin column, centrifuged and the flow through mixed with an equal volume of 70% ethanol to optimise RNA binding. Samples were then transferred to an RNeasy spin column and centrifuged; with RNA now bound to the membrane, flow through was discarded. Buffer RW1, containing guanidine and ethanol, was applied to the column in the first wash step to remove biomolecules including carbohydrate and fat. This was followed by two washes with Buffer RPE, which removes salts from the column. Finally, RNase-free water was added directly to the membrane to elute the RNA.

RNA concentration and quality was determined spectrophotometrically using a NanoDrop ND-1000 Spectrophotometer (Thermo Scientific; Hemel Hempstead, UK). RNA purity was assessed using both the 260/280 and 260/230 ratios. The 260/280 ratio is expected to be 1.8-

2.0; a lower ratio indicates protein contamination; however guanidine, present in the RNeasy reagents, could also result in a lower ratio. The expected 260/230 ratio is approximately 2.0-2.2. A low 260/230 ratio indicates the carry-over of carbohydrates or guanidine thiocyanate ions from the extraction protocol.

2.2.3.2 Reverse transcription

In order to synthesise cDNA, 1 µg RNA and the High-Capacity cDNA Reverse Transcription Kit was used, according to manufacturer's instructions. This kit provides random primers, dNTPs (deoxynucleotide triphosphates, *i.e.* A, T, C and G) and reverse transcriptase, which allows cDNA to be synthesised from RNA. A no-template control (NTC) and no-enzyme control (NEC), which replaced RNA and 20X MultiScribe™ Reverse Transcriptase with nuclease-free water, respectively, were included. Samples were heated to 25°C for 10 minutes, in order for the random primers to anneal to the RNA, before the reaction was increased to 37°C for 120 minutes allowing the Reverse Transcriptase to use the dNTPs for cDNA synthesis. The reaction was terminated after 5 minutes at 85°C and was carried out on an MJ Research Tetrad PTC-225 Thermal Cycler (GMI, Inc; MN, USA).

2.3.3.3 Quantitative PCR

Quantitative PCR was carried out on an ABI PRISM® 7900HT Sequence Detection System (Applied Biosystems; Warrington, UK). TaqMan® assays were used to measure gene expression. During heat cycling the two strands of cDNA separate, and if the gene of interest is present, the TaqMan® probe binds to the 3' to 5' strand. The forward primer, along with DNA polymerase, begins to synthesise a complementary strand of DNA during the annealing

and elongation stages, respectively. When the TaqMan® primer reaches the probe, the probe is cleaved from the cDNA and the fluorescent reporter breaks away from the rest of the probe. Since the probe includes a quencher, the reporter can now fluoresce. Over several cycles a threshold of fluorescence is reached, which allows gene expression to be quantified.

For each gene (Appendix A, Table A.1), samples were measured in triplicate in a 6 µL reaction comprised of 2.7 µL cDNA, 0.3 µL TaqMan® probe labelled with FAM and 3 µL 2X KAPA PROBE FAST Master Mix. The reaction was held at 95°C for 3 minutes, followed by 40 cycles of denaturation and annealing for 3 seconds at 95°C and for 20 seconds 60°C, respectively. A standard curve consisting of pooled cDNA from all samples, diluted in Trizma® hydrochloride 1:10 down to 1:320, was included for each gene, along with the NTC and NEC.

Ct values generated were used to calculate a relative expression ratio as described previously (Pfaffl, 2001). The Ct value represents the number of cycles before logarithmic PCR plots for each sample reaches a threshold fluorescence, with the standard curve values allowing calculation of the assay efficiency, where:

$$\text{Efficiency } (E) = 10^{[-1/\text{slope}]}$$

Ct values for each sample were then expressed relative to a control sample:

$$\text{Delta } (\Delta) \text{ Ct} = (E)^{\text{sample Ct} - \text{control Ct}}$$

And finally corrected to the expression of three reference genes (see below):

$$\text{Ratio} = \frac{\Delta Ct_{target}}{\sqrt[3]{(\Delta Ct_{ref1} * \Delta Ct_{ref2} * \Delta Ct_{ref3})}}$$

2.3.3.4 Determination of reference genes

In order to determine suitable reference genes, seven genes used for correction of gene expression in hepatocytes were identified (Cicinnati *et al.*, 2008; Kim & Kim, 2003). For HepG2 cells, PCR was then carried out with TaqMan® probes on cDNA from the control and DMSO-treated cells, and for Huh7 cells, on control and steatosis-treated cells, and the Ct values were entered into RefFinder software (http://leonxie.esy.es/RefFinder/). This software uses four established methods for ranking the stability of reference genes (BestKeeper; (Pfaffl *et al.*, 2004), NormFinder; (Andersen *et al.*, 2004), Genorm; (Vandesompele *et al.*, 2002) and the comparative delta-Ct method; (Silver *et al.*, 2006)) and combines the scores into one overall ranking (Xie *et al.*, 2012). Based on these scores, the three most stable reference genes were used for correction of target genes for work in HepG2 cells (*B2M*, *HPRT1* and *YWHAZ*; Appendix A, Figure A.1). When analysis was repeated for Huh7 cells, although *B2M* and *YWHAZ* still ranked highly, *HMBS* showed more stability than *HPRT1*, resulting in the use of *B2M*, *HMBS* and *YWHAZ* in Huh7 cells (Appendix A, Figure A.2). As a result, only two reference genes (*B2M* and *YWHAZ*) were used in analyses where HepG2 and Huh7 cells were compared.

2.2.4 Protein extraction and Western blotting

2.2.4.1 Protein extraction and quantification

Collection of protein was carried out with ice-cold reagents and samples were kept on ice throughout to ensure metabolism was stopped. DMSO experiments were run alongside a larger body of work for publication; protein was therefore collected using RIPA

(radioimmunoprecipitation assay) buffer to ensure methodological continuity (Nikolaou *et al.*, 2016). For other experiments, protein was taken from the supernatant collected for TAG analysis. In this case, phosphatase and protease inhibitors (PhosSTOP™ and cOmplete™ ULTRA tablets) were added to the lysis buffer. Where phosphorylation of Akt (ser473) was measured, cells were changed into serum-free media 2 hours prior to collection. Insulin and insulin-like growth factor-1 were added for the final 10 minutes at concentrations of 333, 111, 37, 12.3, 4.1, 1.4, 0.46 or 0 nM (Chapter 3), or 100 nM (Chapter 5). ApoB levels in cell media were measured after concentration of media using Amicon® Ultra-2 mL Centrifugal Filters (first spin at 3750 x g for 15 minutes, second spin at 2000 x g for 2 minutes).

To determine total protein content, the Bio-Rad *DC*™ protein assay was used. This assay is based on the Lowry method of protein quantification; protein first reacts with copper in an alkaline solution, before Folin reagent is reduced by the protein-copper complex, which results in a blue colour change that can be read by spectrophotometer. A standard curve using BSA from concentrations 2 to 0.1 mg/mL, diluted in TAG lysis buffer, was used for quantification. All samples were diluted 1:10 and run in duplicate, with absorbance read at 650 nm on a VERSAmax Microplate Reader (Molecular Devices; CA, USA).

2.2.4.2 Gel electrophoresis and Western blotting

Western blotting separates denatured proteins by gel electrophoresis based on their size. The use of SDS as a buffer ensures proteins are negatively charged, meaning they move toward the positive charge generated at the bottom of the gel. As smaller proteins move more quickly through the gel, proteins become distributed based on their molecular weight. A second

electrophoretic step transfers protein onto a membrane while maintaining this protein size formation. The use of a primary antibody against a protein of interest and a secondary antibody with a reporter enzyme then allows visualisation and quantification of protein bands.

To do this, 20 µg protein, diluted in deionised distilled water and 5 µL loading buffer, was boiled at 95°C for 5 minutes. Denatured protein was then added to Criterion™ TGX Stain-Free™ Precast Gels at a volume of 25 µL, along with 3 µL BLUeye Prestained Protein Ladder, and electrophoresis was carried out for 30 mins at 240 V in 1X Tris Glycine SDS. The gel was activated using the ChemiDoc™ MP System and Image Lab™ Software (Bio-Rad; Hemel-Hempstead, UK) allowing total protein to be visualised and quantified using densitometry using ImageJ software (NIH; MD, USA; http://rsb.info.nih.gov/ij).

Protein was transferred to a polyvinylidene difluoride membrane using the Trans-Blot® Turbo™ Transfer System (Bio-Rad; Hemel-Hempstead, UK) at 25 V for 7 minutes. Membranes were blocked with 5% (w/v) powdered milk or BSA in 1X tris-buffered saline-Tween 20 (TBST, 0.1% Tween 20 v/v) for an hour to prevent non-specific antibody binding, before incubation with primary antibodies diluted 1:1000 in 5% milk at 4°C overnight (Appendix A, Table A.2). The next day, membranes were washed in TBST and the appropriate horseradish peroxidase (HRP)-tagged secondary antibody diluted 1:5000 in 5% milk were added to membranes for one hour (Appendix A, Table A.2). After four washes in TBST, bands were visualised by adding Clarity™ Western ECL Blotting Substrates and using

the ChemiDoc™ MP System (Bio-Rad; Hemel-Hempstead, UK). They were quantified by densitometry and proteins of interest were expressed relative to β-tubulin.

2.2.5 Lipid extraction and gas chromatography-mass spectrometry

2.2.5.1 Lipid extraction

Cells were collected in TAG lysis buffer and sonicated. Lipid was extracted according to the Folch method (Folch *et al.*, 1957). This method uses the differences in polarity between chloroform and methanol, after the addition of water in the form of saline, to sequester salts and hydrophilic cell components in the aqueous phase (3:48:47 (v/v/v) chloroform:methanol:water) and lipids in the largely non-polar, solvent phase (86:14:1 (v/v/v)). To do this, internal standards containing known concentrations of glyceryl triheptadecanoate (15:0), heptade-canoic acid (17:0) and 1,2-diheptanoyl-sn-glycero-3-phosphocholine (17:0) were added to 500 µL cell lysate. Samples were mixed with 5 mL 2:1 chloroform:methanol (v/v) containing 0.01% (w/v) butylated hydroxytoluene before 1 mL 1 M sodium chloride was added and samples were mixed again. Following centrifugation at 800 x g for 10 minutes, the aqueous phase was removed and the solvent phase was evaporated to dryness under nitrogen at 50°C in a TurboVap® LV (Biotage; Uppsala, Sweden).

Samples were reconstituted with 1 mL chloroform and the non-esterified fatty acids (NEFA), TAG and phospholipid fractions were separated using solid-phase extraction (SPE) as described previously (Burdge *et al.*, 2000). SPE columns contain aminopropyl silica, which forms hydrogen bonds with lipids; in combination with specific solvents, different lipid classes can be isolated using selective extraction and elution. First, columns were prewashed

with acetone and chloroform. The samples were then added and TAG and CE, which bond weakly to the silica, were eluted with chloroform. To elute NEFA, diethyl ether containing 2% acetic acid, was added, with the acid weakening the strong bond between the NEFAs carboxyl group and the column's amino group. Finally, PLs were eluted with chloroform and methanol (3:2 v/v) before fractions were evaporated to dryness. The non-polar lipid fraction (TAG and CE) was then reconstituted in 1 mL hexane and fresh SPE columns were prewashed with hexane before the samples were added. Hexane was used to elute CE before hexane, chloroform and ethyl acetate (100:5:5 v/v/v) were used to elute TAG, which was then evaporated to dryness.

Next, samples were methylated in order to reduce the polarity of FAs and allow accurate separation and measurement of FA species *via* gas chromatography (GC). Transesterification was achieved by adding 400 µL toluene and 800 µL sulphuric acid in methanol (1.5% v/v for TAG and NEFA and 6% v/v for PLs) to samples and incubating them in a water bath at 80°C (1 hour for TAG and NEFA and 2 hours for PLs). After cooling to room temperature, 2 mL neutralising solution (25 mM potassium hydrogen carbonate and 25 mM potassium carbonate in water) and 2 mL cyclohexane were added to extract the fatty acid methyl esters (FAMEs). Samples were mixed and centrifuged at 800 x g for 10 minutes before the solvent phase was removed and evaporated to dryness under nitrogen. Fractions were finally reconstituted in 150 µL chloroform and had 20 µL external standard (methyl tricosonate; 23:0) added.

2.2.5.2 Gas chromatography

Reconstituted samples were transferred to a 6890N Network GC System (Agilent Technologies; CA, USA). Gas chromatography allows the separation of compounds within a sample based on the time it takes for them to travel through a column. This depends on the affinity of a compound to remain in the liquid, stationary phase or move with the mobile, gas phase. FAMEs were identified by their retention times compared to a standard containing 31 known fatty acids and quantified in micromolar based on the peak area and molecular weight; they were expressed relative to protein content (as described in section 2.2.4.1). The micromolar quantities were then totalled and each fatty acid was expressed as a percentage of this value (molar percentage; mol%). As a marker of enzyme activity, product to precursor ratios were calculated from molar percentage values. Stearoyl-CoA desaturase activity can be estimated by the ratio of its products, palmitoleate and oleate (C16:1*n*-7 and 18:1*n*-7), to their precursors, palmitate and stearate (C16:0 and C18:0). Likewise, activity of fatty acid elongase 6 (ELOVL6) is estimated by the ratio of stearate (C18:0) to palmitate (C16:0).

2.2.5.3 Stable isotope tracers and gas chromatography-mass spectrometry

For determination of stable isotope enrichment by GC-mass spectrometry, samples are first ionised, before they are accelerated through a column and deflected by a magnetic field. The amount of deflection allows the mass to be determined and the particle identified based on known masses; since mass is also affected by the charge of the particle, mass is corrected to charge and expressed as mass to charge ratio (m/z).

Intracellular DNL was assessed based on the incorporation of deuterium from $^{2}H_2O$ in the media (Finnigan GasBench-II, ThermoFisher Scientific, UK) into [^{2}H]palmitate in intracellular TAG and PL and media TAG. [^{2}H]palmitate enrichments were determined simultaneously by GC-mass spectrometry (GC-MS) using a 5890 GC coupled to a 5973N MSD (Agilent Technologies; CA, USA). Ions with mass-to-charge ratios of 270 (M+0) and 271 (M+1) were determined by selected ion monitoring. In Chapter 4, selected ion monitoring was also carried out for [^{2}H]palmitoleate (268 and 269 m/z), [^{2}H]stearate (298 and 299 m/z) and [^{2}H]oleate/vaccenate (296 and 297 m/z). Calculations of DNL were based on the maximum number of deuterium molecules that can be donated to newly synthesised palmitate (17 *in vitro*, 22 *in vivo*) (Lee *et al.*, 1994a; Lee *et al.*, 1994b) and the amount of deuterium enrichment (Semple *et al.*, 2009).

In Chapter 5, uniformly-labelled ^{13}C-glucose and fructose were used to determine DNL. Media containing 50% labelled and 50% unlabelled sugars was added for every media change, along with ^{2}H-labelled oleate and palmitate (D33 and D31, respectively). Lipids were extracted as described above and enrichments were determined by GC-MS using a 5890 GC coupled to a 5973N MSD (Agilent Technologies; CA, USA). For calculations of DNL, palmitate ions with m/z of 270 to 286 (M + 0 to 16) were determined by selected ion monitoring and the proportion of ^{13}C atoms in palmitate carbons was measured (Tayek & Katz, 1996). For enrichment of labelled palmitate and oleate, selected ion monitoring was also used (270 and 301 m/z; M + 0 and M + 31 for palmitate and 296 and 329 m/z; M + 0 and M + 33 for oleate). Enrichment of labelled FAs were expressed as mole percent excess, which gives the amount of tracer as a percentage of the total (tracer + tracee) pool (Umpleby, 2015).

2.2.6 Imaging and analysis of samples using the IN Cell 6000 Analyzer

2.2.6.1 Preparation of cells for IN Cell analysis

Cells were plated into a 96-well, black-walled, collagen-coated plate with optically clear well bases under normal seeding procedures. After treatment, media was removed from wells and warmed media containing 400 nM MitoTracker Red and 10 μg/mL BODIPY was added to the cells and incubated at 37°C for 30 minutes. After this, cells were washed three times with PBS and media containing 1 μg/mL Hoechst 33342 was added. Cells were incubated at room temperature for 10 minutes and washed three more times with PBS. Paraformaldehyde diluted to 4% was then added and cells were fixed for 15 minutes at room temperature. After a further three PBS washes, cells were covered with PBS and refrigerated until imaging.

2.2.6.2 Image acquisition and analysis using the IN Cell Analyzer 6000

Plates were imaged on the IN Cell Analyzer 6000 (GE Healthcare; IL, USA). Images were taken from five planes and nine fields per well, and four technical replicates were analysed per passage. A Nikon 40X/0.60 objective was used to capture nine fields per well through five Z-slices, with a Z-step of 3 μm, giving a total Z-section of 15 μm. DAPI, FITC and Cy5 channels were used with excitations and emissions of 405 nm and 455 nm for Hoechst (nuclei), 488 nm and 525 nm for BODIPY (lipid droplets; LDs) and 642 nm and 706 nm for Mitotracker (mitochondria), respectively. Before each plate was run, laser autofocus was enabled and optimal exposure settings and focus offsets were determined for each channel.

Images obtained were processed by the IN Cell Investigator-Developer toolbox 1.9.2 (GE Healthcare; IL, USA). Images from the FITC channel were used to analyse LDs; these were

first identified using a pre-processing algorithm and segmented based on their fluorescence intensity. Due to the fact that cells were highly confluent and there were a large number of LDs, post-processing algorithms were also set up. Erosion of LD areas allowed more definition of individual LDs, which, when clump breaking was applied, separated groups of LDs into individual targets. The addition of a form factor ensured that only spherical objects were included, to avoid small LDs that had not been separated being recognised as large LDs. After the algorithm was run, several targets were checked manually before data was exported for analysis.

2.2.7 Determination of oxidative stress

2.2.7.1 ROS-Glo™ H_2O_2 Assay

The ROS-Glo™ H_2O_2 Assay uses a derivatized luciferin substrate, which reacts with H_2O_2 in cultured cells to generate a luciferin precursor. Upon the addition of D-Cysteine, this precursor is converted to luciferin, which then reacts with Ultra-Glo™ recombinant luciferin to produce a luminescent signal. H_2O_2 is a useful marker of ROS, since it has the longest half-life of all ROS in cells, and reflects a general change in levels.

H_2O_2 Substrate was diluted in H_2O_2 Substrate Dilution Buffer to a concentration of 125 µM, which was added to cell media for a final concentration of 25 µM in the final three hours of culture before collection. After this, 25 µL media was removed from cells and added to a half-area, white-walled, 96-well plate. Luciferin Detection Reagent was reconstituted in the Reconstitution Buffer and frozen in single-use aliquots at -20°C. Before use, one aliquot was defrosted and 1% (v/v) D-Cysteine and Signal Enhancer Solution were added to make ROS-

Glo™ Detection Solution. To the collected media, 25 µL ROS-Glo™ Detection Solution was added and incubated in the dark at room temperature for 20 minutes. Luminescence was read on an EnSpire® Multimode Plate Reader (PerkinElmer; Beaconsfield, UK).

2.2.7.2 2′,7′-Dichlorofluorescin diacetate fluorescence

2′,7′-Dichlorofluorescin diacetate (DCF-DA) is a cell-permeable, non-fluorescent probe that is used to detect oxidative stress (Jakubowski & Bartosz, 2000). DCF-DA is first de-acetylated to dihydrodichlorofluorescein before being oxidised to form the highly fluorescent, non-permeant, 2′,7′-dichlorofluorescein (Crow, 1997; Kooy *et al.*, 1997).

A stock solution of 10 mM DCF-DA was dissolved in DMSO. At the time of collection, DCF-DA was diluted in complete, phenol red-free DMEM to a concentration of 10 µM and 100 µl was added to each well for 45 minutes. Fluorescence was red on an EnSpire® Multimode Plate Reader (PerkinElmer; Beaconsfield, UK) at an excitation of 485 nm and an emission of 535 nm.

2.2.8 Lipoprotein separation and lipid content calculation

Size-exclusion chromatography (SEC) was used to separate lipoproteins in the cell media. This technique is similar to other chromatographic techniques and allows large, macromolecular particles contained within a solution to be separated based on their size, with the largest particles eluting first.

Cells were cultured in T75 flasks and 24 hours before collection were washed twice with PBS and once with serum-free DMEM, which was collected for analysis of background. After this,

11 mL of serum-free DMEM was added, and after 24 hours, 10.5 mL was removed and added to Amicon Ultra-15 centrifugal filter devices (Merck Millipore Ltd., Cork, Ireland). These were centrifuged at 4500 x g until approximately 200 µL concentrated media remained (25-35 minutes). Media was removed into Eppendorfs and weighed, to account for differences in concentration efficiency between columns. This became a 'concentration factor', which was used to correct concentrations determined by SEC.

The following analysis was done by Professor Camilla Pramfalk at Karolinska Institutet, Sweden. Methods are taken from (Parini et al., 2006).

Samples were automatically injected at a volume of 30 µL and were carried over the column using an elution buffer (150 mM NaCl, 10 mM Tris-HCl and 0.02% sodium azide, pH7.4); this is delivered by the first pump at a flow-rate of 40 µL/min. Next, the separated lipoprotein fractions were continuously mixed with either cholesterol or triacylglycerol reagents. The reagents were kept on ice and delivered by the second pump at 40 µL/min flow rate. After this, the mixture passed through a 500 µL reaction-coil, PEEK tubing of internal-diameter 0.75 mm (Scantec Laboratory, Partille, Sweden) immersed in a water bath at 37°C. Finally, the absorption was monitored with an UV-VIS detector at 500 nm and data were collected every 20 seconds. Total run-time for each sample was 75 min and 90 min for cholesterol and triacylglycerol analyses, respectively. Chromatograms were integrated by the D-7000 HPLC System Manager software. The lipid content in the respective lipoprotein fraction was calculated as the product of the area percent and the lipid content determined from the injected sample.

2.2.9 Biochemical assays

2.2.9.1 Glycogen assay

The glycogen assay is based on Periodic Acid Schiff (PAS) staining used in pathology samples, with use of a standard curve and spectrophotometry to allow for quantification. Periodic acid oxidizes adjacent hydroxyl groups in sugars, which creates two aldehydes at the tips of each broken monosaccharide. When Schiff reagent is added, these aldehydes react to give a purple colour (McManus, 1962).

Cells were seeded into a 96-well plate and underwent experimental treatments. Upon collection, media was removed and media containing 2 μM hoescht was added to wells and cells were incubated in the dark at 37°C for 30 mins. Cells were then washed and covered in PBS, before fluorescence was read at an excitation of 355 nm and emission of 460 nm on an EnSpire® Multimode Plate Reader (PerkinElmer; Beaconsfield, UK), to measure cell number. Plates were frozen at -80°C until the next stage of analysis.

Plates were defrosted, 1% Triton X-100 was added to samples and the plate was shaken at room temperature for 30 minutes. Next, 100 μL 0.1% periodic acid and 7% acetic acid was added to wells and the plate wrapped in tinfoil. After incubation for 1.5 hours at 37°C, 85 μL Schiff's reagent was added, the plate was wrapped in tinfoil and shaken for 5 minutes before being incubated at room temperature without shaking for a further 25 minutes. Absorbance was read at 550 nm on a VERSAmax Microplate Reader (Molecular Devices; CA, USA).

2.2.9.2 Acetate Assay

The Acetate Assay Kit from Abcam supplies an Enzyme Mix and Substrate Mix, which, when added to media samples, converts free acetate to an intermediate. This, in turn, reduces the supplied probe to produce a strong orange colour, allowing absorbance to be measured.

Media samples were collected from cells and frozen at -20°C until analysis. Samples and a blank media sample were defrosted on ice and diluted 1:5 in Assay Buffer 50 µL was added in duplicate to a 96-well plate. The kit was carried out according to the manufacturer's instructions and absorbance was read at 450 nm on a VERSAmax Microplate Reader (Molecular Devices; CA, USA).

2.2.10 Enzyme-linked immunosorbent assays (ELISAs)

Enzyme-linked immunosorbent assays (ELISAs) utilise antibodies and a detection signal to detect an antigen, usually a protein, peptide, hormone or antibody, from within a liquid sample in a 96-well plate format. Sandwich antibodies, which use a pair of primary antibodies, are commonly used; they have a capture antibody bound to the surface of the well, to which the sample is added and any antigen present is allowed to bind. After washing off any sample that is not bound to the capture antibody, a second primary antibody is added. This antibody may already be labelled, or a secondary, labelled, antibody is added (usually HRP-tagged), which binds to the primary antibody. Addition of a chemical that allows labelling to be quantified is then added. Often, TMB (3,3',5,5'-tetramethylbenzidine) is used, which turns blue when detecting HRP and then yellow when a sulfuric or phosphoric acid-containing stop solution is added. This colour can then be quantified by absorbance measurement.

2.2.10.1 ApoB ELISA

The following analysis was done by Professor Camilla Pramfalk at Karolinska Institutet, Sweden.

The Human apoB ELISA^{PRO} kit came from Mabtech, which measures apoB100 only. Concentrated media from the samples used for SEC (section 2.2.8) were used for the kit, which were diluted 1:1000 Before 100 µL was added to the plate in duplicate. The kit was carried out according to manufacturer's instructions; a Tecan plate reader was used to measure absorbance at 450 nm (Tecan Infinitite F200, Tecan Nordic AB; Stockholm, Sweden) concentrations were determined from the standard curve and corrected for dilution factor described in (section 2.2.8).

2.2.10.2 IL-8 ELISA

Abcam's SimpleStep interleukin (IL)-8 ELISA® kit was used to determine IL-8 levels in cell media. Unlike a sandwich ELISA, the SimpleStep ELISA® utilises wells coated with a generic, anti-tag immobilisation antibody, which allows the tag-labelled capture antibody, sample and a reported-tagged detection antibody to be added at the same time. Complexes of IL-8 and both antibodies are captured by the interaction between the antibody coated on the wells and the capture antibody, with the remaining solution washed away. The detection steps are carried out in the same way as sandwich ELISAs.

Media samples were collected from cells and frozen at -20°C before being defrosted on ice on the day of analysis. Samples were diluted 1:20 in Sample Dilutent NS and 50 µL was added to

wells in duplicate. The kit was carried out according to manufacturer's instructions and absorbance read at 450 nm on a VERSAmax Microplate Reader (Molecular Devices; CA, USA). Sample concentration was determined by the use of a standard curve.

2.2.10.3 Phospho-Akt (ser473) ELISA

In Chapter 3, the AKT (Phospho) [pS473] Human ELISA Kit from Invitrogen was used to measure phosphorylation of Akt; in Chapter 5, a PathScan® Phospho-Akt1 (Ser473) Sandwich ELISA Antibody Pair #7143 from Cell Signalling was used. Cells that had undergone insulin stimulation (see section 2.2.4.1) were defrosted on ice and centrifuged at 10 000 x g for 10 minutes. Cell lysate was diluted 1:10 and added in duplicate to the ELISA plate and kits were carried out according to manufacturer's instructions. For the Invitrogen kit, p-Akt was quantified using a standard curve, expressed relative to protein content and results confirmed by immunoblotting relative to total Akt (section 2.2.4). For the Cell Signalling kit, results were corrected for protein content and expressed relative to unstimulated samples.

2.2.11 Statistics

All experiments consisted of a minimum of three replicates, unless otherwise stated. Where fewer than five replicates are presented, individual data points or ranges and the median are shown, otherwise data are presented as mean ± SEM. GraphPad Prism 6 (GraphPad Software, Inc.; La Jolla, CA) was used for data analysis, unless otherwise stated; one- and two-way ANOVAs with Bonferroni's multiple comparisons tests were used to determine significant differences ($p < 0.05$). Where $n < 5$, equivalent non-parametric tests were used when available, *i.e.* Kruskal-Wallis test with Dunn's multiple comparisons tests and Mann-Whitney tests.

Table 2.1-1. Materials and suppliers used

Item	Supplier	Catalogue number
Routine cell culture		
Corning® cell culture flasks	Sigma-Aldrich; Gillingham, UK	Various
Corning® CellBIND® Multiple Well Plates	Sigma-Aldrich; Gillingham, UK	Various
Dulbecco's modified Eagle's medium (DMEM) + GlutaMAX™, 1 g/L glucose	Gibco™, Life Technologies; Paisley, UK	21885025
Dulbecco's modified Eagle's medium (DMEM) + GlutaMAX™, 4.5 g/L glucose	Gibco™, Life Technologies; Paisley, UK	31966021
Dulbecco's modified Eagle's medium (DMEM), no glucose	Gibco™, Life Technologies; Paisley, UK	A1443001
Foetal bovine serum (FBS)	Seralab; Haywards Heath, UK	EU-000-F
Human male AB serum (Lot# BRH1108782)	Seralab; Haywards Heath, UK	SM-412-HS
MEM Non-essential amino acids (NEAAs) (100X)	Gibco™, Life Technologies; Paisley, UK	11140050
Penicillin-Streptomycin (10,000 U/mL)	Gibco™, Life Technologies; Paisley, UK	15140122
GlutaMAX™ Supplement	Gibco™, Life Technologies; Paisley, UK	35050038
Sodium pyruvate (100 mM)	Gibco™, Life Technologies; Paisley, UK	11360070
Glucose solution (200 g/L)	Gibco™, Life Technologies; Paisley, UK	A2494001
TrypLE™ Express (1X)	Gibco™, Life Technologies; Paisley, UK	12604021
Dulbecco's phosphate-buffered saline (PBS) (10X)	Sigma-Aldrich; Gillingham, UK	D1408-500ML
Cellometer SD100 Counting Chambers	Nexcelom Bioscience; MA, USA	CHT4-SD100-314
Experimental cell culture		
Dimethyl sulfoxide (DMSO)	Sigma-Aldrich; Gillingham, UK	D2650-5X5ML
Bovine serum albumin (BSA)	Sigma-Aldrich; Gillingham, UK	A7030-100G
Oleic acid	Cayman Chemical; MI, USA	90260-1 g-CAY
Palmitic acid	Sigma-Aldrich; Gillingham, UK	P0500-10G
Linoleic acid	Cayman Chemical; MI, USA	90150-1 g-CAY
Alpha-linolenic acid	Cayman Chemical; MI, USA	90210-50 mg-CAY
MTT (3-(4,5-Dimethylthiazol-2-yl)-2,5-Diphenyltetrazolium Bromide)	Invitrogen, ThermoFisher Scientific; Hemel Hempstead, UK	M6494

Table 2.1-1. (continued) Materials and suppliers used

Item	Supplier	Catalogue number
ILab sample preparation and assays		
IL Test™ ReferrIL G	Clinical Chemistry, Instrumentation Laboratory; Milan, Italy	0018257000
IL Test™ SeraChem® Control Level 1	Clinical Chemistry, Instrumentation Laboratory; Milan, Italy	0018162412
IL Test™ SeraChem® Control Level 2	Clinical Chemistry, Instrumentation Laboratory; Milan, Italy	0018162512
Human Assayed Multi-sera Level 2	Acusera, Randox; Crumlin, UK	HN1530 / HS2611
Human Assayed Multi-sera Level 3	Acusera, Randox; Crumlin, UK	HE1532 / HS2611
1% IGEPAL® CA-630 (Nonidet P-40)	Sigma-Aldrich; Gillingham, UK	I8896-50ML
Trizma® hydrochloride	Sigma-Aldrich; Gillingham, UK	T3253-1KG
Sodium chloride	Sigma-Aldrich; Gillingham, UK	S7653-1KG
3-hydroxybutyrate (RANBUT)	Randox; Crumlin, UK	RB1007
Cholesterol	quantILab®, Instrumentation Laboratory; Milan, Italy	0018250540
Glucose/fructose assay	Randox; Crumlin, UK	GF2635
Glucose (Glucose OX)	Clinical Chemistry, Instrumentation Laboratory; Milan, Italy	0018250850
Lactate (LAC)	Randox; Crumlin, UK	LC3980
Triglycerides	quantILab®, Instrumentation Laboratory; Milan, Italy	0018255640
Urea (Urea-N 1)	Clinical Chemistry, Instrumentation Laboratory; Milan, Italy	0018255450
RNA extraction, reverse transcription and real-time PCR		
TRI reagent®	Sigma-Aldrich; Gillingham, UK	T9424-200ML
RNeasy® Plus mini kit	QIAGEN Sciences; MD, USA	74106
2-mercaptoethanol	Sigma-Aldrich; Gillingham, UK	M6250-100ML
High-Capacity cDNA Reverse Transcription Kit	Life Technologies; Paisley, UK	4368813
Nuclease-free water	Ambion, Life Technologies; Paisley, UK	AM9930
KAPA PROBE FAST qPCR Master Mix (2X) Kit	Sigma-Aldrich; Gillingham, UK	KK4703
Trizma® hydrochloride solution	Sigma-Aldrich; Gillingham, UK	T3038-1L
Taqman® probes	Applied Biosystems, ThermoFisher Scientific; Hemel Hempstead, UK	Various

Table 2.1-1. (continued) Materials and suppliers used

Item	Supplier	Catalogue number
Protein extraction and immunoblotting		
RIPA buffer	Sigma-Aldrich; Gillingham, UK	R0278-50ML
PhosSTOP™	Roche, Sigma-Aldrich; Gillingham, UK	000000004906837001
cOmplete™ ULTRA Tablets	Roche, Sigma-Aldrich; Gillingham, UK	000000005892970001
Insulin, human recombinant, zinc solution	Gibco™, ThermoFisher Scientific; Hemel Hempstead, UK	12585014
LONG® R3 insulin-like growth factor (IGF)-1 (human)	Sigma-Aldrich; Gillingham, UK	I1271-1MG
Amicon® Ultra-2 mL Centrifugal Filters	Merck; Watford, UK	UFC210024
Bio-Rad *DC*™ protein assay	Bio-Rad; Hemel-Hempstead, UK	5000116
4X Laemmli Sample Buffer	Bio-Rad; Hemel-Hempstead, UK	1610747
Criterion™ TGX Stain-Free™ Precast Gels	Bio-Rad; Hemel-Hempstead, UK	5678093
BLUeye Prestained Protein Ladder	Geneflow; Lichfield, UK	S6-0024
10X Tris/Glycine/SDS	Bio-Rad; Hemel-Hempstead, UK	1610732
Trans-Blot® Turbo™ Midi PVDF Transfer Packs	Bio-Rad; Hemel-Hempstead, UK	1704157
Primary antibodies	Cell Signalling; MA, USA	Various
Goat anti-Mouse IgG (H+L) Secondary Antibody, HRP	Invitrogen, Thermo Fisher Scientific; Hemel Hempstead, UK	31430
Goat anti-Rabbit IgG (H+L) Secondary Antibody, HRP	Invitrogen, Thermo Fisher Scientific; Hemel Hempstead, UK	31460
Rabbit anti-Sheep IgG (H+L) Secondary Antibody, HRP	Invitrogen, Thermo Fisher Scientific; Hemel Hempstead, UK	31480
Clarity™ Western ECL Blotting Substrates	Bio-Rad; Hemel-Hempstead, UK	1705060

Table 2.1-1. (continued) Materials and suppliers used

Item	Supplier	Catalogue number
Lipid extraction and gas chromatography		
Glyceryl triheptadecanoate	Sigma-Aldrich; Gillingham, UK	T2151-100MG
Heptade-canoic acid	Sigma-Aldrich; Gillingham, UK	H3500-1G
1,2-Diheptanoyl-sn-glycero-3-phosphocholine	Sigma-Aldrich; Gillingham, UK	P4148-100MG
Butylated hydroxytoluene	Sigma-Aldrich; Gillingham, UK	B1378
ISOLUTE® SPE columns	Biotage; Uppsala, Sweden	470-0010-A
Methyl tricosonate	Sigma-Aldrich; Gillingham, UK	T9900-1G
Deuterated water	CK Isotopes; Ibstock, UK	DOLM-242-1
D-Glucose (U-13C6, 99%)	Cambridge Isotope Laboratories, Inc.; MA, USA	CLM-1396-PK
D-Fructose (U-13C6, 99%)	Cambridge Isotope Laboratories, Inc.; MA, USA	CLM-1553-PK
Palmitic acid (D31, 98%)	Cambridge Isotope Laboratories, Inc.; MA, USA	DLM-215-1
Oleic acid (D33, 98%)	Cambridge Isotope Laboratories, Inc.; MA, USA	DLM-1891-PK

Table 2.1-1. (continued) Materials and suppliers used

Item	Supplier	Catalogue number
IN Cell Analyzer		
Nunc™ MicroWell™ 96-Well Optical-Bottom Plates with Coverglass Base	Thermo Fisher Scientific; Hemel Hempstead, UK	164588
BODIPY® 493/503	Thermo Fisher Scientific; Hemel Hempstead, UK	D3922
MitoTracker™ Deep Red	Invitrogen, Thermo Fisher Scientific; Hemel Hempstead, UK	M22426
Hoechst 33342 Solution	Thermo Fisher Scientific; Hemel Hempstead, UK	62249
Oxidative stress assays		
ROS-Glo™ H_2O_2 Assay	Promega; WI, USA	G8820
2′,7′-Dichlorofluorescin diacetate (DCF-DA)	Sigma-Aldrich; Gillingham, UK	D6883
1/2 AreaPlate-96	PerkinElmer; MA, USA	6002299
Biochemical assays		
Triton™ X-100	Sigma-Aldrich; Gillingham, UK	T8787-250ML
PAS staining kit	Merck; Watford, UK	101646
Acetate Assay Kit (Colorimetric)	Abcam; Cambridge, UK	ab204719
ELISAs		
Human apoB ELISA ^{PRO} kit	Mabtach; Nacka, Sweden	3715-1HP-2
Human IL-8 SimpleStep ELISA® Kit	Abcam; Cambridge, UK	ab214030
MIF ELISA Kit	Thermo Fisher Scientific; Hemel Hempstead, UK	EHMIF
AKT (Phospho) [pS473] Human ELISA Kit	Invitrogen, Thermo Fisher Scientific; Hemel Hempstead, UK	KHO0111
PathScan® Phospho-Akt1 (Ser473) Sandwich ELISA Antibody Pair #7143	Cell Signaling; MA, USA	7143S

Chapter 3

Optimisation of existing *in vitro* models of hepatic fatty acid metabolism

3.1 INTRODUCTION

Non-alcoholic fatty liver disease (NAFLD) has become a significant public health burden (Younossi *et al.*, 2016). NAFLD covers a spectrum of conditions, the first of which is steatosis, where lipid droplets (LDs), comprised principally of TAG, form within hepatocytes. Increased intrahepatocellular storage of TAG can result from elevated delivery or synthesis of fatty acids (FAs), reduced secretion or oxidation of FAs, or both. Indeed, several of these processes have been shown to be perturbed in individuals with NAFLD (Diraison *et al.*, 2003; Fabbrini *et al.*, 2008; Lambert *et al.*, 2014). However, the cause of these disturbances is complex, likely resulting from interactions on a systemic level and a cellular level (Berlanga *et al.*, 2014; Sahini & Borlak, 2016). As a result, an approach where each of these factors can be modified and monitored is required to study NAFLD pathophysiology.

Studying metabolic and mechanistic processes is challenging given the limited human NAFLD models available. Investigating liver metabolism in humans *in vivo* presents difficulties and relies on proxy measurements (*e.g.* incorporation of stable isotope tracers into metabolic markers) (Green *et al.*, 2018). In situations where liver biopsies are obtained, only a single time point may be available, the amount of tissue may be limited, or a control group for comparison, lacking (Green *et al.*, 2015b). For *in vitro* cellular studies primary human hepatocytes are considered the gold standard; however, they present issues with availability, inter-donor variability and the short time frame during which they remain differentiated (Green *et al.*, 2018). As a result, proliferating human hepatoma cell models are the most widely-used option.

Two well-established cell lines are HepG2 and Huh7; however, these models are poorly differentiated, often resemble foetal liver cells and have limited ability to carry out metabolic processes including TAG hydrolysis and very low-density lipoprotein (VLDL) secretion (Gibbons *et al.*, 1994; Javitt, 1990; Wu *et al.*, 1996). Due to these limitations, work to improve the metabolic phenotype of hepatoma cell lines has been undertaken. In stem cells, addition of dimethyl sulfoxide (DMSO) promotes differentiation toward functional derivatives (Chetty *et al.*, 2013; Pal *et al.*, 2012) and this approach has also been used in HepG2 and Huh7 cells. Although results relating to differentiation markers are mixed (Choi *et al.*, 2009; Mowbray, 2011; Sivertsson *et al.*, 2010), available data suggests TAG accumulation is reduced and lipid metabolism altered, in the presence of DMSO (Nikolaou *et al.*, 2016; Song *et al.*, 2012). In addition, both cell lines demonstrate changes in their metabolic phenotype when cultured in human serum (HS), including improvements in expression of lipid metabolism-regulating nuclear receptors and lipoprotein secretion (Pramfalk *et al.*, 2016; Steenbergen *et al.*, 2013).

As a result of the limitations of using primary hepatocytes and the metabolic defects of hepatoma cells, the aim of this chapter was:

1. To create a physiologically relevant, replicable *in vitro* hepatocyte model for studying NAFLD by investigating the effects of DMSO, glucose and culturing sera on cell function and FA metabolism

3.2 METHODS

3.2.1 DMSO experiments

Cells were seeded in maintenance media (see Chapter 2, section 2.2.1.1) and cultured for 72 hours. After this, cells were washed twice with PBS and treatment media was added. Treatment media consisted of glucose-free DMEM with the addition of 10% FBS, 1% NEAAs and 10,000 U/ml penicillin-streptomycin, as well as 5.5 mM glucose, 1% sodium pyruvate, 1% Glutamax^{TM} and 1% DMSO. Media was changed every 48-72 hours with collection of cells and media after 48 hours, 72 hours and seven, 14 and 21 days. For the control condition, treatment media without DMSO was added, with samples collected after 48 hours.

3.2.2 Glucose experiments

After passaging, cells were seeded into three flasks in maintenance media. Once adhered, cells were washed twice with PBS and treatment media was added. Treatment media consisted of glucose-free DMEM, 10% FBS, 1% NEAAs and 10,000 U/ml penicillin-streptomycin, sodium pyruvate and Glutamax^{TM}, with either 5.5 mM, 11 mM or 22 mM glucose. Cells were grown for 3-4 days in treatment media before being dissociated and seeded at 4 x 10^4 cells per cm^2 in treatment media. They were then grown for a further four days to confluence before cells and media were collected. Media was changed every 48-72 hours throughout.

3.2.3 Serum experiments

Cells were seeded and grown for 72 hours to confluence in maintenance media. Upon reaching confluence they were washed twice with PBS and treatment media was added.

Treatment media consisted of phenol red-free DMEM, 11 mM glucose, 1% NEAAs, 10,000 U/ml penicillin-streptomycin, sodium pyruvate and Glutamax™, with 10% FBS or 2% HS. For assessment of *de novo* lipogenesis (DNL), 10% heavy water (^2H_2O) was added to media and for all experiments, media was changed every 48-72 hours.

Data was initially analysed after three, seven and 14 days in FBS or HS, but since longer culture time did not affect RNA expression, intracellular or media TAG, and some transcription factors did not demonstrate a change in expression until day seven, only the seven day results are presented (for all results, see Appendix B, Figures B.1 & 2, Tables B.1 & 2). Preliminary results were also obtained for TAG, media TAG and 3-hydroxybutyrate (3-OHB) at 21 and 28 days, however, the only metabolite that showed a change at later time points was media 3-OHB, which was approximately two-fold higher at day 21 compared to day 14, but did not increase any further at day 28 (data not shown). In addition, cells were cultured in 2% FBS to ensure differences between FBS and HS were not due to serum content of media; however, cell death occurred in Huh7 cells after three days and this condition was, therefore, not pursued further.

3.2.4 Analytical techniques

RNA extraction and RT-PCR, biochemical analyses, protein extraction and immunoblotting, lipid extraction and gas chromatography-mass spectrometry and the phospho-Akt ELISA was carried out as described in Chapter 2, sections 2.2.2-5 & 2.2.10.

3.3 RESULTS

3.3.1 The effect of DMSO on metabolic phenotype and function in HepG2 cells

3.3.1.1 The effect of DMSO on the metabolic phenotype of HepG2 cells

Based on previous work suggesting DMSO may improve metabolism under high glucose (25 mM) conditions (Nikolaou *et al.*, 2016), similar investigations were undertaken in HepG2 cells in low glucose media (5.5 mM). Levels of intracellular TAG appeared lower in DMSO-treated cells at day seven, 14 and 21 compared to control, although this was only significant ($p < 0.05$) at day 14 (Figure 3.3.1-1A). Decreasing intracellular TAG was mirrored by reduced gene expression of the lipogenic enzymes acetyl-CoA carboxylase 1 (ACC1; *ACACA*) and fatty acid synthase (FAS; *FASN*) in DMSO-treated cells at days 14 and 21 (both $p < 0.05$, Table 3.3.1-1), suggesting a downregulation of the DNL pathway. In addition, media TAG, a marker of TAG secretion, and media 3-hydroxybutyrate (3-OHB), a marker of FA oxidation, were found to be significantly ($p < 0.05$) higher at day 21 in DMSO-treated cells compared to control cells (Figure 3.3.1-1B & C). Overall, reduced lipogenic gene expression and TAG accumulation, along with increased media TAG and 3-OHB, suggest DMSO exposure improved the elevated lipogenesis and suppressed FA mobilisation characteristic of HepG2 cells.

Table 3.3.1-1. The effect of dimethyl sulfoxide (DMSO) on differentiation, tumour and fatty acid metabolism gene expression in HepG2 cells.

	Control	Day 2	Day 4	Day 7	Day 14	Day 21
Differentiation and tumour genes						
ALB	1.04 (0.70 - 1.39)	0.29 (0.20 - 0.35)	0.34 (0.27 - 0.55)	0.30 (0.27 - 0.65)	0.24 (0.13 - 0.36)*	0.27 (0.25 - 0.35)
AFP	1.00 (0.85 - 1.18)	0.58 (0.53 - 0.61)	0.55 (0.45 - 0.82)	0.28 (0.26 - 0.59)	0.11 (0.07 - 0.16)*	0.11 (0.08 - 0.14)*
HNF4A	1.00 (0.99 - 1.02)	0.84 (0.65 - 0.97)	0.85 (0.80 - 1.02)	0.70 (0.65 - 0.99)	0.59 (0.51 - 0.68)*	0.68 (0.63 - 0.77)
Fatty acid metabolism genes						
ACACA	1.04 (0.89 - 1.09)	0.71 (0.67 - 0.86)	0.67 (0.60 - 0.82)	0.66 (0.60 - 0.88)	0.51 (0.47 - 0.52)*	0.45 (0.36 - 0.46)*
ACACB	1.05 (0.82 - 1.16)	0.82 (0.55 - 0.90)	0.77 (0.57 - 0.90)	0.57 (0.35 - 0.79)	0.58 (0.46 - 0.82)	0.82 (0.72 - 0.91)
FASN	1.01 (0.76 - 1.31)	0.67 (0.66 - 1.09)	0.52 (0.51 - 0.86)	0.56 (0.42 - 0.83)	0.33 (0.27 - 0.47)*	0.39 (0.38 - 0.41)*
SCD	0.99 (0.83 - 1.22)	0.97 (0.77 - 1.05)	0.86 (0.82 - 1.17)	0.87 (0.79 - 1.04)	1.19 (0.76 - 1.29)	1.01 (1.00 - 1.19)

Cells were confluent at Day 0 and grown for a further 2, 4, 7, 14 and 21 days in 1% DMSO, with the control condition grown to Day 2 without DMSO. All genes were expressed as a relative expression ratio to the mean control value and corrected to three reference genes (*B2M*, *HPRT1* and *YWHAZ*). Data are presented as median (range), $n = 3$. * $p < 0.05$ compared to control; Kruskal-Wallis test with Dunn's multiple comparisons test.

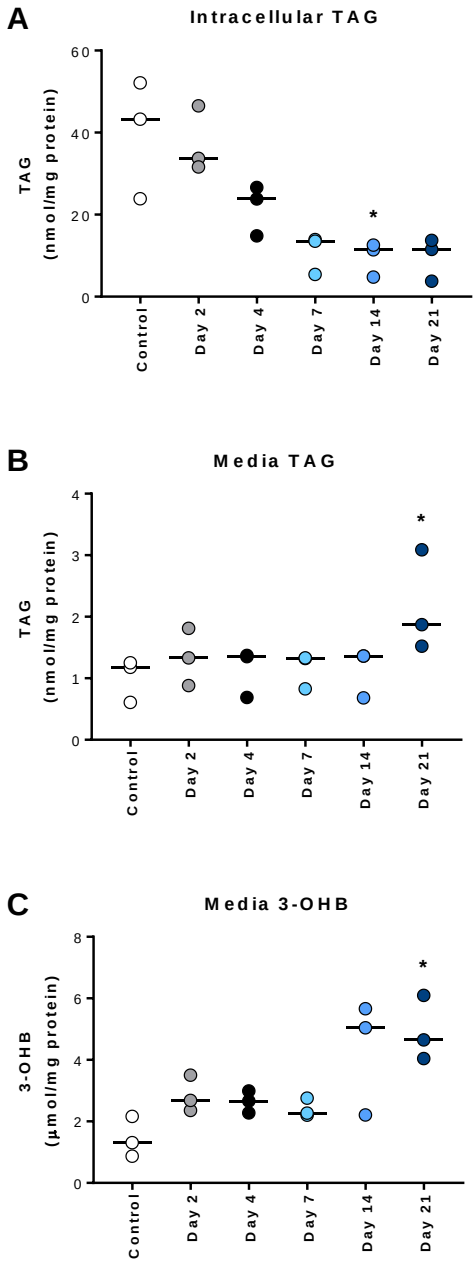


Figure 3.3.1-1. The effect of dimethyl sulfoxide (DMSO) on metabolic parameters in HepG2 cells. Cells were confluent at Day 0 and grown for a further 2, 4, 7, 14 and 21 days in 1% DMSO, with the control condition grown to Day 2 without DMSO. Intracellular triacylglycerol (TAG) content was measured (**A**), as were levels of media TAG (**B**) and 3-hydroxybutyrate (3-OHB; **C**), as markers of fatty acid secretion and oxidation, respectively. Media was added to cells 48 hours prior to collection and all results were corrected to protein content of cells. Data are presented as individual values and median, $n = 3$. * $p < 0.05$ compared to control; Kruskal-Wallis test with Dunn's multiple comparisons test.

3.3.1.2 The effect of DMSO on liver function and endoplasmic reticulum stress markers in HepG2 cells

DMSO has previously been used to induce differentiation in stem cells; since HepG2 cells show signs of dedifferentiation, and therefore lack some hepatocyte characteristics, the effect of DMSO treatment on markers of differentiation and cancer were investigated. Treatment with DMSO caused a reduction in albumin (*ALB*) and hepatocyte nuclear factor (HNF)4-α mRNA expression (*HNF4A*), two markers of differentiation and hepatocyte function, which was evident in cells throughout the treatment period and became significant at 14 days compared to control cells for both genes ($p < 0.05$; Table 3.3.1-1). However, expression of the tumour marker alpha fetoprotein (*AFP*) was also suppressed in DMSO-treated cells at both 14 and 21 days (both $p < 0.05$; Table 3.3.1-1).

Endoplasmic reticulum (ER) stress markers were measured to assess DMSO toxicity, which is known to occur at high exposure levels. There was no effect of DMSO on levels of CCAAT/enhancer-binding protein homologous protein (CHOP), or inositol-requiring enzyme-1α (IRE-1α) in HepG2 cells (Figure 3.3.1-2A & B). However, there was a trend for increased levels of both markers at days 14 and 21, suggesting an induction of the unfolded protein response (UPR) with prolonged exposure to 1% DMSO.

Overall, despite the positive effects of 1% DMSO on glucose and FA metabolism, the less conclusive effect on differentiation markers, and possibility of cell stress indicated by UPR induction, meant DMSO treatment was not pursued further.

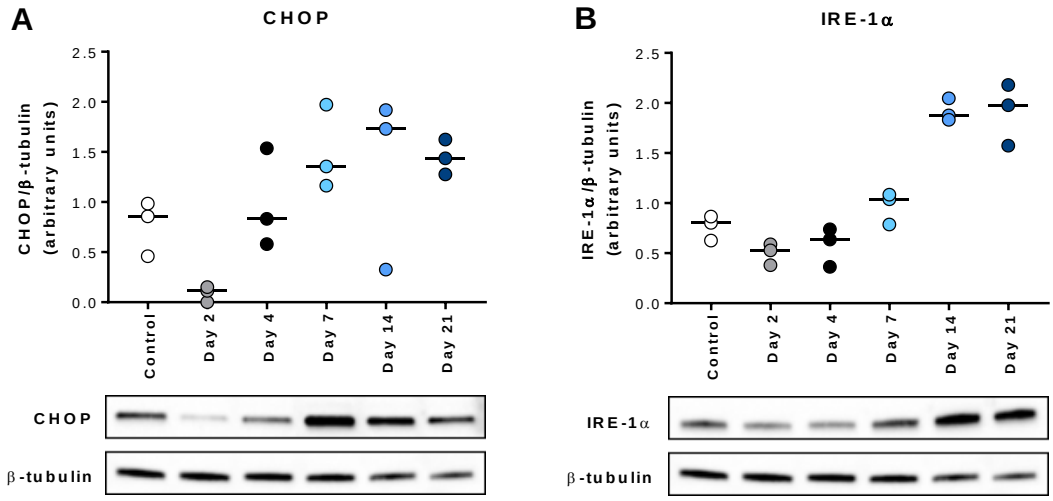


Figure 3.3.1-2. The effect of dimethyl sulfoxide (DMSO) on endoplasmic reticulum (ER) stress markers in HepG2 cells. Cells were confluent at Day 0 and grown for a further 2, 4, 7, 14 and 21 days in 1% DMSO, with the control condition grown to Day 2 without DMSO. Representative immunoblots of CCAAT/enhancer-binding protein homologous protein (CHOP; **A**) and inositol-requiring enzyme-1α (IRE-1α; **B**). Results are expressed relative to β-tubulin. Data are presented as individual values and median, $n = 3$. * $p < 0.05$ compared to control; Kruskal-Wallis test with Dunn's multiple comparisons test.

3.3.2 The effect of glucose concentration on Huh7 and HepG2 function and metabolism

3.3.2.1 The effect of media glucose concentration on the metabolic phenotype of HepG2 and Huh7 cells

To investigate the optimal concentration of media glucose to maintain cell metabolism and health, HepG2 and Huh7, another well-established hepatocyte cell line, were grown in three different glucose concentrations. After culture for 48 hours in 5.5, 11 or 22 mM glucose, both cell lines had taken up almost all glucose provided at 5.5 mM and 11 mM (Figure 3.3.2-1A & B). At the highest concentration of glucose, HepG2 used approximately 50% of available glucose, while Huh7 cells had around 75% glucose disappearance from the media (Figure 3.3.2-1A & B). Although glycolytic gene expression was unchanged in both cell lines (Table 3.3.2-1), Huh7 cells had elevated media lactate levels when cultured in 22 mM glucose ($p < 0.05$, Figure 3.3.2-1D), suggesting an upregulation of glycolysis. Increasing glucose availability also resulted in a significant upregulation of intracellular and media TAG in HepG2 cells and media TAG in Huh7 cells in the 22 mM compared to the 5.5 mM glucose condition, likely through an upregulation of DNL (Figure 3.3.2-2A-D). A concurrent decrease in media 3-OHB in Huh7 cells ($p < 0.05$, Figure 3.3.2-2F) suggests that an elevation in DNL suppressed FA oxidation. Thus, a high glucose concentration tended to augment the already elevated rates of lipogenesis and glycolysis in these cell lines.

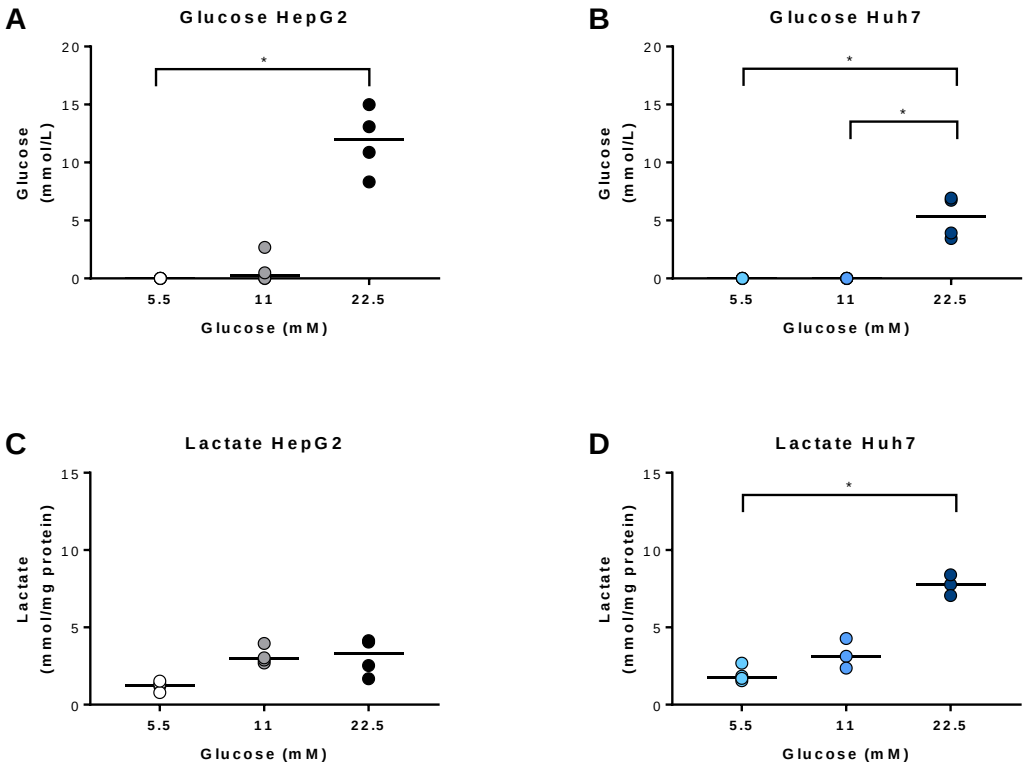


Figure 3.3.2-1. The effect of media glucose concentration on glucose metabolism and cell function in HepG2 (**A, C**) and Huh7 (**B, D**) cells. Cells were grown for 3 days in flasks before being transferred to plates and grown for a further 4 days in 5.5 mM, 11 mM or 22.5 mM glucose. Glucose remaining in the media (**A, B**) and lactate content of the media (**C, D**) were measured and expressed relative to protein content. For media glucose, this value was multiplied by the average protein content to approximate total remaining glucose. Media was added to cells 48 hours prior to collection. Data are presented as individual values and median, $n = 4$. * $p < 0.05$; Kruskal-Wallis test with Dunn's multiple comparisons test.

Table 3.3.2-1. The effect of glucose concentration on differentiation, tumour and fatty acid metabolism gene expression in Huh7 and HepG2 cells.

	HepG2			Huh7		
	5.5 mM	**11 mM**	**22.5 mM**	**5.5 mM**	**11 mM**	**22.5 mM**
Proliferation, differentiation and tumour genes						
ALB	1.01 (0.93 - 1.07)	1.03 (0.97 - 1.17)	0.90 (0.83 - 0.95)	0.98 (0.27 - 1.00)	0.64 (0.41 - 0.87)	0.71 (0.21 - 0.73)
AFP	1.00 (0.93 - 1.07)	1.13 (1.07 - 1.18)	1.15 (1.08 - 1.18)	1.28 (0.65 - 1.35)	1.30 (0.81 - 1.33)	1.00 (0.60 - 1.42)
HNF4A	1.01 (0.95 - 1.05)	1.17 (0.94 - 1.36)	1.16 (0.92 - 1.35)	1.04 (0.79 - 1.23)	0.82 (0.58 - 0.96)	0.81 (0.70 - 1.05)
MKI67	1.00 (0.92 - 1.09)	1.13 (0.82 - 1.39)	2.23 (2.03 - 2.44)	1.02 (0.91 - 1.08)	0.84 (0.46 - 1.20)	1.13 (0.82 - 1.46)
Fatty acid metabolism genes						
ACACA	1.01 (0.86 - 1.15)	0.73 (0.52 - 1.01)	1.02 (0.78 - 1.29)	1.01 (0.87 - 1.15)	0.87 (0.71 - 1.01)	0.79 (0.71 - 0.88)
ACACB	0.92 (0.90 - 1.23)	1.09 (0.60 - 1.49)	1.68 (1.32 - 1.76)	1.01 (0.77 - 1.32)	0.80 (0.60 - 1.12)	0.96 (0.86 - 1.23)
FASN	1.05 (0.83 - 1.15)	1.01 (0.87 - 1.29)	1.09 (0.76 - 1.30)	1.02 (0.93 - 1.05)	0.84 (0.53 - 1.13)	1.10 (0.88 - 1.39)
SCD	1.03 (0.88 - 1.11)	1.09 (0.99 - 1.15)	0.79 (0.75 - 0.87)	1.00 (0.95 - 1.05)	0.77 (0.61 - 0.96)	0.89 (0.72 - 1.01)
Glycolysis genes						
G6PC	1.03 (0.62 - 1.67)	1.55 (0.60 - 2.37)	1.51 (0.73 - 2.32)	1.09 (0.48 - 2.45)	2.11 (1.61 - 2.64)	1.92 (1.09 - 3.25)
PDHA1	1.02 (0.91 - 1.08)	0.96 (0.91 - 1.04)	0.95 (0.93 - 0.97)	1.02 (0.90 - 1.09)	0.87 (0.74 - 1.11)	1.08 (0.98 - 1.17)

Cells were grown for 3 days in flasks before being transferred to plates and grown for a further 4 days in 5.5 mM, 11 mM or 22.5 mM glucose. All genes were expressed as a relative expression ratio to the mean control value and corrected to two reference genes (*B2M* and *YWHAZ*). Data are presented as median (range), $n = 4$. Kruskal-Wallis test with Dunn's multiple comparisons test.

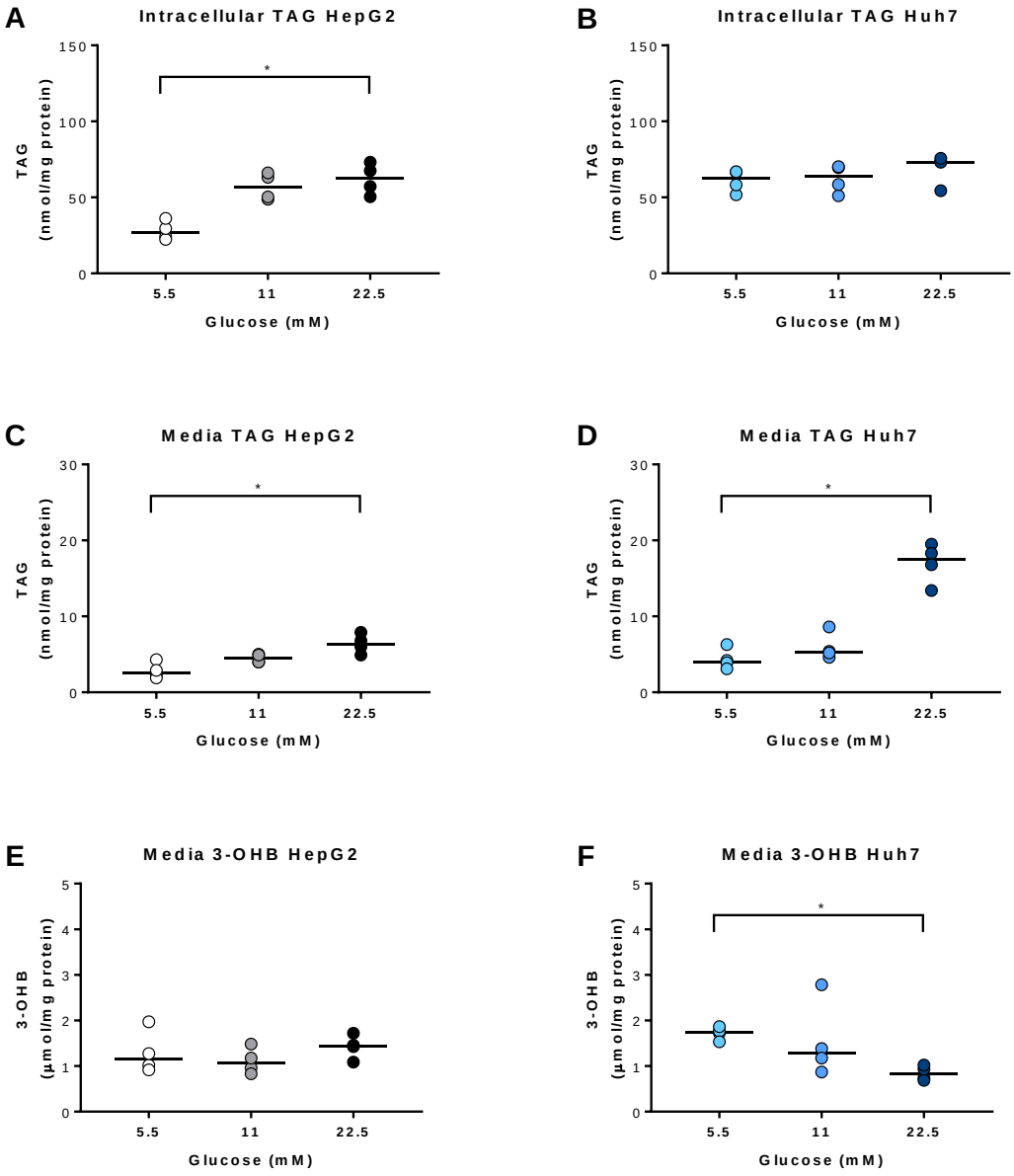


Figure 3.3.2-2. The effect of media glucose concentration on FA metabolism in HepG2 (**A, C, E**) and Huh7 (**B, D, F**) cells. Cells were grown for 3 days in flasks before being transferred to plates and grown for a further 4 days in 5.5 mM, 11 mM or 22.5 mM glucose. Intracellular triacylglycerol (TAG) content was measured (**A, B**), as were levels of media TAG (**C, D**) and 3-hydroxybutyrate (3-OHB; **E, F**), as markers of fatty acid secretion and oxidation, respectively. Media was added to cells 48 hours prior to collection and all results were corrected to protein content of cells. Data are presented as individual values and median, $n = 4$. * $p < 0.05$; Kruskal-Wallis test with Dunn's multiple comparisons test.

3.3.2.2 The effect of media glucose concentration on liver function and endoplasmic reticulum stress markers in HepG2 and Huh7 cells

In order to determine whether these changes resulted from the cells displaying more cancerous characteristics, differentiation and tumour markers were measured. Expression of *AFP* and *HNF4A* were unchanged in response to differing levels of media glucose. In Huh7 cells, albumin transcripts tended to be expressed more highly in cells grown in 5.5 mM and 11 mM glucose compared to 22 mM, while Ki-67 mRNA (*MKI67*), a marker of proliferation, was higher in the 22 mM condition compared to 5.5 or 11 mM, although these results did not reach significance (Table 3.3.2-1, all $p = 0.056$).

Urea levels, which can be a marker of amino acid catabolism, were significantly higher at 5.5 mM compared to 22 mM glucose in Huh7 cells but remained unchanged in HepG2 cells (Figure 3.3.2-3A & B). In addition, levels of CHOP and IRE-1α were higher in low glucose in HepG2 and Huh7 cells, although this only reached significance for CHOP in Huh7 cells (Figure 3.3.2-3C-F). Further investigation based on these results demonstrated that most glucose provided at 5.5 mM and 11 mM was taken up within 24 hours (Appendix B, Figure B-3). The lower glucose availability may explain the elevated stress markers seen in cells at 5.5 mM, whereas 11 mM glucose appeared to be sufficient to prevent a catabolic state. These results, combined with the excess glucose that remained after treatment with 22 mM glucose, led to 11 mM glucose being used for subsequent experiments, in line with that used for primary hepatocyte culture (Green *et al.*, 2017).

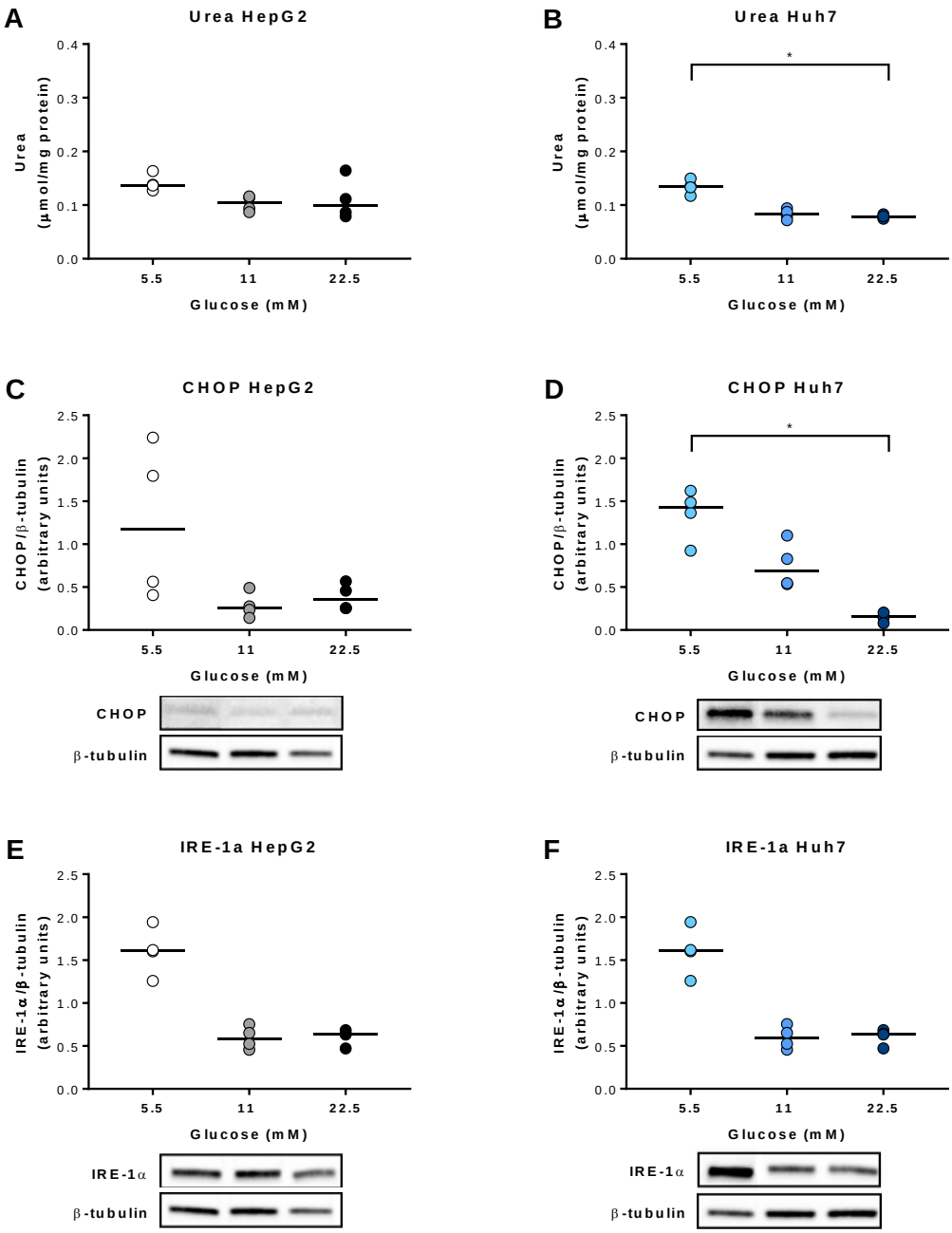


Figure 3.3.2-3. The effect of glucose on amino acid catabolism and endoplasmic reticulum (ER) stress markers in HepG2 and (**A, C, E**) and Huh7 (**B, D, F**) cells. Cells were grown for 3 days in flasks before being transferred to plates and grown for a further 4 days in 5.5 mM, 11 mM or 22.5 mM glucose. Urea content of the media was measured (**A, B**) as a marker of amino acid catabolism. Representative immunoblots of CCAAT/enhancer-binding protein homologous protein (CHOP; **C, D**) and inositol-requiring enzyme-1α (IRE-1α; **E, F**) were quantified as markers of ER stress and expressed relative to β-tubulin. All samples were run on a single gel and bands from one replicate were represented. Data are presented as individual values and median, $n = 4$. * $p < 0.05$; Kruskal-Wallis test with Dunn's multiple comparisons test.

3.3.3 The effect of human serum and foetal bovine serum on HepG2 and Huh7 function and metabolism

3.3.3.1 The effect of culturing sera on storage and synthesis of TAG in HepG2 and Huh7 cells

Previous work has demonstrated that using human serum for culture may promote a more differentiated phenotype, as well as improving cholesterol and bile acid metabolism (Pramfalk *et al.*, 2016; Steenbergen *et al.*, 2013); these findings were extended to investigate FA and TAG metabolism. Levels of intracellular TAG were found to be significantly higher in Huh7 than HepG2 cells when cultured in both sera (Figure 3.3.3-1A). Huh7 cells also had a significantly higher proportion of DNL-derived palmitate than HepG2 cells independently of culturing serum; for both cell lines DNL was higher when cultured in FBS compared to HS (all $p < 0.05$; Figure 3.3.3-1B).

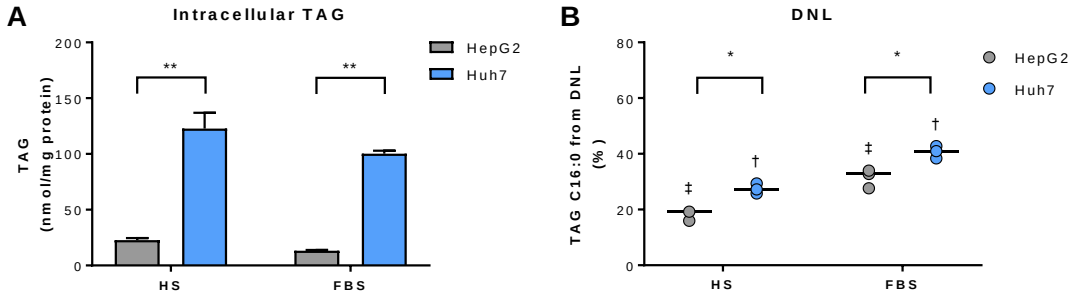


Figure 3.3.3-1. Storage and synthesis of triacylglycerol (TAG) in HepG2 and Huh7 cells. Cells were cultured in either human serum (HS) or foetal bovine serum (FBS)-containing media for seven days. Intracellular TAG content was measured (**A**); data are mean ± SEM, $n = 5$. Palmitate (C16:0) in TAG derived from *de novo* lipogenesis (DNL) was measured (**B**); data are presented as individual values and median, $n = 3$. * $p < 0.05$, ** $p < 0.001$; two-way ANOVA with Bonferroni's multiple comparisons test.

Table 3.3.3-1. mRNA expression of lipid metabolism genes in Huh7 and HepG2 cells

	HS		FBS	
	HepG2	**Huh7**	**HepG2**	**Huh7**
FA transport and synthesis genes				
ACACA	1.44 (1.27 - 1.50)**‡	0.60 (0.56 - 0.68)	1.42 (1.33 - 1.57)**‡	0.69 (0.68 - 0.74)
ACACB	2.04 (1.14 - 2.41)*‡	0.90 (0.77 - 1.20)	1.20 (0.95 - 1.22)‡	0.92 (0.71 - 1.00)
CIDEC	0.35 (0.33 - 0.43)**	1.29 (1.17 - 1.68)†	0.26 (0.25 - 0.29)*	0.78 (0.71 - 0.88)†
DGAT2	1.18 (1.05 - 1.23)	1.38 (1.08 - 1.68)	0.71 (0.57 - 0.88)*	1.52 (0.75 - 1.91)
FASN	1.18 (0.97 - 1.21)*‡	0.56 (0.49 - 0.59)	1.49 (1.16 - 1.72)**‡	0.61 (0.52 - 0.79)
FABP1	0.79 (0.71 - 0.85)*	1.31 (1.01 - 1.61)	0.76 (0.63 - 0.82)*	1.34 (1.07 - 1.45)
SCD1	1.40 (1.36 - 1.57)	0.89 (0.73 - 1.05)	1.59 (1.13 - 1.81)	0.99 (0.76 - 1.13)
FA elongation and desaturation genes				
ELOVL2	1.95 (1.89 - 1.97)**‡	0.69 (0.68 - 0.75)	1.27 (1.05 - 1.43)*‡	0.78 (0.74 - 0.90)
ELOVL5	1.17 (1.16 - 1.21)	0.87 (0.73 - 0.89)	1.34 (1.25 - 1.38)	0.97 (0.94 - 0.99)
ELOVL6	0.82 (0.82 - 1.02)*	1.20 (0.92 - 1.37)	0.91 (0.86 - 1.03)**	1.47 (1.26 - 1.74)
FADS1	0.65 (0.59 - 0.76)*	1.01 (0.84 - 1.16)	0.69 (0.48 - 0.70)*	1.14 (0.89 - 1.39)
FADS2	0.54 (0.52 - 0.63)**	1.34 (1.22 - 1.39)	0.55 (0.45 - 0.68)**	1.47 (1.38 - 1.63)
Lipolysis, secretion and oxidation genes				
APOB	1.81 (1.58 - 2.19)**‡	0.58 (0.47 - 0.62)	0.97 (0.87 - 1.04)*	0.55 (0.49 - 0.59)
CES1	0.01 (0.01 - 0.02)**	1.24 (1.18 - 1.32)†	0.01 (<0.01 - 0.01)**	2.08 (1.91 - 2.21)†
CIDEB	0.25 (0.23 - 0.27)**	1.17 (0.84 - 1.27)	0.23 (0.15 - 0.32)*	0.87 (0.79 - 1.41)
CPT1A	0.67 (0.62 - 0.75)*	1.26 (0.88 - 1.36)	0.75 (0.69 - 0.81)**	1.41 (1.17 - 1.58)
LIPC	0.34 (0.34 - 0.43)**	1.29 (1.04 - 1.61)	0.20 (0.16 - 0.26)*	0.86 (0.81 - 1.56)
MTTP	0.83 (0.78 - 0.85)*	1.57 (1.07 - 1.66)	0.42 (0.40 - 0.48)**	1.50 (1.41 - 1.95)
PNPLA2	1.44 (1.27 - 1.50)**‡	0.60 (0.56 - 0.68)	1.42 (1.33 - 1.57)**‡	0.69 (0.68 - 0.74)
PNPLA3	1.04 (0.77 - 1.22)	1.10 (0.93 - 1.17)	0.56 (0.45 - 0.65)*	1.08 (0.89 - 1.26)
TM6SF2	0.67 (0.40 - 0.75)**	1.35 (1.25 - 1.48)	0.38 (0.35 - 0.56)*	1.06 (0.91 - 1.26)
Hepatic nuclear receptors				
HNF4A	1.16 (1.16 - 1.55)	1.26 (0.98 - 1.40)	0.95 (0.88 - 1.00)*	1.26 (1.11 - 1.33)
NR1H3	1.03 (1.00 - 1.40)*	1.30 (1.28 - 1.32)	0.80 (0.52 - 1.05)**	1.16 (1.10 - 1.51)
NR1H4	0.62 (0.58 - 0.69)	1.29 (1.05 - 1.40)	0.18 (0.17 - 0.35)*	1.33 (0.97 - 1.63)
Transcription factors				
MLXIPL	3.09 (1.85 - 4.45)**‡	0.19 (0.13 - 0.24)	1.31 (1.05 - 1.42)*‡	0.19 (0.17 - 0.23)
PPARA	0.87 (0.72 - 1.07)*	1.13 (1.07 - 1.30)	0.72 (0.64 - 0.84)*	1.04 (0.91 - 1.20)
PPARG	0.53 (0.29 - 0.87)*	1.04 (0.81 - 1.30)	0.31 (0.27 - 0.39)*	1.04 (0.88 - 1.21)
PPARGC1A	3.32 (2.75 - 3.57)**	0.01 (0.01 - 0.03)	3.00 (1.94 - 3.36)**	0.01 (0.01 - 0.02)
SREBF1	0.69 (0.64 - 0.81)*	0.91 (0.79 - 1.00)	0.86 (0.77 - 0.96)	0.83 (0.78 - 0.91)

Cells were cultured in either human serum (HS) or foetal bovine serum (FBS)-containing media for seven days. mRNA expression is presented relative to a calibrator sample, all genes were corrected to two reference genes (*B2M* and *YWHAZ*). Data are presented as median (range), $n = 4$. * $p < 0.05$, ** $p < 0.001$ *vs.* Huh7 cells in the same serum condition; matching symbols denote significant differences between means for HepG2 cells (‡) and Huh7 cells (†), $p < 0.05$; two-way ANOVA with Bonferroni's multiple comparisons tests.

In contrast, gene expression analysis showed an upregulation of DNL-related genes (*ACACA* and *FASN*) in HepG2 compared to Huh7 cells in HS ($p < 0.05$, Table 3.3.3-1), potentially due to a 14-fold higher expression of the lipogenic transcription factor carbohydrate-responsive element binding protein (ChREBP; *MLXIPL*) in HepG2 cells, compared to a more modest elevation of sterol-regulatory element binding protein (SREBP)-1c (*SREBF1*) expression in Huh7 cells (both $p < 0.05$ in HS, Table 3.3.3-1). Genes involved in lipid transport (liver fatty acid binding protein 1; *FABP1*) and storage (cell death inducing DFFA like effector C; *CIDEC)* were expressed more highly in Huh7 compared to HepG2 cells ($p < 0.05$; Table 3.3.3-1), suggesting Huh7 cells synthesised and stored TAG more efficiently than HepG2 cells.

3.3.3.2 The effect of culturing sera on FA composition in TAG and PL fractions in HepG2 and Huh7 cells

Given the differences observed in TAG synthesis and accumulation, the FA composition of TAG and PLs were measured. Total saturated fatty acids (SFAs) in both lipid fractions were similar between cell lines and sera (Figure 3.3.3-2A & B). Huh7 cells had a greater proportion of stearate (C18:0) in the PL fraction while HepG2 cells had more myristate (C14:0) and palmitate (C16:0) (all $p < 0.05$, Table 3.3.3-3). Total intracellular monounsaturated FA (MUFA) composition showed an effect of serum on the PL fraction, with higher levels in FBS-cultured compared to HS-cultured cells ($p < 0.05$, Figure 3.3.3-2C & D). Inter-cell line differences were apparent in individual FA composition, with significantly higher proportions of palmitoleate (C16:1*n*-7) and oleate (C18:1*n*-9) and lower levels of vaccinate (C18:1*n*-7) in Huh7 compared to HepG2 cells (Table 3.3.3-2 & 3.3.3-3).

Differences in polyunsaturated FA (PUFA) content were more marked between the cell lines for both TAG and PL fractions (Figure 3.3.3-2E & F). Notably, the two essential FAs, linoleate (C18:2*n*-6) and α-linolenate (C18:3*n*-3), were significantly higher in abundance in the TAG and PL fractions in both cell lines as a result of culturing in HS rather than FBS (Figure 3.3.3-2E & F, Table 3.3.3-2 & 3.3.3-3). However, partitioning of these FAs was dependent on cell line: in the TAG fraction, PUFAs were higher in HepG2 cells ($p < 0.05$, Figure 3.3.3-2E), while Huh7 cells had a significantly higher abundance of PUFA in the PL fraction compared to HepG2 cells (Figure 3.3.3-2F). This was reflected in all individual PUFAs except linoleate (Table 3.3.3-3), suggesting that Huh7 cells partition PUFAs into PLs rather than store them in the TAG fraction.

Differences in FA composition can result from intracellular metabolism or exogenous supply. As essential FAs cannot be synthesized *de novo*, the increase in intracellular content can be attributed to higher levels contained in HS; this was confirmed when serum alone was analysed (Appendix B, Table B-3). Media with 2% HS contained twice as much TAG compared to media with 10% FBS, including 10 times the amount of linoleate and a small amount of α-linolenate, which was undetectable in FBS. However, longer chain *n*-3 FAs were not detected in either serum, demonstrating the ability of both cell lines to elongate and desaturate FAs, although potentially to different degrees. Expression of FA desaturases (*FADS1* and *FADS2*) were expressed more highly in Huh7 cells, regardless of culturing serum, but elongases were differentially upregulated in Huh7 cells (*ELOVL6*) and HepG2 cells (*ELOVL2*; all $p < 0.05$, Table 3.3.3-1).

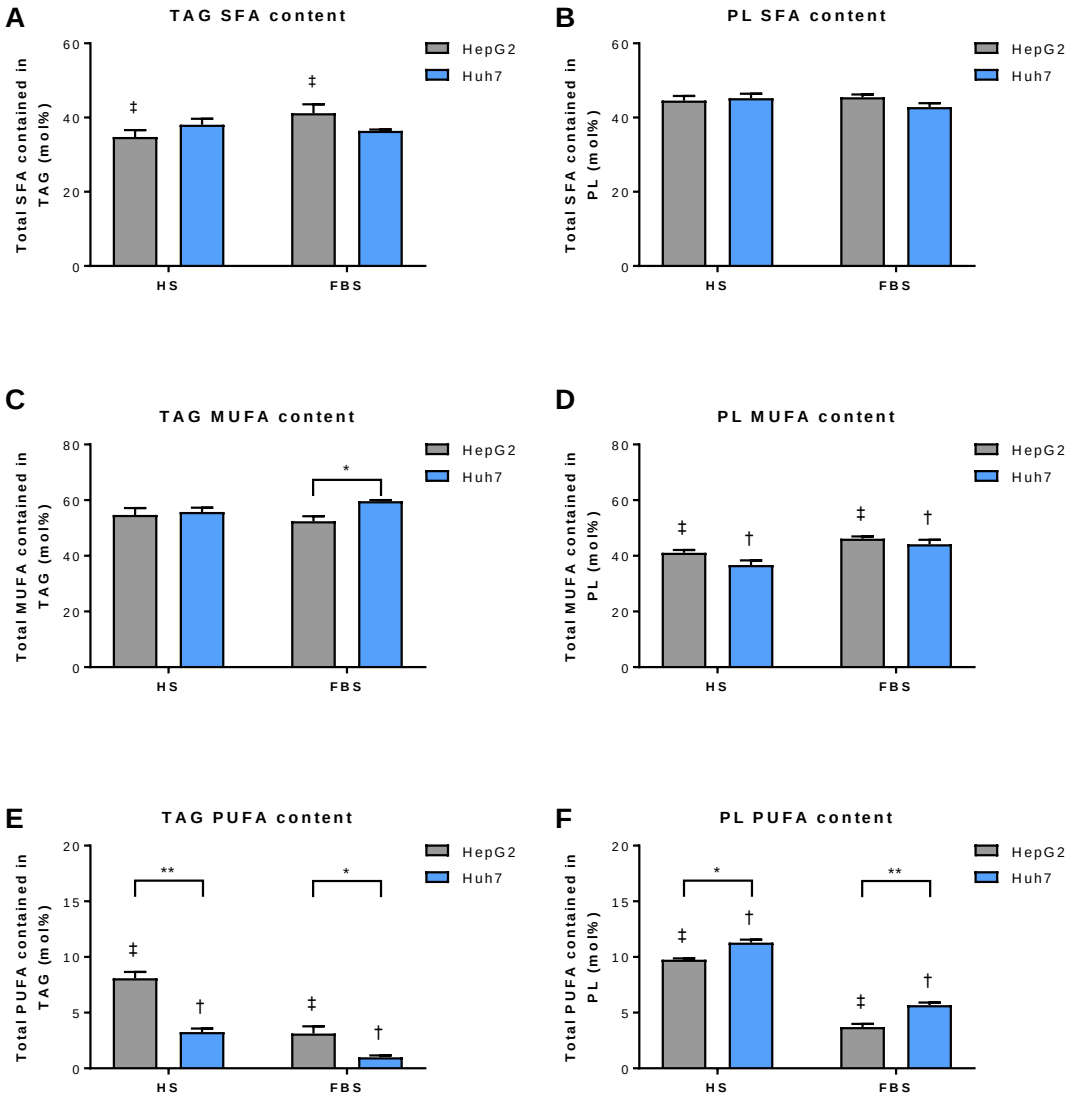


Figure 3.3.3-2. Metabolism and composition of triacylglycerol (TAG) and phospholipid (PL) fractions in Huh7 and HepG2 cells. Cells were cultured in either human serum (HS) or foetal bovine serum (FBS)-containing media for seven days. Intracellular TAG was extracted and the contribution of saturated, monounsaturated and polyunsaturated fatty acids (SFA, MUFA and PUFA) was determined for TAG (**A, C, E**) and PL (**B, D, F**). Data are mean ± SEM, n = 5. * $p < 0.05$, ** $p < 0.001$; matching symbols denote significant differences between means for Huh7 (†) and HepG2 cells (‡), $p < 0.05$; two-way ANOVA with Bonferroni's multiple comparisons test.

Table 3.3.3-2. Fatty acid composition of triacylglycerol in Huh7 and HepG2 cells cultured with HS or FBS (mol%)

	HS		FBS	
	HepG2	**Huh7**	**HepG2**	**Huh7**
C14:0	4.72 ± 0.16	5.90 ± 0.25	6.25 ± 0.46	4.22 ± 0.09
C16:0	26.1 ± 1.3	27.0 ± 1.1	29.1 ± 1.6*	24.8 ± 0.40
C18:0	3.95 ± 0.55‡	5.17 ± 0.28†	5.84 ± 0.47*‡	7.44 ± 0.40†
C16:1*n*-7	8.3 ± 0.6**‡	15.2 ± 0.4	11.8 ± 0.4*‡	14.0 ± 0.5
C18:1*n*-9	25.6 ± 0.6**‡	30.1 ± 0.8†	22.9 ± 0.9**‡	35.6 ± 0.4†
C18:1*n*-7	20.8 ± 1.7**	10.5 ± 0.5	17.7 ± 1.3**	10.1 ± 0.2
C18:2*n*-6	4.71 ± 0.33**‡	2.29 ± 0.17†	0.78 ± 0.13‡	0.30 ± 0.01†
C18:3*n*-6	0.44 ± 0.09	0.19 ± 0.03	0.54 ± 0.08	0.31 ± 0.09
C18:3*n*-3	0.39 ± 0.07*‡	0.14 ± 0.05†	0.0 ± 0.0‡	0.0 ± 0.0†
C20:4*n*-6	0.66 ± 0.05*	0.18 ± 0.04	0.72 ± 0.2*	0.09 ± 0.02
C20:5*n*-3	1.97 ± 0.47*	0.47 ± 0.12	1.08 ± 0.27	0.29 ± 0.06

Cells were cultured in human serum (HS) or foetal bovine serum (FBS)-containing media for seven days. Data are mean ± SEM, n = 5. Two-way ANOVA with Bonferroni's multiple comparisons test. * $p < 0.05$, ** $p < 0.001$ *vs.* Huh7 cells in the same serum condition; matching symbols denote significant differences between means for Huh7 (†) and HepG2 cells (‡), $p < 0.05$.

Table 3.3.3-3. Fatty acid composition of phospholipids in Huh7 and HepG2 cells cultured with HS or FBS (mol%)

	HS		FBS	
	HepG2	**Huh7**	**HepG2**	**Huh7**
C14:0	3.76 ± 0.31**‡	0.90 ± 0.05	6.38 ± 0.78**‡	0.83 ± 0.10
C16:0	35.8 ± 0.9*	31.2 ± 0.7	33.4 ± 0.7*	30.5 ± 0.7
C18:0	5.1 ± 0.2**	13.1 ± 0.6	5.7 ± 0.4**	11.5 ± 0.5
C16:1*n*-7	9.75 ± 0.72	8.50 ± 0.83	13.85 ± 2.05*	9.20 ± 0.91
C18:1*n*-9	15.9 ± 0.6**‡	20.9 ± 0.5†	19.0 ± 0.6**‡	29.2 ± 1.1†
C18:1*n*-7	14.9 ± 1.5**	7.0 ± 0.7	12.5 ± 1.5**	5.4 ± 0.1
C20:1*n*-9	0.57 ± 0.03*	0.29 ± 0.06	0.73 ± 0.03**	0.29 ± 0.06
C18:2*n*-6	5.58 ± 0.45‡	5.16 ± 0.07†	0.69 ± 0.05‡	0.49 ± 0.02†
C18:3*n*-6	0.26 ± 0.01**‡	0.47 ± 0.03†	0.18 ± 0.02‡	0.19 ± 0.01†
C18:3*n*-3	0.1 ± 0.0	0.07 ± 0.01†	0.09 ± 0.02**	0.16 ± 0.01†
C20:4*n*-6	1.51 ± 0.12**	2.79 ± 0.27†	0.97 ± 0.02*	1.70 ± 0.08†
C20:5*n*-3	0.48 ± 0.06‡	0.38 ± 0.02†	0.31 ± 0.06**‡	0.61 ± 0.02†
C22:5*n*-3	0.57 ± 0.02**	1.22 ± 0.13	0.92 ± 0.11*	1.49 ± 0.11
C22:6*n*-3	1.77 ± 0.16*‡	1.21 ± 0.21	0.84 ± 0.05‡	1.04 ± 0.03

Cells were cultured in human serum (HS) or foetal bovine serum (FBS)-containing media for seven days. Data are mean ± SEM, n = 5. Two-way ANOVA with Bonferroni's multiple comparisons test. * $p < 0.05$, ** $p < 0.001$ *vs.* Huh7 cells in the same serum condition; matching symbols denote significant differences between means for Huh7 (†) and HepG2 cells (‡), $p < 0.05$.

3.3.3.3 The effect of culturing sera on TAG and FA disposal in HepG2 and Huh7 cells

The ability of hepatocytes to mobilise TAG for secretion in lipoproteins and FAs for oxidation is an important part of their metabolic function, and is often lacking in hepatoma cell lines. We assessed the cell media TAG concentration as a proxy marker of TAG secretion and found it to be significantly higher in Huh7 compared to HepG2 cells in FBS (Figure 3.3.3-3A). In both cell lines media TAG was significantly higher when cultured in HS compared to FBS, but the levels did not significantly differ between Huh7 and HepG2 cells after culturing in HS (Figure 3.3.3-3A). ApoB, the apolipoprotein associated with lipoprotein particles secreted from hepatocytes, was significantly more abundant in the media after culturing in HS than FBS in HepG2 and Huh7 cells, but did not differ between cell lines (Figure 3.3.3-3B). Levels of *APOB* mRNA were also elevated after culturing in HS in HepG2 cells ($p < 0.05$), and were significantly higher in HepG2 cells than Huh7 cells in both conditions. Expression of *MTTP*, *CIDEB* and *TM6SF2*, genes related to the transfer of TAG to apoB-containing particles and their secretion, were significantly higher in Huh7 cells (Table 3.3.3-1).

As a marker of FA oxidation, 3-OHB in the media was measured and was significantly higher in both cells lines after culturing in HS compared to FBS. Media 3-OHB concentrations were also significantly higher in HepG2 compared to Huh7 cells when cultured in HS (Figure 3.3.3-3C). In contrast, the expression of oxidative genes (peroxisome proliferator-activated receptor-γ; *PPARG* and carnitine palmitoyltransferase 1A; *CPT1A*) were more highly expressed in Huh7 cells in HS and FBS (all $p < 0.05$, Table 3.3.3-1). In line with the ability of both cells to mobilise TAG for secretion and oxidation, expression of lipases were present,

although *LIPC*, *PNPLA3* and *CES1* were all as expressed more highly in Huh7 cells and only *PNPLA2* in HepG2 cells (all $p < 0.05$, Table 3.3.3-1).

3.3.3.4 The effect of culturing sera on insulin and insulin-like growth factor-1 signalling in HepG2 and Huh7 cells

Given the role of insulin in regulating FA metabolism, phosphorylation of Akt in response to insulin and insulin-like growth factor (IGF)-1 stimulation was measured. While healthy human hepatocytes do not express the IGF-1 receptor, due to de-differentiation, hepatoma cell lines do express the receptor and respond to IGF-1 by phosphorylating Akt in the same way as insulin (Waraky *et al.*, 2016). HS increased Akt phosphorylation in response to insulin to similar extents in both Huh7 and HepG2 cells, although there was considerable variation between replicates (Figure 3.3.3-4A - D). However, in HepG2 cells, IGF-1 also phosphorylated Akt at a similar magnitude to insulin in HS compared to FBS, which was less evident in Huh7 cells, indicating a suppression of perturbed IGF-1 signalling in Huh7 cells cultured in HS (Figure 3.3.3-4A - D). Immunoblotting of the 111 nM samples confirmed that both cell lines were significantly more insulin sensitive when cultured in HS ($p < 0.05$, Figure 3.3.3-4E & F). However, there was also evidence that when cultured in HS, IGF-1 stimulation significantly increased Akt phosphorylation in HepG2 cells, which was not seen in Huh7 cells (Figure 3.3.3-4E & F). These results indicate a suppression of perturbed IGF-1 signalling in Huh7 cells cultured in HS.

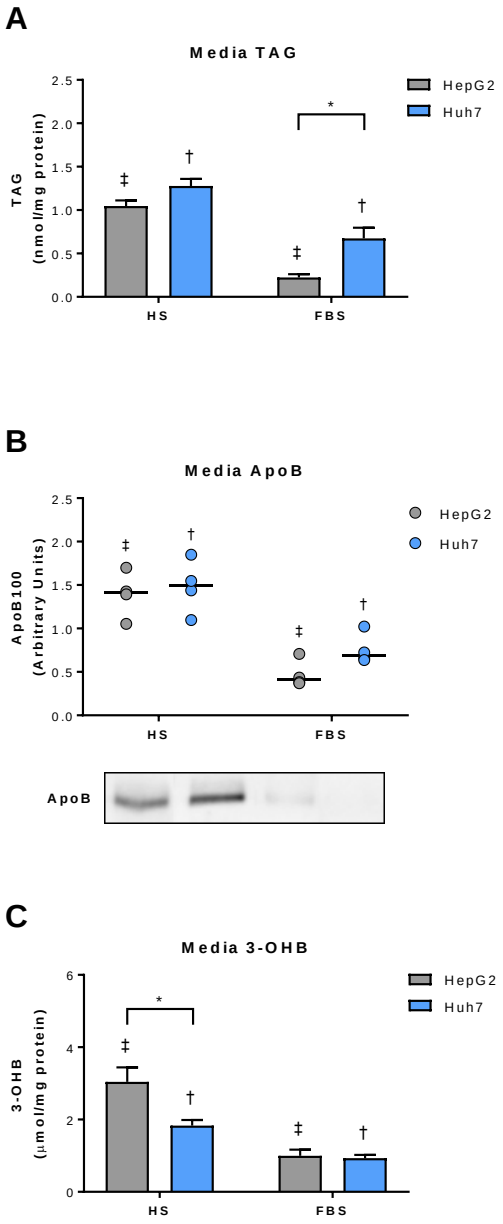


Figure 3.3.3-3. Secretion of triacylglycerol (TAG) and fatty acid oxidation in Huh7 and HepG2 cells. Cells were cultured in either human serum (HS) or foetal bovine serum (FBS)-containing media for seven days. TAG (**A**), apolipoprotein (apo)B (**B**) and 3-hydroxybutyrate (3-OHB; **C**) in cell media were measured. Media TAG and 3-OHB (**A, C**) are mean ± SEM, $n = 5$. Media apoB (**B**) are presented as individual values and median, $n = 4$. An apoB antibody was used and the appropriate molecular weight band for apoB100 (550 kDa) was quantified. * $p < 0.05$; matching symbols denote significant differences between means for Huh7 (†) and HepG2 cells (‡), $p < 0.05$; two-way ANOVA with Bonferroni's multiple comparisons test.

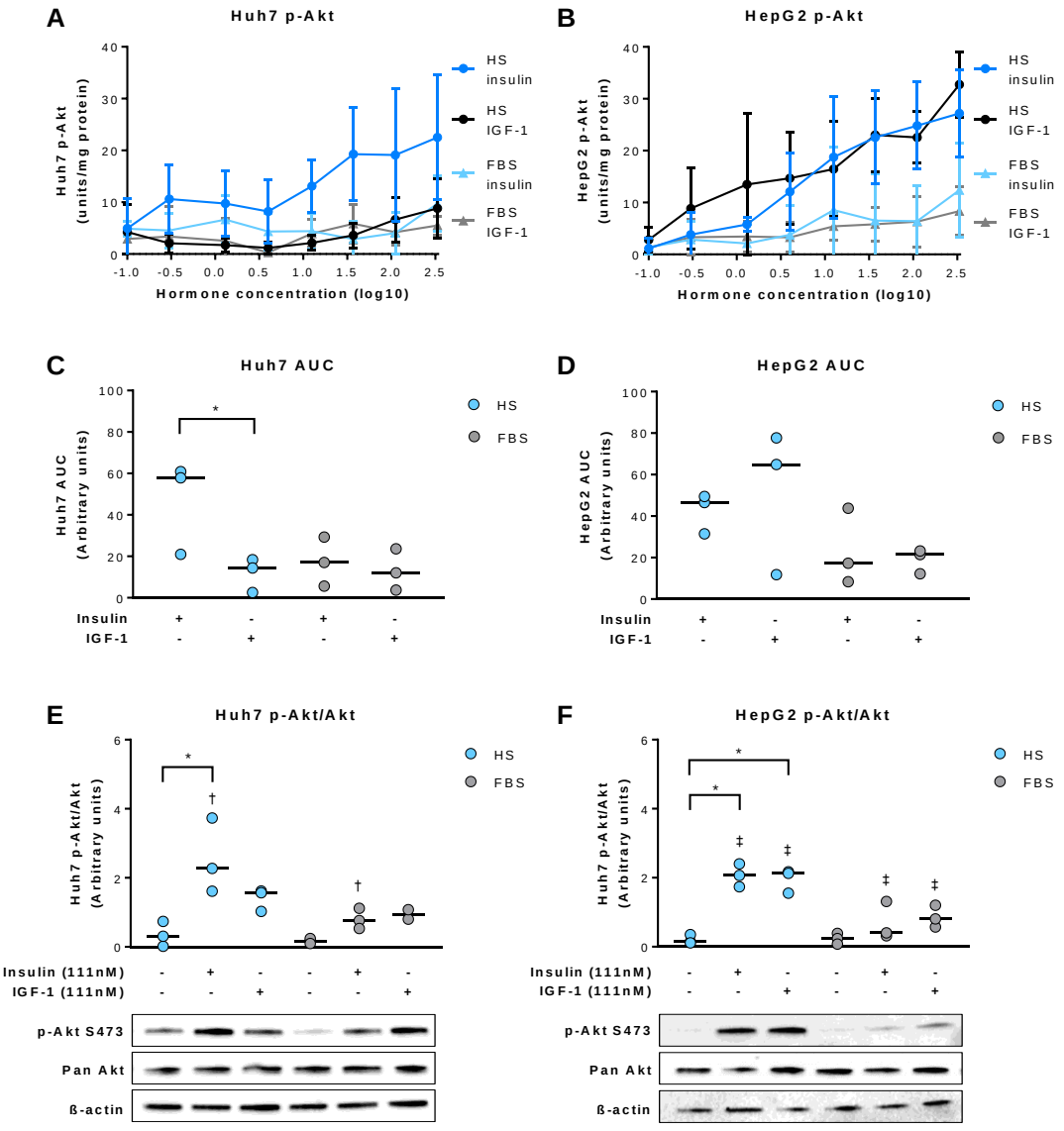


Figure 3.3.3-4. Insulin and insulin-like growth factor 1 (IGF-1) signalling in Huh7 and HepG2 cells. Cells were cultured in either human serum (HS) or foetal bovine serum (FBS)-containing media for three days before serum starvation and stimulation with insulin or IGF-1 at 0, 0.46, 1.4, 4.1, 12.3, 37, 111 and 333 nM. Insulin/IGF-1 stimulated Akt serine 473 phosphorylation was measured by ELISA in Huh7 (**A**) and HepG2 cells (**B**) and area under the curve (AUC) for p-Akt serine 473 ELISA was quantified (Huh7 cells: **C**; HepG2 cells: **D**). p-Akt/Akt quantification was confirmed by immunoblotting of 111 nM samples and results were expressed relative to β-tubulin in Huh7 (**E**) and HepG2 cells (**F**). Data are presented as individual values and median, $n = 3$. * $p < 0.05$; matching symbols denote significant differences between means for Huh7 (†) and HepG2 cells (‡), $p < 0.05$; two-way ANOVA with Bonferroni's multiple comparisons test. *This analysis was carried out by Dr. Charlotte Green and Mr. Thomas Cornfield.*

3.4 DISCUSSION

The aim of this chapter was to determine optimal cell culture conditions for creating a model for the investigation of NAFLD *in vitro*. Building on our previous work in high glucose conditions (Nikolaou *et al.*, 2016), DMSO was initially found to exert some positive effects on HepG2 cells when cultured in low glucose (5.5 mM) media. Notably, the expression of the tumour marker *AFP* was reduced, as was TAG accumulation and expression of the DNL genes *ACACA* and *FASN*, representing a correction of dysregulated lipid metabolism commonly seen in hepatoma cells. Although in line with previous studies (Nikolaou *et al.*, 2016; Song *et al.*, 2012), the strength of the results presented here are less striking, meaning DMSO treatment was not pursued further. This difference was likely due to cells being cultured in low glucose media only: it may be that with less substrate available for TAG synthesis DMSO confers little benefit.

When the effect of glucose on both Huh7 and HepG2 cells lines was investigated, metabolic responses, and particularly an increase in DNL, in higher glucose levels were evident in both cell lines. Huh7 cells upregulated TAG secretion in response to elevated glucose supply, while HepG2 cells increased TAG content and secretion; this increase in TAG synthesis is unsurprising given the additional substrate in cells known to have high levels of DNL (Daniels *et al.*, 2014). The apparent divergence in glycolysis and FA oxidation between cell lines, with an increase in lactate and decrease in media 3-OHB seen in Huh7 cells, but not HepG2 cells, may be due to a reported reduction in activation of AMP-activated protein kinase (AMPK) seen in HepG2 cells cultured in high glucose media (Berger *et al.*, 2015), since AMPK

signalling would normally activate and inhibit these pathways, respectively. These results suggest Huh7 cells show more metabolic flexibility in differentially partitioning substrates towards glucose or FA metabolism.

Culturing serum also had an effect on FA synthesis and storage. Huh7 cells stored more TAG than HepG2 cells in both culturing conditions, which may in part be explained by higher DNL in Huh7 cells. Although Steenbergen *et al.* (Steenbergen *et al.*, 2013) did not measure intracellular TAG, they reported an increase in LDs in Huh7 cells after 21 days of culture in HS; this was attributed to elevated liver X receptor (LXR; *NR1H3*), peroxisome proliferator-activated receptor (PPAR)-α and PPAR-γ expression. We did not observe changes in these transcripts or an increase in intracellular TAG in response to HS in either cell line, which may be due to the difference in culturing time. However, they were all expressed to a higher degree in Huh7 compared to HepG2 cells, as was farnesoid X receptor (FXR; *NR1H4*). LXR is a lipogenic nuclear receptor, which promotes transcription of genes related to DNL and TAG uptake from lipoproteins; FXR, which primarily regulates bile acids and induces lipid disposal, also increases hepatic TAG uptake (Lopez-Velazquez *et al.*, 2012). It may be that the increased expression of LXR and FXR in Huh7 cells led to increased TAG uptake and storage, suggesting that Huh7 cells are more responsive to the effects of exogenous fat supply than HepG2 cells.

When cultured in FBS with 11 mM glucose, the amount of DNL in both Huh7 and HepG2 cells could be considered supraphysiological; however, when cultured in HS with the same level of glucose DNL accounted for 18-25% in both cell lines, which is comparable to that

reported for subjects with NAFLD (Diraison *et al.*, 2003; Donnelly *et al.*, 2005; Lambert *et al.*, 2014). The lower amount of DNL in cells cultured in HS may be due to the higher quantity of TAG in this serum: both SFA and PUFA are known inhibitors of the two major lipogenic transcription factors, SREBP-1c and ChREBP (Dentin *et al.*, 2008; Ye & DeBose-Boyd, 2011). In addition, we found that insulin signalling improved in both cell lines as a result of culture in HS, possibly due to FBS being rich in insulin and albumin (Gstraunthaler & Lindl, 2011), both of which can lead to insulin resistance (IR). The relative insulin insensitivity in cells cultured in FBS compared to HS may have caused a reduction in glycogenesis; this would provide increased precursors for DNL. Although limited to Akt phosphorylation, the available data indicates that culture of both cell lines in HS results in a more insulin-sensitive phenotype, providing the opportunity for IR in steatosis development to be investigated.

Although both Huh7 and HepG2 cells have been found to secrete dense, lipid-poor lipoproteins (Gibbons *et al.*, 1994; Javitt, 1990; Meex *et al.*, 2011), culturing in HS improves lipoprotein profiles in both cell lines (Pramfalk *et al.*, 2016; Steenbergen *et al.*, 2013). Whether this results from a change in function due to HS-cultured hepatocytes displaying a more differentiated phenotype, or simply an increase in FA availability for transfer to apoB-containing particles, is not clear. It is well established that provision of exogenous FAs results in increased TAG content of lipoprotein particles secreted from HepG2 cells (Dashti *et al.*, 1987; Ellsworth *et al.*, 1986; Wu *et al.*, 1996). It is plausible that both the increase in secretion and oxidation in hepatoma cells in HS is a result of increased supply of FA. In the present study, the only exogenous FAs provided were that in the culturing sera. The low levels of

essential FAs appear to have led to the elongation and desaturation of the DNL product palmitate (C16:0): the most notable difference between FA composition of our cells and that seen *in vivo*, was an increase in palmitoleate (C16:1*n*-7) and vaccenate (C18:1*n*-7), and a reduction in linoleate (C18:2*n*-6) and α-linolenate (C18:3*n*-3) and their products (Arendt *et al.*, 2015; Hodson *et al.*, 2008). This suggests the use of HS, as well as routine supply of exogenous FAs in the culture media, may assist in overcoming FA depletion, thus lowering DNL and increasing TAG secretion and FA oxidation.

Culturing in HS altered the intracellular FA composition of the cells, resulting in a higher PUFA content. PUFAs were primarily abundant in the PL fraction of Huh7 cells; however, they were more abundant in the TAG fraction of HepG2 cells. HepG2 cells carry the I148M variant of the *PNPLA3* gene, which causes remodelling of hepatocellular LDs and results in increased PUFA and reduced stearate in intracellular TAG (Luukkonen *et al.*, 2016; Peter *et al.*, 2014; Romeo *et al.*, 2008; Ruhanen *et al.*, 2014), in line with our results. In contrast, Huh7 cells have limited protein levels of PNPLA3, which results in enzyme activity equivalent to cells expressing the wild type protein (Ruhanen *et al.*, 2014). Additionally, carriers of the *PNPLA3* I148M variant are suggested to have lower DNL-derived intrahepatic fat and to secrete poorly-lipidated apoB particles (Luukkonen *et al.*, 2016; Pirazzi *et al.*, 2012; Sevastianova *et al.*, 2012), which may explain the consistently lower rate of DNL and the tendency (in FBS but not HS) to secrete less TAG in HepG2 compared to Huh7 cells. The effect of this genotype on models investigating FA metabolism is, therefore, an important consideration.

Although we have focused primarily on cellular FA metabolism, culture conditions may also affect whether these cell lines present with a more differentiated, or conversely, more cancerous, phenotype. HepG2 cells have previously been shown to express the interleukin-6 receptor, a tumour marker, to a greater extent and to be a more proliferative cell line than Huh7 cells (Berger *et al.*, 2015). When cultured in high glucose, which may promote a more cancerous phenotype, we found a significant reduction in albumin expression in Huh7 cells at 22 mM glucose and a trend for increased *MKI67* expression, suggesting a shift to a less differentiated, more proliferative phenotype in Huh7 cells, but not HepG2 cells. A similar divergence in the proliferative response of these cell lines to high glucose has been observed previously, and was attributed to glucose activating the LKB1/AMPK signalling pathway in Huh7 cells (Berger *et al.*, 2015).

In terms of promoting a more differentiated hepatocyte phenotype, previous studies using HS have shown that functional outcomes including bile acid and cholesterol metabolism are improved in HepG2 cells (Pramfalk *et al.*, 2016), while hepatocyte morphology, cytochrome P450 enzyme function and differentiation markers are improved in both cell types (Pramfalk *et al.*, 2016; Steenbergen *et al.*, 2013). The mechanism by which HS may exert its effect remain unclear. HS results in growth arrest of cells, allowing them to be cultured for longer, which has been found to independently promote differentiation in Huh7 cells (Sivertsson *et al.*, 2010), however, these benefits were augmented when used in parallel with HS, suggesting an independent mechanism (Steenbergen *et al.*, 2013). When comparing HepG2 and Huh7 cells, we did not measure any specific markers of differentiation; however, the suppression in IGF-

1 signalling in Huh7 cells compared to HepG2 cells after culture in HS, may suggest a more differentiated phenotype in these cells. Huh7 cells therefore appear to be a more responsive cell line to the effects of glucose and HS on proliferation and differentiation, respectively.

There are some limitations to this work. The sera were used at different concentrations: HS at 2% and FBS 10%. We found cells were not viable when cultured with 2% FBS (data not shown), while previous work did not find any difference between culturing HepG2 cells in 2% or 5% HS (Pramfalk *et al.*, 2016). Given that the FA content of media was higher in 2% HS than 10% FBS, it is likely an increase in HS content would only have exaggerated the current findings. Media TAG was measured as a surrogate measure of lipoprotein secretion, which means differences in particle density may have been missed: this has previously been shown to be lower in HepG2 compared to Huh7 cells when cultured in FBS (Meex *et al.*, 2011). Finally, two widely-available and well-characterised hepatocyte cell models have been investigated; however, as development and validation of other models (*e.g.* iPSC and HepaRG) continues, investigation of the use of HS in these cells may lead to a FA metabolism model that more closely recapitulates a human hepatocyte phenotype.

3.5 SUMMARY

- The addition of 1% DMSO to the culture medium of HepG2 cells resulted in limited improvement of FA metabolism and differentiation markers, meaning DMSO was not pursued further
- While insufficient glucose (5.5 mM) appeared to cause ER stress and amino acid catabolism, high levels of glucose (22 mM) had the potential to enhance proliferation and TAG synthesis in HepG2 and Huh7 cells, resulting in 11 mM glucose being chosen for subsequent experiments
- Compared to FBS, culturing cells in HS conveyed a number of benefits to both cell lines including provision of essential and long-chain FAs, reduced DNL and improved mobilisation of intracellular FAs for oxidation and secretion; measurement of Akt phosphorylation also suggested improved insulin signalling after culture in HS
- HepG2 and Huh7 differ in their response to change in glucose and serum composition of the culturing media, which may result from HepG2 cells carrying the *PNPLA3* I148M mutation
- Due to the improvement in metabolic function with HS and the defects in HepG2 cells that are relevant to a model of FA metabolism, Huh7 cells and HS will be used for further development of an *in vitro* model of macrovesicular steatosis

Chapter 4

Development of a new *in vitro* model of hepatic lipid droplet pattern and fatty acid metabolism

4.1 INTRODUCTION

The first stage of non-alcoholic fatty liver disease (NAFLD) is steatosis, where lipid droplets (LDs) begin to accumulate within hepatocytes. Lipid droplets consist of a core of triacylglycerol (TAG) and cholesterol esters (CEs) surrounded by a protein-containing phospholipid (PL) monolayer. Traditionally thought to have an inert role in energy metabolism, LDs are now recognised to be involved in diverse cellular processes including storage of vitamins and signalling molecules, management of cell stress and protein handling (Welte & Gould, 2017). Moreover, the chronic presence of LDs in non-adipose tissue organs (ectopic fat) has been implicated in both the development and progression of metabolic disease (Shulman, 2014). Further investigation has highlighted the role of distinct LD populations and characteristics in mediating disease pathogenesis (Gemmink *et al.*, 2017; Straub *et al.*, 2008; Tandra *et al.*, 2011).

In hepatic steatosis, LDs may be mostly small, with poorly-defined edges (microvesicular steatosis) or much larger, which can result in engorgement of the cytoplasm and displacement of the nucleus (macrovesicular steatosis) (Takahashi & Fukusato, 2014). Macrovesicular steatosis is more commonly seen in NAFLD, although microvesicular steatosis is present in around 10-15% of cases (Masterton *et al.*, 2011; Takahashi & Fukusato, 2014; Tandra *et al.*, 2011). How these two steatotic patterns might determine disease pathogenesis has not been well investigated, and the evidence available is mixed. Microvesicular steatosis has been reported to associate positively and negatively with progression to non-alcoholic steatohepatitis (NASH) (Masterton *et al.*, 2011; Tandra *et al.*, 2011), as well as with a

decreased risk of insulin resistance (IR) and diabetes compared to macrovesicular steatosis (Masterton *et al.*, 2011). That the two patterns have different disease trajectories is supported by their different LD protein compositions (Pawella *et al.*, 2014).

In association with steatosis, patients with NAFLD display changes in hepatocyte and whole-body metabolism (reviewed in Chapter 1, section 1.3.2). Briefly, steatosis is associated with increased availability of circulating non-esterified fatty acids (FAs) (Perla *et al.*, 2017), which are elevated as a result of impaired suppression of adipose tissue lipolysis due to IR; in the liver, IR can increase DNL (Diraison *et al.*, 2003; Donnelly *et al.*, 2005; Lambert *et al.*, 2014). Sucrose is proposed to play a causal role in DNL through its stimulation of insulin release, promotion of DNL-stimulating transcription factors and use as a substrate (Sanders & Griffin, 2016). In response to an increase in intracellular TAG, very low-density lipoprotein (VLDL)-TAG secretion is increased (Chan *et al.*, 2010; Fabbrini *et al.*, 2008), while markers of β-oxidation show evidence of both increased (Sanyal *et al.*, 2001) and unchanged levels (Kotronen *et al.*, 2009; Sunny *et al.*, 2011).

Currently, LD patterns in *in vitro* models are poorly-defined. Although nutritional composition of media can be used successfully to induce the cellular stress associated with NAFLD *in vitro* (Kostrzewski *et al.*, 2017), whether it is a micro or macrovesicular LD pattern that develops is rarely reported; as a result, the applicability of these models to the predominantly macrosteatotic phenotype of NAFLD is unclear. Where large LDs have been reported, cellular metabolism and function were not investigated (Pawella *et al.*, 2014). In addition, cellular models often lack the addition of essential FAs and due to the limited

capacity of cell lines to replicate hepatic metabolism seen in humans *in vivo*, the metabolic phenotype of steatosis has not been well modelled or investigated *in vitro*.

Given the lack of reported data on LD characteristics *in vitro* and their impact on hepatocyte metabolism, the aims of this chapter were:

1. to create a model of macrovesicular steatosis in Huh7 cells for the study of NAFLD by manipulating nutritional substrates
2. to investigate the effects of FAs and simple sugars on LD size and FA metabolism in Huh7 cells

4.2 METHODS

4.2.1 Experimental treatments

4.2.1.1 Single vs. repeated FA dose experiments

Preliminary work to investigate the frequency of FA treatments in lipid loading was carried out in HepG2 cells after the addition of 1% dimethyl sulfoxide (DMSO) for seven days; remaining work in this chapter was carried out in Huh7 cells. HepG2 cells were seeded in maintenance media (see Chapter 2, section 2.2.1.1) and cultured for 72 hours. After this, cells were washed twice with PBS and media consisting of glucose-free DMEM with the addition of 2% human serum (HS), 1% NEAAs and 10,000 U/ml penicillin-streptomycin, 5.5 mM glucose, 1% sodium pyruvate, 1% Glutamax™ and 1% DMSO was added. Media was changed every 48-72 hours for seven days before the same media with the addition of 5.5 mM fructose, 0.5 nM insulin and 800 µM FAs was added at time point 0 h. FAs consisted of a physiological mix of oleate, palmitate, linoleate and α-linolenate at a ratio of 45:30:24:1 (Chapter 2, section 2.2.1.6). The same FA mix was used for all experiments outlined in this chapter. This media either remained on cells for a total of 72 hours, with samples collected every 24 hours, or was replenished every 24 hours, again, with cells and media collected every 24 hours.

4.2.1.2 FA concentration experiments

Cells were seeded and grown to confluence in maintenance media, before being cultured in HS-containing media for seven days. HS media consisted of phenol red-free DMEM, 11 mmol/L glucose, 1% NEAAs, 10,000 U/mL penicillin-streptomycin, 1% sodium pyruvate and 1% Glutamax™, with 2% HS. After this, cells continued to be treated with HS media (0 µM

FAs), or were treated with one of three experimental treatments. All treatments consisted of HS media with an additional 5.5 mM fructose and either 200, 1000 or 2000 μM FAs. Light microscopy showed larger LDs when media was changed alternative days (data not shown), resulting in a protocol consisting of four media changes every 48 hours, with collection occurring 24 hours after the final media change, for remaining experiments.

4.2.1.3 Cell viability experiments

Cells were seeded into 96-well plates and grown to confluence in maintenance media, before being cultured in human serum HS-containing media for seven days. Cells then continued to be cultured in this media with either 0, 200, 400, 600, 800 or 1000 μM FAs, or with FAs and 5.5 mM fructose for a further seven days. After this, a 3-(4, 5-dimethylthiazol-2-yl)-2, 5-diphenyltetrazolium bromide (MTT) assay was carried out as described in Chapter 2, section 2.2.1.7).

4.2.1.4 Steatosis induction experiments

After passaging, cells were seeded and grown to confluence in maintenance media, before being cultured in HS-containing media for seven days. After this, cells were treated with one of three experimental treatments. All treatments consisted of HS media (described in section 4.2.1.2) with a combination of supplementary FAs and fructose. Low fat low sugar (LFLS) media had 200 μM FAs, low fat high sugar (LFHS) media had 200 μM FAs and 5.5 mM fructose added and the high fat high sugar (HFHS) media had 800 μM FAs and 5.5 mM fructose added; all treatments contained 0.5 nM insulin. For assessment of DNL, 10% heavy water (^2H_2O) was added to media and for all experiments, media was changed every 48–72 h.

4.2.1.5 Glucose and fructose disappearance experiments

Cells were seeded at 100,000 cells per mL into 24-well plates. When confluence was reached, cells were treated with HS media for seven days, with media replenished every 48-72 hours. After this, cells were exposed to either the LFHS or HFHS treatments. Media was collected 8, 16, 24, 32, 40 and 48 h.

4.2.2 Analytical techniques

RNA extraction and RT-PCR, ILab analyses, lipid extraction and gas chromatography-mass spectrometry, IN Cell analysis, size-exclusion chromatography determination of oxidative stress and biochemical assays were carried out as described in Chapter 2 (sections 2.2.2-2.2.9).

4.3 RESULTS

4.3.1 Optimisation of steatosis treatment protocol

4.3.1.1 The effect of single or repeated FA doses on TAG accumulation

To enable maximal TAG storage in cells and replicate TAG accumulation seen in a human steatotic liver, the effect of regular media changes on HepG2 cells was investigated. When media containing 800 μM FAs was changed 72 hours prior to collection, around 85% of the provided FAs were taken up in the first 24 hours, with a further 10-12% taken up over the next 48 hours. However, when media was changed every 24 hours, 80-85% of media FAs were taken up with every media change, equating to a total uptake of approximately 2000 μM when media was changed daily, compared to 750 μM FAs when media was not changed (Figure 4.3.1-1A & C). This was reflected in TAG content of the cells: daily media changes resulted in a median TAG content of 395 nmol/mg protein compared to 140 nmol/mg protein in the absence of media changes (Figure 4.3.1-1B & D). These results demonstrated that HepG2 cells had the capacity to accumulate higher levels of TAG with repeated, rather than a single, dose of FAs.

4.3.1.2 The effect of media FA concentration on FA metabolism and lipid droplet accumulation

To further investigate optimal conditions in which to stimulate intracellular TAG accumulation, different concentrations of FAs were added to the media of Huh7 cells after culture in HS. Metabolic parameters were not changed significantly when 200 μM FA was added to the media compared to 0 μM (Figures 4.3.1-2A-C). Accumulation of intracellular

TAG was, however, higher when 1000 µM FAs were added to the media compared to 0 µM, but there was no further increase with the addition of 2000 µM, suggesting cells had reached their maximum capacity for TAG storage (Figure 4.3.1-2A).

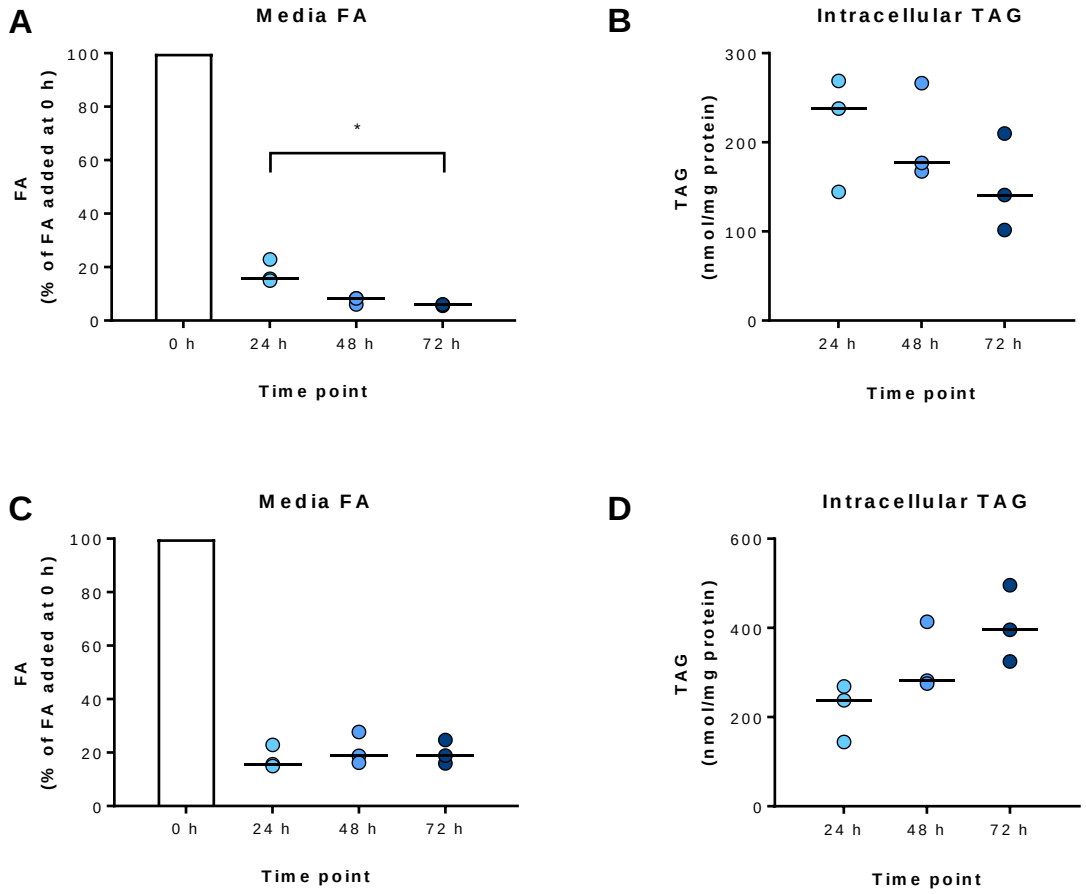


Figure 4.3.1-1. The effect of changing media daily on uptake of fatty acids (FAs) and intracellular triacylglycerol (TAG) levels in HepG2 cells. Cells were confluent at Day 0 and grown for a further 7 days in 1% DMSO with human serum before having media containing 5.5 mM glucose, 5.5 mM fructose, 800 µM FAs (45% oleate (C18:1*n*-9), 30% palmitate (C16:0), 24% linoleate (C18:2*n*-6) and 1% α-linolenate (C18:3*n*-3) and 0.5 nM insulin added. Cells were then either left in this media for 72 hours (**A, B**), or had media replenished every 24 hours (**C, D**). Lipid was extracted an analysed *via* gas chromatography and media FA (**A, C**) and intracellular TAG (**B, D**) was measured. Media FA is expressed as a percentage of total FA added (0 h). Intracellular TAG is expressed relative to protein content of cells. Data are presented as individual values and median, $n = 3$, * $p < 0.05$; Kruskal-Wallis test with Dunn's multiple comparisons test.

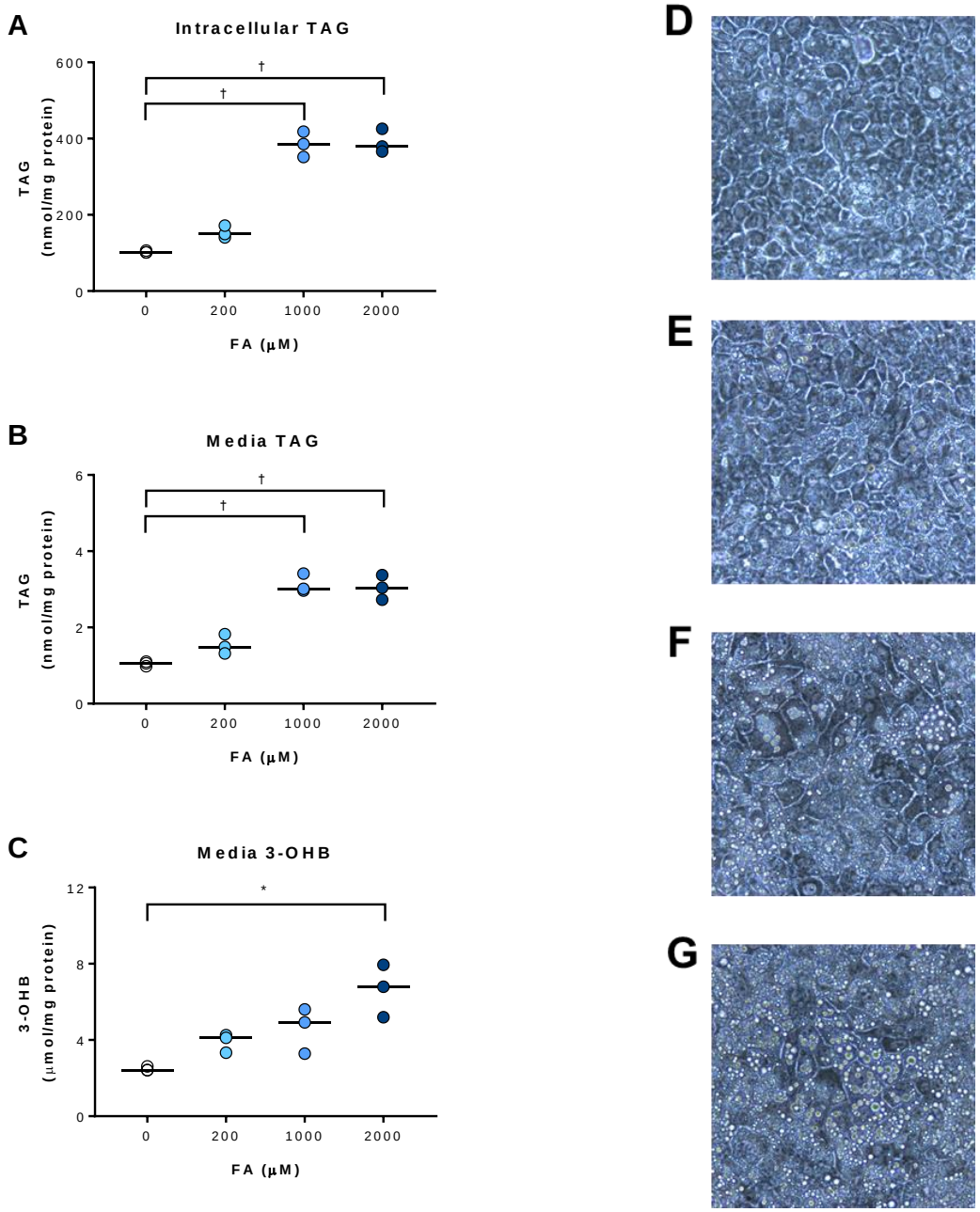


Figure 4.3.1-2. The effect of fructose and fatty acids (FAs) on metabolic parameters in Huh7 cells. Upon reaching confluence, cells were cultured in 11 mM glucose and 2% HS for 7 days, before culture in this media for a further 7 days (0 μM FA) or in media with an additional 5.5 mM fructose and 200, 1000 or 2000 μM FA and 0.5 nM insulin. Intracellular triacylglycerol (TAG) content was measured (**A**), as were levels of media TAG (**B**) and 3-hydroxybutyrate (3-OHB; **C**), as markers of fatty acid secretion and oxidation, respectively. Images of fat accumulation were taken via light microscopy (X40 magnification) for 0 μM (**D**), 200 μM (**E**), 1000 μM (**F**) and 2000 μM (**G**). Media was changed every 48 to 72 hours and 24 hours prior to collection. All results were corrected to protein content of cells. Data are presented as individual values and median, $n = 3$. * $p < 0.05$, † $p < 0.08$; Kruskal-Wallis test with Dunn's multiple comparisons test.

Likewise, TAG in the media was higher ($p = 0.055$) after treatment with both 1000 and 2000 μM FAs compared to 0 μM, but values were similar (median of 3.0 nmol/mg protein for both 1000 μM and 2000 μM; Figure 4.3.1-2B). Only the addition of 2000 μM FAs resulted in a significantly higher media 3-OHB concentration than the 0 μM treatment ($p < 0.05$; Figure 4.3.1-2C). In line with this, expression of hepatic lipase (*LIPC*) was significantly higher after the 2000 μM treatment compared to 0 μM (Table 4.3.1-1), suggesting increased mobilisation of intracellular FA for oxidation. Light microscopy demonstrated similarities in lipid droplet accumulation in 0 and 200 μM treatments (Figure 4.3.1-2D & E) and 1000 and 2000 μM treatments (Figure 4.3.1-2F & G). Expression of LD genes was largely unchanged by FA treatment, although there were increases in *CIDEB* and *PLIN5* in cells treated with 2000 and 1000 μM, respectively (Table 4.3.1-1). To replicate *in vivo* physiology, where the liver would be exposed to FAs, 200 μM was chosen as a baseline 'low fat' FA concentration, since there were minimal differences compared to 0 μM.

4.3.1.3 The effect of media monosaccharide and FA concentration on cell viability

Cell viability was measured to ensure high concentrations of FAs and sugars were not toxic to cells. In order to replicate the intake of sucrose, fructose was added to the media in combination with glucose and different concentrations of FAs. Viability tended to increase with the addition of increasing FA concentrations up to 800 μM (Figure 4.3.1-3). However, in both glucose only, and glucose and fructose-treated cells, there was a reduction in viability when 1000 μM FAs were added. On the basis of these observations, 800 μM was chosen as the maximum concentration of FAs added to cells with 11 mM of glucose and 5.5 mM of fructose.

Table 4.3.1-1. The effect of fructose and fatty acids (FAs) on gene expression in Huh7 cells.

	0 µM	200 µM	1000 µM	2000 µM
Lipid droplet genes				
BSCL2	0.18 (0.17 - 0.21)	0.25 (0.25 - 0.27)	0.24 (0.23 - 0.29)	0.23 (0.18 - 0.27)
CIDEB	0.23 (0.21 - 0.28)	0.20 (0.20 - 0.23)*	0.29 (0.28 - 0.32)	0.33 (0.31 - 0.33)*
CIDEC	0.22 (0.19 - 0.26)	0.45 (0.40 - 0.48)	0.39 (0.36 - 0.44)	0.42 (0.42 - 0.52)
PLIN1	0.07 (0.06 - 0.11)	0.09 (0.08 - 0.12)	0.12 (0.10 - 0.14)	0.13 (0.11 - 0.19)
PLIN2	0.51 (0.27 - 1.08)	0.70 (0.41 - 0.82)	0.39 (0.20 - 0.51)	0.33 (0.23 - 0.35)
PLIN3	0.23 (0.23 - 0.28)†	0.30 (0.28 - 0.33)	0.28 (0.26 - 0.32)	0.33 (0.30 - 0.33)†
PLIN5	0.18 (0.10 - 0.21)*	0.32 (0.27 - 0.33)	0.34 (0.32 - 0.34)*	0.33 (0.31 - 0.34)
Fatty acid metabolism genes				
DGAT1	0.19 (0.14 - 0.19)	0.44 (0.37 - 0.45)	0.41 (0.38 - 0.45)	0.39 (0.38 - 0.39)
DGAT2	0.29 (0.29 - 0.31)	0.31 (0.27 - 0.31)	0.31 (0.30 - 0.34)	0.30 (0.29 - 0.34)
LIPC	0.31 (0.29 - 0.33)*	0.34 (0.33 - 0.37)	0.37 (0.32 - 0.39)	0.39 (0.38 - 0.39)*
MTTP	0.35 (0.33 - 0.53)	0.45 (0.38 - 0.46)	0.36 (0.30 - 0.43)	0.42 (0.37 - 0.43)

Upon reaching confluence, cells were cultured in 11 mM glucose and 2% HS for 7 days, before they continued to be cultured in this media for a further 7 days (0 µM FA) or in media with an additional 5.5 mM fructose and 200, 1000 or 2000 µM FA and 0.5 nM insulin. Media was changed every 48 to 72 hours and 24 hours prior to collection. All genes were expressed as a relative expression ratio to the mean control value and corrected to three reference genes (*B2M, HMBS* and *YWHAZ*). Data are presented as median (range), $n = 3$. Matching symbols denote significant differences between means * $p < 0.05$, † $p < 0.08$; Kruskal-Wallis test with Dunn's multiple comparisons test.

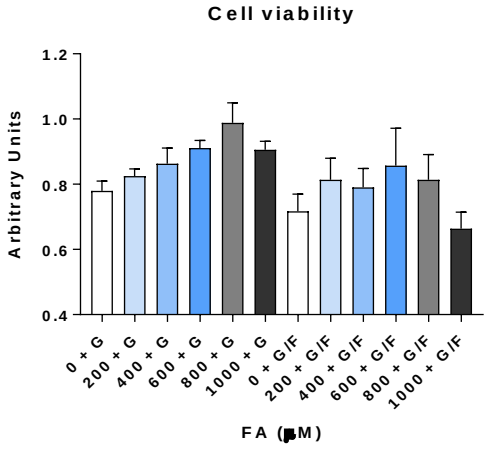


Figure 4.3.1-3. The effect of fructose and fatty acids (FA) on cell viability determined by a 3-(4,5-dimethylthiazol-2-yl)-2,5-diphenyltetrazolium bromide (MTT) assay in Huh7 cells. Upon reaching confluence, cells were cultured in 11 mM glucose and 2% HS for 7 days, before culture for another 7 days with 0.5 nM insulin and 0, 200, 400, 600, 800 or 1000 µM FA in media with 11 mM glucose only (G) or glucose with an additional 5.5 mM fructose (G/F). Media was changed every 48 to 72 hours and 24 hours prior to collection. Data are mean ± SD, $n = 5$ technical replicates.

4.3.2 Development of an *in vitro* model of macrovesicular steatosis

4.3.2.1 The effect of media composition on lipid droplet size

In order to determine whether the LD population was altered by different media compositions, LD size was assessed using the IN Cell Analyzer 6000. LDs were identified, counted and their area quantified. Absolute LD number did not differ significantly between treatments (LFLS: 32575 ± 2222, LFHS: 34673 ± 2794, HFHS: 37112 ± 2657; mean ± SEM). However, because of variation across passages, data was expressed relative to the mean LD count for each passage. In this case, there were significantly fewer LDs in the LFLS-treated compared to the LFHS and HFHS-treated cells (Figure 4.3.2-1A).

LDs were also stratified by area; there were significant differences between LD populations after media treatments. Cells treated with LFLS and LFHS media had significantly more small LDs (<1 μm^2) compared to HFHS-treated cells, and significantly fewer large LDs (2-200 μm^2; Figure 4.3.2-1C). These differences in LD size distribution were also evident from confocal microscopy (Figures 4.3.2-1D-F), although expression of LD proteins at the mRNA level was not altered (Table 4.3.2-1). When the LD population from HFHS cells was compared to primary cells isolated from fatty liver tissue (for method, see Appendix C, section C.1), primary cells had significantly more LDs between 10-50 μm^2, and fewer small LDs (1-2 μm^2), although the population distribution overall was similar (Figure 4.3.2-1B).

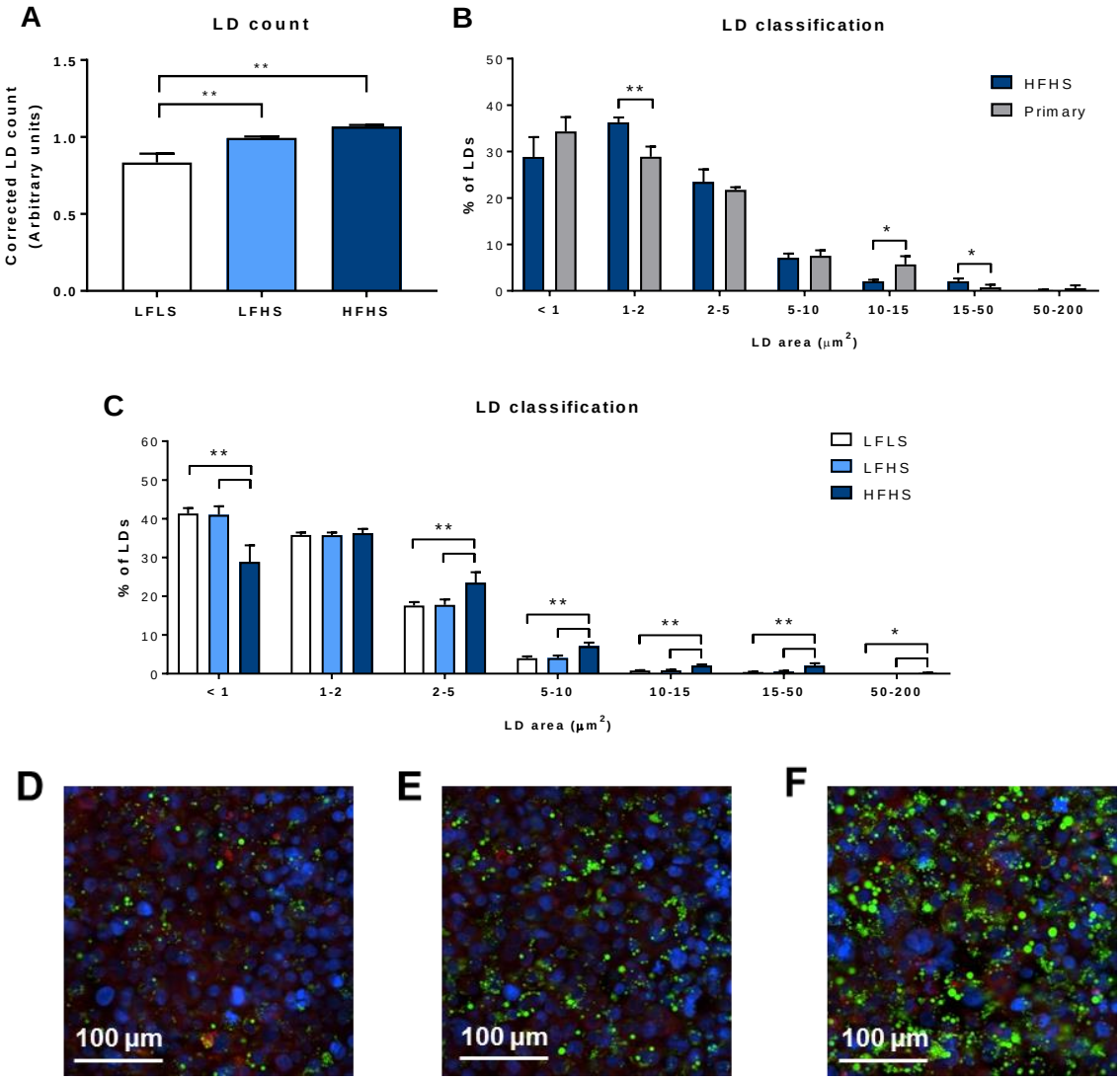


Figure 4.3.2-1. The effect of media composition on lipid droplet (LD) characteristics in Huh7 cells. Once confluent, cells were treated with media containing 2% human serum and 11 mM glucose for seven days before treatment media was added. Treatments consisted of either low fat low sugar (LFLS; 11 mM glucose + 200 µM fatty acids), low fat high sugar (LFHS; 200 µM fatty acids + 11 mM glucose + 5.5 mM fructose) or high fat high sugar (HFHS; 800 µM fatty acids + 11 mM glucose + 5.5 mM fructose); all treatments contained 0.5 nM insulin. LDs were identified, counted and their area quantified using the IN Cell Analyzer 6000. Total LD counts (**A**) were obtained and LD population was stratified by size (**C**). Primary hepatocytes isolated from liver tissue (one non-steatotic and two steatotic) were cultured for 24 hours and LD populations were compared to HFHS-treated cells (**B**). Cells were stained with Hoechst (nuclei; blue), BODIPY (LDs; green) and Mitotracker (mitochondria; red) and representative fluorescence images were obtained for cells treated with LFLS (**D**), LFHS (**E**) and HFHS (**F**) at 40X magnification. Data are mean ± SEM, $n = 6$ for Huh7 cells and $n = 3$ for primary cells. * $p < 0.05$, ** $p < 0.001$; two-way ANOVA with Bonferroni's multiple comparisons test.

Table 4.3.2-1. The effect of media composition on gene expression in Huh7 cells.

	LFLS	LFHS	HFHS
FA and TAG synthesis genes			
ACACA	1.08 ± 0.08[a]	1.02 ± 0.06[a]	0.72 ± 0.02[b]
ACACB	0.96 ± 0.04	0.89 ± 0.06	0.93 ± 0.04
DGAT1	0.91 ± 0.06	0.92 ± 0.07	0.79 ± 0.02
DGAT2	0.98 ± 0.06	1.09 ± 0.05	0.97 ± 0.05
FASN	0.88 ± 0.12	1.12 ± 0.17	0.87 ± 0.10
SCD	1.07 ± 0.06	1.31 ± 0.12	1.00 ± 0.10
FA elongation and desaturation genes			
ELOVL2	1.05 ± 0.04	0.98 ± 0.06	0.91 ± 0.04
ELOVL5	1.01 ± 0.01[a]	0.96 ± 0.03	0.89 ± 0.03[b]
ELOVL6	1.02 ± 0.09	1.05 ± 0.09	0.94 ± 0.05
FADS1	0.86 ± 0.03[a]	1.07 ± 0.06[b]	0.85 ± 0.05[a]
FADS2	0.97 ± 0.04	1.14 ± 0.06[a]	0.87 ± 0.04[b]
Lipid droplet protein genes			
BSCL2	0.79 ± 0.02	0.82 ± 0.04	0.80 ± 0.04
CIDEB	0.91 ± 0.11	1.06 ± 0.11	0.96 ± 0.07
CIDEC	0.91 ± 0.09	0.92 ± 0.11	0.99 ± 0.11
PLIN1	0.79 ± 0.05	0.98 ± 0.10	1.04 ± 0.09
PLIN2	0.95 ± 0.05	1.02 ± 0.05	0.99 ± 0.04
PLIN3	0.95 ± 0.04	1.06 ± 0.08	0.98 ± 0.07
PLIN5	0.78 ± 0.05	0.89 ± 0.05	0.92 ± 0.12
Hepatic nuclear receptors & transcription factors			
MLXIPL	0.95 ± 0.03	1.09 ± 0.08	0.97 ± 0.07
NR1H3	0.94 ± 0.03	1.07 ± 0.07	0.90 ± 0.06
NR1H4	0.93 ± 0.05	0.96 ± 0.06	0.91 ± 0.05
SREBF1	0.96 ± 0.06	1.15 ± 0.05[a]	0.81 ± 0.04[b]

Once confluent, cells were treated with media containing 2% human serum and 11 mM glucose for seven days before treatment media was added. Treatments consisted of either low fat low sugar (LFLS; 11 mM glucose + 200 μM fatty acids), low fat high sugar (LFHS; 200 μM fatty acids + 11 mM glucose + 5.5 mM fructose) or high fat high sugar (HFHS; 800 μM fatty acids + 11 mM glucose + 5.5 mM fructose); all treatments contained 0.5 nM insulin. All genes were expressed as a relative expression ratio to a pooled sample and corrected to three reference genes (*B2M*, *HMBS* and *YWHAZ*). Data are mean ± SEM, $n = 6$. Different letters denote significant differences between means, $p < 0.05$; two-way ANOVA with Bonferroni's multiple comparisons test.

4.3.2.2 The effect of media composition on FA synthesis and storage

To investigate how media composition affected FA synthesis and storage, intracellular TAG and DNL was measured. Although typically only C16:0 is measured to determine DNL, since C16:0 can be elongated to C18:0 and desaturated to C16:1*n*-7 and C18:1*n*-7/9, these FAs were also included in the determination of DNL (Wilke *et al.*, 2009). While there were no differences in intracellular TAG between the LFLS and LFHS conditions, there was significantly more TAG stored in the HFHS-treated cells compared to both LFLS and LFHS (Figure 4.3.2-2A). However, there were no differences in the total amount of TAG derived from DNL (Figure 4.3.2-2C), suggesting that the additional TAG resulted from the esterification of exogenous FAs. However, when TAG and PL fractions were combined, differences in total DNL-derived FAs between treatments were evident: HFHS-treated cells had a lower proportion of DNL-derived FAs compared to LFLS and LFHS-treated cells (both $p < 0.05$; Figure 4.3.2-2B & D). In line with this finding, expression of acetyl-CoA carboxylase 1 (*ACACA*) was significantly lower in cells treated with HFHS media compared to both LFLS and LFHS media ($p < 0.05$; Table 4.3.2-1). In addition, *SREBF1* was significantly higher in LFHS-treated cells compared to HFHS-treated cells, whilst differences in *SCD* followed the same pattern, although differences were not significant ($p = 0.10$; Table 4.3.2-1).

4.3.2.3 The effect of media composition on FA composition, elongation and desaturation

Differences in TAG accumulation were further investigated *via* analysis of FA composition. Cells treated with HFHS media had a significantly lower proportion of saturated FAs in their TAG fraction and a significantly higher proportion of polyunsaturated (PU)FAs ($p < 0.05$;

Table 4.3.2-2). Similar results were seen in the PL fraction, with HFHS-treated cell PLs also having a lower proportion of MUFAs ($p < 0.05$; Table 4.3.2-3; absolute values can be found in the Appendix C, Tables C.1 & C.2).

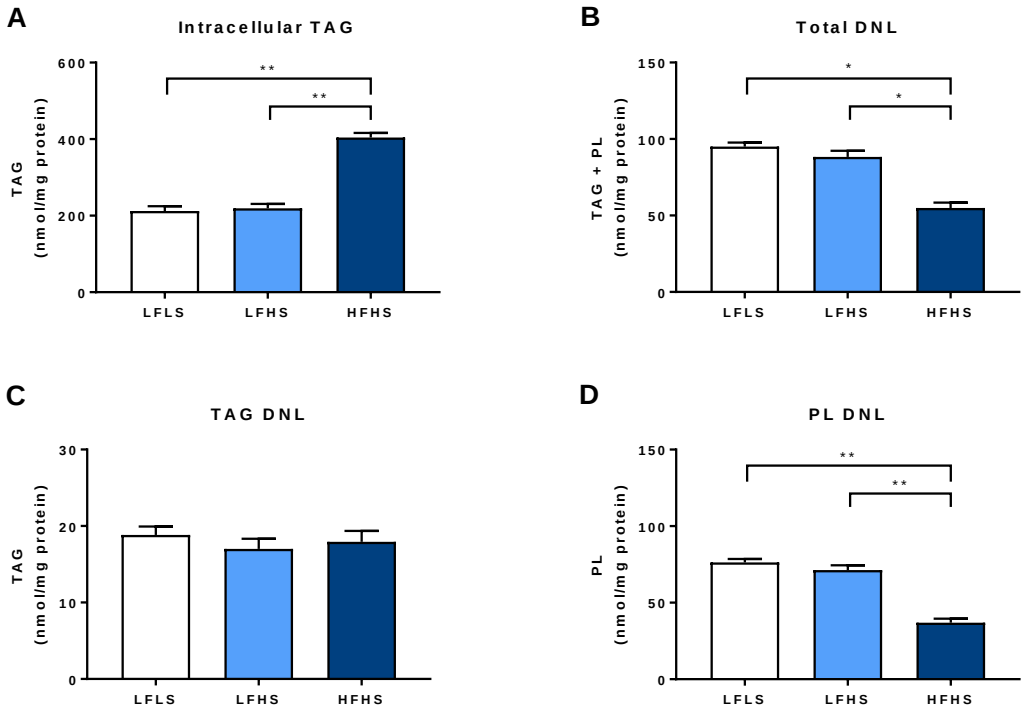


Figure 4.3.2-2. The effect of media composition on fatty acid (FA) synthesis and storage in Huh7 cells. Upon reaching confluence, cells were treated with media containing 2% human serum and 11 mM glucose for seven days before treatment media was added. Treatments consisted of either low fat low sugar (LFLS; 11 mM glucose + 200 µM FAs), low fat high sugar (LFHS; 200 µM FAs + 11 mM glucose + 5.5 mM fructose) or high fat high sugar (HFHS; 800 µM FAs + 11 mM glucose + 5.5 mM fructose); all treatments contained 0.5 nM insulin. Intracellular triacylglycerol (TAG; **A**) was measured. The contribution of *de novo* lipogenesis was calculated from deuterium appearance in C16:0, C16:1*n*-7, C18:0 and C18:1*n*-7 & 9 in total FAs (**B**), TAG (**C**) and PLs (**D**). Media was changed every 48 to 72 hours and 24 hours prior to collection and results are corrected to protein content. Data are mean ± SEM, $n = 6$. * $p < 0.05$; ** $p < 0.001$; two-way ANOVA with Bonferroni's multiple comparisons test.

Of the four exogenous FAs given to cells (C16:0, C18:1*n*-9, C18:2*n*-6 and C18:3*n*-3), only palmitate (C16:0) was present at significantly lower proportions in HFHS-treated cells compared to LF-treated cells in both TAG and PL fractions, suggesting cells were particularly efficient at further metabolising this FA.

In line with this, elongation and desaturation indices were significantly different in HFHS-treated cells. To avoid ratios being affected by the higher absolute amount of the precursor (16:0) in HFHS cells, only DNL-derived FAs that could be traced (*i.e.* C16:0, C16:1*n*-7, C18:0 and C18:1*n*-7/9) were used. The total FA pool from TAG and PLs showed that both the

Table 4.3.2-2. The effect of media composition on fatty acid composition of triacylglycerol in Huh7 cells (mol%)

	LFLS	LFHS	HFHS
C14:0	3.79 ± 0.13**	3.81 ± 0.10**	2.15 ± 0.07
C16:0	26.1 ± 0.38*	26.1 ± 0.45*	23.8 ± 0.21
C18:0	3.89 ± 0.16**	3.94 ± 0.15**	2.47 ± 0.10
SFA	**33.7 ± 0.65****	**33.9 ± 0.70****	**28.4 ± 0.38**
C16:1*n*-7	7.50 ± 0.11**	7.60 ± 0.06**	3.80 ± 0.07
C18:1*n*-9	38.0 ± 0.58**	38.4 ± 0.59**	45.3 ± 0.36
C18:1*n*-7	5.36 ± 0.09**	5.60 ± 0.10**	2.05 ± 0.12
C20:1*n*-9	0.51 ± 0.02	0.50 ± 0.02	0.49 ± 0.02
MUFA	**51.4 ± 0.45**	**52.1 ± 0.53**	**51.7 ± 0.23**
C18:2*n*-6	8.54 ± 0.18**	8.62 ± 0.17**	16.5 ± 0.18
C18:3*n*-6	3.58 ± 0.66*	2.75 ± 0.45*	0.81 ± 0.13
C18:3*n*-3	0.07 ± 0.02**	0.06 ± 0.02**	0.74 ± 0.03
C20:4*n*-6	0 ± 0**	0 ± 0**	0.20 ± 0.01
C20:5*n*-3	0.16 ± 0.03	0.10 ± 0.02	0.09 ± 0.01
PUFA	**12.3 ± 0.68****	**11.5 ± 0.42****	**18.3 ± 0.18**

Once confluent, cells were treated with media containing 2% human serum and 11 mM glucose for seven days before treatment media was added. Treatments consisted of either low fat low sugar (LFLS; 11 mM glucose + 200 μM fatty acids), low fat high sugar (LFHS; 200 μM fatty acids + 11 mM glucose + 5.5 mM fructose) or high fat high sugar (HFHS; 800 μM fatty acids + 11 mM glucose + 5.5 mM fructose); all treatments contained 0.5 nM insulin. Data are mean ± SEM, $n = 6$. * $p < 0.05$; ** $p < 0.001$ compared to HFHS-treated cells; two-way ANOVA with Bonferroni's multiple comparisons test.

desaturation (C16:1/C16:0) and elongation (C18:0/C16:0) ratios were higher in HFHS-treated cells (all $p < 0.05$; Figure 4.3.2-3A & B); these results were largely consistent within TAG and PL FAs (Appendix C, Figure C.1A-E). Despite being desaturated by the same enzyme as C16:0 (SCD), the C18:1/C18:0 ratio was significantly lower in HFHS cells compared to both low fat treatments, as well as in the LFHS treatment compared to LFLS (Figure 4.3.2-3C).

Table 4.3.2-3. The effect of media composition on fatty acid composition of phospholipids in Huh7 cells (mol%)

	LFLS	LFHS	HFHS
C14:0	0.40 ± 0.02**	0.37 ± 0.02**	0.15 ± 0.01
C16:0	26.4 ± 0.42*	26.2 ± 0.31*	24.1 ± 0.29
C18:0	16.2 ± 0.14**	16.5 ± 0.10*	17.2 ± 0.20
SFA	**43.0 ± 0.34***	**43.0 ± 0.27***	**41.5 ± 0.32**
C16:1*n*-7	2.97 ± 0.25**	2.53 ± 0.07**	0.83 ± 0.08
C18:1*n*-9	19.2 ± 0.15	19.3 ± 0.17	18.6 ± 0.28
C18:1*n*-7	3.51 ± 0.13**	3.50 ± 0.15**	1.57 ± 0.03
C20:1*n*-9	0.28 ± 0.02	0.30 ± 0.02	0.34 ± 0.02
MUFA	**26.0 ± 0.29****	**25.6 ± 0.08****	**21.4 ± 0.36**
C18:2*n*-6	17.2 ± 0.35**	17.1 ± 0.19**	24.7 ± 0.31
C18:3*n*-6	0.66 ± 0.09*	0.53 ± 0.02	0.38 ± 0.04
C18:3*n*-3	0.19 ± 0.01*	0.20 ± 0.01*	0.26 ± 0.02
C20:4*n*-6	4.52 ± 0.19*	4.84 ± 0.18	5.58 ± 0.28
C20:5*n*-3	0.44 ± 0.01*	0.45 ± 0.01*	0.51 ± 0.02
C22:5*n*-3	1.19 ± 0.05**	1.21 ± 0.06**	0.85 ± 0.05
C22:6*n*-3	0.70 ± 0.02**	0.73 ± 0.02*	0.82 ± 0.02
PUFA	**24.9 ± 0.45****	**25.1 ± 0.30****	**34.0 ± 0.97**

Once confluent, cells were treated with media containing 2% human serum and 11 mM glucose for seven days before treatment media was added. Treatments consisted of either low fat low sugar (LFLS; 11 mM glucose + 200 µM fatty acids), low fat high sugar (LFHS; 200 µM fatty acids + 11 mM glucose + 5.5 mM fructose) or high fat high sugar (HFHS; 800 µM fatty acids + 11 mM glucose + 5.5 mM fructose); all treatments contained 0.5 nM insulin. Data are mean ± SEM, $n = 6$. * $p < 0.05$; ** $p < 0.001$ compared to HFHS-treated cells; two-way ANOVA with Bonferroni's multiple comparisons test.

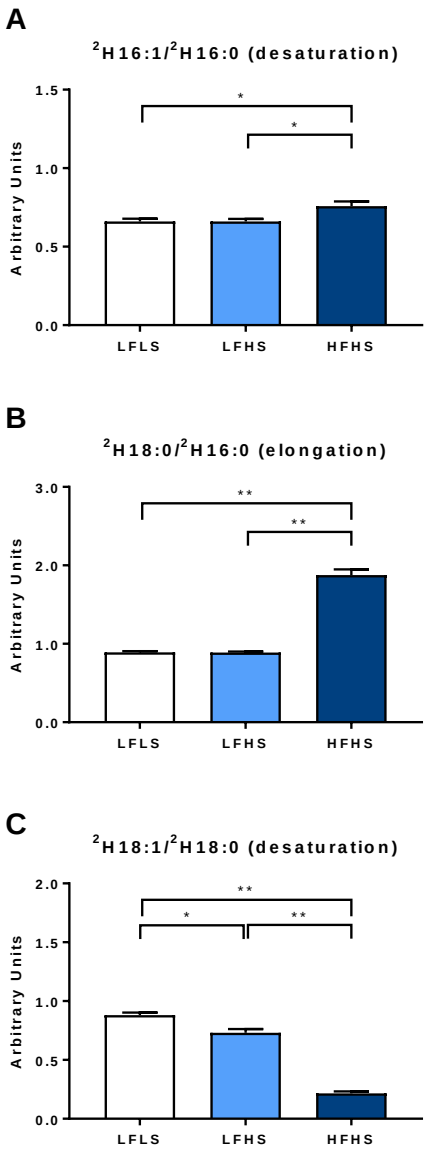


Figure 4.3.2-3. The effect of media composition on fatty acid (FA) metabolism in Huh7 cells. Upon reaching confluence, cells were treated with media containing 2% human serum and 11 mM glucose for seven days before treatment media was added. Treatments consisted of either low fat low sugar (LFLS; 11 mM glucose + 200 µM FAs), low fat high sugar (LFHS; 200 µM FAs + 11 mM glucose + 5.5 mM fructose) or high fat high sugar (HFHS; 800 µM FAs + 11 mM glucose + 5.5 mM fructose). The contribution of *de novo* lipogenesis was calculated from deuterium appearance in C16:0, C16:1*n*-7, C18:0 and C18:1*n*-7 & 9 and indices of C16:0 desaturation (**A**) and elongation (**B**) and C18:0 desaturation (**C**) were calculated. Media was changed every 48 to 72 hours and 24 hours prior to collection. Data are mean ± SEM, $n = 6$. * $p < 0.05$, ** $p < 0.001$; two-way ANOVA with Bonferroni's multiple comparisons test.

Although total proportion of PUFA content in HFHS cells was higher than LFLS and LFHS cells, there were differences in FA species. Particularly in PLs, HFHS-treated cells had differences in *n*-6 FAs, with more arachidonate (C20:4*n*-6) and less γ-linolenate (C18:3*n*-6) than LF-treated cells ($p < 0.05$; Table 4.3.2-3). Cells treated with HFHS media also had a significantly lower proportion of the *n*-3 FA docosapentaenoate acid (DPA; C22:5*n*-3), but higher proportions of eicosapentaenoic acid (EPA; C20:5*n*-3) and docosahexaenoic acid (DHA; C22:6*n*-3; Table 4.3.2-3). Overall, the PL *n*-6/*n*-3 ratio was higher in HFHS-treated cells compared to LF-treated cells (12.7 ± 0.25 *vs.* 8.89 ± 0.26 in LFLS and 8.70 ± 0.29 in LFHS, both $p < 0.001$). Gene expression in HFHS cells showed a significantly lower expression of *FADS1* and *2* compared to LFHS cells, and of *ELOVL5* compared to LFLS cells (all $p < 0.05$; Table 4.3.2-1).

4.3.2.4 The effect of media composition on lipoprotein secretion

One fate of mobilised FA within hepatocytes is secretion as VLDL particles, which, in steatosis, results in an increase in VLDL production. When TAG in the media was measured as a marker of TAG secretion, it was significantly higher in the media of HFHS-treated cells compared to LFLS and LFHS-treated cells ($p < 0.05$; Figure 4.3.2-4A). VLDL particles contain the apolipoprotein B100; however, apoB levels were not different between treatments, indicating more TAG per apoB particle (Figure 4.3.2-4B). In line with this, size-exclusion chromatography indicated that the HFHS-treated cells were capable of secreting VLDL (TAG-rich) particles. The majority of the TAG from these cells was secreted as VLDL, whereas LFLS and LFHS-treated cells secreted more LDL-sized particles (Figure 4.3.2-4C).

Similar results were seen in cholesterol content, with most cholesterol secreted in VLDL, rather than LDL, particles in HFHS compared to low fat-treated cells (Figure 4.3.2-4D).

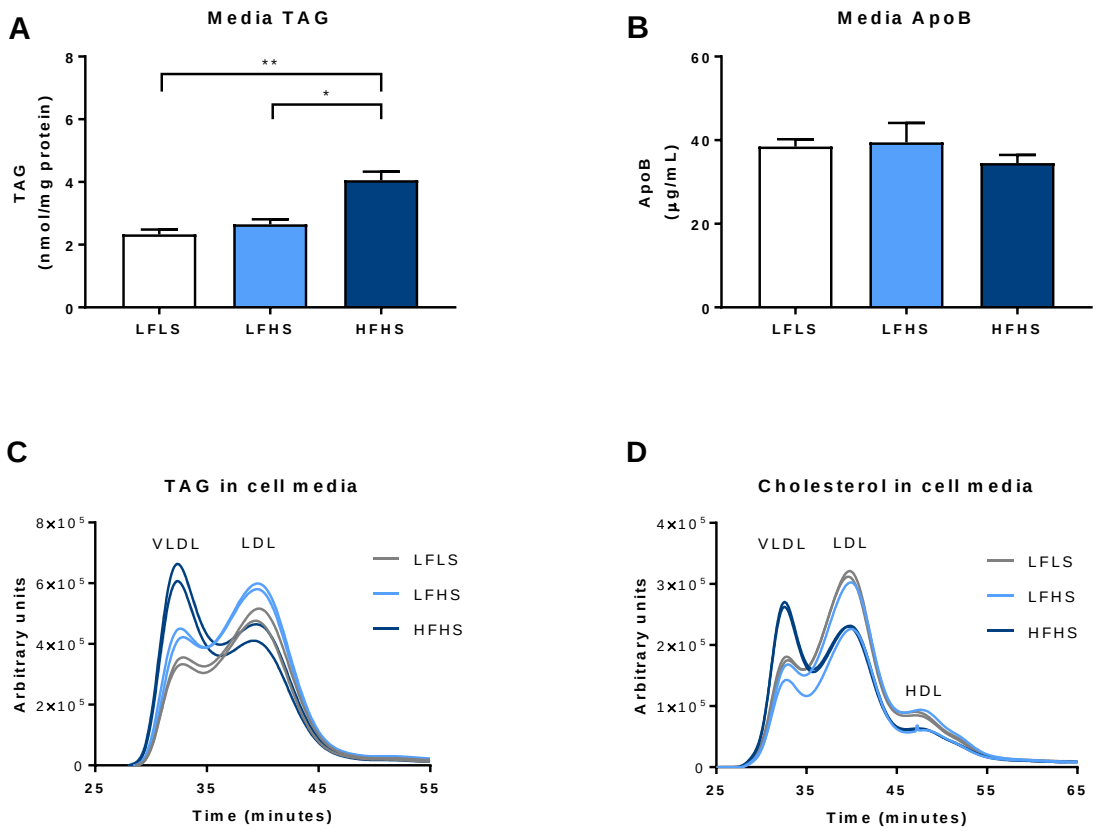


Figure 4.3.2-4. The effect of media composition on lipoprotein secretion. Upon reaching confluence, cells were treated with media containing 2% human serum and 11 mM glucose for seven days before treatment media was added. Treatments consisted of either low fat low sugar (LFLS; 11 mM glucose + 200 µM fatty acids), low fat high sugar (LFHS; 200 µM fatty acids + 11 mM glucose + 5.5 mM fructose) or high fat high sugar (HFHS; 800 µM fatty acids + 11 mM glucose + 5.5 mM fructose). Media triacylglycerol (TAG; **A**) and apoB (**B**) were measured as markers of secretion. Media TAG (**C**) and cholesterol (**D**) content were measured in lipoproteins of different sizes by size exclusion chromatography (SEC; $n = 2$). Media was changed every 48 to 72 hours and 24 hours prior to collection. For media TAG, results are corrected to protein content and data are mean ± SEM, $n = 6$. * $p < 0.05$, ** $p < 0.001$; two-way ANOVA with Bonferroni's multiple comparisons test. For media apoB, data are mean ± SD, $n = 2$; for curves, data from two replicates are presented. *ApoB and SEC curves were analysed by Professor Camilla Pramfalk at Karolinska Institutet, Sweden.*

4.3.2.5 The effect of media composition on FA oxidation and oxidative stress

Mobilised FA within hepatocytes may also be used for energy production: as a marker of FA oxidation, 3-OHB was measured in cell media. There was a significant increase in 3-OHB in the HFHS condition compared to the LFHS condition ($p < 0.05$), with a similar trend ($p = 0.09$) observed compared to the LFLS condition (Figure 4.3.2-5A). Elevated oxidative activity may result in oxidative stress within the cell; however, cellular 2',7'-dichlorofluorescein (DCF) fluorescence demonstrated no differences seen between treatments, a result confirmed with measurement of H_2O_2 *via* the ROS-Glo™ H_2O_2 Assay (Figure 4.3.2-5B & C).

4.3.2.6 The effect of media composition on glucose metabolism

Since the liver shows metabolic flexibility in substrate use, changes in FA metabolism may also alter glucose metabolism. HFHS-treated cells had significantly more intracellular glycogen than the LF-treated cells, and less media lactate (all $p < 0.05$; Figure 4.3.2-6A & B), suggesting that the provision of additional FAs diverted glucose away from anaerobic glycolysis and towards storage.

4.3.2.7 The effect of media monosaccharide and FA concentration on glucose and fructose disappearance

Finally, disappearance of glucose and fructose in the media was measured, to investigate how substrates were being used by cells. In both the LFHS and the HFHS condition, glucose concentration rapidly decreased over the first 16 hours in culture (Figure 4.3.2-7), with almost none detectable after 32 hours. In contrast, fructose disappearance was slower: after 48 hours, 2.85 ± 0.21 mM remained in HFHS media and 4.15 ± 0.07 mM in LFHS media (mean ± SD).

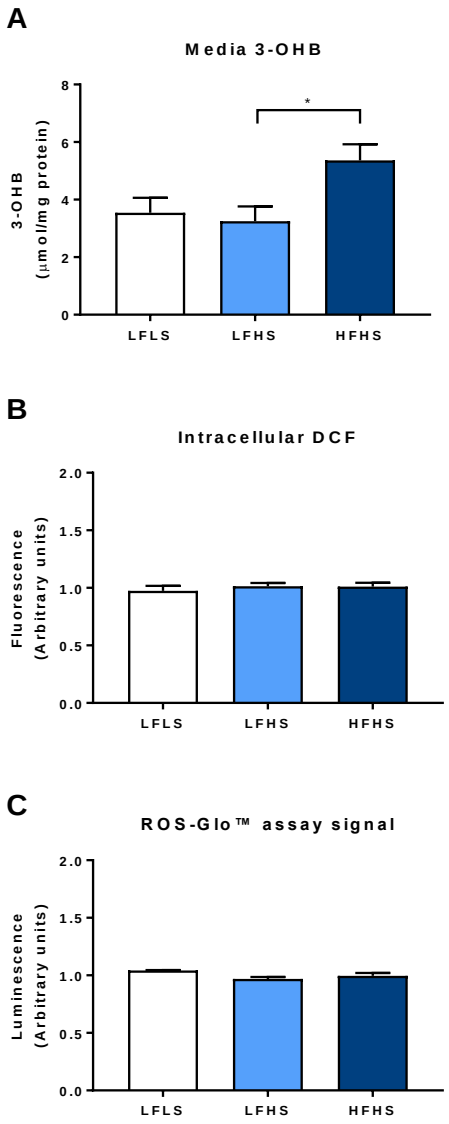


Figure 4.3.2-5. The effect of media composition on fatty acid (FA) oxidation and oxidative stress in Huh7 cells. Upon reaching confluence, cells were treated with media containing 2% human serum and 11 mM glucose for seven days before treatment media was added. Treatments consisted of either low fat low sugar (LFLS; 11 mM glucose + 200 µM FAs), low fat high sugar (LFHS; 200 µM FAs + 11 mM glucose + 5.5 mM fructose) or high fat high sugar (HFHS; 800 µM FAs + 11 mM glucose + 5.5 mM fructose); all treatments contained 0.5 nM insulin. Media 3-hydroxybutyrate (3-OHB; **A**), fluorescence of 2',7'-dichlorofluorescein (DCF; **B**) and ROS-Glo™ luminesce (**C**) were measured as markers of FA oxidation and oxidative stress, respectively. Media was changed every 48 to 72 hours and 24 hours prior to collection. 3-OHB results are corrected to protein content and ROS-Glo™ signal to Hoechst staining. Data are mean ± SEM, $n = 6$. * $p < 0.05$; two-way ANOVA with Bonferroni's multiple comparisons test.

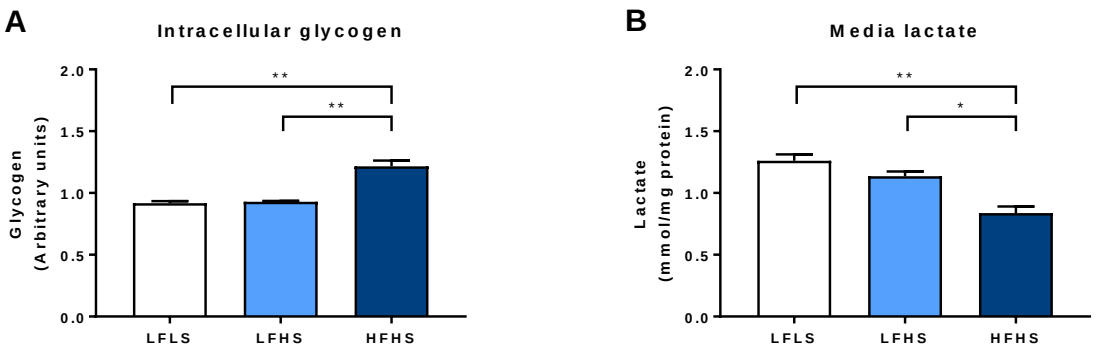


Figure 4.3.2-6. The effect of media composition on glucose metabolism in Huh7 cells. Upon reaching confluence, cells were treated with media containing 2% human serum and 11 mM glucose for seven days before treatment media was added. Treatments consisted of either low fat low sugar (LFLS; 11 mM glucose + 200 µM fatty acids), low fat high sugar (LFHS; 200 µM fatty acids + 11 mM glucose + 5.5 mM fructose) or high fat high sugar (HFHS; 800 µM fatty acids + 11 mM glucose + 5.5 mM fructose); all treatments contained 0.5 nM insulin. Intracellular glycogen (**A**) and media lactate (**B**) were measured as markers of glucose storage and anaerobic glycolysis, respectively. Media was changed every 48 to 72 hours and 24 hours prior to collection and results are corrected to nuclei staining (glycogen) or protein content (lactate). Data are mean ± SEM, $n = 6$. * $p < 0.05$, ** $p < 0.001$; two-way ANOVA with Bonferroni's multiple comparisons test.

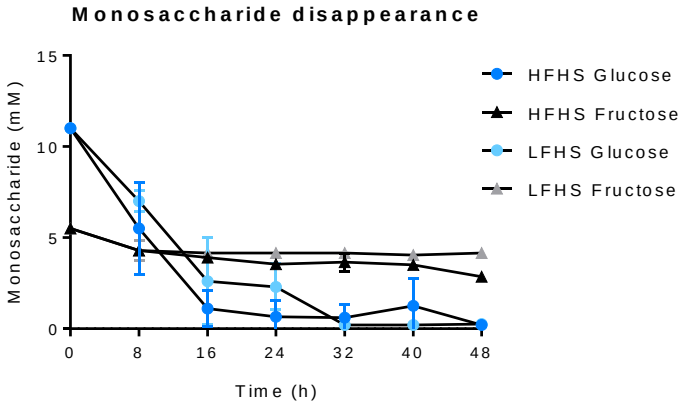


Figure 4.3.2-7. Disappearance of glucose and fructose in Huh7 cells. Upon reaching confluence, cells were treated with media containing 2% human serum and 11 mM glucose for seven days before treatment media was added. Treatments consisted of either low fat high sugar (LFHS; 200 µM fatty acids + 11 mM glucose + 5.5 mM fructose) or high fat high sugar (HFHS; 800 µM fatty acids + 11 mM glucose + 5.5 mM fructose); both treatments contained 0.5 nM insulin. Media was collected at 0, 8, 16, 24, 32, 40 and 48 h and concentration of glucose and fructose in the media was measured. Data are mean ± SD, $n = 2$.

4.4 DISCUSSION

The aims of this chapter were to create a physiological, *in vitro* model of TAG accumulation and macrovesicular steatosis in Huh7 cells using mixed substrate media and to investigate the effect of this media on metabolism. In line with previous studies that had specifically set out to create large LDs (Nativ *et al.*, 2013; Pawella *et al.*, 2014; Yarmush *et al.*, 2016), more than one dose of FA-containing media was required for maximal storage of TAG. However, we found a levelling off of intracellular TAG storage and a tendency toward reduced cell viability when media FAs were increased above 800 μM. Previous work has reported that treating primary rat hepatocytes and HepG2 cells with 4 mM palmitic and oleic acid over six days successfully induced macrovesicular steatosis in rat hepatocytes (Nativ *et al.*, 2013; Yarmush *et al.*, 2016). However the authors did not comment on the viability of the cells and the LD pattern was not reported in HepG2 cells. Our preliminary results suggested that such high levels of FAs are not utilised, resulting in 800 μM FAs being used for subsequent experiments.

Building on work from Chapter 3, 11 mM glucose was used as a baseline monosaccharide concentration. In addition, a 'high sugar' condition, containing an additional 5.5 mM fructose, was used. When given with a low level of FAs (200 μM), fructose had little impact on any metabolic parameters measured. Indeed, measurement of its disappearance from the media suggested that even after 48 hours approximately 3-4 mM of the 5.5 mM fructose remained in the media, compared to glucose, which was undetectable. Similar results have been found in HepG2 cells, where in the presence of 5 mM glucose, only a small quantity of the 20 mM fructose provided was taken up (Maldonado, 2016). This preference for glucose

may be due to hepatoma cells having high expression of the GLUT1 and GLUT12 transporters (Brito *et al.*, 2015), which have a high affinity for glucose (Mueckler & Thorens, 2013), whereas GLUT2, which transports both glucose and fructose, is predominantly expressed in healthy liver (Karim *et al.*, 2012).

Despite low levels of fructose uptake, there was still an effect of fructose at the gene expression level, with *SREBF1*, a key regulator in DNL, more highly expressed in the LFHS condition compared to the HFHS condition. The *SREBF1* targets *FADS1* and *FADS2* were also upregulated, while *SCD* showed a trend toward increased expression in LFHS-treated cells. To date, *in vitro* literature regarding the lipogenic effects of fructose is conflicting (Gnocchi *et al.*, 2014; Hirahatake *et al.*, 2011; Huang *et al.*, 2011; Lanaspa *et al.*, 2012), while human studies where a fructose intervention diet is fed in isocaloric amounts relative to a control diet, do not support fructose as a cause of liver fat accumulation (Chiu *et al.*, 2014; Chung *et al.*, 2014; Ter Horst & Serlie, 2017). Nonetheless, the present data supports one of the proposed pathways of fructose-induced lipogenesis, which is to upregulate DNL genes; however, it may be that in association with high FA levels, the inhibitory effects of unsaturated FAs on *SREBF1* expression (Hannah *et al.*, 2001; Shimano & Sato, 2017) balances any stimulatory effect that fructose has.

Addition of 800 μM FAs to the media resulted in increased total TAG accumulation, with the quantity of intracellular TAG in the HFHS-treated cells placing them in the 'NAFL2' grade of steatosis based on previously defined cut-offs (220 - 465.5 nmol/mg of protein) (Chiappini *et al.*, 2017; Peng *et al.*, 2015). The LFLS and LFHS-treated cells would also be defined as

steatotic by these guidelines, (> 41.7 nmol/mg protein) (Chiappini *et al.*, 2017), although the proportion of larger LDs in HFHS cells demonstrate a more macrosteatotic phenotype under this condition. Despite this, expression of LD proteins were unchanged, except for a trend of increased *PLIN1* expression in HFHS-treated cells compared the LFLS condition. *PLIN1* is not normally expressed in hepatocytes, but is expressed in adipocytes; however, in macrovesicular steatosis, PLIN1 expression is increased as LDs increase in size (Straub *et al.*, 2008). Previously, long term culture (up to 40 days) of Huh7 cells with a combination of DMSO and a preadipocyte-adipocyte differentiation medium increased the expression of PLIN1 (Pawella *et al.*, 2014); it is therefore possible that longer culture time would have resulted in even larger LDs forming in the HFHS condition. When culture time was extended to 10 and 14 days, LD size did appear to increase, although this was not quantified (Appendix C, Figure C.2A-C). Use of extended culture time to create larger LDs could, therefore, be considered for future models.

HFHS-treated cells also had an LD pattern similar to that seen in primary hepatocytes isolated from fatty liver tissue, although these LDs are still smaller than those seen in histology samples from fatty livers (up to 5000 μm^2; Appendix C, Figure C.3). When isolating cells from transplant-rejected fatty livers, we found very poor viability of hepatocytes where severe steatosis is present. It is likely that the 3D architecture of the liver allows these LDs to form, and once broken down, a single cell can no longer facilitate large LDs. As a result, it's possible that primary hepatocytes successfully isolated and cultured from fatty livers represent a population with small LDs. Histology commonly shows heterogeneity in LD size across liver tissue (Appendix C, Figure C.4A-C); if subpopulations of hepatocytes with different LD sizes

are primarily located in different regions (*i.e.* periportal or pericentral), primary hepatocytes successfully isolated may not be representative of the whole liver. The potential of single-cell technologies to further investigate and phenotype different hepatocyte populations would help to elucidate how biased toward cells with small LDs current methods of hepatocyte isolation are.

As well as HFHS-treated cells, LFHS-treated cells appeared to have a higher number of LDs than LFLS-treated cells, although the size distribution of LDs and total area of LDs was unaffected. LDs have a core of neutral lipids, namely TAG and CEs; however, neither intracellular TAG nor cholesterol was different in response to LFLS and LFHS treatments. Likewise, expression of LD proteins at RNA level were not different between the low fat treatments. Further stratification of the smallest LDs (into <0.75 and 0.75-1 μm^2) did not reveal any difference between LFLS and LFHS-treated cells (data not shown). Similar to the gene expression data, it may be that the addition of fructose exerts a subtle effect on LD accumulation, which is only evident in the measurement of certain parameters.

In response to high levels of FA in the cell media, contribution of DNL FAs to the cellular FA pool was significantly reduced. Unsaturated FAs are known to inhibit/downregulate DNL through liver X receptor and SREBP-1c (Dentin *et al.*, 2008; Hannah *et al.*, 2001; Ye & DeBose-Boyd, 2011), while increasing levels of palmitate have been shown to down-regulate DNL in human adipocytes (Collins *et al.*, 2011). Nonetheless, in human NAFLD, DNL is increased in the presence of 'selective' IR, where lipogenic and gluconeogenic pathways are upregulated (Schwarz *et al.*, 2003). In our model, all treatments had the same amount of

insulin added to the media (0.5 nM), meaning that any effect of systemic hyperinsulinaemia were not distinguishable. In response to these results, the HFHS condition was repeated with both 1 nM and 10 nM insulin; however, DNL was not affected. That this substantial increase in insulin did not further stimulate DNL suggests that the cells may be at their maximum capacity, or, similarly to the results obtained with HS (Chapter 3), that the provision of exogenous FAs inhibits DNL in cells while insulin has a minimal stimulatory effect. The extent to which DNL is controlled by insulin signalling in these cells requires further investigation.

The secreted lipoprotein profile was affected by the addition of FAs to the media. Previous work has demonstrated that supplying exogenous FAs to culture media improves lipoprotein secretion in both HepG2 and Huh7 cells (Dashti *et al.*, 1987; Ellsworth *et al.*, 1986; Meex *et al.*, 2011; Wu *et al.*, 1996). As shown in Chapter 3, use of HS in the culture media improved total TAG secretion, and lipoprotein lipidation in HepG2 and Huh7/7.5 cells (Gunn *et al.*, 2017; Pramfalk *et al.*, 2016; Steenbergen *et al.*, 2013). The combination of both HS and FAs in the current model not only resulted in cells secreting VLDL-sized particles under all treatments, but the HFHS-treated cells secreted the majority of TAG and cholesterol as VLDL particles. Although the use of HS over 30 days has previously been shown to replicate TAG and cholesterol lipoprotein profiles of human blood in Huh7 cells (Steenbergen *et al.*, 2013), experimental evidence is limited. The present results show that with the addition of FAs to the media, lipoprotein profiles can be improved over a much shorter time frame and replicates the increase in TAG secretion seen *in vivo* in humans in response to increased hepatic TAG storage (Fabbrini *et al.*, 2008).

The provision of additional FAs in the media of HFHS-treated cells also resulted in an increase in FA oxidation, as measured by 3-OHB in the media. Despite this increase, ROS levels were not changed. It has recently been proposed that as a result of the fat accumulation characteristic of NAFLD, there is an initial increase in mitochondrial activity in order to dispose of FA, before the mitochondria become overloaded, oxidative stress occurs and mitochondrial activity decreases (Koliaki *et al.*, 2015; Peng *et al.*, 2018). This dynamic response of mitochondrial activity to steatosis may explain the inconclusive evidence on whether there is increased or decreased FA oxidation in human NAFLD (Fabbrini & Magkos, 2015). There is, however, evidence that ROS plays a key role in NAFLD pathogenesis, and particularly its progression to NASH (Koliaki *et al.*, 2015; Peng *et al.*, 2018; Polimeni *et al.*, 2015; Spahis *et al.*, 2017). It may be that in our model, although mitochondrial activity is increased, it is not yet overloaded to the point where oxidative stress occurs.

A shift away from glycolysis towards β-oxidation and a reduction in DNL in HFHS cells resulted in partitioning of glucose toward glycogen storage. Glycogenesis is an insulin-stimulated process, and although data on hepatic glycogen storage in NAFLD patients is limited, it is believed that glucose is directed away from glycogen storage toward DNL (Byrne & Targher, 2015). This can stem from selective IR within the liver, or peripheral IR, which prevents glucose being used for synthesis of muscle glycogen (Byrne & Targher, 2015; Fabbrini & Magkos, 2015). Indeed, disruption of glycogen synthesis in primary mouse hepatocytes caused increased lipogenesis and IR, implying reduced glycogen synthesis could be causal in the hepatic IR present in NAFLD (Irimia *et al.*, 2017). Given that the HFHS cells

were able to dispose of glucose *via* glycogen synthesis, this may also explain why DNL was not elevated in HFHS-treated cells.

A common approach to induce hepatocyte lipid accumulation and cellular stress in cell models of NAFLD is the addition of oleate and palmitate to the cell media; in previous studies this resulted in increased lipid accumulation, inflammatory markers and ROS (Chavez-Tapia *et al.*, 2012; Cui *et al.*, 2010; Kostrzewski *et al.*, 2017). In contrast, when given in combination with linoleate and α-linolenate, we found that cells were able to tolerate high concentrations of FAs despite lipid accumulation. Neither ROS, nor preliminary data collected for IL-8 secretion (see Appendix C, Figure C.5), showed any change under the HFHS condition. This data supports existing literature, which showed that when given in combination with linoleate, palmitate did not induce the same inflammatory response in Huh7 cells as it did when given alone (Maruyama *et al.*, 2014). The authors reported that this was due to linoleate reducing activation of c-Jun N-terminal kinase by palmitate, a pathway also linked to apoptosis (Sommerfeld *et al.*, 2015); this may explain the good viability seen in our results, even at high concentrations of FAs.

Apart from the anti-inflammatory effects of linoleate, we also found that cells adapted to high palmitate concentrations: despite being exposed to a fourfold higher concentration of palmitate, HFHS-treated cells had a significantly lower proportion of intracellular palmitate, as opposed to significantly higher levels of oleate, linoleate and α-linolenate. This suggests that the cells were highly efficient in further metabolising palmitate *via* desaturation or elongation, or partitioning palmitate towards oxidation and secretion. Analysis of PL

composition also showed that there was a significantly lower proportion of saturated FAs in PLs of HFHS-treated cells and no significant difference in absolute amounts. Due to their effect on membrane fluidity, having saturated FAs in PL membranes are considered potentially pathogenic, while presence of unsaturated FAs improve fluidity (Stubbs & Smith, 1984). In the HFHS condition, the remodelling of PLs to contain more PUFAs and less SFAs and MUFAs may support the idea that cells are able to adapt to the high quantity of FAs they have been exposed to. Although the *n*-6/*n*-3 ratio of PLs was significantly higher in HFHS-treated cells, which is associated with a proinflammatory state and has been reported in PLs of NAFLD patients compared to controls upon liver biopsy (Araya *et al.*, 2004; Elizondo *et al.*, 2007), we did not note any detrimental effects of this change.

Although we measured a large number of metabolic parameters in this chapter, there were some limitations to the work. Firstly, we only measured media 3-OHB as a marker of FA oxidation. When FAs are oxidised *via* β-oxidation, acetyl-CoA is produced: a major pathway for this is further condensation to ketone bodies, one of which is 3-OHB. Although this is a well-established marker for hepatic FA oxidation, it does not account for the proportion of acetyl-CoA that enters the electron transport chain and results in CO_2 production, meaning differences in this pathway were not accounted for. In addition, we did not measure insulin sensitivity in the samples analysed in this chapter. Data from Chapter 3 suggest that Huh7 cells cultured in HS are insulin-sensitive, however, we cannot be sure of the effect of the 7-day FA treatment on insulin signalling. Due to the time required to culture and insulin-stimulate samples for analysis, it was not pursued for the present results, but will be considered in future studies.

4.5 SUMMARY

- Repeated doses of a high concentration of a physiological mix of FAs was well tolerated by cells and promoted maximal FA storage and LD size
- The combination of HS-containing media, mixed substrates including essential FAs and longer culture time facilitated a more physiological profile of FA metabolism
- The highest dose of FAs (800 μM) in association with glucose (11 mM) and fructose (5.5 mM) promoted formation of larger LDs that had a similar distribution to primary hepatocytes
- This condition also resulted in metabolic changes including elevated lipoprotein secretion and FA oxidation, but no change in DNL, ROS or cytokine production
- This model therefore offers a relatively benign steatosis phenotype in which to investigate pathogenic effects of gene editing

Chapter 5

Investigating the interaction between DGAT2 activity and substrate availability *in vitro*

5.1 INTRODUCTION

Diacylglycerol acyltransferase (DGAT) carries out the final step of triacylglycerol (TAG) synthesis, catalysing the addition of a fatty acyl-CoA to diacylglycerol (DAG). Two isoforms of DGAT exist, 1 and 2, which both carry out this function, although they differ significantly in sequence homology, cellular topology and tissue expression (Cases *et al.*, 1998; Cases *et al.*, 2001; Lardizabal *et al.*, 2001) (reviewed in Chapter 1, section 1.2). The differences in topology, with DGAT2 present on lipid droplets (LDs) and appearing to have more cytosolic activity, while DGAT1 has both cytosolic and luminal activity at the ER, have been suggested to contribute to preferential growth of cytosolic and luminal LDs, respectively. Based on the differences in expression pattern, some of the earliest work investigating DGAT activities hypothesised that DGAT1 was particularly important in intestinal TAG re-esterification, while DGAT2 used *de novo*-synthesised fatty acids and was vital in very low-density lipoprotein (VLDL) assembly in the liver (Meegalla *et al.*, 2002). Subsequent work in animal and *in vitro* models has offered some experimental support to this hypothesis, although not all evidence is conclusive.

The findings relating to the role of DGAT2 in *de novo* lipogenesis (DNL) appear consistent across a number of models. DGAT inhibition in HepG2 cells incubated with isotope tracers demonstrated reduced DNL: this was especially evident when DGAT2 activity was reduced (Qi *et al.*, 2012; Wurie *et al.*, 2012). Tracer work in mouse models has also shown suppressed DNL when DGAT2 activity is reduced *in vivo* (Qi *et al.*, 2012) and *in vitro* (Choi *et al.*, 2007; Yu *et al.*, 2014), while *Dgat1*$^{-/-}$ mice were protected from steatosis after increased exogenously-

derived FAs, but not endogenously-derived (Villanueva *et al.*, 2009). In addition, DNL-related genes have demonstrated concomitant up or downregulation in association with changes in *Dgat2* expression in mice (Choi *et al.*, 2007; Jornayvaz *et al.*, 2011; Qi *et al.*, 2012; Yu *et al.*, 2005). This, along with the observation of colocalisation of DGAT2 and SCD1 (Man *et al.*, 2006), further supports the assertion that DGAT2 may preferentially use DNL-derived FAs as a substrate.

However, the roles of the DGAT enzymes in VLDL secretion and oxidation remain unclear. There is evidence that both DGAT1 and DGAT2 have regulatory roles in VLDL secretion in *in vitro* and *in vivo* animal models (Choi *et al.*, 2007; Liang *et al.*, 2004; Yamazaki *et al.*, 2005; Yu *et al.*, 2005). In primary human hepatocytes, use of DGAT inhibitors suggested that DGAT2 was rate-limiting in VLDL secretion (Li *et al.*, 2015a), but this has not been confirmed in the same model more recently (McLaren *et al.*, 2018). Interestingly, human DGAT1 loss-of-function is associated with hypertriglyceridaemia, which is hypothesised to result from increased activity of DGAT2 and subsequent VLDL production (Haas *et al.*, 2012; Stephen *et al.*, 2016). Paradoxically, DGAT1 is thought to have more luminal activity at the ER, contributing towards luminal LDs that would lipidate primordial VLDL particles before secretion (Bhatt-Wessel *et al.*, 2018). Although study of FA oxidation is limited, reduction in DGAT2 activity particularly appears to increase FA oxidation (Choi *et al.*, 2007; Li *et al.*, 2015a; McLaren *et al.*, 2018; Yu *et al.*, 2005), potentially through an inhibition of DNL.

Given this background and preliminary results from the Oxford Biobank (Karpe *et al.*, 2018) linking a DGAT2 mutation to adverse metabolic parameters, the aims of this chapter were:

1. To establish models of altered DGAT2 activity using both knockdown (siRNA) and knockout (CRISPR-Cas9) technologies
2. To investigate the metabolic effects of, and interaction between, nutritional substrates and changes in DGAT2 activity

5.2 METHODS

5.2.1 CRISPR-Cas9 modification of Huh7 cells

This work was carried out by Dr. Tomas Jakobsson and Professor Camilla Pramfalk at Karolinska Institutet, Sweden. The protocol used for CRISPR-Cas9 editing is based on a published method (Ran et al., 2013b) and is summarised below.

CRISPR-Cas9 is a powerful technology that can be used to edit an organism's genome. First observed in the DNA of bacteria in 1987 (Mojica *et al.*, 1993), Clustered Regularly Interspaced Short Palindromic Repeats (CRISPR) have now been established as places where viral DNA are stored in a form of immune memory (Barrangou *et al.*, 2007). When the bacteria is infected again, these sequences, which identify viral DNA, are transcribed and processed into small CRISPR RNAs (crRNAs), which can form a complex with a DNA nuclease, Cas (CRISPR-associated) 9. Upon identifying matching DNA, the Cas9-crRNA complex begins to make cuts in order to disable the virus. Protospacer-adjacent motif (PAM) sites adjacent to the target gene are required for the Cas9 to cut, which stop the complex targeting the bacteria's own CRISPR sequences (Doudna & Charpentier, 2014).

It has now been established that by complexing artificial, guide RNAs (gRNA) with Cas9, any part of an organism's genome can be cut (Jinek *et al.*, 2012). When this occurs, the organism tries to repair this break; however, although the break in the DNA can be repaired through non-homologous end joining (NHEJ), the length and sequence of base pairs will be different, resulting in insertion/deletion (*indel*) mutations. Within coding exons, a frameshift mutation

and premature stop codon can result, which prevents transcription and translation, therefore 'knocking out' the gene. Homology-directed repair (HDR) requires the provision of a repair template, which, if successful, will be used by the organism to repair the break in DNA elicited by Cas9, allowing mutations of interest (*e.g.* SNPs) to be inserted or removed from an organisms DNA (Ran *et al.*, 2013b).

5.2.1.1 Design of targeting components for the CRISPR/Cas9 system and transfection of Huh7 cells

Reagents were purchased from Thermo Fisher Scientific; Hemel Hempstead, UK, unless otherwise stated. Single-guide (sg)RNAs upstream of a PAM sequence (5'-NGG) in the early exons of *DGAT2* were selected and off-targets were identified using the CRISPR design tool (Zhang lab; http://crispr.mit.edu/). A double nicking strategy was used, which introduces two, targeted single-strand nicks, rather than a single, double-strand break. Since both nicks would have to be aligned in order for NHEJ to occur, this doubles the specificity of the target and greatly reduces off-target effects (Ran *et al.*, 2013a). The sgRNA sequences for allele 1 (sgRNA_A #6; Figure 5.3.1.1A) were 5'-GCCCGGAGTAGGCGGCTATGA-3' and 5'-CGGGCCTCATCCGCCGATACT-3', and for allele 2 (sgRNA_B #6; Figure 5.3.1.1A), 5'-GCGCGGCGAGCGTCAGGCCG-3' and 5'-CGCGCCGCTCGCAGTCCGGC-3'. An extra G was appended at the 5′ of the sgRNA where the guide sequence did not begin with G and a BpiI (BbsI) site was inserted at the 5' end for cloning into a GFP-tagged vector, pSpCas9n(BB)-2A-GFP (PX461; Addgene; MA, USA). To do this, sgRNAs were annealed and the PX461 vector digested with FastDigest BbsI before ligation of the annealed sgRNAs and digested plasmid. This was then transformed into competent cells and clones that were picked

were, after purification, sent for sequencing to verify that they contained the correct insert. Huh7 cells were seeded into 6-well plates 24 hours prior to transfection. Plasmids containing the sgRNA were transfected by combining 2 μg of the plasmids with 8 μL Lipofectamine CRISPRMAX reagent in Opti-MEM so that a total of 1 mL was added per well for 5 hours, before being removed and normal culturing media added for 48 hours.

5.2.1.2 Functional validation of sgRNA

Upon collection, cells were washed with PBS and trypsinised, before centrifugation at 800 rpm (300 x g) for 5 minutes. Cells were resuspended in PBS with 2% penicillin-streptomycin, passed through cell strainers and put on ice. Next, SYTOX™ Green was added to the cell suspension at a ratio of 1:5000 to identify dead cells, and fluorescence-activated cell sorting (FACS) for GFP was carried out. Sorted cells were centrifuged at 300 x g for 5 minutes and plated into 24-well plates, before expanding into T25 flasks. After this, gDNA was isolated from edited and wildtype (WT) cells using the DNeasy blood and tissue kit from Qiagen (QIAGEN Sciences; MD, USA) and the SURVEYOR nuclease assay was carried out. This assay uses polymerase chain reaction (PCR; see Chapter 6, section 6.2.1) to detect base substitutions and *indels*. Primers were designed using the CRISPR design tool (Zhang lab; http://crispr.mit.edu/) as follows; forward primer: 5'-GCTGGGGTCTAGGCTGTTTC-3', reverse primer: 5'-GAAGGGAGAGGGGAGGGAAG-3'. Regions 200-400 bp either side of the Cas9 target were amplified in both WT and edited cells, before PCR products were purified. Next, samples underwent hybridization using 1X Taq PCR buffer, which allows strands from WT and edited cells to form a heteroduplex, before the SURVEYOR Nuclease

and Enhancer were added to the annealed product 1:25 and incubated for 30 minutes at 42°C. SURVEYOR Nuclease cleaves the heteroduplex where a mismatch occurs (*i.e.* where the sequence of edited cells differ to the WT cells). Samples were then run through a 10% Tris borate EDTA gel *via* gel electrophoresis at 200V for 45 minutes, and cleaved products were visualised by incubating the gel for 30 mins in 1X SYBR® Gold Nucleic Acid Gel Stain.

5.2.1.3 Culturing and sequencing of edited cells

A confluent flask of a heterogeneous (WT and edited cells) was washed and trypsinised, before centrifugation at 300 x g for 5 minutes. The cell pellet was resuspended in media and cells were counted. In order to culture single cell colonies, the cell suspension was diluted such that there were 0.5 cells plated per well in a 96-well plate. Media was changed every 2-4 days until single cell colonies could be identified, and, once confluent, the wells that had originated from a single cell colony were trypsinised. These were first reseeded into a 12-well plate and when these became confluent, into a T25 flask. For DNA sequencing, cells were trypsinised and centrifuged at 300 x g for 5 minutes; media was removed and the pellet was frozen at -20°C until analysis. DNA was isolated using the DNeasy blood and tissue kit from Qiagen. The same primers that were used for the SURVEYOR assay were used for PCR amplification of the Cas9-targeted region. PCR products then had 3' A overhangs added and were cloned into TOPO pCR-II vectors, to ensure full and accurate sequencing for each allele. Colonies were grown, isolated and inoculated, before centrifugation and isolation of plasmid DNA using the QIAprep Spin Miniprep for sequencing (QIAGEN Sciences; MD, USA).

5.2.2 siRNA knockdown of *DGAT2*

Small interfering RNA (siRNA) are double stranded RNA molecules that prevent translation of target genes, reducing their protein expression. Once inside the cell, siRNA is unwound to form single-stranded RNA, before becoming part of the RNA-induced silencing complex (RISC). Endogenous RNA complementary to the siRNA contained within the RISC is identified and cleaved, causing it to be degraded and preventing translation and protein expression. siRNA is delivered to the cell *via* a lipid-based transfection reagent.

5.2.2.1 Optimisation with siGLO Green Transfection Indicator

Reagents were purchased from Dharmacon, GE Healthcare Life Sciences; CO, USA, unless otherwise stated. In order to optimise siRNA and transfection reagent concentrations to treat cells with, siGLO Green Transfection Indicator was used. This is a fluorescent, RISC-independent, oligonucleotide duplex that localises to the nucleus to confirm transfection.

Cells were seeded into 96-well, black-walled plates and grown to confluence. After this, media was changed to HS-containing media, and cells were cultured for seven days with media changes every 48-72 hours. After this, Dharmafect 4, recommended for Huh7 cells, was combined with Opti-MEM (Thermo Fisher Scientific; Hemel Hempstead, UK) at a 10X concentration and incubated at room temperature for 5 minutes. siRNA was also diluted in Opti-MEM at a 10X concentration and incubated at RT for 5 minutes. Transfection reagent and siRNA were then combined at a 1:1 ratio (1:2 dilution) and incubated at RT for 20 minutes. For Dharmafect-only controls, diluted transfection reagent was combined with equal parts Opti-MEM. After this, the siRNA and transfection reagent mix was diluted 1:5

(therefore total dilution of 1:10) in penicillin-streptomycin and serum-free media. Treatments were added to wells in triplicate and left for 24 or 48 hours. After this, media was changed to low fat low sugar (LFLS) media and fluorescence was read at 494/520 nm. If required, cells were returned to the incubator and LFLS media was replenished every 48 hours, before fluorescence was read again after seven days.

5.2.2.2 DGAT2 knockdown

ON-TARGET*plus* siRNA was used for DGAT2 knockdown studies. ON-TARGET*plus* siRNA uses four individual RNA sequences to increase potency of knockdown studies. In addition, by phosphorylating the antisense strand to increase RISC association and adding a 2′-*O*-methyl modification within the seed region, specificity is improved and off-target effects are reduced. Furthermore, 2′-*O*-methyl modifications of the sense strand reduce potential off-target silencing (Jackson *et al.*, 2006).

DGAT2 ON-TARGET*plus* siRNA (Appendix D, Table D.1) and the ON-TARGET*plus* Non-targeting Control Pool (Appendix D, Table D.2) were used for knockdown experiments as described above, at a final concentration of 100 nM and 10 uL/mL Dharmafect 4.

5.2.3 Analytical techniques

RNA extraction and RT-PCR, ILab analyses, lipid extraction and gas chromatography-mass spectrometry, IN Cell analysis, size-exclusion chromatography, determination of oxidative stress, biochemical assays and ELISAs were carried out as described in Chapter 2 (sections 2.2.2-2.2.10).

5.3 RESULTS

5.3.1 Creation of a *DGAT2* knockout cell line

Sanger sequencing of edited cells confirmed that there were *indels* in exon 1 of the *DGAT2* gene (Figure 5.3.1.1). Both alleles had frameshift mutations and premature stop codons, with allele 1 having a 74 bp insertion and allele 2 a 41 bp deletion. DGAT2 KO cells were viable and proliferated normally. At 100% confluence, compared to WT cells, DGAT2 KO cells appeared slightly larger (Figure 5.3.1.2A & C). After seven days in HS-containing media, cell sizes looked similar, although cell-to-cell junctions were more defined in DGAT2 KO cells (Figure 5.3.1.2B & D). Measurement of protein and phospholipids were not different between cells (data not shown) indicating there was a similar amount of cellular material in both cell types.

5.3.2 Optimisation of siRNA knockdown in Huh7 cells

Unlike normal transfection conditions, the seven day HS protocol required transfection to occur in 100% confluent cells, and for transfection to persist for the following seven day FA treatment. Initially, different concentrations of siGLO green and Dharmafect 4 were investigated to ensure the method of siRNA would still be effective on confluent cells. After both 24 and 48 hours, there was increased fluorescence relative to the Dharmafect only control (Figure 5.3.2-1A&B). There were minimal differences in culturing the cells with siRNA for a further 24 hours, with the biggest differences seen at higher concentrations of siRNA (40 and 50 nM). An MTT assay showed that cell viability was not affected at higher concentrations of transfection reagent or siRNA (data not shown). Based on this data, cells

were cultured with *DGAT2* or non-targeting (NT) siRNA at 50 nM, with 10 µL/mL transfection reagent for 24 hours, which resulted in a knockdown of approximately 35%. At this level of knockdown (*DGAT2* relative expression ratio 0.65 ± 0.05 *vs.* 1.00 ± 0.01 with *DGAT2* or NT siRNA, respectively, mean ± SD, $n = 2$), preliminary analysis suggested that there were differences in metabolic parameters (Figure 5.3.2-2A-F).

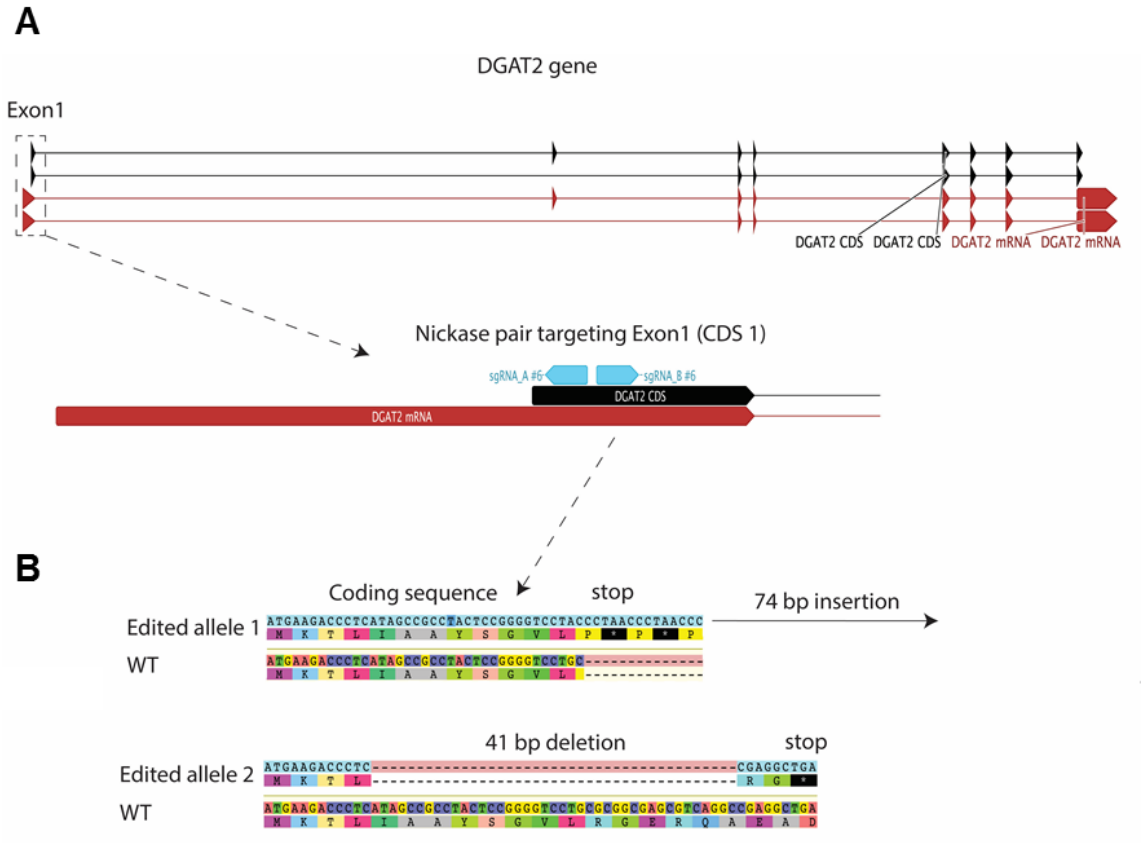


Figure 5.3.1-1. Targeting strategy for diacylglycerol acyltransferase 2 (DGAT2) deletion *via* CRISPR-Cas9 mediated non-homologous end joining. Single guide RNAs (sgRNAs) were targeted upstream of a protospacer adjacent motif (PAM) sequence (5'-NGG) in the coding sequence (CDS) of exon 1 in the *DGAT2* gene (**A**). Sanger sequencing was used to confirm *indels* producing a frameshift and premature stop codon on both alleles of the *DGAT2* gene (**B**). *This work was carried out by Dr. Tomas Jakobsson and Professor Camilla Pramfalk at Karolinska Institutet, Sweden; the figure was provided by Dr. Tomas Jakobsson.*

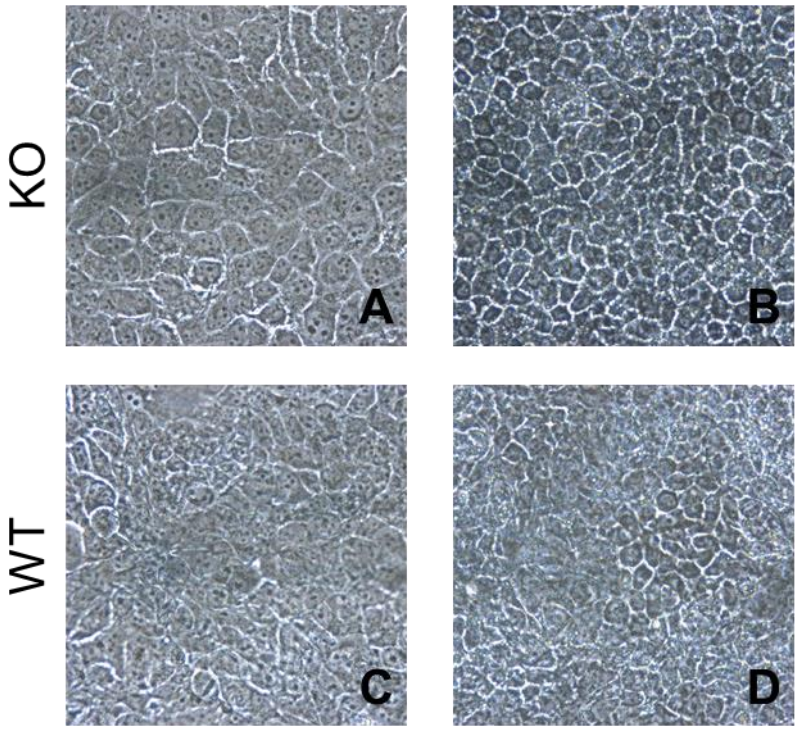


Figure 5.3.1-2. Light microscopy images of knockout (KO; **A, B**) and wildtype (WT; **C, D**) Huh7 cells. Images (40X magnification) were taken at confluence, (**A, C**) and after seven days growth in human serum-containing media (**B, D**). Media was changed every 48-72 hours.

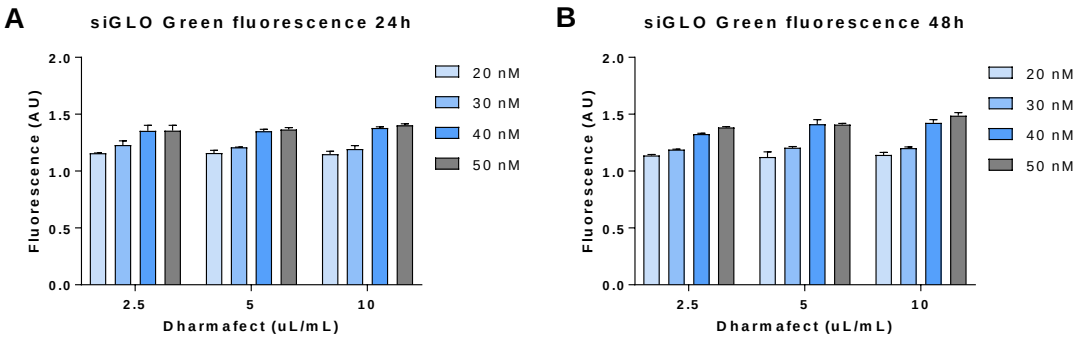


Figure 5.3.2-1. siGLO Green fluorescence in Huh7 cells as a marker of transfection efficiency. Cells were seeded into 96-well, black-walled plates and grown to confluence. Upon reaching confluence, cells were grown in human serum media for seven days, with media changed every 48-72 hours. After this, cells were exposed to varying levels of transfection reagent (Dharmafect 4) in combination with siGLO green in antibiotic and serum-free media for either 24 hours (**A**) or 48 hours (**B**). Data are mean ± SD, $n = 2$.

Previous work utilising siRNA knockdown in confluent Huh7 cells generated efficient (approximately 60%) knockdown with 200 nM siRNA and 20 µL/mL Dharmafect (Sivertsson *et al.*, 2013). For this reason, siGLO green transfection was repeated at higher concentrations, and fluorescence was measured at 24 hours and 7 days, in order to replicate the steatosis induction timeline. Higher concentrations of siRNA made a marked impact of fluorescence at 24 h (100 – 200 nM; Figure 5.3.2-3A), particularly in combination with higher concentrations of transfection reagent (10 and 20 µL/mL). Although to a lesser extent, these differences persisted at 7 days (Figure 5.3.2-3B). At both 10 and 20 µL/mL transfection reagent, there was a particular increase in expression when the siRNA concentration went from 50 to 100 nM, with a more subtle increase beyond this. With a target of approximately 50% *DGAT2* knockdown, a combination of 100 nM siRNA and 10 µL/mL transfection reagent was used for subsequent experiments.

Despite successful preliminary experiments, when knockdown was pursued across treatment conditions and samples were collected for a number of outcome measures, PCR data showed very inconsistent results; *DGAT2* knockdown varied from 0 to 45% (Appendix D, Figure D.1A & B). Due to time constraints, experiments for siRNA knockdown of *DGAT2* were not repeated and no further data is presented.

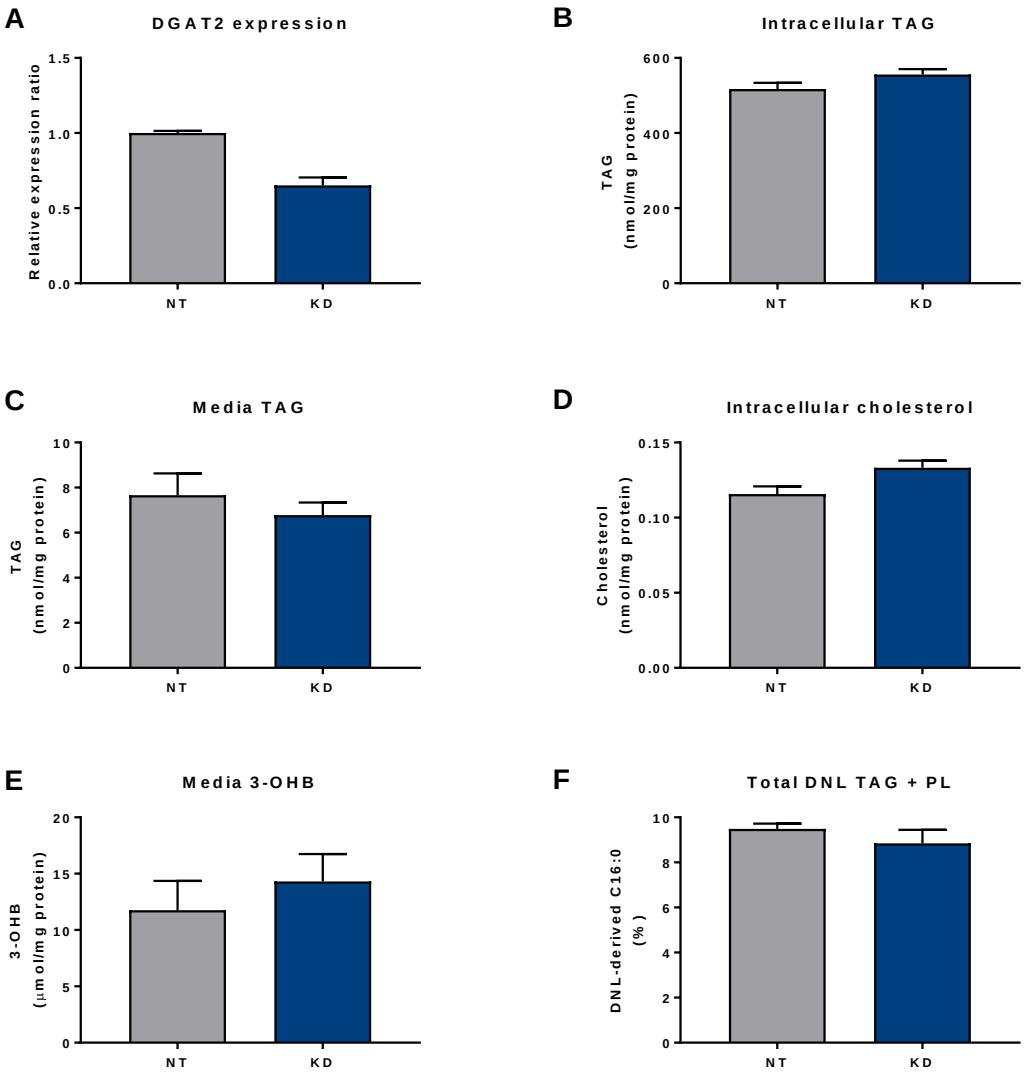


Figure 5.3.2-2. Preliminary results investigating the efficiency and effect of *DGAT2* knockdown (KD) in Huh7 cells. After seeding, cells were cultured in maintenance media until confluence, before being cultured in human serum-containing media for seven days. After this, 50 nM siRNA either targeting *DGAT2* or a non-targeting (NT) control was added to cells with 10 µL/mL Dharmafect 4 in antibiotic and serum-free media for 24 hours before high fat high sugar (800 µM fatty acids + 11 mM glucose + 5.5 mM fructose and 0.5 nM insulin) media was added for a further seven days. To confirm knockdown, *DGAT2* mRNA expression was measured (**A**). Metabolic parameters including intracellular storage of triacylglycerol (TAG; **B**) and cholesterol (**D**) were measured, as was media TAG (**C**) and 3-hydroxybutyrate (3-OHB; **E**) as measures of fatty acid secretion and oxidation, respectively. Deuterated water (^2H_2O) was added to cell media to determine *de novo* lipogenesis (DNL) from deuterium appearance in palmitate (C16:0; **F**). Media was changed every 48 to 72 hours and 24 hours prior to collection and results are corrected to protein content. Data are mean ± SD, $n = 2$.

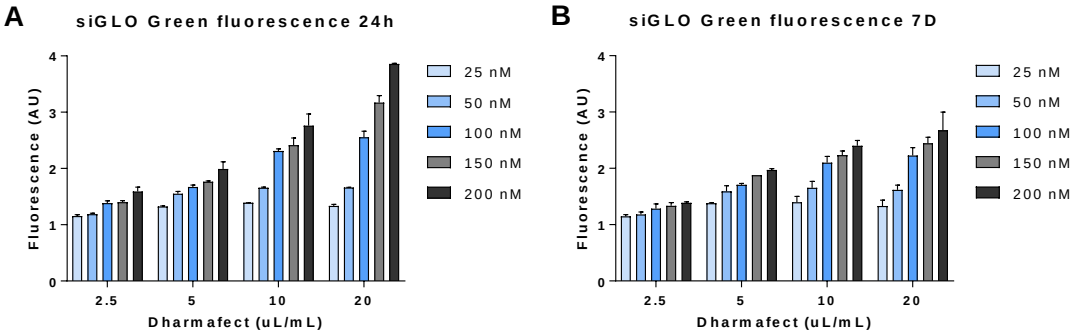


Figure 5.3.2-3. siGLO green fluorescence in Huh7 cells as a marker of transfection efficiency. Cells were seeded into 96-well, black-walled plates and grown to confluence. Upon reaching confluence, cells were grown in human serum media for seven days, with media changed every 48-72 hours. After this, cells were exposed to varying levels of transfection reagent (Dharmafect 4) in combination with siGLO green in antibiotic and serum-free media for 24 hours (**A**). After this, cells were exposed to human serum-containing media for a further seven days (**B**), with media changed every 48-72 hours. Data are mean ± SD, $n = 2$.

5.3.3 Investigating the effects of *DGAT2* knockout on FA storage and metabolism in the presence of different nutritional substrates in Huh7 cells

5.3.3.1 The effect of DGAT2 knockout on intracellular lipid accumulation in Huh7 cells

DGAT2 WT and KO cells were cultured and underwent treatment with LFLS, LFHS and HFHS media (see Chapter 4, section 4.2.1.2). Given that DGAT2 is a TAG-synthesising enzyme, the accumulation of TAG within the cell was measured. After all treatments, and despite an approximate doubling of *DGAT1* expression ($p < 0.001$ for all treatments; Table 5.3.3-1), there was a consistent reduction in intracellular TAG as a result of DGAT2 KO of Huh7 cells (all $p < 0.05$; Figure 5.3.3-1A). There were also differences between treatments regardless of gene editing, with the amount of intracellular TAG in LF-treated cells being lower than that in HFHS-treated cells (all $p < 0.05$; Figure 5.3.3-1A). Data on LD counts from IN Cell 6000 analysis supported TAG analysis, with significantly more LDs present in cells cultured in HFHS media compared to LFLS media, although there were no differences

between WT and KO cells (Figure 5.3.3-1B). Since LDs consist of TAG and cholesterol ester, intracellular cholesterol was also measured. In contrast to TAG, cholesterol tended to be increased in DGAT2 KO cells, although not significantly (Figure 5.3.3-1C). When TAG and cholesterol were combined, the trend of there being more intracellular lipid in WT compared to KO cells persisted, but was only significant in the HFHS condition (Figure 5.3.3-1D).

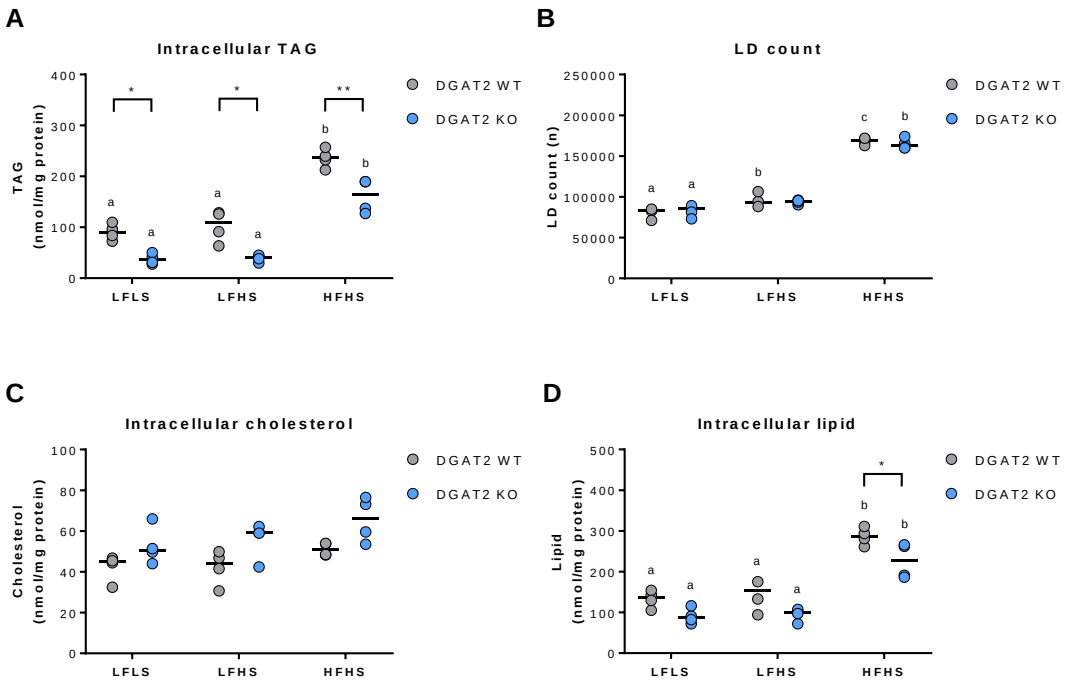


Figure 5.3.3-1. The effect of media composition on lipid storage in Huh7 cells with wildtype (WT) or knockout (KO) of the *DGAT2* gene. Once confluent, cells were treated with media containing 2% human serum and 11 mM glucose for seven days before treatment media was added. Treatments consisted of either low fat low sugar (LFLS; 11 mM glucose + 200 µM fatty acids), low fat high sugar (LFHS; 200 µM fatty acids + 11 mM glucose + 5.5 mM fructose) or high fat high sugar (HFHS; 800 µM fatty acids + 11 mM glucose + 5.5 mM fructose); all treatments contained 0.5 nM insulin. Intracellular triacylglycerol (TAG; **A**) was measured and LDs were identified and counted using the IN Cell Analyzer 6000 (**B**). Intracellular cholesterol was also measured (**C**) and TAG and cholesterol were combined to determine total intracellular lipid content (**D**). Media was changed every 48 to 72 hours and 24 hours prior to collection and results are corrected to protein content. Data are presented as individual values and median, $n = 4$. * $p < 0.05$, ** $p < 0.001$; different letters denote significant differences between means within WT or KO cells, $p < 0.05$; two-way ANOVA with Bonferroni's multiple comparisons tests.

To determine whether these differences between WT and KO cells were due to changes in FA uptake from the media, media NEFA concentrations were measured. After 24 hours, NEFA remaining in the media from the WT cells ranged from 74.5 μM in the LFHS-treated cells, to 83.2 μM in HFHS-treated cells (Table 5.3.3-2). However, in the KO cells, while NEFA concentrations in the LFLS and LFHS cells were comparable to the WT cells, the HFHS-treated KO cells had approximately 200 μM FA remaining ($p < 0.05$ *vs.* LFLS and LFHS KO and HFHS WT cells). Although there were significantly higher levels of FAs remaining in the media in HFHS-treated KO cells compared to WT cells, the was not uniform across all those supplied: while oleate (C18:0) and palmitate (C16:0) levels were 40-50% higher in KO cells, the essential FAs remained at levels more than six and four times higher than in WT HFHS media (linoleate (C18:2*n*-6) and α-linolenate (C18:3*n*-3), respectively; Table 5.3.3-2).

5.3.3.2 The effect of DGAT2 knockout on FA synthesis in Huh7 cells

Since DGAT2 is believed to play a role in DNL, which is an important contributor to the FA pool of hepatocytes, the effect of DGAT2 KO on DNL was investigated. Incorporation of ^{13}C from labelled glucose and fructose into palmitate (C16:0) was used as a measure of DNL in TAG and PLs; in both fractions, DNL was markedly suppressed in DGAT2 KO cells (all $p < 0.001$; Figure 5.3.3-2A). There was also an effect of media composition, with a significantly lower proportion of DNL-derived palmitate in TAG of HFHS-treated cells compared to those treated with LFLS (in WT and KO, $p < 0.05$) and LFHS (in WT, $p < 0.05$; Figure 5.3.3-2A). However, when expressed as an absolute value, although differences between WT and KO cells appeared even more dramatic and remained statistically significant, there were no differences between cells treated with different media (Figure 5.3.3-2C).

Table 5.3.3-1. The effect of media composition on gene expression in Huh7 cells with wildtype (WT) or knockout (KO) of the *DGAT2* gene.

	LFLS		LFHS		HFHS	
	WT	**KO**	**WT**	**KO**	**WT**	**KO**
FA and TAG synthesis genes						
ACACA	0.99 (0.83 - 1.10)	1.19 (1.17 - 1.25)	0.85 (0.74 - 1.18)	1.06 (1.02 - 1.12)	0.89 (0.79 - 1.14)	0.95 (0.87 - 1.07)
DGAT1	0.65 (0.63 - 0.74)**	1.41 (1.24 - 1.42)**	0.71 (0.62 - 0.80)**	1.50 (1.24 - 1.58)**	0.86 (0.72 - 1.09)**	1.55 (1.53 - 1.56)**
DGAT2	0.78 (0.64 - 0.89)*	1.30 (1.18 - 1.52)*	0.76 (0.64 - 1.09)	1.13 (1.08 - 1.38)	0.68 (0.66 - 1.00)*	1.30 (1.29 - 1.45)*
FASN	1.16 (0.80 - 1.44)*	1.03 (0.99 - 1.15)*	1.06 (0.78 - 1.45)*	0.86 (0.83 - 0.90)*	1.29 (1.15 - 1.42)*	0.71 (0.70 - 0.79)*
SCD	1.11 (1.10 - 1.28)*	0.68 (0.65 - 1.03)*	1.43 (1.23 - 1.49)**	0.73 (0.63 - 0.86)**	1.36 (1.25 - 1.47)*	0.85 (0.70 - 0.92)*
FA elongation and desaturation genes						
ELOVL2	0.89 (0.80 - 1.01)	1.15 (1.12 - 1.16)	0.80 (0.79 - 0.87)*	1.23 (1.07 - 1.34)*	1.00 (0.85 - 1.09)	1.13 (0.73 - 1.26)
ELOVL5	0.97 (0.92 - 1.33)	0.87 (0.81 - 0.92)	1.14 (1.01 - 1.16)	0.80 (0.70 - 1.04)	1.16 (1.06 - 1.17)	0.99 (0.97 - 1.22)
ELOVL6	1.32 (1.25 - 1.99)**	0.80 (0.72 - 0.81)**	1.28 (1.24 - 1.41)*	0.75 (0.73 - 0.75)*	1.19 (1.17 - 1.22)*	0.74 (0.72 - 0.78)*
FADS1	1.51 (1.03 - 1.55)*	0.64 (0.58 - 0.85)*	1.22 (1.12 - 1.55)*	0.70 (0.67 - 0.75)*	1.40 (1.29 - 1.57)*	0.83 (0.69 - 1.11)*
FADS2	1.25 (1.04 - 1.37)*	0.82 (0.70 - 0.83)*	1.30 (0.98 - 1.50)*	0.77 (0.74 - 0.85)*	1.29 (1.12 - 1.39)*	0.87 (0.78 - 0.92)*
Lipid droplet protein genes						
CIDEB	0.61 (0.54 - 0.78)**	1.73 (1.70 - 1.77)**	0.59 (0.48 - 0.72)**	1.39 (1.37 - 1.70)**	0.59 (0.58 - 0.78)**	1.75 (1.36 - 1.79)**
PLIN2	1.02 (0.74 - 1.32)	1.04 (0.91 - 1.18)	1.06 (0.82 - 1.07)	1.02 (0.93 - 1.04)	1.06 (0.97 - 1.07)	0.93 (0.89 - 1.08)
PLIN3	0.82 (0.76 - 1.17)	1.20 (1.01 - 1.27)	0.91 (0.77 - 1.15)	0.99 (0.97 - 1.16)	0.83 (0.77 - 0.96)	1.25 (0.85 - 1.52)
PLIN5	1.24 (0.88 - 1.35)	1.00 (0.86 - 1.20)	0.92 (0.72 - 1.06)	1.10 (0.96 - 1.13)	1.08 (0.99 - 1.09)	0.96 (0.7 - 1.00)
Hepatic nuclear receptors & transcription factors						
MLXIPL	3.35 (3.27 - 3.47)**	0.29 (0.20 - 0.37)**	2.96 (2.89 - 3.94)**	0.41 (0.38 - 0.45)**	3.14 (2.38 - 4.15)**	0.26 (0.22 - 0.29)**
SREBF1	1.41 (1.37 - 1.77)*	0.92 (0.83 - 1.17)*	1.41 (0.94 - 1.52)	0.85 (0.81 - 0.98)	1.22 (0.78 - 1.27)*	0.60 (0.52 - 0.63)*

Once confluent, cells were treated with media containing 2% human serum and 11 mM glucose for seven days before treatment media was added. Treatments consisted of either low fat low sugar (LFLS; 11 mM glucose + 200 μM fatty acids), low fat high sugar (LFHS; 200 μM fatty acids + 11 mM glucose + 5.5 mM fructose) or high fat high sugar (HFHS; 800 μM fatty acids + 11 mM glucose + 5.5 mM fructose); all treatments contained 0.5 nM insulin. All genes were expressed as a relative expression ratio to a pooled sample and corrected to three reference genes (*B2M*, *HMBS* and *YWHAZ*). Data are presented as median (range), $n = 4$. Two-way ANOVA with Bonferroni's multiple comparisons test, * $p < 0.05$, ** $p < 0.001$.

Table 5.3.3-2. The effect of media composition on fatty acids remaining in the media (μM) after 24 hours on Huh7 cells with wildtype (WT) or knockout (KO) of the *DGAT2* gene

	LFLS		LFHS		HFHS	
	WT	**KO**	**WT**	**KO**	**WT**	**KO**
C16:0	51.5 (35.9 - 58.9)	40.7 (35.2 - 44.6)[a]	37.9 (30.4 - 46.8)	42.2 (34.4 - 57.5)[a]	52.8 (38.2 - 63.4)*	70.6 (62.3 - 80.4)*[b]
C18:1*n*-9	12.4 (11.0 - 19.0)	17.6 (15.8 - 19.2)[a]	13.0 (10.8 - 18.0)	18.0 (15.0 - 25.1)	16.0 (14.6 - 19.4)*	24.9 (23.8 - 25.7)*[b]
C18:2*n*-6	3.98 (2.91 - 5.82)	7.96 (6.42 - 23.3)[a]	4.26 (3.07 - 12.3)	9.47 (7.58 - 9.77)[a]	18.5 (7.56 - 21.2)*	105.0 (89.7 - 105.6)*[b]
C18:3*n*-3	0.57 (0.51 - 0.61)	0.56 (0.48 - 1.32)[a]	0.40 (0.35 - 1.13)	0.57 (0.48 - 0.71)[a]	0.76 (0.65 - 1.15)*	4.10 (3.32 - 4.41)*[b]
Total	74.5 (53.8 - 74.9)	66.8 (59.0 - 87.4)[a]	54.8 (46.9 - 76.7)	73.9 (61.1 - 85.6)[a]	83.2 (69.3 - 101.6)*	201.1 (182.7 - 216.1)*[b]

Once confluent, cells were treated with media containing 2% human serum and 11 mM glucose for seven days before treatment media was added. Treatments consisted of either low fat low sugar (LFLS; 11 mM glucose + 200 μM fatty acids), low fat high sugar (LFHS; 200 μM fatty acids + 11 mM glucose + 5.5 mM fructose) or high fat high sugar (HFHS; 800 μM fatty acids + 11 mM glucose + 5.5 mM fructose); all treatments contained 0.5 nM insulin. Data are presented as median (range), $n = 4$. * $p < 0.05$, different letters denote significant differences between means within WT or KO cells, $p < 0.05$; two-way ANOVA with Bonferroni's multiple comparisons tests.

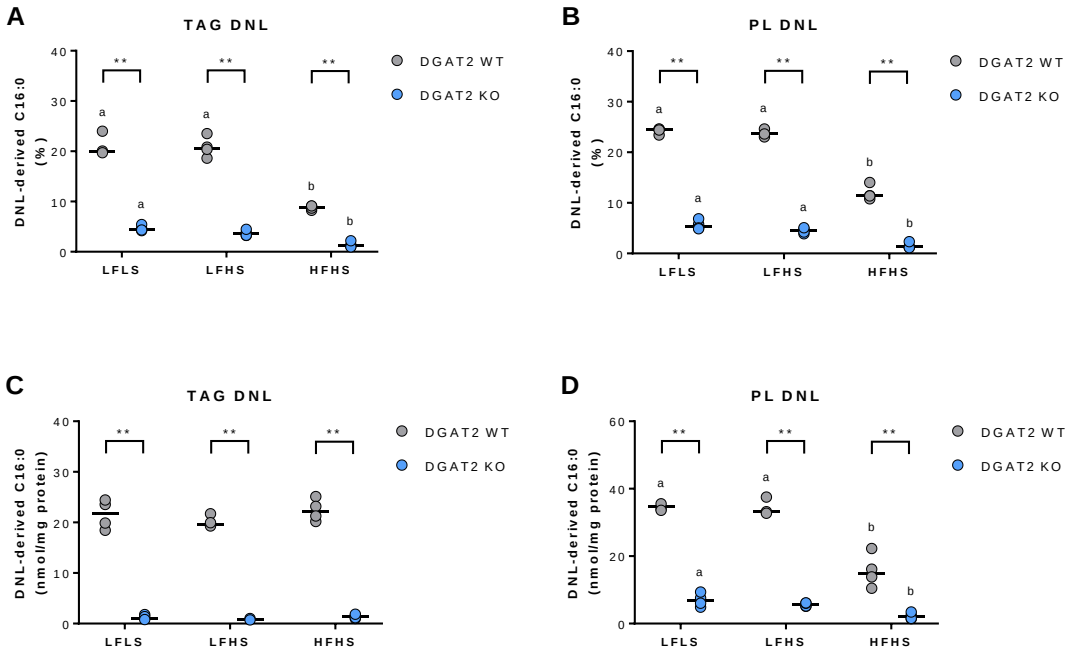


Figure 5.3.3-2. The effect of media composition on *de novo* lipogenesis (DNL) in Huh7 cells with wildtype (WT) or knockout (KO) of the *DGAT2* gene. Once confluent, cells were treated with media containing 2% human serum and 11 mM glucose for seven days before treatment media was added. Treatments consisted of either low fat low sugar (LFLS; 11 mM glucose + 200 µM fatty acids), low fat high sugar (LFHS; 200 µM fatty acids + 11 mM glucose + 5.5 mM fructose) or high fat high sugar (HFHS; 800 µM fatty acids + 11 mM glucose + 5.5 mM fructose); all treatments contained 0.5 nM insulin. Glucose and fructose consisted of 50% ^{12}C and 50% ^{13}C to allow tracing of carbon into *de novo* synthesised palmitate. Contribution of DNL as a percentage of total TAG (**A**) and PLs (**B**) was calculated, and used to determine the absolute (nmol/mg protein) amount of DNL-derived palmitate in TAG (**C**) and PLs (**D**). Media was changed every 48 to 72 hours and 24 hours prior to collection. Data are presented as individual values and median, $n = 4$. * $p < 0.05$, ** $p < 0.001$; different letters denote significant differences between means within WT or KO cells, $p < 0.05$; two-way ANOVA with Bonferroni's multiple comparisons tests.

Similar differences were seen in the PL fraction: LFLS-treated cells had significantly more palmitate from DNL than HFHS-treated cells regardless of DGAT2 function (all $p < 0.05$; Figure 5.3.3-2B & D). When expressed as either mol% or as an absolute amount, there were clear differences in DNL contribution to palmitate in the PL fraction: like TAG, this was

significantly lower in the KO compared to WT cells (all $p < 0.001$; Figure 5.3.3-2B & D). In line with this, expression of the DNL regulators ChREBP (*MLXIPL*) and SREBP-1c (*SREBF1*) were strongly affected by the knockout of *DGAT2* (Table 5.3.3-1). Although it varied across treatment, *MLXIPL* expression was up to 12-fold higher in DGAT2 WT cells compared to KO cells (all $p < 0.001$); *SREBF1* expression was also downregulated in KO cells ($p < 0.05$ for LFLS and HFHS; Table 5.3.3-1). In line with this, expression of FAS (*FASN*) and stearoyl-CoA desaturase (*SCD*) were lower in *DGAT2* KO cells (all $p < 0.05$; Table 5.3.3-1).

5.3.3.3 The effect of DGAT2 knockout on exogenous FA storage in Huh7 cells

Along with ^{13}C sugars, deuterated (^{2}H) palmitate and oleate were added to cell media to trace the contribution of exogenous FAs to intracellular and secreted TAG and PLs. In TAG, when expressed as absolute amounts, both D31 palmitate and D33 oleate followed a similar pattern to total intracellular TAG: all WT cells had significantly higher levels than KO cells across treatments, and HFHS-treated cells had higher levels than low fat-treated cells within WT or KO cells (all $p < 0.05$; Figure 5.3.3-3A & C). In agreement with HFHS-treated cells having similar DNL-derived palmitate, but more palmitate overall, HFHS-treated cells had a higher relative amount of D31 palmitate than low fat-treated cells (all $p < 0.05$; Figure 5.3.3-3B). Relative D33 oleate enrichment differed to palmitate: whereas high palmitate enrichment in HFHS-treated cells suggested a net retention of this FA over the four media changes, oleate was maintained at approximately 15% of TAG oleate. Although D33 oleate levels were significantly higher in WT compared to KO cells, the low variation indicates regulation of exogenous FA turnover and partitioning into non-TAG pathways (Figure 5.3.3-3B & D).

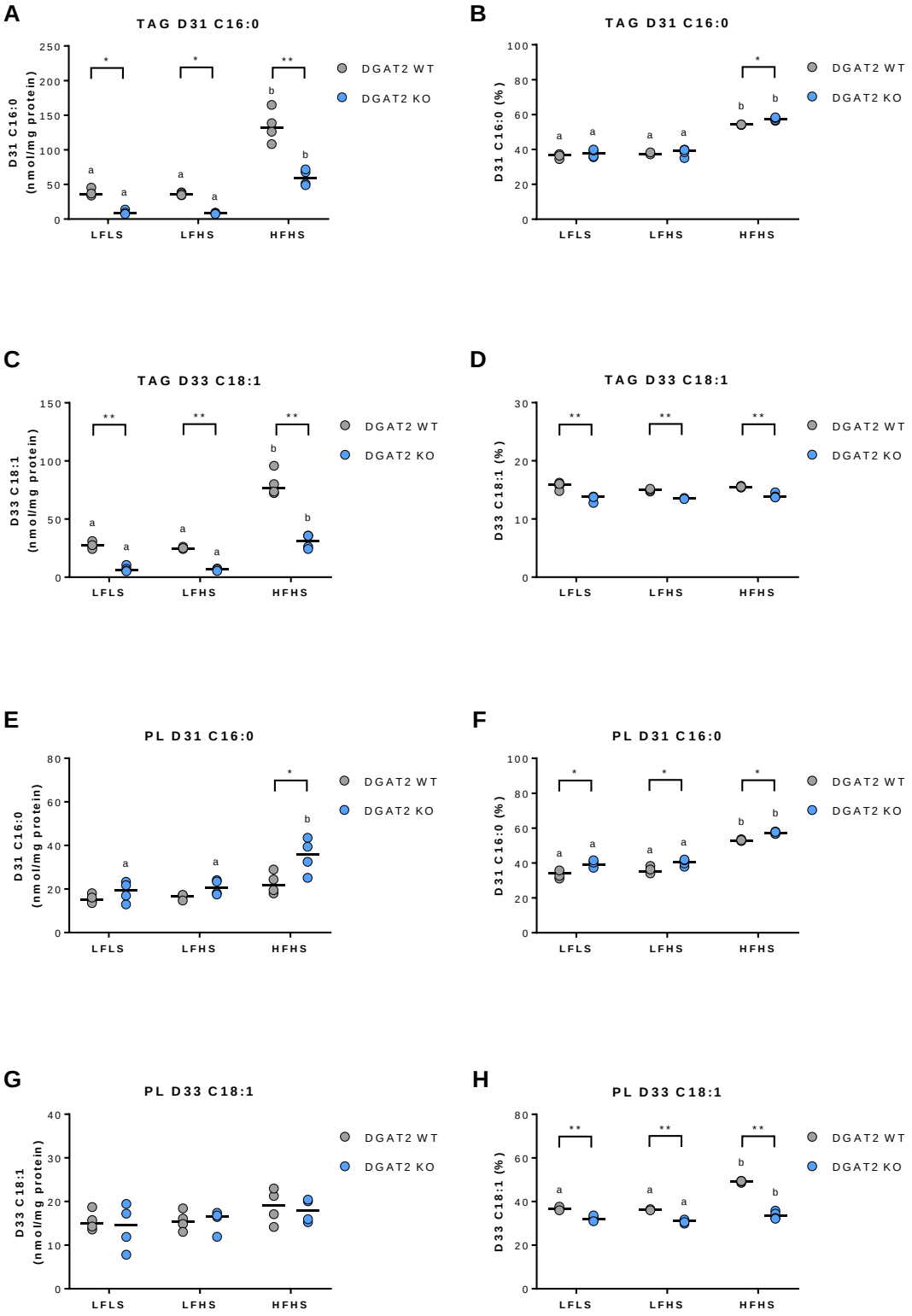


Figure 5.3.3-3. Figure legend can be found on the next page.

Figure 5.3.3-3. (Previous page) The effect of media composition on exogenous fatty acid (FA) storage and partitioning in Huh7 cells with wildtype (WT) or knockout (KO) of the *DGAT2* gene. Once confluent, cells were treated with media containing 2% human serum and 11 mM glucose for seven days before treatment media was added. Treatments consisted of either low fat low sugar (LFLS; 11 mM glucose + 200 μM FAs), low fat high sugar (LFHS; 200 μM FAs + 11 mM glucose + 5.5 mM fructose) or high fat high sugar (HFHS; 800 μM FAs + 11 mM glucose + 5.5 mM fructose); all treatments contained 0.5 nM insulin. The FA mix contained 100% labelling of $^{2}H_{31}$[palmitate] (D31) and $^{2}H_{33}$[oleate] (D33) to allow tracing of exogenous FAs into the intracellular FA pool. Contribution of exogenous D31 palmitate to total intracellular TAG (**A**) and PLs (**E**) was calculated (nmol/mg protein), which was determined from the percentage enrichment in TAG (**B**) and PLs (**F**). Contribution of exogenous D33 oleate to total intracellular TAG (**C**) and PLs (**G**) was calculated (nmol/mg protein), which was determined from the percentage enrichment in TAG (**D**) and PLs (**H**). Media was changed every 48 to 72 hours and 24 hours prior to collection. Data are presented as individual values and median, $n = 4$. * $p < 0.05$, ** $p < 0.001$; different letters denote significant differences between means within WT or KO cells, $p < 0.05$; two-way ANOVA with Bonferroni's multiple comparisons tests.

Unlike DNL-derived TAG, which was similar in absolute values across treatment media, proportions of DNL-derived palmitate were lower in HFHS-treated cells (section 5.3.3.2). Enrichment of D31 palmitate suggests that this was compensated for by exogenous palmitate, since this was higher in HF-treated cells than LF-treated KO cells; when expressed as a percentage of total palmitate, differences were evident in both cell types (Figure 5.3.3-3E & F). In contrast to D31 palmitate, which was higher in KO cells compared to WT, D33 oleate was more enriched in WT cells when relative values were analysed (all $p < 0.05$; Figure 5.3.3-3H). Whereas D33 oleate enrichment was consistent in the TAG fraction, it was higher overall in the PL fraction (~40%), and around 50% in the WT HFHS-treated cells: this suggests a preferential partitioning of exogenous oleate to the PL fraction of these cells (Figure 5.3.3-3H).

Table 5.3.3-3. The effect of media composition on fatty acid composition of triacylglycerol in Huh7 cells with wildtype (WT) or knockout (KO) of the *DGAT2* gene (mol%)

	LFLS		LFHS		HFHS	
	WT	**KO**	**WT**	**KO**	**WT**	**KO**
C14:0	3.18 (3.05 - 3.23)^{**a}	1.61 (1.54 - 1.67)^{**a}	3.07 (2.96 - 3.25)^{**a}	1.50 (1.44 - 1.70)^{**a}	1.37 (1.34 - 1.39)^{**b}	0.53 (0.49 - 0.61)^{**b}
C16:0	19.8 (19.6 - 20.6)^{**a}	16.3 (15.2 - 17.4)^{**a}	19.4 (19.2 - 19.9)^{**a}	15.2 (14.9 - 16.8)^{**a}	9.25 (9.10 - 9.39)^{**b}	6.38 (5.91 - 7.44)^{**b}
C18:0	4.56 (4.45 - 4.82)^{**a}	3.52 (3.36 - 3.74)^{**a}	4.42 (4.24 - 4.54)^{**a}	3.30 (3.17 - 3.51)^{**a}	2.12 (2.10 - 2.40)^{**b}	1.57 (1.46 - 1.75)^{**b}
SFA	34.8 (34.6 - 35.2)^{**a}	30.3 (29.3 - 31.2)^{**a}	34.2 (34.2 - 35.0)^{**a}	29.1 (28.9 - 30.9)^{**a}	27.9 (27.7 - 28.1)^{*b}	26.2 (26.1 - 26.9)^{*b}
C16:1*n*-7	6.94 (6.86 - 7.28)^{**a}	3.10 (3.00 - 3.28)^{**a}	6.91 (6.83 - 7.07)^{**a}	2.99 (2.75 - 3.05)^{**a}	2.86 (2.83 - 2.90)^{**b}	0.98 (0.91 - 1.16)^{**b}
C18:1*n*-9	39.6 (39.6 - 40.4)^{**a}	48.8 (46.8 - 49.6)**	40.3 (39.7 - 40.9)^{**a}	49.2 (48.6 - 50.8)**	46.8 (46.7 - 47.0)^{*b}	48.9 (48.0 - 49.3)*
C18:1*n*-7	6.15 (6.02 - 6.40)^{**a}	5.16 (4.64 - 5.33)^{**a}	6.08 (5.94 - 6.14)^{**a}	4.77 (4.56 - 5.02)^{**a}	2.39 (2.35 - 2.40)^{*b}	1.82 (1.61 - 2.24)^{*b}
C20:1*n*-9	0.39 (0.37 - 0.40)^{**a}	0.63 (0.45 - 0.69)^{**a}	0.39 (0.37 - 0.39)^{a}	0.41 (0.36 - 0.53)^{b}	0.16 (0.15 - 0.16)^{*b}	0.29 (0.22 - 0.35)^{*c}
MUFA	53.4 (53.0 - 53.7)**	57.3 (55.8 - 58.6)^{**a}	53.8 (52.9 - 54.2)^{**a}	57.4 (56.7 - 59.0)^{**a}	52.2 (52.1 - 52.3)^{b}	51.9 (51.7 - 52.2)^{b}
C18:2*n*-6	9.14 (9.01 - 9.40)^{**a}	10.7 (9.80 - 10.9)^{**a}	9.29 (9.11 - 9.56)^{**a}	10.9 (10.6 - 11.2)^{**a}	17.7 (17.5 - 17.9)^{**b}	19.4 (18.8 - 19.5)^{**b}
C18:3*n*-6	0.20 (0.19 - 0.24)	0.18 (0.13 - 0.20)^{a}	0.22 (0.20 - 0.24)	0.22 (0.21 - 0.23)^{a}	0.33 (0.30 - 0.37)	0.43 (0.28 - 0.68)^{b}
C18:3*n*-3	0.18 (0.17 - 0.19)^{*a}	0.27 (0.25 - 0.33)^{*a}	0.19 (0.17 - 0.19)^{**a}	0.28 (0.23 - 0.41)**	0.35 (0.34 - 0.37)^{b}	0.35 (0.33 - 0.39)^{b}
C20:4*n*-6	0.16 (0.15 - 0.19)^{a}	0.26 (0.13 - 0.36)	0.17 (0.15 - 0.18)^{*a}	0.29 (0.28 - 0.32)*	0.27 (0.26 - 0.28)^{b}	0.30 (0.24 - 0.38)
PUFA	9.70 (9.58 - 9.93)^{**a}	11.3 (10.4 - 11.8)^{**a}	9.84 (9.70 - 10.1)^{**a}	11.8 (11.4 - 12.0)^{**a}	18.7 (18.4 - 18.8)^{**b}	20.3 (20.2 - 20.7)^{**b}

Once confluent, cells were treated with media containing 2% human serum and 11 mM glucose for seven days before treatment media was added. Treatments consisted of either low fat low sugar (LFLS; 11 mM glucose + 200 µM fatty acids), low fat high sugar (LFHS; 200 µM fatty acids + 11 mM glucose + 5.5 mM fructose) or high fat high sugar (HFHS; 800 µM fatty acids + 11 mM glucose + 5.5 mM fructose); all treatments contained 0.5 nM insulin. Data are presented as median (range), $n = 4$. * $p < 0.05$, ** $p < 0.001$; different letters denote significant differences between means within WT or KO cells, $p < 0.05$; two-way ANOVA with Bonferroni's multiple comparisons tests.

Table 5.3.3-4. The effect of media composition on fatty acid composition of phospholipids in Huh7 cells with wildtype (WT) or knockout (KO) of the *DGAT2* gene (mol%)

	LFLS		LFHS		HFHS	
	WT	**KO**	**WT**	**KO**	**WT**	**KO**
C14:0	0.34 (0.31 - 0.36)**[a]	0.16 (0.15 - 0.18)**[a]	0.35 (0.33 - 0.36)**[a]	0.17 (0.15 - 0.19)**[a]	0.18 (0.17 - 0.19)**[b]	0.06 (0.05 - 0.07)**[b]
C16:0	21.3 (20.0 - 21.8)*[a]	16.9 (16.1 - 17.4)*[a]	21.1 (19.3 - 21.5)*[a]	16.6 (16.0 - 18.0)*[a]	11.9 (11.3 - 13.1)*[b]	6.99 (6.55 - 14.6)*[b]
C18:0	14.5 (14.2 - 14.6)**[a]	11.2 (10.6 - 12.8)**[a]	14.1 (14.1 - 14.4)**[a]	10.1 (9.81 - 11.9)**[a]	11.6 (10.9 - 12.1)**[b]	7.43 (7.31 - 8.20)**[b]
SFA	41.9 (41.2 - 43.0)[a]	38.3 (38.0 - 41.1)	42.5 (39.7 - 42.6)*[a]	37.7 (35.5 - 38.4)*	37.4 (34.2 - 38.5)b	35.8 (34.3 - 40.6)
C16:1*n*-7	2.33 (2.20 - 2.42)**[a]	0.76 (0.70 - 0.90)**[a]	2.31 (2.30 - 2.41)**[a]	0.75 (0.72 - 1.19)**[a]	0.70 (0.61 - 0.80)*[b]	0.20 (0.19 - 0.71)*[b]
C18:1*n*-9	21.4 (21.1 - 22.3)	22.4 (18.5 - 22.5)[a]	21.6 (20.6 - 22.0)	22.6 (22.3 - 23.6)	19.9 (19.0 - 23.9)*	24.4 (22.8 - 24.6)*[b]
C18:1*n*-7	3.48 (3.35 - 3.60)[a]	3.09 (1.74 - 3.15)[a]	3.48 (3.36 - 4.83)[a]	3.25 (3.08 - 3.51)[a]	1.72 (1.58 - 2.48)[b]	1.35 (1.32 - 1.43)[b]
C20:1*n*-9	0.18 (0.16 - 0.25)[a]	0.24 (0.18 - 0.27)[a]	0.22 (0.16 - 0.25)[a]	0.18 (0.17 - 0.21)[a]	0.10 (0.09 - 0.15)[b]	0.11 (0.07 - 0.14)[b]
MUFA	27.4 (27.2 - 28.9)[a]	26.4 (21.4 - 26.6)	28.1 (27.5 - 29.6)[a]	27.0 (26.5 - 27.8)	22.4 (21.5 - 27.1)[b]	26.0 (24.9 - 26.3)
C18:2*n*-6	16.5 (16.3 - 17.2)**[a]	23.0 (22.0 - 24.5)**	16.4 (16.2 - 16.7)**[a]	21.0 (20.8 - 23.0)**[a]	25.5 (24.1 - 27.1)*[b]	23.8 (21.4 - 25.2)*[b]
C18:3*n*-6	0.60 (0.53 - 0.65)	0.29 (0.25 - 0.57)	0.53 (0.23 - 0.81)	0.32 (0.31 - 0.57)	0.64 (0.62 - 0.86)*	0.38 (0.21 - 0.46)*
C18:3*n*-3	0.12 (0.12 - 0.18)*	0.06 (0.05 - 0.07)*	0.13 (0.09 - 0.18)	0.09 (0.04 - 0.13)	0.15 (0.13 - 0.21)*	0.07 (0.06 - 0.10)*
C20:4*n*-6	4.90 (4.47 - 4.97)	4.75 (3.96 - 5.64)[a]	4.92 (4.56 - 5.08)	5.43 (5.12 - 5.66)[a]	6.46 (6.00 - 6.81)	7.21 (5.07 - 9.74)[b]
C20:5*n*-3	0.29 (0.24 - 0.43)	0.23 (0.18 - 0.32)	0.24 (0.05 - 0.27)	0.20 (0.15 - 0.26)	0.34 (0.29 - 0.41)	0.13 (0.13 - 0.39)
C22:5*n*-3	1.34 (1.18 - 1.70)*[a]	0.89 (0.83 - 1.15)*	1.23 (1.05 - 1.48)*[a]	0.89 (0.76 - 1.06)*	0.80 (0.77 - 1.07)[b]	0.86 (0.82 - 0.91)
C22:6*n*-3	1.33 (1.27 - 1.51)**[a]	1.80 (1.65 - 2.02)**[a]	1.36 (1.30 - 1.42)**[a]	1.88 (1.82 - 1.97)**[a]	1.11 (1.11 - 1.19)**[b]	1.47 (1.27 - 1.58)**[b]
PUFA	25.2 (24.6 - 25.9)**[a]	30.6 (30.1 - 33.9)**[a]	24.8 (24.2 - 25.4)**[a]	30.4 (30.0 - 31.9)**[a]	35.0 (32.5 - 37.5)[b]	34.4 (31.6 - 35.7)[b]

Once confluent, cells were treated with media containing 2% human serum and 11 mM glucose for seven days before treatment media was added. Treatments consisted of either low fat low sugar (LFLS; 11 mM glucose + 200 µM fatty acids), low fat high sugar (LFHS; 200 µM fatty acids + 11 mM glucose + 5.5 mM fructose) or high fat high sugar (HFHS; 800 µM fatty acids + 11 mM glucose + 5.5 mM fructose); all treatments contained 0.5 nM insulin. Data are presented as median (range), $n = 4$. * $p < 0.05$, ** $p < 0.001$; different letters denote significant differences between means within WT or KO cells, $p < 0.05$; two-way ANOVA with Bonferroni's multiple comparisons tests.

5.3.3.4 The effect of DGAT2 knockout on FA composition, elongation and desaturation in Huh7 cells

Building on the differences in DNL, FA composition was further investigated. In agreement with changes in DNL, there were significantly less of the FAs that can be derived from DNL in DGAT2 KO cells (*e.g.* myristate (C14:0), palmitate (C16:0), palmitoleate (C16:1*n*-7), stearate (C18:0) and vaccinate (C18:1*n*-7; Table 5.3.3-3); comparable differences of a larger magnitude in TAG content between cells were noted when expressed as absolute values (Appendix D, Table D.3). Similar differences were seen in the PL fraction in DNL-derived FAs, with lower levels of these FAs in DGAT2 KO cells (Table 5.3.3-4; absolute values found in Appendix D, Table D.4). Both SCD1 (*SCD*) and ELOVL6, the enzymes that desaturate and elongate palmitate (C16:0), were expressed at significantly lower levels in DGAT2 KO cells (all $p < 0.05$; Table 5.3.3-1). When TAG and PL FAs were combined, the product-to-precursor ratios of these enzymes were lower for SCD1 in KO cells (C16:1*n*-7/C16:0 and C18:1*n*-9/C18:0; all $p < 0.001$; Figure 5.3.3-4A & B), but higher for ELOVL6 in low fat-treated KO cells (C18:0/C16:0, all $p < 0.05$; Figure 5.3.3-4C).

In contrast to palmitate (C16:0), KO cells tended to have higher intracellular proportions of the other contributors to the exogenous FAs in the media. In the TAG fraction, LFLS and LFHS-treated KO cells had approximately 9% more oleate (C18:1*n*-9) than WT cells (both $p < 0.001$), while differences in the HFHS-treated cells were less dramatic, although still significant ($p < 0.05$; Table 5.3.3-3). In the PL fraction, media treatments had the opposite effect, with significantly more oleate in HFHS-treated KO cells compared to WT ($p < 0.05$),

but no differences in LFLS an LFHS-treated cells (Table 5.3.3-4). In the TAG fraction, there was a small but significant increase in the proportion of linoleate (C18:2*n*-6) in KO across media treatments, which persisted in the PL fraction (Tables 5.3.3-3&4). In PLs, differences in *n*-3 FAs were apparent, with lower levels of α-linolenate (C18:3*n*-3) in the KO cells compared to WT ($p < 0.05$ for LFLS and HFHS) and higher levels of docosahexaenoate (C22:6*n*-3, all $p < 0.001$; Table 5.3.3-4). In line with the formation of longer chain FAs, levels of *ELOVL2* tended to be higher in KO cells ($p < 0.05$ for LFHS, Table 5.3.3-1).

5.3.3.5 The effect of DGAT2 knockout on lipid droplet pattern in Huh7 cells

To investigate differences in lipid accumulation further, size of LDs was determined with the IN Cell 6000. Stratification of LDs by size within treatments demonstrated that under HFHS conditions, in DGAT2 KO cells there were fewer of the smallest (< 1 μm^2) LDs, but more in the 1-5 μm^2 range (all $p < 0.05$; Figure 5.3.3-5G). Confocal microscopy showed well-defined LDs in KO cells, with fewer patches of very small LDs accumulating, as seen in the WT cells (Figure 5.3.3-5H & I). Apart from CIDEB, which was significantly upregulated, expression of LD-related genes did not change in response to DGAT2 KO (Table 5.3.3-1). A similar trend for changes in LD distribution was seen in the LFLS and LFHS-treated cells (Figure 5.3.3-5A-F). Although there was more variation in LD distribution in KO cells, the percentage falling within the 1-2 μm^2 range persisted in being significantly higher in KO cells compared to WT cells (both $p < 0.05$), primarily driven by a shift away from LDs < 1μm^2 in area (Figure 5.3.3-5A-F).

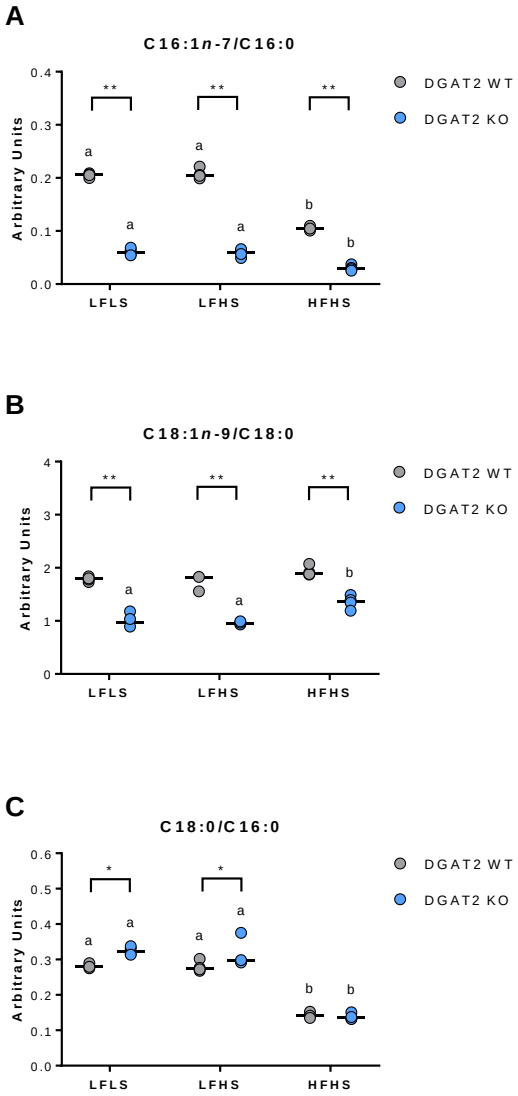


Figure 5.3.3-4. The effect of media composition on fatty acid desaturation and elongation in Huh7 cells with wildtype (WT) or knockout (KO) of the *DGAT2* gene. Once confluent, cells were treated with media containing 2% human serum and 11 mM glucose for seven days before treatment media was added. Treatments consisted of either low fat low sugar (LFLS; 11 mM glucose + 200 µM fatty acids), low fat high sugar (LFHS; 200 µM fatty acids + 11 mM glucose + 5.5 mM fructose) or high fat high sugar (HFHS; 800 µM fatty acids + 11 mM glucose + 5.5 mM fructose); all treatments contained 0.5 nM insulin. Indices of stearoyl-CoA desaturase activities for C16:0 (**A**) and C18:0 (**B**) and fatty acid elongase 6 activity (**C**) were calculated. Media was changed every 48 to 72 hours and 24 hours prior to collection. Data are presented as individual values and median, $n = 4$. * $p < 0.05$, ** $p < 0.001$; different letters denote significant differences between means within WT or KO cells, $p < 0.05$; two-way ANOVA with Bonferroni's multiple comparisons tests.

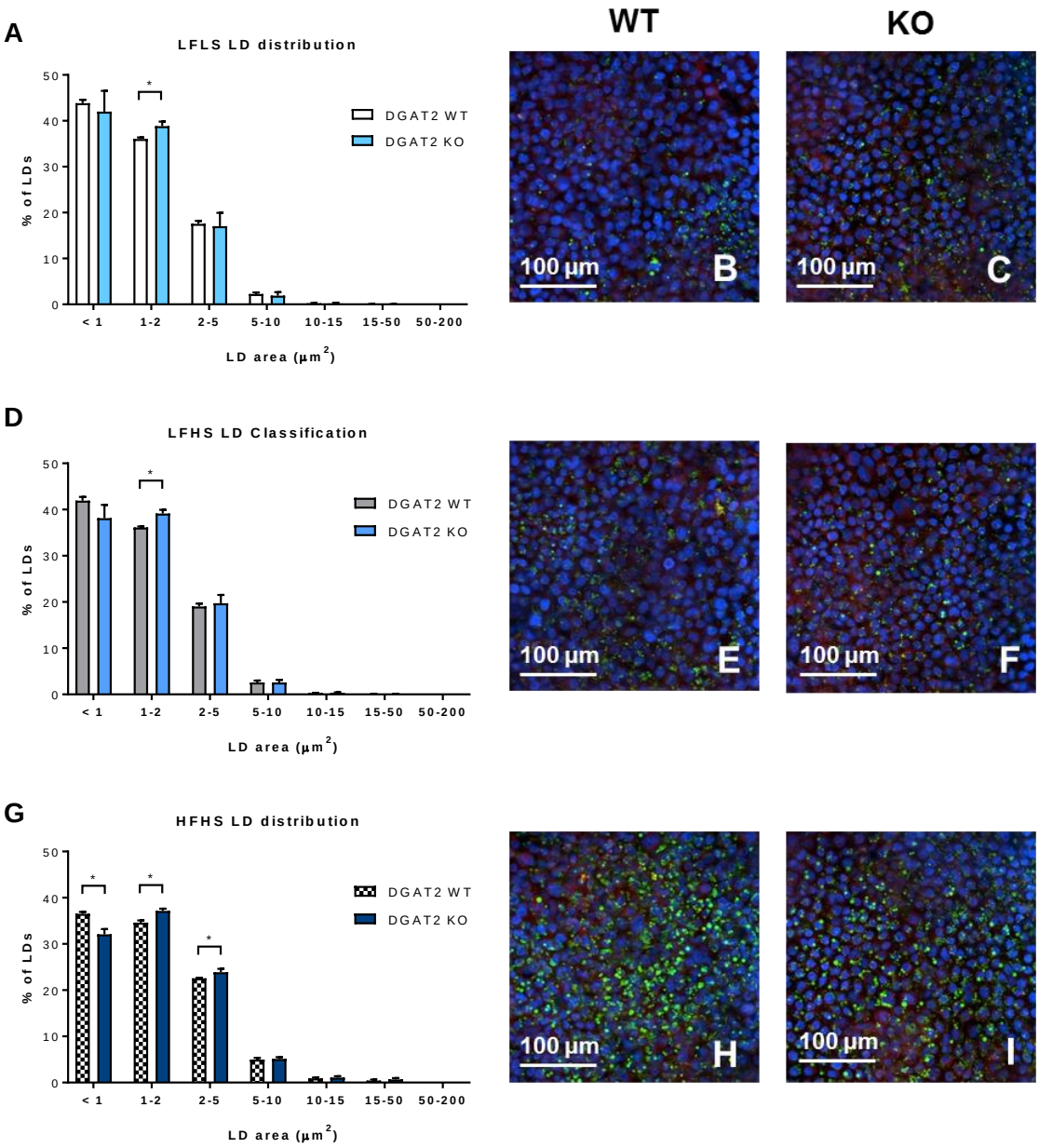


Figure 5.3.3-5. The effect of media composition on lipid droplet (LD) characteristics in Huh7 cells with wildtype (WT) or knockout (KO) of the *DGAT2* gene. Once confluent, cells were treated with media containing 2% human serum and 11 mM glucose for seven days before treatment media was added. Treatments consisted of either low fat low sugar (LFLS; 11 mM glucose + 200 µM fatty acids), low fat high sugar (LFHS; 200 µM fatty acids + 11 mM glucose + 5.5 mM fructose) or high fat high sugar (HFHS; 800 µM fatty acids + 11 mM glucose + 5.5 mM fructose); all treatments contained 0.5 nM insulin. LDs were identified and their area quantified using the IN Cell Analyzer 6000. Total LD populations were stratified by size in LFLS (**A**), LFHS (**D**) and HFHS (**G**) treated cells. Cells were stained with Hoechst (nuclei), BODIPY (LDs) and Mitotracker (mitochondria) and representative fluorescence images were obtained for WT (**B, E, H**) and KO (**C, F, I**) cells treated with LFLS (**B, C**), LFHS (**E, F**) and HFHS (**H, I**) at 40X magnification. Data are mean ± SD, $n = 4$, * $p < 0.05$ between WT and KO, Mann-Whitney test.

5.3.3.6 The effect of DGAT2 knockout on lipid secretion in Huh7 cells

Since there is conflicting evidence on how DGAT2 may affect lipoprotein secretion from the liver, media lipoproteins were analysed. Overall, less lipid was secreted from KO cells compared to WT cells (Figure 5.3.3-6A-F). In line with this, there was less TAG and fewer apoB particles secreted under all conditions in DGAT2 KO cells (all $p < 0.05$; Figure 5.3.3-6A & C), although no differences between media treatments were found in these parameters. As an indicator of lipoprotein lipidation, the amount of TAG per apoB particle was calculated, which was significantly lower as a result of DGAT2 KO ($p < 0.001$; Figure 5.3.3-6E); lipidation was also higher in HFHS-treated WT cells compared to KO cells ($p < 0.05$; Figure 5.3.3-6E). FPLC curves supported this finding, with larger areas displayed in WT cells and peaks at both VLDL and LDL-sized particles, in contrast to KO cells, which had a very small peak noticeable at only the LDL size (Figure 5.3.3-6G).

When cholesterol secretion was analysed, there were also consistently lower levels in the media of DGAT2 KO cells compared to WT (Figure 5.3.3-6B, D & F). Particularly, a divergence in secretion between WT and KO cells was evident in VLDL and total cholesterol secretion, with more cholesterol secreted in WT cells across all treatments; this was especially noticeable in HFHS-treated cells (all $p < 0.001$; Figure 5.3.3-6B & F). FPLC confirmed this pattern, with HFHS-treated KO cells displaying the smallest cholesterol curves, whereas WT cells treated with HFHS media had the largest curves (Figure 5.3.3-6H). In addition, there was significantly less cholesterol secreted in LDL-sized particles in HFHS-treated KO cells compared to LFLS-treated KO cells ($p < 0.05$; Figure 5.3.3-6D & F); this difference was also apparent in cholesterol secretion curves (Figure 5.3.3-6H).

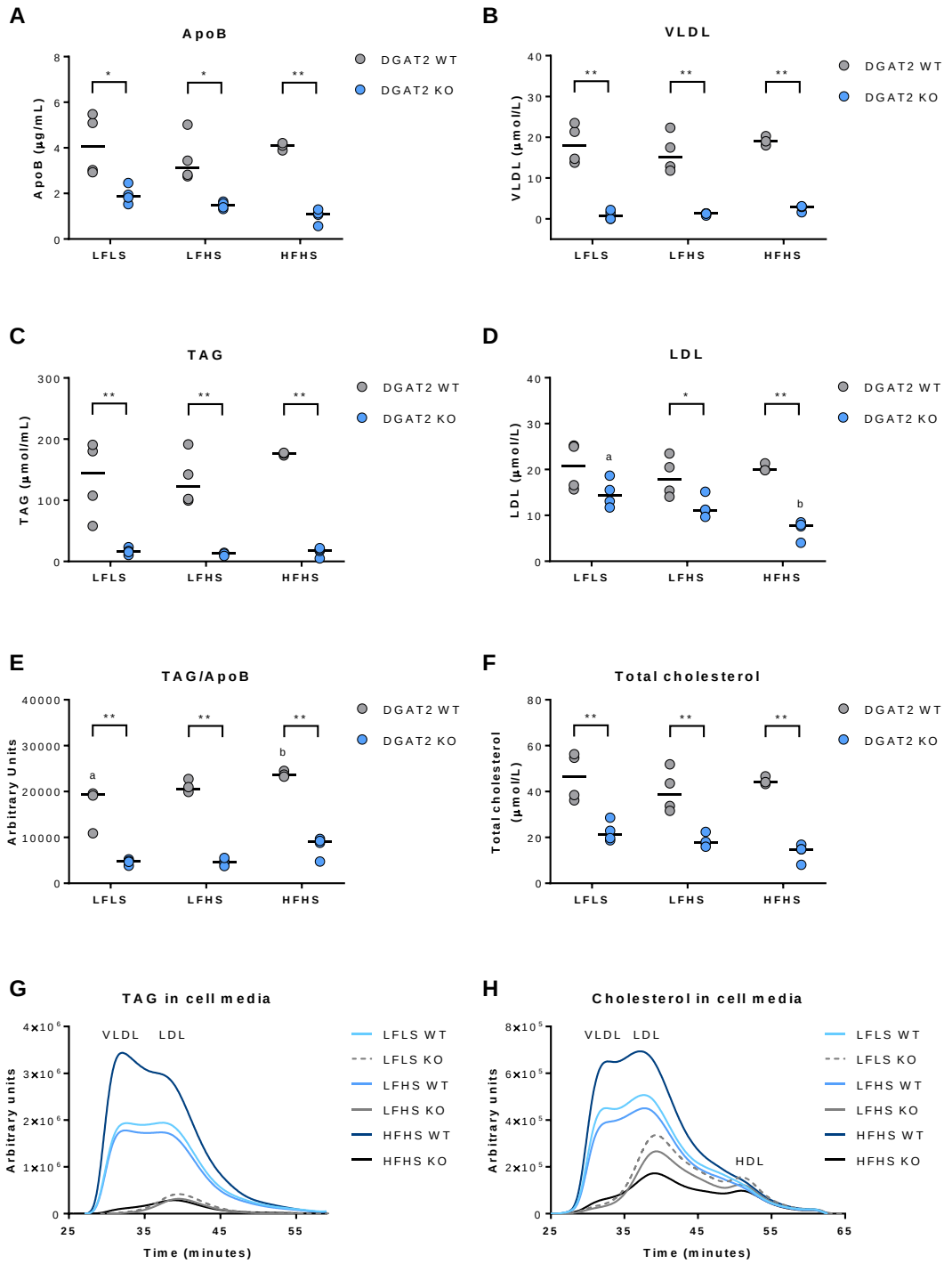


Figure 5.3.3-6. Figure legend can be found on the next page.

Figure 5.3.3-6. (Previous page) The effect of media composition on lipoprotein secretion in Huh7 cells with wildtype (WT) or knockout (KO) of the *DGAT2* gene. Once confluent, cells were treated with media containing 2% human serum and 11 mM glucose for seven days before treatment media was added. Treatments consisted of either low fat low sugar (LFLS; 11 mM glucose + 200 µM fatty acids), low fat high sugar (LFHS; 200 µM fatty acids + 11 mM glucose + 5.5 mM fructose) or high fat high sugar (HFHS; 800 µM fatty acids + 11 mM glucose + 5.5 mM fructose); all treatments contained 0.5 nM insulin. Cell media was collected and apolipoprotein B (ApoB) was measured (**A**). Media underwent size-exclusion chromatography to identify very low-density lipoprotein (VLDL) and LDL-sized lipoproteins and cholesterol content (**B** & **D**) was measured. Total triacylglycerol (TAG) in VLDL and LDL was also calculated (**C**), as was total cholesterol (**F**). TAG was expressed relative to as an indicator of particle size (**E**). Curves obtained for TAG (**G**) and cholesterol (**H**) from size-exclusion chromatography show the distribution of lipoprotein particle sizes in samples. Data are presented as individual values and median, or mean for curves, n = 3-4. * $p < 0.05$, ** $p < 0.001$; different letters denote significant differences between means within WT or KO cells, $p < 0.05$; two-way ANOVA with Bonferroni's multiple comparisons tests. *These samples were analysed by Professor Camilla Pramfalk at Karolinska Institutet, Sweden.*

5.3.3.7 The effect of DGAT2 knockout on FA composition secreted from Huh7 cells

As well as the amount and size of lipoproteins secreted, the origin and composition of FAs in the TAG and PL fractions were investigated. When WT and KO cells were compared, there were some consistent trends in the TAG composition in the media: KO cells tended to secrete more palmitoleate, stearate and linoleate than WT cells, but less oleate (Table 5.3.3-5; absolute values found in Appendix D, Table D.5). In the PL fraction, a similar pattern was seen in stearate and oleate (Table 5.3.3-6; absolute values found in Appendix D, Table D.6), as well as increased arachidonate secretion in PLs from LFLS-treated cells ($p < 0.05$; Table 5.3.3-6).

Table 5.3.3-5. The effect of media composition on fatty acid composition of triacylglycerol secreted in the media of Huh7 cells with wildtype (WT) or knockout (KO) of the *DGAT2* gene (mol%)

	LFLS		LFHS		HFHS	
	WT	**KO**	**WT**	**KO**	**WT**	**KO**
C16:0	28.3 (27.4 - 30.0)	29.2 (27.5 - 34.7)	27.8 (26.4 - 28.2)	30.3 (24.9 - 32.0)	26.8 (25.9 - 27.2)	29.2 (26.9 - 30.0)
C18:0	5.75 (4.97 - 7.55)^{a}	7.55 (6.07 - 8.61)	5.68 (5.14 - 6.21)^{*a}	7.96 (6.32 - 9.07)*	3.36 (3.30 - 4.12)^{**b}	6.63 (6.24 - 6.99)**
C16:1*n*-7	4.92 (4.82 - 5.74)^{**a}	3.33 (3.03 - 4.08)^{**a}	5.11 (4.64 - 5.60)^{**a}	3.50 (2.95 - 3.66)^{**a}	2.05 (2.02 - 2.10)^{b}	2.60 (2.23 - 2.68)^{b}
C18:1*n*-9	41.8 (41.1 - 42.5)^{*a}	38.3 (35.6 - 39.7)*	41.6 (41.5 - 44.1)^{*a}	37.9 (37.2 - 41.3)*	45.8 (45.2 - 46.7)^{**b}	40.0 (38.8 - 41.9)**
C18:1*n*-7	4.01 (3.50 - 4.95)^{*a}	2.57 (2.19 - 3.21)*	4.31 (4.17 - 5.71)^{**a}	2.56 (2.10 - 2.84)**	2.33 (1.86 - 2.46)^{b}	2.18 (1.68 - 2.86)
C18:2*n*-6	14.6 (13.3 - 15.4)^{**a}	17.7 (17.5 - 20.5)**	14.9 (13.8 - 15.8)^{*a}	17.9 (16.8 - 20.8)*	19.9 (18.6 - 20.1)^{b}	19.5 (18.7 - 20.9)

Once confluent, cells were treated with media containing 2% human serum and 11 mM glucose for seven days before treatment media was added. Treatments consisted of either low fat low sugar (LFLS; 11 mM glucose + 200 μM fatty acids), low fat high sugar (LFHS; 200 μM fatty acids + 11 mM glucose + 5.5 mM fructose) or high fat high sugar (HFHS; 800 μM fatty acids + 11 mM glucose + 5.5 mM fructose); all treatments contained 0.5 nM insulin. Data are presented as median (range), $n = 4$. * $p < 0.05$, ** $p < 0.001$; different letters denote significant differences between means within WT or KO cells, $p < 0.05$; two-way ANOVA with Bonferroni's multiple comparisons tests.

Table 5.3.3-6. The effect of media composition on fatty acid composition of phospholipids secreted in the media of Huh7 cells with wildtype (WT) or knockout (KO) of the *DGAT2* gene (mol%)

	LFLS		LFHS		HFHS	
	WT	**KO**	**WT**	**KO**	**WT**	**KO**
C16:0	28.3 (27.4 - 30.0)	29.2 (27.5 - 34.7)	27.8 (26.4 - 28.2)	30.3 (24.9 - 32.0)	26.8 (25.9 - 27.2)	29.2 (26.9 - 30.0)
C18:0	16.7 (16.2 - 17.7)*	20.7 (20.0 - 21.1)*	17.6 (16.4 - 20.0)*	20.5 (18.6 - 25.6)*	15.8 (15.1 - 16.6)*	20.6 (17.4 - 23.0)*
C18:1*n*-9	41.8 (41.1 - 42.5)*[a]	38.3 (35.6 - 39.7)*	41.6 (41.5 - 44.1)*[a]	37.9 (37.2 - 41.3)*	45.8 (45.2 - 46.7)[b]**	40.0 (38.8 - 41.9)**
C18:1*n*-7	2.12 (1.74 - 2.52)*[a]	2.00 (1.64 - 2.13)*	2.38 (2.11 - 2.62)**[a]	1.98 (1.39 - 2.57)**	1.39 (1.18 - 1.68)[b]	1.78 (1.59 - 2.17)
C18:2*n*-6	20.9 (20.3 - 21.5)[a]	22.0 (19.3 - 24.1)	22.4 (20.8 - 24.2)[a]	21.9 (20.0 - 23.5)	28.4 (26.4 - 29.9)*[b]	23.4 (21.2 - 25.2)*
C20:4*n*-6	6.13 (5.35 - 6.64)*	9.25 (7.58 - 9.95)*	7.27 (5.95 - 7.94)	8.14 (7.06 - 10.5)	7.04 (5.58 - 7.69)	8.65 (7.42 - 10.5)

Once confluent, cells were treated with media containing 2% human serum and 11 mM glucose for seven days before treatment media was added. Treatments consisted of either low fat low sugar (LFLS; 11 mM glucose + 200 μM fatty acids), low fat high sugar (LFHS; 200 μM fatty acids + 11 mM glucose + 5.5 mM fructose) or high fat high sugar (HFHS; 800 μM fatty acids + 11 mM glucose + 5.5 mM fructose); all treatments contained 0.5 nM insulin. Data are presented as median (range), $n = 4$. * $p < 0.05$, ** $p < 0.001$; different letters denote significant differences between means within WT or KO cells, $p < 0.05$; two-way ANOVA with Bonferroni's multiple comparisons tests.

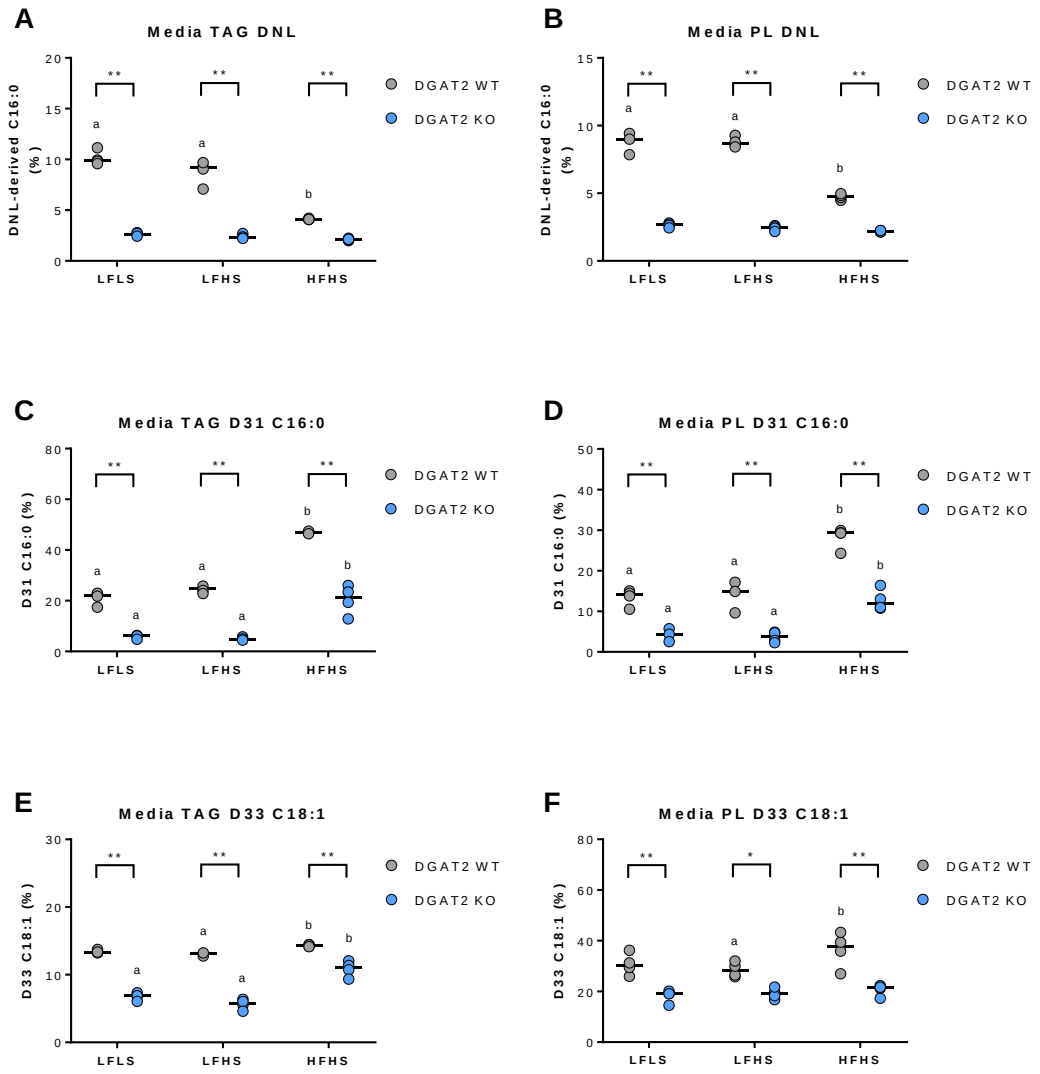


Figure 5.3.3-7. The effect of media composition on exogenous fatty acid (FA) secretion in Huh7 cells with wildtype (WT) or knockout (KO) of the *DGAT2* gene. Once confluent, cells were treated with media containing 2% human serum and 11 mM glucose for seven days before treatment media was added. Treatments consisted of either low fat low sugar (LFLS; 11 mM glucose + 200 µM FAs), low fat high sugar (LFHS; 200 µM FAs + 11 mM glucose + 5.5 mM fructose) or high fat high sugar (HFHS; 800 µM FAs + 11 mM glucose + 5.5 mM fructose); all treatments contained 0.5 nM insulin. Glucose and fructose consisted of 50% ^{12}C and 50% ^{13}C to allow tracing of carbon into *de novo* synthesised palmitate and contribution of DNL as a percentage of total TAG (**A**) and PLs (**B**) was calculated. The FA mix contained 100% labelling of $^{2}H_{31}$[palmitate] (D31) and $^{2}H_{33}$[oleate] (D33) to allow tracing of exogenous FAs into the media FA pool. Percentage enrichment of D31 palmitate in TAG (**C**) and PLs (**D**) was calculated as was enrichment of D33 oleate (TAG, **E**; PLs, **F**). Media was changed every 48 to 72 hours and 24 hours prior to collection. Data are presented as individual values and median, $n = 4$. * $p < 0.05$, ** $p < 0.001$; different letters denote significant differences between means within WT or KO cells, $p < 0.05$; two-way ANOVA with Bonferroni's multiple comparisons tests.

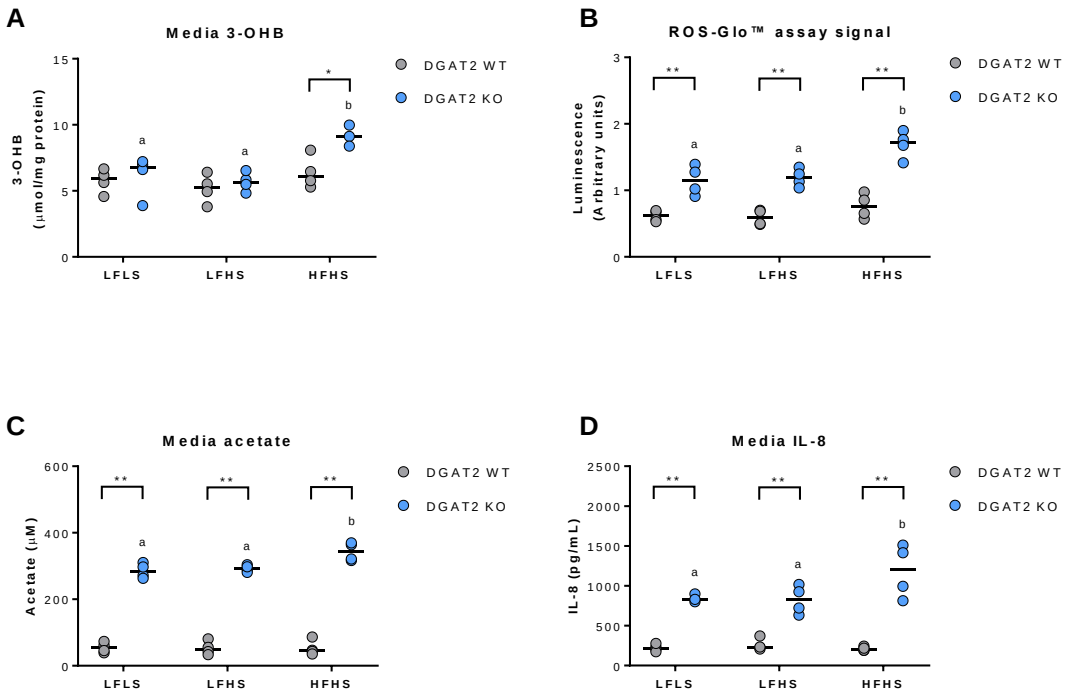


Figure 5.3.3-8. The effect of media composition on markers of fatty acid oxidation, oxidative stress and inflammation in Huh7 cells with wildtype (WT) or knockout (KO) of the *DGAT2* gene. Once confluent, cells were treated with media containing 2% human serum and 11 mM glucose for seven days before treatment media was added. Treatments consisted of either low fat low sugar (LFLS; 11 mM glucose + 200 μM fatty acids), low fat high sugar (LFHS; 200 μM fatty acids + 11 mM glucose + 5.5 mM fructose) or high fat high sugar (HFHS; 800 μM fatty acids + 11 mM glucose + 5.5 mM fructose); all treatments contained 0.5 nM insulin. As a marker of β-oxidation, media 3-hydroxybutyrate (3-OHB) was measured (**A**). Reactive oxygen species (ROS) were measured using the ROS-Glo™ assay (**B**) and media acetate was measured as a marker of peroxisomal β-oxidation (**C**). Interleukin (IL)-8 was measured as a marker of inflammation (**D**). Media was changed every 48 to 72 hours and 24 hours prior to collection and 3-OHB results are corrected to protein content. Data are presented as individual values and median, $n = 4$. * $p < 0.05$, ** $p < 0.001$; different letters denote significant differences between means within WT or KO cells, $p < 0.05$; two-way ANOVA with Bonferroni's multiple comparisons tests.

Tracer analysis of ^{13}C enrichment of palmitate (from labelled sugars) in media TAG was similar to that seen intracellularly, with KO cells and HFHS-treated cells having a smaller proportion of DNL-derived FAs (Figure 5.3.3-7A & B). However, when D31 palmitate in media TAG and PL was measured, there were some differences from what was seen in intracellular data: namely, the relative enrichment in KO cells appeared lower than WT cells (all $p < 0.001$, Figure 5.3.3-7C & D). In addition, whereas D33 oleate enrichment in intracellular TAG was relatively uniform in WT and KO cells, in the media, there was a more noticeable reduction in exogenous oleate in TAG and PLs from KO cells (all $p \leq 0.001$; Figure 5.3.3-7E & F). These lower enrichments in KO cells may be indicative of more exogenous palmitate and oleate being retained. When absolute values were analysed, results were similar (Appendix D, Figure D.3).

5.3.3.8 The effect of DGAT2 knockout on FA oxidation, oxidative stress and inflammation in Huh7 cells

It has been hypothesised that DGAT1 directs TAG toward a pool destined for oxidation, while DGAT2 has a larger role in directing TAG towards secretion (Li *et al.*, 2015a). There were no obvious differences between rates of β-oxidation, as measured by 3-OHB concentration in the media, between LF-treated WT and KO cells (Figure 5.3.3-8A). However, under HFHS treatment, media 3-OHB was significantly elevated in KO cells compared to WT cells and LF-treated KO cells ($p < 0.05$; Figure 5.3.3-8A); there was also more ROS in KO cells under all conditions ($p < 0.001$; Figure 5.3.3-8B). Oxidative stress can result from mitochondrial overload, or FAs being oxidised by alternative organelles. Measurement of acetate in the media, which is produced by peroxisomal β-oxidation, suggested that this may account for

the increase in ROS: not only was there significantly more acetate in the media KO cells compared to WT, there was also a significantly higher level in HFHS KO cells compared to their LF counterparts (all $p < 0.05$, Figure 5.3.3-8C). These results mirrored those observed in ROS, indicating that these two measures are closely related. Since ROS is associated with inflammation, interleukin (IL)-8, an inflammatory cytokine, was measured in the media; IL-8 was higher in DGAT2 KO cells compared to WT cells when cultured in all media and in HF *vs.* LF-treated KO cells (all $p < 0.05$; Figure 5.3.3-8D).

5.3.3.9 The effect of DGAT2 knockout on glucose metabolism in Huh7 cells

To further investigate hepatic metabolism in Huh7 cells, aspects of glucose metabolism were measured. Intracellular glycogen did not differ as a result of media treatments or between WT and KO cells (Figure 5.3.3-9A). In contrast, media lactate tended to be lower in DGAT2 KO cells across treatments, reaching significance under LFLS and LFHS conditions ($p < 0.05$; Figure 5.3.3-9B). Since glucose within the cell may be directed to DNL, glycogenesis or glycolysis, all of which were either downregulated or unchanged in KO cells, the amount of glucose remaining in cell media was determined: glucose was significantly higher in the media of KO cells compared to WT cells (all $p < 0.001$; Figure 5.3.3-9A). Although glucose uptake itself is not insulin-mediated in hepatocytes, its downstream pathways are, meaning it can be indirectly stimulated by insulin. When phosphorylation of Akt was measured as a marker of insulin sensitivity, there were consistently lower levels of phosphorylation in KO cells in response to insulin stimulation than WT cells (all $p < 0.001$; Figure 5.3.3-9D).

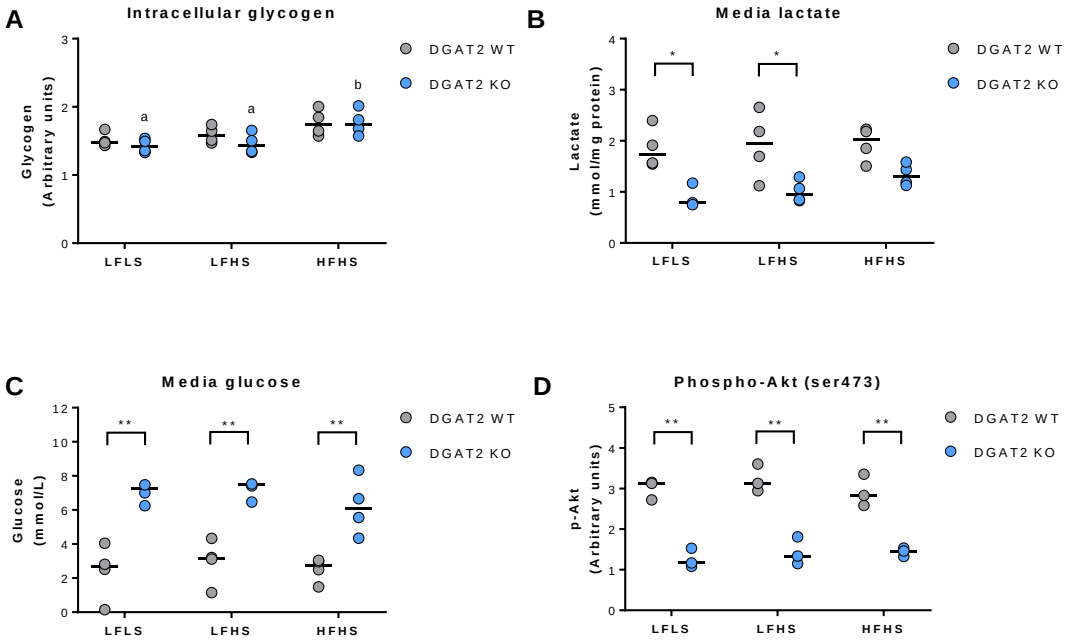


Figure 5.3.3-9. The effect of media composition on markers of glucose metabolism in Huh7 cells with wildtype (WT) or knockout (KO) of the *DGAT2* gene. Once confluent, cells were treated with media containing 2% human serum and 11 mM glucose for seven days before treatment media was added. Treatments consisted of either low fat low sugar (LFLS; 11 mM glucose + 200 µM fatty acids), low fat high sugar (LFHS; 200 µM fatty acids + 11 mM glucose + 5.5 mM fructose) or high fat high sugar (HFHS; 800 µM fatty acids + 11 mM glucose + 5.5 mM fructose); all treatments contained 0.5 nM insulin. Intracellular glycogen (**A**) and media lactate (**B**) were measured as markers of glucose storage and anaerobic glycolysis, respectively. Glucose remaining in the media after 24 hours was also measured (**C**). Phosphorylation of Akt at serine 473 was measured in samples stimulated for 10 minutes with 100 nM insulin and expressed relative to non-stimulated samples (**D**). Media was changed every 48 to 72 hours and 24 hours prior to collection and results are corrected to nuclei staining (glycogen) or protein content (lactate); for media glucose, this value was multiplied by the average protein content to approximate total remaining glucose. Data are presented as individual values and median, $n = 4$. * $p < 0.05$, ** $p < 0.001$; different letters denote significant differences between means within WT or KO cells, $p < 0.05$; two-way ANOVA with Bonferroni's multiple comparisons tests.

5.4 DISCUSSION

The aims of this chapter were to investigate the effect of a reduction in DGAT2 activity through both siRNA and CRISPR-Cas9 technologies and how this would interact with nutritional substrates as developed in Chapter 4. Although siRNA treatments were optimised through both a transfection indicator and targeting siRNA for the cells and protocol used, the final experiments showed high variation in transfection efficiency. Whilst some replicates showed the level of transfection desired, others did not display any reduction in *DGAT2* expression compared to their non-targeting control. Why this inconsistency occurred during this round of experiments is unclear. Although cells were from the same source, the latter experiment was from a fresh vial of Huh7 cells brought up from liquid nitrogen; the *DGAT2* siRNA was also from a new vial: whether these differences effected efficiency would require some further investigation, which unfortunately there was insufficient time to pursue.

In contrast, complete knockout of *DGAT2* using the CRISPR-Cas9 system was successful, providing a robust model in which to investigate the role of DGAT2 in FA metabolism in hepatocyte cells. Along with DGAT1, DGAT2 is a TAG-synthesising enzyme, meaning complete KO of one of these enzymes would be expected to reduce intracellular TAG storage. Despite an approximate two-fold increase in DGAT1 mRNA, a reduction in TAG was observed in KO cells. The differences in intracellular TAG could be accounted for by a number of observations; firstly, there was a tendency for cholesterol to increase, suggesting diversion of TAG precursors into alternative lipid synthesis pathways; secondly, there was a lower contribution of DNL-derived TAG; finally, there were more exogenous FAs remaining

in the media of KO cells, meaning there was less intracellular substrate available. Nonetheless, with only DGAT1 functioning, cells were able to store intracellular lipid and were responsive to the increased exogenous FAs in the HFHS condition, which stimulated intracellular TAG storage and LD synthesis in both cell types.

Analysis of LD distribution also highlighted differences between cell types, particularly that DGAT2 KO cells tended to have proportionally fewer of the smallest LDs, resulting in a shift towards more in the 1-5 μm^2 range. DGAT2 is known to bud off from the ER with LDs and is present with a number of other enzymes required for TAG synthesis, thus allowing LD growth within the cytosol (Kuerschner *et al.*, 2008; Wilfling *et al.*, 2013). In addition, inhibition of DGAT2 in hepatocytes has been found to cause accumulation of small LDs, suggesting DGAT2 has a role in LD growth (Becuwe *et al.*, 2018; Li *et al.*, 2015a; Wilfling *et al.*, 2013). Our data does not fully support this, since there were large LDs present even in the absence of DGAT2. However, Wilfling *et al.*, Li *et al.* and Becuwe *et al.* only treated cells with a single dose of one FA (oleate), for a shorter time period (12, 4 and 48 hours) and used rat hepatocytes, mouse hepatocytes and human breast cancer cells, respectively: results are therefore not directly comparable to our findings.

In fact, the differences observed in the present study are in line with what is currently hypothesised about protein targeting and LD growth. The presence of TAG-synthesising enzymes (GPAT4 and DGAT2) on LDs is hypothesised to occur *via* the ARF/COP-I complex, which removes a small LD from existing cytosolic LDs, in order to increase surface tension and allow the larger LD to reconnect with the ER. This allows these ER-resident proteins to

embed in the PL membrane of the LD, before it again buds off (Gluchowski *et al.*, 2017a). By abolishing *DGAT2* expression, this system may also have been downregulated, thus preventing the ARF/COP-I-mediated synthesis of small LD; although plausible, confocal microscopy with a higher resolution would be required to confirm this hypothesis. In addition, the absence of DGAT2 would not stop the coalescence of LDs or diffusion of lipid between LDs; these are the two main mechanisms through which LDs grow (Gluchowski *et al.*, 2017a; Walther *et al.*, 2017). We did not measure *CIDEC* expression in these experiments, which facilitates lipid diffusion between LDs: if expression is maintained or increased in DGAT2 KO, this would support the continued LD growth in KO cells.

Previous studies have suggested that DGAT2 preferentially uses *de novo*-derived FAs as a substrate (Choi *et al.*, 2007; Li *et al.*, 2015a; Qi *et al.*, 2012; Wurie *et al.*, 2012); the present results certainly support an interaction of DGAT2 activity with DNL. There was a striking downregulation in DNL-derived palmitate in DGAT2 KO cells, which accounted for less than 2 nmol/mg protein (~1-2% of total TAG), suggesting that in the absence of DGAT2, DNL is either downregulated, or DNL-derived FAs are diverted into alternative pathways. However, reduced expression of two key regulators of DNL, ChREBP (*MLXIPL*) and SREBP-1c (*SREBF1*), suggest that downregulation is more likely, which may indicate an adaptive, transcription factor-mediated mechanism that protects the cell from free, DNL-derived FAs that cannot be esterified without the activity of DGAT2. Although both transcription factors tended to be downregulated in KO cells compared to WT controls, ChREBP downregulation was particularly apparent.

This decrease in ChREBP transcription and activity appears to have had a number of effects on cellular FA metabolism. ChREBP is a known regulator of several GLUT transporters, including GLUT1, GLUT2, GLUT4 and GLUT5 (Iizuka, 2017; Iizuka *et al.*, 2004; Ma *et al.*, 2006; Yu *et al.*, 2014); GLUT2 is the main hepatic glucose transporter, although GLUT1 is also upregulated in hepatoma cells (Amann *et al.*, 2009). We did not measure the expression of these GLUT transporters; however, glucose was found to be present at higher concentrations in the media of KO cells after 24 hours (approximately 7 mM *vs.* 3 mM in WT cells), suggesting less glucose uptake in these cells. It has previously been reported that *Chrebp*$^{-/-}$ mice are intolerant to a high sucrose diet, likely due to downregulated GLUT expression in the small intestine (Iizuka, 2017). ChREBP also regulates the glycolytic enzymes glucose 6-phosphatase and glucokinase regulatory protein. In line with this, anaerobic glycolysis, as measured by increased media lactate levels, was reduced, although the apparent reduction in intracellular glucose did not affect glycogen content, demonstrating a reduction in ChREBP-specific pathways.

Apart from *MLXIPL* suppression reducing substrate availability, it may also have affected insulin signalling in DGAT2 KO cells, which tended to be lower than the WT cells. In mouse models, *Chrebp* deletion and overexpression has been implicated in reduced and increased insulin sensitivity, respectively (Benhamed *et al.*, 2012; Jois *et al.*, 2017), while cross-sectional data from liver biopsies has shown reduced *MLXIPL* expression in insulin resistant patients (Benhamed *et al.*, 2012). *SREBF1*, the other master regulator of hepatic DNL, also showed a tendency for reduced expression in KO cells, the transcription of which is known to be

insulin-mediated (Tarling *et al.*, 2004). Downregulation of both of these transcription factors would therefore account for the reduction in DNL, as well as the reduced expression in a number of DNL genes observed, including *SCD*, *ELOVL6*, *FADS1* and *FADS2*. It would therefore be plausible to suggest that the effect of DGAT2 on DNL was mediated by lower mRNA expression, and presumably activity, of ChREBP and SREBP-1c.

How DGAT2 regulates the expression of *MLXIPL* and *SREBF1* is not clear and is complicated by the fact that some factors (*e.g.* insulin signalling) could be both a cause and consequence (Benhamed *et al.*, 2012; Sirek *et al.*, 2009; Tarling *et al.*, 2004). *MLXIPL* transcription was particularly suppressed and although relatively little is known about the transcriptional regulation of this gene (Iizuka & Horikawa, 2008; Uyeda & Repa, 2006), one study has identified a region in the *MLXIPL* promoter that interacts with octamer transcription factor-1 (Oct-1), which was found to suppress *MLXIPL* transcription (Sirek *et al.*, 2009). Oct-1 is also known to be regulated by cellular stress (Tantin *et al.*, 2005; Wang & Jin, 2010b) and specifically by H_2O_2 (Wang & Jin, 2010a). We found increased H_2O_2 (as measured by the ROS-Glo™ assay) in DGAT2 KO cells, which may have increased Oct-1 levels, thus downregulating *MLXIPL* expression; however, more experiments would be required to confirm this, and other, mechanisms behind *MLXIPL* suppression in DGAT2 KO cells.

Differences between WT and DGAT2 KO cells were also noted in their FA composition. As expected, DGAT2 cells tended to have proportionally lower levels of FAs that can be derived from DNL in the TAG and PL fraction. In addition, there were differences evident in PUFA content of FAs: a high level of linoleate remaining in the media of HFHS-treated KO cells,

despite there being, in absolute amounts, similar concentrations in PL, and a much lower amount in the TAG fraction. Previously, *Dgat2*$^{-/-}$ mice were found to have reduced linoleate content in TAG, FFA and CEs, as well as acylceramide, for which linoleate is a precursor, despite maternal levels being normal (Senkal et al., 2017; Stone *et al.*, 2004). In both TAG and PL fractions in the present study, linoleate accounted for a similar percentage of FAs in both WT and KO cells in the HFHS condition, suggesting an optimal ratio of intracellular linoleate to other FAs. Taken together, these results may imply that linoleate is a preferred substrate for DGAT2, which, when not functioning, results in impaired disposal and selective uptake of alternative FAs, in contrast to the canonical viewpoint of FA uptake proportional to extracellular concentration (Mashek, 2013).

Apart from differences in FA uptake, DGAT2 KO cells also seemed to have altered levels of elongation and desaturation of the essential PUFAs. *ELOVL2* expression tended to be increased and specifically in the PL fraction, there tended to be more docosahexaenate (DHA; C22:6*n*-3), which was accompanied by a decrease in the precursor FAs, especially α-linolenate (C18:3*n*-3), suggesting further metabolism of this FA to long chain (LC) *n*-3s. Given both *FADS1* & *2* appeared to be downregulated and *ELOVL5* expression was unchanged, this increased production of DHA in KO cells is counterintuitive. However, it has been shown that C20 and C22 *n*-3 and *n*-6 FAs can inhibit earlier desaturation steps in LCPUFA synthesis (Fisher *et al.*, 1989), meaning the lower absolute amounts of FAs in KO cells may have allowed more desaturase activity despite lower mRNA expression levels. There is also emerging evidence that DNL-derived palmitate may be desaturated to sapienate (C16:1*n*-10) *via*

FADS2 (Park *et al.*, 2016): low levels of DNL in KO cells may therefore have decreased competition for the FADS2 enzyme.

The observed increase in DHA abundance is supported by an increase in media acetate, which is a marker of peroxisomal FA oxidation (Leighton *et al.*, 1989); this process is required to produce DHA (C22:6*n*-3) from nisiniate (C24:6*n*-3) *via* removal of one acetyl-CoA for oxidation (Poirier *et al.*, 2006; Su *et al.*, 2001). In addition, peroxisomal β-oxidation is a source of ROS (Sandalio *et al.*, 2013), as is ω-oxidation in the ER (Miura, 2013). We did not measure ω-oxidation, which occurs during oxidative overload in the liver to maintain FA homeostasis (Miura, 2013); however, considering changes in ROS levels were very closely associated with acetate levels, peroxisomal oxidative activity seemed to be the primary source of ROS in the cells. In addition, mitochondrial β-oxidation, measured by 3-OHB production, did not differ between low fat-treated WT and KO cells, suggesting that the oxidative pathway was not saturated, but peroxisomal activity was increased primarily for its LCFA-shortening capacity.

That a more dramatic difference in mitochondrial β-oxidation wasn't seen between DGAT2 KO and WT cells may be unexpected, since loss of DGAT2 activity has previously been shown to increase hepatic FA oxidation (Choi *et al.*, 2007; Li *et al.*, 2015a; McLaren *et al.*, 2018; Yu *et al.*, 2014). If increased DGAT1 or decreased DGAT2 activity does mediate elevated FA oxidation, our results may be for two reasons. Firstly, a lack of substrate (*i.e.* less intracellular TAG) in the DGAT2 KO cells may have masked a potential upregulation of this pathway; in line with this, the biggest difference between WT and KO cells in FA oxidation was in the HFHS condition, where FA availability would have been increased. In addition, certainly in

comparison to HepG2 cells, *PNPLA2* expression was low in Huh7 cells (see Chapter 3, section 3.3.3.3). This lipase (adipose triglyceride lipase; ATGL) is thought to generate FAs specifically targeted for FA oxidation; with increased ATGL activity, bigger differences in FA oxidation may have been evident.

The effect of low TAG levels was also noted in relation to secretion. Previously, DGAT2 has been hypothesised to have a role in VLDL assembly and secretion (Li *et al.*, 2015a; Wurie *et al.*, 2012; Zammit, 2013): our results confirm that DGAT2 is required for this process and that it cannot be fully compensated for by DGAT1. Work from Chapter 4, along with previous research (Dashti *et al.*, 1987; Ellsworth *et al.*, 1986; Wu *et al.*, 1996), suggests that by increasing the amount of substrate with exogenous FAs, lipoprotein secretion profiles could be improved. Reduced VLDL secretion in DGAT2 KO cells could have been due to their tendency to have less intracellular TAG, and therefore less substrate, with which to lipidate apoB particles. However, the magnitude of difference seen between WT and KO cells and the fact that even under HFHS conditions, when intracellular TAG was higher in KO cells than LF-treated WT cells, TAG secretion was still supressed suggesting a more regulatory role of DGAT2 in lipoprotein assembly.

Results obtained from primary mouse hepatocytes and DGAT1 and 2 inhibitors led Li *et al.*, to hypothesise that both DGATs direct some TAG towards luminal LDs and primordial apoB particles for use in the assembly of VLDL particles, but most synthesised by DGAT1 are incorporated into luminal and cytosolic LDs, while DGAT2 presence at the ER was additionally required to re-esterify lipolysed TAG from cytoplasmic and luminal LDs for

maturation of VLDL particles (Li *et al.*, 2015a). This is in line with the observations of Gibbons *et al.*, who, using primary rat hepatocytes and [^{3}H]oleate, demonstrated that there is a time lag between maximal TAG storage and maximal VLDL secretion (Gibbons *et al.*, 1992), leading to the theory of a secretory pool of lipid within the ER, which requires exogenous FAs to undergo esterification into a LD, before lipolysis and re-esterification to enter the secretory pool (Gibbons *et al.*, 1992). A role for DGAT2 in this process is supported by the present results, where DGAT2 KO cells appeared to have intracellular TAG sequestered in a pool that was not accessible for VLDL secretion.

Furthermore, by tracing stable isotopes in Huh7 cells both intracellularly, and into secreted particles, we noticed a difference in enrichment between *de novo*-derived and exogenous FAs in secreted particles. Whereas DNL-derived palmitate in the media was reflective of the enrichment pattern seen intracellularly, both D31 palmitate and D33 oleate were enriched at a much lower extent in the media of KO cells. Taken together with previous work, these results may indicate that upon synthesis, DNL-derived TAG is distributed equally to the cytosolic and secretory (apoB-associated) pools, whereas the majority of exogenous FAs are directed first to a cytosolic or luminal LD, which is then lipolysed and re-esterified for lipidation of VLDL particles as they mature. In human participants, the proportions of DNL, diet and adipose-derived TAG in VLDL closely matched intracellular pools determined by liver biopsy (Donnelly *et al.*, 2005); it may therefore be that our DGAT2 KO model represents an 'early stage' lipoprotein particle that has enough lipid for secretion, but has not fully undergone lipidation with exogenous FA.

Whether the DGAT enzymes themselves have a direct role on partitioning TAG to different storage pools or for VLDL maturation is unknown. In contrast, another ER-resident protein, fat storage-inducing transmembrane protein 2 (FIT2), is believed to be involved with this process (Choudhary *et al.*, 2015; Goh & Silver, 2013). This enzyme has a regulatory role in LD synthesis (see Chapter 1, section 1.1.3.3) and has been found to function in association with both DGAT proteins, but particularly DGAT2 (Becuwe *et al.*, 2018; Cai *et al.*, 2017). Previously, in response to *FIT2* KO, both *DGAT1* and *DGAT2* expression were downregulated (Becuwe *et al.*, 2018). If a reciprocal mechanism in DGAT2 KO cells exists, it may not be DGAT2 activity *per se* that is responsible for the additional lipidation step of lipoproteins, but that a change in the expression or function of FIT2 prevented re-esterified exogenous FAs being directed to a luminal LD for later VLDL maturation in the DGAT2 KO cells. The interaction between DGAT enzymes and FIT2 in partitioning of lipid for storage and secretion would be interesting to investigate further.

The inclusion of three media treatments in comparing DGAT2 WT and KO cells was to allow assessment of how gene editing may interact with nutrient availability, and particularly the steatotic model induced by the HFHS treatment. Although DGAT2 KO cells seemed to adapt well to a complete removal of DGAT2 activity, including by upregulating expression of *DGAT1*, there were some signs of cellular stress that were augmented in the HFHS-treated cells, namely ROS production and IL-8 secretion. Since DGAT1 is primarily believed to use exogenous FAs as a substrate (Li *et al.*, 2015a; Villanueva *et al.*, 2009) and be important in protecting cells from free FA toxicity (Chitraju *et al.*, 2017), it may be that the increased

supply of FA in the HFHS treatment was sufficient to overload DGAT1 in these cells, which began to switch from a 'benign' steatotic phenotype, as described in Chapter 4, to a more 'progressive' phenotype. This may suggest that DGAT2 offers a protective role in hepatic steatosis; however, a complete knockout is clearly an extreme model and while useful for determining the function of DGAT2, only offers limited insight into its pathogenic role. Therefore, how partial impairment of the DGAT2 enzyme affects metabolism and cellular stress would be of interest.

There were some limitations to this work. Firstly, although we confirmed DGAT2 KO by sequencing, confirmation of this at the protein level is required: to our knowledge, no good DGAT2 antibodies currently exist. In addition, we only measured FAs present in TAG and PLs; DGAT2 may have a role in the formation of other lipid species, including DAG and acylceramides (Senkal *et al.*, 2017). As a result, measurement of more lipid classes may have offered additional insight into the pathogenic and signalling effects of DGAT2 activity. Only labelled sugars were used to measure DNL in this chapter, as opposed to heavy water in previous chapters; this may therefore have underestimated total DNL, since contribution from non-sugar sources would have been missed. However, given the downregulation of DNL genes in KO cells, even though absolute amounts may have differed slightly if heavy water had been used, it's likely the same pattern of reduced DNL in KO cells would have been observed. Finally, it has been shown that monoacylglycerol transferase (MGAT)3 possesses some DGAT activity (Brandt *et al.*, 2016): some contribution of compensatory MGAT activity in DGAT2 KO cells therefore cannot be excluded.

5.5 SUMMARY

- Although there were promising preliminary results, siRNA knockdown of *DGAT2* was not successful for the final experiments, meaning the impact of a partial reduction in DGAT2 activity was not investigated
- CRISPR-Cas9 mediated knockout of *DGAT2* was successful and created a viable, proliferative cell line in which to investigate FA metabolism in response to different concentrations of sugars and fat
- There were several changes in DGAT2 KO cells, particularly, lower intracellular TAG levels, a marked reduction in DNL and *MLXIPL* expression and secretion of very TAG-poor lipoprotein particles
- Although the cells seemed able to adapt to not having DGAT2 activity, in the HFHS condition, designed to increase TAG and LD accumulation similar to that seen in NAFLD, there were increases in ROS and IL-8 levels, possibly due to a saturation of DGAT1 activity
- Overall, results confirmed previous reports of DGAT2 using DNL-derived substrates and was required for addition of TAG to VLDL particles; however, how a less extreme, physiological, change in DGAT2 activity contributes to metabolism remains to be investigated

Chapter 6

Investigating the interaction between *DGAT2* mutations and sugar overfeeding in humans

6.1 INTRODUCTION

In the last several decades, there has been an increase in the prevalence of obesity and obesity-related disease, including NAFLD (Younossi *et al.*, 2016). Sugar has been postulated to be a driver of this trend; epidemiological data suggest increasing fructose intakes track with the rise in obesity and metabolic disease (Lim *et al.*, 2010; Tappy & Le, 2010). Particularly relevant to NAFLD is the stimulatory role sucrose, which is composed of equimolar amounts of glucose and fructose, may have on hepatic *de novo* lipogenesis (DNL) (Hudgins *et al.*, 2011; Sanders & Griffin, 2016; Tappy & Le, 2010). This process would contribute newly-synthesised fat directly to the hepatic lipid pool and is known to be upregulated in individuals with NAFLD, although whether it precedes, or is a consequence of, NAFLD is less certain (Diraison *et al.*, 2003; Donnelly *et al.*, 2005; Lambert *et al.*, 2014). Although both cross-sectional and dietary intervention studies exist linking fructose overfeeding to increases in liver fat, meta-analyses have shown that when fed isocalorically, there is no significant impact of fructose on liver fat accumulation (Chiavaroli *et al.*, 2015; Chiu *et al.*, 2014; Chung *et al.*, 2014). Nonetheless, speculation as to the role of sugar in NAFLD development continues.

Since DGAT2 has a key role in DNL and very low-density lipoprotein (VLDL) secretion, it has been hypothesised to be the link between a high-carbohydrate 'Western' diet and hypertriglyceridaemia present in cardiometabolic disorders (Zammit, 2013). As a result, investigation of the effect of DGAT2 inhibitors in humans and higher primates has been undertaken; however, these have yielded modest and inconclusive results. McClaren *et al.* carried out a number of studies using DGAT2 inhibitors and siRNA in non-human primates:

they found that reducing DGAT2 activity via either method did not affect VLDL secretion, although DNL was not measured (McLaren *et al.*, 2018). Nicotinic acid, or niacin (vitamin B3), has also been used therapeutically as a DGAT2 inhibitor (Ganji *et al.*, 2004). To date, all interventions resulted in significant reductions in plasma triglycerides and increases in high-density lipoprotein cholesterol; however, these improvements in plasma lipids were seen alongside a reduction in insulin sensitivity (Blond *et al.*, 2014; Fabbrini *et al.*, 2010; Hu *et al.*, 2012).

In addition, Hu *et al.*, looked at the effects of two common *DGAT2* single nucleotide polymorphisms (SNPs; rs3060 and rs101899116) on participant response to Niacin therapy (Hu *et al.*, 2012). Both of these SNPs resulted in a smaller reduction in liver fat than seen in the cohort as a whole. A similar finding was reported previously in subjects with the rs1944438 SNP in *DGAT2*, who had a smaller reduction in liver fat in response to a lifestyle intervention than non-carriers (Kantartzis *et al.*, 2009). In line with the inhibitor data, *DGAT2* mutations in this study were related to a dissociation between liver fat and insulin sensitivity (Kantartzis *et al.*, 2009). Although neither of these studies reported significant effects of *DGAT2* SNPs on plasma biochemistry, a *de novo* missense mutation (p.Y223H) in DGAT2 found in a Korean male with Charcot-Marie-Tooth disease was associated with a reduction in plasma triacylglycerol (TAG) (Hong *et al.*, 2016).

Given the conflicting evidence regarding the role of sugar in liver fat accumulation and the evidence of *DGAT2* mutations mediating liver fat changes, a pilot study was undertaken with the following aims:

1. To investigate the effect of a sugar overfeeding intervention on hepatic *de novo* lipogenesis, liver fat content and whole-body metabolism
2. To establish whether SNPs in the *DGAT2* gene may modify the impact of sugar overfeeding on metabolic responses

6.2 METHODS

6.2.1 Identification of *DGAT2* mutations and participant characteristics in the Oxford Biobank cohort

This analysis was carried out by Dr. Matthew Neville.

The Oxford Biobank (OBB) is a cohort of healthy 30- to 55-year-old men and women from Oxfordshire. Participants undergo a range of biochemical and anthropometric measures and blood is collected for DNA extraction (Karpe *et al.*, 2018). SNPs are identified using the Illumina Infinium Core Exome 24 v1 array ($n = 4500$) and the Affymetrix UK Biobank Axiom array ($n = 7122$) and genotypes called using standard quality control criteria. Allele frequencies and association statistics were generated in the PLINK whole genome association analysis toolset (Purcell *et al.*, 2007). The impact of the missense variants on the protein were assessed in the online consensus tool predictSNP (https://loschmidt.chemi.muni.cz/predictsnp2/). Two SNPs of interest were found that were associated with an altered metabolic phenotype, rs151179593 and rs140793537: participants with these mutations were selected for a recruit-by-genotype study.

6.2.2 DNA sequencing of Huh7 cells

As a result of identification of these SNPs, sequencing of *DGAT2* was undertaken in Huh7 cells. Polymerase chain reaction (PCR) was used to amplify the region of interest within the *DGAT2* gene. By combining appropriate primers, DNA polymerase and nucleotides with DNA and then cycling temperatures for denaturation, annealing and extension, a particular

region of interest is amplified for analysis. In Sanger sequencing, once the region of interest has been amplified and purified, PCR is repeated. Fluorescently labelled, chain-terminating dideoxynucleotides are used, allowing each base pair to be identified as fragments migrate through a capillary based on size, before fluorescence of deoxynucleotide is detected.

6.2.2.1 Primer design for DGAT2 Exon 6 & 7

DGAT2 is located on the long arm of chromosome 11 (11q13.5), and has nine exons. Forward and reverse primers for Exon 6 and Exon 7 of *DGAT2* were designed using Primer-BLAST (https://www.ncbi.nlm.nih.gov/tools/primer-blast/). Sequences and characteristics of primers can be found in Appendix E, Table E.1. Two forward and reverse primers were designed for each exon and ordered from Sigma-Aldrich (Gillingham, UK). Primers were selected based on a melting temperature between 57°C and 63°C, a G/C content between 30 and 80%, a length between 18 and 22 base pairs and a difference in melting temperature between the two primers of less than 2°C.

6.2.2.2 DNA extraction of Huh7 cells

DNA was extracted from HS-treated Huh7 cells using the QIAGEN AllPrep DNA/RNA Mini Kit (QIAGEN Sciences; MD, USA). This kit utilises microspin columns and selective binding to purify genomic DNA from samples. Samples were collected as described for RNA extraction in Chapter 2, section 2.2.3.1. After samples were defrosted to room temperature, they were heated 37°C to ensure samples were thawed and salts dissolved, before being transferred into an AllPrep DNA spin column. Columns were washed first with buffer AW1 to denature proteins, followed by buffer AW2 to remove salts. Finally, buffer EB, a Tris-based

solution, was added to columns in two elution steps. All centrifugation was carried out at 15,000 x g for 1-2 minutes. DNA was quantified using the NanoDrop ND-1000 Spectrophotometer (Thermo Scientific; Hemel Hempstead, UK), as described in Chapter 2, section 2.2.3.1.

6.2.2.3 Polymerase chain reaction

DNA amplification was carried out with REDTaq® ReadyMix™ PCR Reaction Mix (Sigma-Aldrich; Gillingham, UK). REDTaq® ReadyMix is a mixture of Taq DNA polymerase, deoxynucleotides, reaction buffer, and a red dye, which eliminate the need to add a loading buffer/tracking dye prior to electrophoresis. PCR was carried out with a 10 µL reaction consisting of 5 µL REDTaq, 1 ng DNA, 5 µM forward and reverse primers and nuclease-free water. For each exon, all combinations of forward and reverse combinations were used. Samples were first heated to 95°C for 10 mins, before 30 cycles of 94°C for 30 seconds, annealing for 30 seconds and extension at 72°C for 1 minute. Annealing was initially run at 55.0, 55.4, 56.3, 57.5, 59.2, 61.4, 63.9, 66.7, 67.7, 68.9, 69.7 and 70.0°C.

6.2.2.4 Agarose gel electrophoresis

To determine the most effective combination of primers and annealing temperature for DNA amplification, electrophoresis was carried out using 2% (w/v) agarose gels. Gels were prepared using 5 g agarose in 250 mL 1X Tris Borate EDTA (TBE) buffer (pH 8.3); a 10X stock of TBE containing 1 M Tris base, 1 M boric acid and 0.02 M EDTA (0.5M) was diluted and the mixture was heated in a microwave oven until the agarose had completely dissolved. Ethidium bromide was then added and the gel was cast using a Multi Sub tank (Appleton

Woods Ltd, Birmingham, UK). Once set, combs were removed and the gel was covered with TAE and 3 µL of a 1 Kb Plus DNA Ladder (Invitrogen, Thermo Scientific; Hemel Hempstead, UK) and 10 µL of PCR product was loaded. Electrophoresis was carried out 150 V for 30 minutes. Bands were visualised using the ChemiDoc™ MP System (Bio-Rad; Hemel-Hempstead, UK).

6.2.2.5 PCR product cleanup

For exon 6 and 7, forward primer 2 and reverse primer 1 at an annealing temperature of 59.2°C was found to be optimal. PCR and electrophoresis was repeated under these conditions, before 1 µL ExoSAP-IT™ PCR Product Cleanup Reagent (Applied Biosystems, ThermoFisher Scientific; Hemel Hempstead, UK) was added to samples, which hydrolyses any remaining primers or nucleotides. Samples were heated to 37°C for 30 mins to enable hydrolysis, and then 80°C for 15 minutes for enzyme denaturation. SureClean Plus (Bioline Reagents Ltd.; London, UK) was next added, and the sample was centrifuged at 14,000 x g for 10 minutes. Supernatant was removed and the pellet was twice resuspended in ethanol and centrifuged at 14,000 x g for 10 minutes. Finally, the pellet was dried, resuspended in 10 µL Tris EDTA buffer and sent for Sanger sequencing.

6.2.3 Dietary intervention and postprandial study days

6.2.3.1 Subjects

We initially identified 25 individuals with *DGAT2* rs151179593 Gly250Asp variant (G>A); Group A) and 57 individuals with *DGAT2* rs140793537 Arg297Gly variant (G>A); Group B) within the Oxford BioBank (Karpe *et al.*, 2018) (www.oxfordbiobank.org.uk) and they were

invited to take part in the study. To date, four individuals (one rs151179593 carrier; group A and three rs140793537 carriers; group B) volunteered to participate. We then recruited (to date) three age and BMI matched individuals (wild-type for *DGAT2*; controls). All volunteers were considered non-diabetic and free from any known disease, had a body mass index <35 kg/m^2, were not taking medication known to affect lipid or glucose metabolism, did not smoke and did not consume alcohol above recommended limits (Chalasani *et al.*, 2012). The study was approved by North East - Tyne & Wear South Research Ethics Committee (17/NE/0031); all subjects gave written informed consent.

6.2.3.2 Dietary intervention

Subjects consumed a standardised diet (based on the EatWell Plate) for 5 days prior to the baseline study day, to ensure all participants had a similar starting point of dietary intake for carbohydrate, fat and protein. Participants then underwent a metabolic study day (detailed below). Over the course of the study day, participants met with the study dietitian (Dr. Pamela Dyson) who instructed them on how to change their diet so that it was isocaloric but included a higher amount of free sugars. Participants were provided with foods such as soft drinks and sweets, along with written instructions on how to achieve the dietary targets; the study team were in regular contact with participants to provide support and help compliance; the aim was a free sugar intake of 25% total energy for 2-3 weeks. Participants filled in 3-day diet diaries (including at least one weekend day) every week during the study and dietary analysis was carried out using Nutritics software (Nutritics Ltd.; Swords, Ireland).

6.2.3.3 Determination of liver fat and body composition

Intra-hepatic fat was measured by magnetic resonance spectroscopy (MRS) after an overnight fast and within one week of the study day (Banerjee *et al.*, 2014). On the study day, whole body composition and fat quantification and distribution were assessed by dual-energy X-ray absorptiometry (DXA) using the GE Lunar iDXA and all data are analysed with Encore software (version 11.0; GE Medical Systems; WI, USA), which beyond regional body composition also includes an algorithm for quantification of visceral adipose tissue (VAT) (Karpe *et al.*, 2018). Quantification of intra-hepatic fat using MRS and whole body composition and fat quantification using DXA were performed at before and after the dietary intervention.

6.2.3.4 Postprandial study day

Prior to the study day, participants were asked to avoid foods naturally enriched in ^{13}C (*e.g.* corn based foods such as cornflakes) and refrain from strenuous exercise and alcohol for 24 hours. The evening prior to the study day, subjects consumed deuterated water ($^{2}H_2O$) (3 g/kg body water) and continued to consume $^{2}H_2O$ during the course of the study day. To maintain a plasma water enrichment of 0.3% they consumed 4.5 g $^{2}H_2O$/L of filtered water for the measurement of fasting and postprandial hepatic DNL.

On the study day, after an overnight fast and consumption of $^{2}H_2O$, subjects came to the clinical research unit and a cannula was inserted into an antecubital vein, and baseline (time point 0 hours) blood and breath samples taken. Participants were then fed a mixed test meal, consisting of 40 g Rice Krispies (Kelloggs; Manchester, UK), 200 g skimmed milk and a

chocolate drink containing 40 g olive oil (the test meal contained 40g fat, 40g carbohydrate). Two hundred mg of [U^{13}C]palmitic acid was added to the chocolate milkshake to trace the fate of the dietary fatty acids.

Repeated blood and breath samples were taken at 0, 30, 60, 120, 180, 240, 300 and 360 minutes after consumption of the meal over the course of the study day. Indirect calorimetry was performed 120 minutes after consumption of the meal using a Gem Calorimeter (GEMNutrition Ltd.; Daresbury, UK), to determine whole body CO_2 production and whole body respiratory exchange ratio (RER), and net carbohydrate and fat oxidation rates.

6.2.3.5 Analytical methods

Whole blood was collected into heparinized syringes (Starstedt; Leicester, UK) and plasma was rapidly separated by centrifugation at 4˚C for the measurement of plasma metabolite and insulin concentrations as outlined in Chapter 2, section 2.2.2 and as previously described (Hodson *et al.*, 2007). Separations of chylomicron-Svedberg flotation rate (S_f) >400 and VLDL-rich fraction (S_f20-400) were made by sequential flotation using density gradient ultracentrifugation (Hodson *et al.*, 2007). Ultracentrifugation was performed in a SW40Ti swinging bucket rotor (Beckman Instruments; CA, USA) at 40 000 rpm at 14°C. The gradients were run for 32 min to float S_f >400 and for a further 16 h to float S_f 20 – 400 lipoproteins.

Samples were taken at 0, 30, 60, 90, 120, 180, 240, 300, and 360 min after the consumption of the test meal for the measurement of plasma glucose, insulin, TAG, NEFA, 3-hydroxybutyrate (3-OHB) and at 0, 120, 180, 240, 300, and 360 min for the analysis of chylomicron-TAG and VLDL-TAG. For calculation of DNL, VLDL-TAG fractions underwent lipid extraction and

gas chromatography-mass spectrometry as described in Chapter 2, section 2.2.5. Breath samples were collected at 0, 30, 60, 90, 120, 180, 240, 300, and 360 min into EXETAINER® tubes (Labco Ltd.; High Wycombe, UK) for measurement of $^{13}CO_2$ enrichment.

6.2.3.6 $^{13}CO_2$ enrichment analysis

Fasting and postprandial breath samples were analysed using gas chromatography-combustion-isotope ratio mass spectrometry (GC-C-IRMS). A capillary column (CPPoraPLOTQ, VarianLtd; Oxford, United Kingdom) was used to separate CO_2 from the presence of other gases. The column had dimensions of 30 m by 0.32 mm by 10 µm. Samples were injected at 100 µL using the split injection mode at 110°C with the column flow kept at 2.0 mL/min. The sampling time was 10 mins with the oven temperature at 35°C (Chong *et al.*, 2007).

From each sample, the machine generates a delta value ($\delta^{13}C$ 0/00), which was then converted into a tracer-to-tracee ratio (TTR) using the following equation (Chong *et al.*, 2007):

$$TTR\ (^{13}C{:}^{12}C) = [(\delta^{13}C\ 0/00/1000) + 1] \times 0.0112372$$

To account for the natural abundance of ^{13}C, the TTR of the fasting breath sample was later subtracted from the TTR of each postprandial sample. The $^{13}CO_2$ production rate was determined by multiplying the TTR for $^{13}CO_2$ of each breath sample by the CO_2 production rate (VCO_2 in mmol/min).

6.2.3.7 Calculations and statistical analysis

Data were analysed using SPSS for Windows v25 (SPSS, UK, Chertsey, UK) and. Statistical significance was set at $p < 0.05$ and data are presented as median (range) unless otherwise stated. Homeostatic model assessment of insulin resistance (HOMA-IR) was calculated as described (Matthews *et al.*, 1985). Areas under the curve (AUC) were calculated by the trapezoid method and divided by the relevant period to give a time-averaged value. GraphPad Prism 6 (GraphPad Software, Inc.; La Jolla, CA) was used to compare AUCs, anthropometric and fasting parameters between the DGAT2 and control groups using a two-way ANOVA with repeated measures for time (visits A and B). For postprandial data, repeated measures ANOVA, with time and group as factors, were used to investigate the difference between visits over time and the differences between groups over time.

6.3 RESULTS

6.3.1 Identifying *DGAT2* variants from the Oxford Biobank

Since DGAT2 has an important role in DNL, which may impact hepatic fat content and whole-body metabolism, associations between *DGAT2* mutations and metabolic parameters were investigated in the Oxford Biobank (OBB) (Karpe *et al.*, 2018). Initial data suggested that people carrying the rs151179593 Gly250Asp variant (G>A) had significantly ($p < 0.05$) elevated circulating insulin (22%), glucose (5%), TAG (20%) and HOMA-IR (30%) compared to non-carriers. This SNP had a MAF in the OBB of 0.18% and predicted outcome of 'damaging' and 'probably damaging' according to SIFT and PolyPhen, respectively. Based on this data, a recruit-by-genotype study was designed to investigate stimulation of DNL by sugar overfeeding in this population.

However, due to low numbers of people within the OBB carrying this variant ($n = 20$), additional analysis was carried out to identify other detrimental SNPs with a higher frequency. The rs140793537 Arg297Gly variant (G>A) had a MAF of 0.39% and a predicted outcome of 'damaging' and 'possibly damaging' according to SIFT and PolyPhen, respectively. Fifty-seven carriers of this variant were identified in the OBB, who had significant ($p < 0.05$) reductions in fasting circulating insulin (6.4%) and HOMA-IR (6.8%) compared to non-carriers ($n = 7063$); analysed alone, women had a 2.6% reduction in circulating glucose ($p = 0.061$; Table 6.3.1-1). Repeated analysis of the rs151179593 variant, now with an additional five carriers and 2090 controls, showed that the significant associations seen previously were no longer present (Table 6.3.1-1).

Table 6.3.1-1. Fasting metabolic characteristics of carriers (A/G) compared to non-carriers (G/G) of two *DGAT2* single nucleotide polymorphisms from the Oxford Biobank

	rs151179593						rs140793537					
	Male		Female		All		Male		Female		All	
n (A/G)	16		9		25		32		25		57	
n (G/G)	3087		4008		7095		3073		3990		7063	
Insulin	↓1.1%	0.958	↑6.3%	0.629	↑3.6%	0.773	↓4.4%	0.357	↓11.3%	0.020*	↓6.4%	0.024*
Glucose	↑1.6%	0.716	↑0.9%	0.572	↑2.6%	0.528	↑0.6%	0.647	↓2.6%	0.061	↔0%	0.388
HOMA-IR	↓1.4%	0.938	↑7.3%	0.575	↑4.9%	0.756	↓4.3%	0.401	↓13.8%	0.011*	↓6.8%	0.020*
TAG	↓5.9%	0.255	↑29.0%	0.020	↑14.1%	0.691	↓2.8%	0.689	↓2.3%	0.494	↓2.0%	0.442
NEFA	↑5.6%	0.760	↑3.6%	0.819	↑0.7%	0.680	↓11.3%	0.186	↓3.2%	0.731	↓10.3%	0.228
TC	↑3.6%	0.670	↓3.4%	0.789	↑2.0%	0.825	↑2.8%	0.305	↑2.5%	0.461	↑5.7%	0.209
HDL-C	↑1.3%	0.510	↑12.4%	0.070	↑0.5%	0.123	↑2.2%	0.487	↑3.1%	0.237	↓0.3%	0.190
LDL-C	↑6.6%	0.450	↓17.3%	0.079	↑0.4%	0.590	↑5.0%	0.203	↑3.3%	0.584	↑5.7%	0.188

Carriers of two single nucleotide polymorphisms were identified from the Oxford Biobank and fasting metabolic parameters were compared to non-carriers. Differences are reported as a fold change from non-carriers with p values; * $p < 0.05$. HOMA-IR, homeostatic model assessment of insulin resistance; TAG, triacylglycerol; NEFA, non-esterified fatty acids; TC, total cholesterol; HDL-C, high-density lipoprotein-cholesterol; LDL-C, low-density lipoprotein-cholesterol.

6.3.2 Sequencing exon 6 and 7 of *DGAT2* in Huh7 cells

In order to complement recruitment of human participants, homology directed repair (HDR) of Huh7 cells via the CRISPR-Cas9 system was pursued. Sanger sequencing of the two SNPs (rs151179593 and rs140793537) in the *DGAT2* gene revealed Huh7 cells were homozygous for the wild type allele (G/G; Figure 6.3.2-1). However, initial attempts to introduce the rs140793537 Arg297Gly variant (G>A) were unsuccessful and due to time restrictions, HDR for the rs151179593 Gly250Asp variant (G>A) was not pursued.

6.3.3 Sugar overfeeding intervention and postprandial study days

6.3.3.1 Subject recruitment and observational data

Letters sent out to rs151179593 and rs140793537 carriers resulted in recruitment of one male participant with the rs151179593 SNP and three (two male and one female) carriers of the rs140793537 SNP. Initially, these carriers were compared to clusters of 15 age, sex, weight, height and BMI-matched controls from the OBB (Table 6.3.3-1 & 2). The most consistent trends, seen across all four carriers, were increases in circulating glucose, total lean mass and leg lean mass. Elevations in glucose ranged from 0.2 to 0.5 mmol/L (Table 6.3.3-2), while lean mass was, on average, 9.2% higher in people with *DGAT2* mutations (range: 6.9 – 11.3%); increases in leg lean mass ranged from 1.5% to 13.6% in carriers (Table 6.3.3-1). In participants with the rs140793537 SNP, there was also a tendency for elevated plasma TAG (0.3 – 2.1 mmol/L higher) and HDL-C (0.1 – 0.6 mmol/L higher) concentrations in carriers compared to control clusters (Table 6.3.3-2).

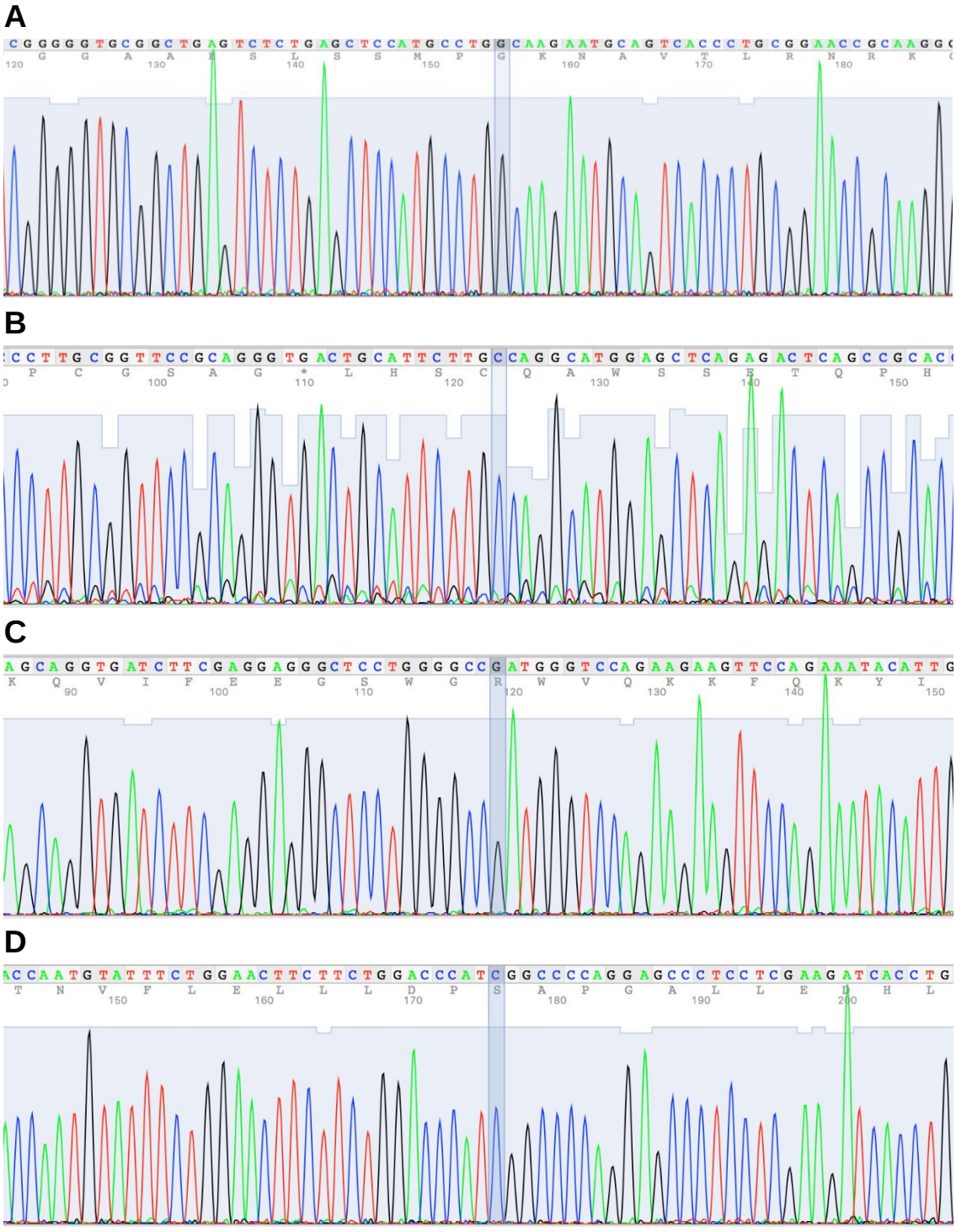


Figure 6.3.2-1. Sequencing results from exon 6 (**A, B**) and 7 (**C, D**) of the *DGAT2* gene in Huh7 cells. Cells were shown to be homozygous (wild type) for two single nucleotide polymorphisms (SNP), rs151179593; allele G > A, p.Gly250Asp (forward **A**, reverse **B**) and rs140793537; allele G > A, p.Arg297Gln (forward **C**, reverse **D**). SNP locations are highlighted with the cursor in blue.

Table 6.3.3-1. Anthropometric and body composition characteristics of people carrying the single nucleotide polymorphisms rs151179593 (**A**) and rs140793537 (**B**) compared to a cluster of matched non-carriers from the Oxford Biobank

	Cluster 1		**Cluster 2**		**Cluster 3**		**Cluster 4**	
	Case	Control	Case	Control	Case	Control	Case	Control
	A		**B**		**B**		**B**	
	(*n*=1)	(*n*=15)	(*n*=1)	(*n*=15)	(*n*=1)	(*n*=15)	(*n*=1)	(*n*=15)
Sex	Male	Male	Male	Male	Male	Male	Female	Female
Height (cm)	168	177.3 (5.8)	180	179.1 (4.1)	178	177.3 (3.4)	167	163.3 (4.8)
Weight (kg)	78.7	81.6 (10.9)	84	86.2 (15.2)	97.9	82.2 (11.3)	74.5	65.6 (11.7)
BMI (kg/m^2)	27.9	25.9 (2.6)	25.9	26.8 (4.6)	30.9	26.2 (3.7)	26.7	24.6 (4.0)
Waist (cm)	89	91.1 (8.1)	87	93.3 (12.9)	103	90.5 (11.3)	89	79.6 (10.6)
Hip (cm)	102	99.2 (5.1)	99	102 (6.9)	108	101 (6.9)	103	100 (8.3)
SBP (mmHg)	153	121 (10)	128	125 (11)	125	129 (10)	135	116 (12)
DBP (mmHg)	86	76 (7.4)	71	76 (9.4)	75	80 (8.5)	85	73 (10.6)
Total fat (kg)	11.3	20.4 (5.6)	16.8	22.8 (10.1)	33.6	22.7 (6.6)	28.2	23.1 (9.5)
Android fat (kg)	0.89	2.0 (0.7)	1.5	2.2 (1.5)	3.4	2.2 (0.9)	2.6	1.7 (1.1)
Gynoid fat (kg)	1.5	3.0 (0.8)	2.6	3.5 (1.2)	4.7	3.2 (0.8)	4.5	4.3 (1.3)
Leg fat (kg)	2.6	5.5 (1.4)	4.1	6.3 (2.1)	8.7	6.0 (1.5)	7.9	8.5 (2.6)
Visceral fat (kg)*	0.18	1.1 (0.7, 1.5)	0.7	0.9 (0.4, 1.1)	1.9	1.2 (0.5, 1.3)	1.2	0.3 (0.2, 0.6)
Arm fat (kg)	1.1	2.1 (0.5)	1.6	2.2 (0.8)	3.7	2.4 (0.7)	3.4	2.7 (1.1)
Total lean mass (kg)	63.8	57.3 (7.5)	62.9	58.8 (6.2)	60.9	55.8 (5.6)	43.4	39.7 (4.7)
Lean mass arms (kg)	7.5	7.7 (1.3)	8.6	7.4 (0.8)	7.6	7.2 (1.1)	5	4.0 (0.5)
Lean mass legs (kg)	21.2	19.8 (2.9)	21.7	19.9 (2.5)	21.7	19.1 (2.5)	13.6	13.4 (2.2)

Data presented as mean (standard deviation) for normally distributed variables and *median (inter-quartile range) for skewed variables. Cases and controls matched for age, sex, height, weight and BMI. SBP, systolic blood pressure; DBP, diastolic blood pressure. *This analysis was carried out by Dr. Senthil Vasan.*

Table 6.3.3-2. Fasting plasma biochemistry characteristics of people carrying the single nucleotide polymorphisms rs151179593 (**A**) and rs140793537 (**B**) compared to a cluster of matched non-carriers from the Oxford Biobank

	Cluster 1		**Cluster 2**		**Cluster 3**		**Cluster 4**	
	Case	Control	Case	Control	Case	Control	Case	Control
	A		**B**		**B**		**B**	
	(*n*=1)	(*n*=15)	(*n*=1)	(*n*=15)	(*n*=1)	(*n*=15)	(*n*=1)	(*n*=15)
Glucose (mmol/L)	5.5	5.3 (0.5)	5.5	5.3 (0.5)	5.7	5.2 (0.5)	5.3	5.1 (0.4)
Insulin (mU/L)*	12.1	11.5 (10.2, 17.2)	8.4	10.1 (8.1, 15.9)	13.9	9.1 (7.9, 10.9)	16.1	5.5 (3.2, 10.8)
Cholesterol (mmol/L)	5.6	5.6 (1.0)	4.7	4.9 (0.8)	5	5.5 (0.7)	5.4	5.2 (1.0)
Triglycerides (mmol/L)*	0.9	1.2 (0.8, 1.9)	1.3	0.9 (0.8, 1.2)	1.5	1.2 (0.6, 1.5)	3	0.9 (0.7, 1.4)
HDL-C (mmol/L)	1.6	1.2 (0.3)	1	1.3 (0.3)	1.1	1.2 (0.3)	0.9	1.5 (0.4)
LDL-C (mmol/L)	3.6	3.7 (0.9)	3.1	3.3 (0.8)	3.3	3.7 (0.7)	3.2	3.1 (0.9)
Apolipoprotein-B (g/L)	1	1.0 (0.2)	1	0.9 (0.2)	0.9	1.1 (0.2)	1.2	0.9 (0.2)
NEFA (µmol/L)	278	482 (202)	674	366 (206)	377	429 (152)	492	466 (210)
3-OHB (µmol/L)*	45	89 (41.6, 129.6)	112.3	49.5 (27.7, 534)	37.5	60 (31.6, 218)	33.4	51.5 (29.5, 108.3)

Data presented as mean (standard deviation) for normally distributed variables and *median (inter-quartile range) for skewed variables. Cases and controls matched for age, sex, height, weight and BMI. HDL-C, high-density lipoprotein-cholesterol; LDL-C, low-density lipoprotein-cholesterol; NEFA, non-esterified fatty acids; 3-OHB, 3-hydroxybutyrate. *This analysis was carried out by Dr. Senthil Vasan.*

6.3.3.2 Baseline characteristics and dietary adherence

To date, we have full data for four cases and three controls in this pilot dietary intervention study; all but one case had a control participant recruited. Since only one carrier of the rs151179593 SNP was recruited, all carriers of *DGAT2* mutations were analysed together as there was no obvious divergence in results between the two SNPs. The median age was 50 years for *DGAT2* mutation carriers and 48 years for controls (Table 6.3.3-3). Although waist circumference and total fat mass appeared to be slightly higher in control participants (median: 90 *vs.* 85 cm and 21.7 *vs.* 15.7 kg), no statistically significant differences were detected. Visceral fat mass also tended to be higher in control participants (median: 1127 *vs.* 642.2 g); however, in both groups, this varied highly between participants (Table 6.3.3-3). In addition, similar to the observational data from control clusters, *DGAT2* mutation carriers had a non-significant trend for increased total lean mass (median: 59.8 *vs.* 54.9 kg; Table 6.3.3-3).

Table 6.3.3-3. (Next page) Participants with a mutation in the *DGAT2* gene (DGAT2) or matched controls (Control) were recruited and anthropometric and fasting plasma biochemistry measurements were taken before (visit A), and at the end of (visit B), a sugar overfeeding intervention that lasted 15-20 days. Data are presented as median (range). ‡ $p < 0.1$, * $p < 0.05$ compared to pre-intervention within groups, different letters denote significant ($p < 0.05$) differences between groups; two-way ANOVA with Bonferroni's multiple comparisons tests. HOMA-IR, homeostatic model assessment of insulin resistance; NEFA, non-esterified fatty acids; HDL-C, high-density lipoprotein-cholesterol; VLDL, very low-density lipoprotein-cholesterol; 3-OHB, 3-hydroxybutyrate; ALT, alanine aminotransferase.

Table 6.3.3-3. Participant characteristics and fasting plasma biochemistry before and after a sugar overfeeding intervention in people carrying a *DGAT2* mutation and controls

	DGAT2 (*n* = 4)		Control (*n* = 3)	
	Visit A	**Visit B**	**Visit A**	**Visit B**
Participant characteristics				
Sex (M/F)	(3/1)		(2/1)	
Days on diet	19.5 (15 - 20)		18 (17 - 20)	
Age (y)	50 (47 - 53)		48 (45 - 51)	
Weight (kg)	76.0 (63.5 - 94.2)	76.9 (63.7 - 93.2)	80.2 (52.9 - 101)	81.7 (54.5 - 102)‡
BMI (kg/m^2)	25.5 (23.0 - 29.7)	25.8 (23.1 - 29.4)	24.8 (22.0 - 34.2)	25.2 (22.7 - 34.5)‡
Waist circumference (cm)	85 (75 - 104)	85 (74 - 103)	90 (71 - 110)	91 (70 - 111)
Total fat mass (kg)	15.7 (11.8 - 32.5)	15.8 (11.3 - 31.6)	21.7 (14.7 - 41.9)	23.4 (15.0 - 42.5)
Total lean mass (kg)	59.8 (41.4 - 62.6)	59.8 (41.2 - 61.8)	54.9 (36.2 - 55.1)	55.2 (36.2 - 55.2)
Visceral fat (g)	642.2 (44.1 - 2109)	591.5 (160.3 - 1907)	1127 (0.2 - 3347)	1148 (74.2 - 3326)
Liver fat (%)	2.0 (1.5 - 3.5)	2.1 (0.7 - 3.5)	2.7 (1.4 - 19.5)	4.9 (1.7 - 24.1)‡
Fasting plasma biochemistry				
HOMA-IR	1.4 (1 - 3.1)	1.3 (1.2 – 4.0)	2.2 (0.4 – 7.0)	3.0 (0.3 – 6.0)
Glucose (mmol/L)	5.1 (4.8 - 5.6)	4.9 (4.7 – 6.0)	4.8 (4.6 - 5.4)	5.1 (5.1 - 5.2)
Insulin (mU/L)	6.1 (4.5 - 12.5)	6.1 (4.9 - 12.3)	10.3 (2.2 - 29.2)	11.9 (1.0 – 21.0)
NEFA (µmol/L)	370.8 (263.7 - 1054)	438.6 (249.0 - 637.4)	650.9 (339.9 – 662.0)	464.9 (239.3 - 573.9)
Total cholesterol (mmol/L)	4.4 (3.8 – 5.0)	4.6 (4.1 - 5.2)	4.1 (4.0 - 4.5)	4.4 (3.7 - 4.7)
HDL-C (mmol/L)	1.3 (0.9 - 1.6)	1.2 (1.0 - 1.5)	0.9 (0.7 - 2.2)	0.9 (0.8 - 1.8)
Non-HDL-C (mmol/L)	3.1 (2.5 - 3.7)	3.4 (3.0 - 3.8)	3.2 (2.3 - 3.3)	3.6 (1.9 - 3.8)
TAG (mmol/L)	1374 (595.9 - 2035)	1469 (533.7 - 2603)	1153 (361.7 - 1937)	1481 (415.0 - 2263)
VLDL-TAG (µmol/L)	859.4 (266.5 - 1183)	1009 (274.6 - 1596)	547.8 (64.4 - 1282)	946 (141.6 - 992.1)
3-OHB (µmol/L)	37.6 (20.6 - 83.1)[a]	27.5 (13.3 - 34.7)	228.1 (106.7 - 280.2)[b]	28.9 (23.9 - 46.6)*
ALT (IU/L)	10 (7 - 15)	11.5 (7 - 21)	27 (10 - 32)	16 (11 - 34)

The duration of dietary intervention in subjects ranged from 15 to 20 days, with a median of 19.5 days for *DGAT2* carriers and 18 days for controls (Table 6.3.3-3). Over the dietary intervention period, most participants increased their caloric intake; this was by approximately 500 kcals in the DGAT2 group ($p < 0.05$) and 350 kcal in the control group, although the female participant in this group reduced their intake by 240 kcal (Table 6.3.3-4). Both groups significantly ($p < 0.05$) increased their carbohydrate and sugar intake over the study period, with free sugars accounting for 24.3% of energy intake in *DGAT2* carriers and 28.7% in controls at the end of the intervention, an increase of 14.9% and 20.7%, respectively (Table 6.3.3-4). This increase in carbohydrate intake largely displaced fat in the diet, which contributed less to dietary intake at the end of the study compared to baseline ($p < 0.06$ in *DGAT2* carriers and $p < 0.05$ in controls).

Table 6.3.3-4. Dietary intake before and after a sugar overfeeding intervention in people carrying a *DGAT2* mutation and controls

	DGAT2 (*n* = 4)		**Control (*n* = 3)**	
% Energy	**Habitual**	**Intervention**	**Habitual**	**Intervention**
Carbohydrate	51.0 (42.1 - 54.3)	65.5 (63.5 - 67.0)*	47.5 (31.5 - 53.5)	67.4 (64.3 - 68.9)*
Sugars	19.6 (15.4 - 26.1)	34.5 (30.2 - 39.1)*	17.8 (13.7 - 20.4)	38.5 (34.3 - 39.5)*
Free sugars	6.7 (3.8 - 14.2)	24.3 (19.7 - 25.1)*	7.6 (2.6 - 12.0)	28.7 (21.2 - 32.9)*
Protein	17.4 (14.0 - 22.3)	13.3 (12.5 - 15.1)	18.9 (16.6 - 19.2)	14.5 (13.2 - 15.9)
Fat	30.6 (25.1 - 35.0)	20.0 (18.0 - 20.4)‡	33.6 (29.9 - 49.2)	17.3 (16.4 - 19.9)*
SFA	11.2 (5.2 - 15.4)	6.5 (4.8 - 7.9)‡	13.4 (10.4 - 15.0)	6.3 (5.7 - 7.1)*
MUFA	10.9 (8.9 - 12.3)	7.0 (4.1 - 7.3)‡	11.7 (10.8 - 19.0)	6.2 (5.6 - 6.5)*
PUFA	3.9 (3.6 - 6.5)	3.2 (1.6 - 4.2)	5.9 (3.5 - 12.8)	3.3 (2.7 - 4.8)
Energy intake (kcal)	2222 (1706 - 2592)	2741 (1973 - 2936)*	1920 (1872 - 2192)	2266 (1634 - 2442)

Participants with a mutation in the *DGAT2* gene (DGAT2) or matched controls (Control) were recruited and completed a three-day food diary before (habitual), and at the end of (intervention), a sugar overfeeding intervention that lasted 15-20 days. Data are presented as median (range). * $p < 0.05$, ‡ $p < 0.1$ compared to pre-intervention; two-way ANOVA with Bonferroni's multiple comparisons tests. *Dietary analysis was carried out by Dr. Fredrik Rosqvist.*

6.3.3.3 The effect of sugar overfeeding on anthropometry and fasting plasma biochemistry

Despite a tendency to increase energy intake over the intervention period, neither group had significantly elevated body weight or BMI post-intervention, although there was a trend in the control group, with median body weight increasing by 1.5 kg (p = 0.069), and BMI by 0.4 kg/m^2 (p = 0.073; Table 6.3.3-3). In addition, while the DGAT2 group had almost no change in liver fat after sugar overfeeding (2.0% to 2.1%), the control group had an increase from 2.7% to 4.9% (p = 0.066; Table 6.3.3-3). Fasting plasma biochemistry markers did not differ between groups at baseline, with the exception of 3-OHB, which was markedly lower in *DGAT2* mutation carriers (median: 37.6 μmol/L) compared to controls (median: 228.1 μmol/L, p = 0.001; Table 6.3.3-3). After sugar overfeeding, only 3-OHB changed in either group, with a reduction of 199.2 μmol/L in the control group (p = 0.008; Table 6.3.3-3). Individual changes in plasma biochemistry can be found in Appendix E, Figures E.1 & 2).

6.3.3.4 The effect of sugar overfeeding on postprandial substrate appearance and hormonal response to a mixed meal

In response to the feeding of a mixed test meal including sugar and fat, both groups displayed an increase in chylomicron TAG; in the DGAT2 group, this had occurred by 120 minutes, but was not noted until 180 minutes in the control group (Figure 6.3.3-1A & B). Moderate differences were seen between visits A and B in the DGAT2 group: there appeared to be an earlier peak and plateau in chylomicron TAG post-intervention, resulting in a non-significant augmentation of the AUC (median: 369.0 *vs.* 271.6, Table 6.3.3-5). In the control group, there was a sharp elevation in chylomicron TAG at 300 minutes during visit B, rather than the

plateau seen at 180 minutes in visit A (Figure 6.3.3-1B). Although absolute values were different, this pattern occurred in all individuals in the control group after the sugar overfeeding intervention.

Consumption of the test meal caused an increase in blood glucose over time; this peaked at 30 minutes in the *DGAT2* mutation carriers before and after the sugar over feeding intervention, while in controls, the highest levels were seen at 60 and 90 minutes pre and post-intervention, respectively (Figure 6.3.3-1C & D). This difference in pattern between groups was significant when the effect of time was measured (pre-intervention, $p = 0.073$; post-intervention, $p < 0.05$). While *DGAT2* mutation displayed a consistent peak at 30 minutes in blood glucose before and after sugar overfeeding, the prolonged increase up to 90 minutes in the control groups resulted in a significantly different ($p < 0.05$) glucose response before and after the intervention (Figure 6.3.3-1D), although AUC levels were not changed (Table 6.3.3-5).

Figure 6.3.3-1. (Next page) The effect of sugar overfeeding on postprandial substrate appearance and hormonal response to a mixed meal. Participants with a mutation in the *DGAT2* gene (DGAT2; **A, C, E, G**) or matched controls (Control; **B, D, F, H**) were recruited and underwent postprandial study days before (visit A), and at the end of (visit B), a sugar overfeeding intervention that lasted 15-20 days. Participants were given a mixed meal at time point 0, and blood was collected every 30 – 60 minutes for 6 hours. Triacylglycerol (TAG) content in chylomicrons was measured (**A, B**), as were glucose (**C, D**), insulin (**E, F**) and non-esterified fatty acids (NEFA; **G, H**). Data are presented as mean ± SD. Statistics are reported from a two-way, repeated measures ANOVA.

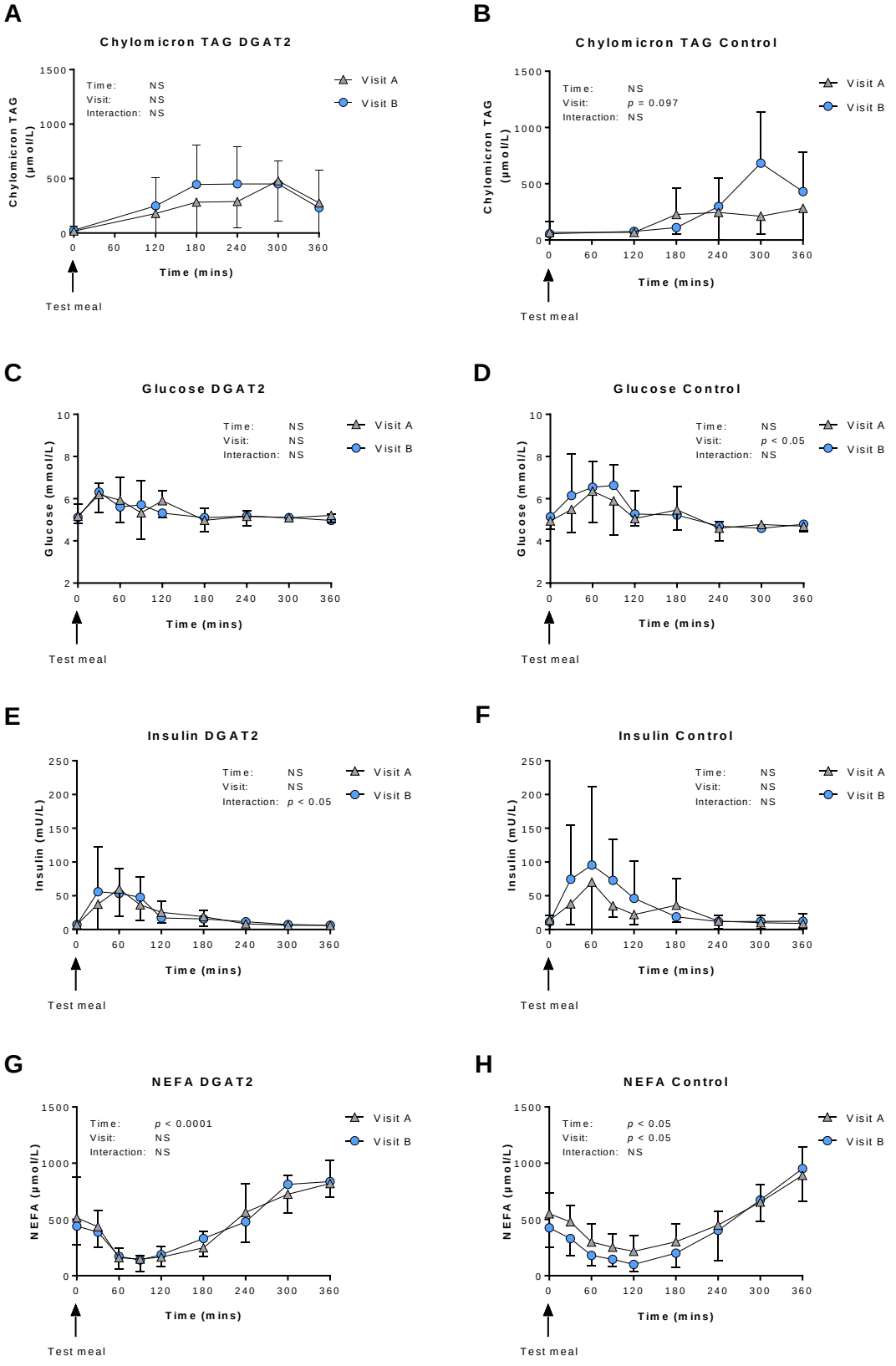


Figure 6.3.3-1. Figure legend can be found on previous page

Patterns of insulin secretion, which is stimulated by glucose, were similar to those of blood glucose. Participants with *DGAT2* mutations showed minimal difference in response to the test meal at visit A and B, although there was a time x visit interaction ($p < 0.05$, Figure 6.3.3-1E). In contrast, controls appeared to have higher levels post-intervention (median AUC: 34.3 *vs.* 19.9 mU/L), although this was not significant (Figure 6.3.3-1F, Table 6.3.3-5). When responses of the DGAT2 and control group were compared, there was a significant effect of time at visits A and B (both $p < 0.05$). One action of insulin is to suppress NEFA release from adipose tissue. In line with this, while plasma NEFA concentrations were largely unchanged in *DGAT2* mutation carriers pre and post-intervention, similar to glucose and insulin, in controls, NEFA levels were higher post-intervention (visit effect: $p < 0.05$; Figure 6.3.3-1G & H). Like insulin, there was a time effect at visits A and B in the between-group analysis (both $p < 0.0001$).

6.3.3.5 The effect of sugar overfeeding on postprandial hepatic fatty acid synthesis and metabolism and substrate utilisation in response to a mixed test meal

Sugar overfeeding would be expected to stimulate DNL through pathway upregulation and increased substrate supply. In *DGAT2* mutation carriers and controls, a significant ($p < 0.05$) post-intervention increase in DNL was seen (Figure 6.3.3-2A & B). Differences were also evident from calculation of AUC, with an increase from a median of 5.85 to 9.99% in the DGAT2 group and 5.94 to 11.0% in the control group (both $p < 0.05$; Table 6.3.3-5). One fate of DNL-derived fatty acids is to be incorporated in VLDL particles for secretion. In both groups, there appeared to be an increase in VLDL TAG levels after the sugar overfeeding

intervention (Figure 6.3.3-2C & D). However, due to one control participant exhibiting a decrease in VLDL TAG post-intervention and higher inter-individual variability, the AUC values demonstrated a decrease in this group and no significant differences were noted for either group (Figure 6.3.3-2; Table 6.3.3-5).

An upregulation of DNL would result in the production of malonyl-CoA, which can inhibit hepatic fatty acid oxidation, a marker of which is 3-OHB. At baseline it was noted that fasting 3-OHB levels were significantly higher in controls ($p < 0.05$; Table 6.3.3-3); before the sugar overfeeding intervention, 3-OHB AUC was also significantly lower in *DGAT2* mutation carriers compared to controls ($p < 0.05$; Table 6.3.3-5). During the postprandial study days, time had a significant ($p < 0.05$) effect on 3-OHB levels, with an increase particularly apparent after 180 minutes (Figure 6.3.3-2E & F). A significant time x group interaction was also noted pre and post-intervention (both $p < 0.05$). Although there appeared to be a slight suppression of 3-OHB at 360 minutes in the DGAT2 group during visit B compared to visit A, a suppressed elevation from 180 minutes onwards in the control group was more evident, meaning a significant ($p < 0.05$) reduction in 3-OHB AUC was evident post-intervention (median: 92.8 *vs.* 209.4 μmol/L; Table 6.3.3-5).

Although 3-OHB is an established marker of hepatic FA oxidation, feeding of ^{13}C-labelled palmitate allows whole-body FA oxidation to be measured by the production of $^{13}CO_2$. Similarly to the 3-OHB results, suppression of $^{13}CO_2$ production also appeared to be blunted in *DGAT2* mutation carriers after sugar overfeeding, although it was evident at later time points, resulting in significant time and interaction effect ($p < 0.01$; Figure 6.3.3-2G).

Compared to visit A, a suppression in $^{13}CO_2$ production in the control group post-intervention was apparent from 120 minutes to the end of the study duration (Figure 6.3.3-2H), resulting in a significantly reduced AUC from visit A to B (median: 0.04 to 0.02 μmol/min/kg lean mass, $p < 0.05$).

Differences in substrate utilisation between groups were also evident from the respiratory quotient (RQ). Median values 120 minutes after the test meal during visit A were 0.86 in *DGAT2* mutation carriers and 0.72 in controls ($p = 0.068$), suggesting a stronger preference for carbohydrate in the DGAT2 group. This was confirmed by direct measurement of carbohydrate oxidation at 120 minutes during visit A (178.7 *vs.* 11.7 mg/min, $p < 0.05$; Table 6.3.3-5). While sugar overfeeding resulted in a significant increase in RQ in the control group ($p < 0.05$, Table 6.3.3-5), there were no significant differences in substrate utilisation post-intervention in *DGAT2* mutation carriers and carbohydrate oxidation remained elevated compared to the control group ($p = 0.095$; Table 6.3.3-5).

Figure 6.3.3-2. (Next page) The effect of sugar overfeeding on postprandial hepatic fatty acid and metabolism and substrate utilisation in response to a mixed meal. Participants with a mutation in the *DGAT2* gene (DGAT2; **A, C, E, G**) or matched controls (Control; **B, D, F, H**) were recruited and underwent postprandial study days before (visit A), and at the end of (visit B), a sugar overfeeding intervention that lasted 15-20 days. Participants were given deuterated water (^2H_2O) to drink overnight before the study day and a mixed meal containing ^{13}C palmitate at time point 0. Blood and breath were collected every 30 – 60 minutes for 6 hours. Incorporation of ^2H into very low-density lipoprotein (VLDL) palmitate was used to measure *de novo* lipogenesis (DNL; **A, B**). Total VLDL triacylglycerol (TAG; **C, D**) and 3-hydroxybutyrate (3-OHB; **E, F**) were also measured. Appearance of $^{13}CO_2$ in collected breath (**G, H**) was used to measure whole-body palmitate oxidation. Data are presented as mean ± SD. Statistics are reported from a two-way, repeated measures ANOVA.

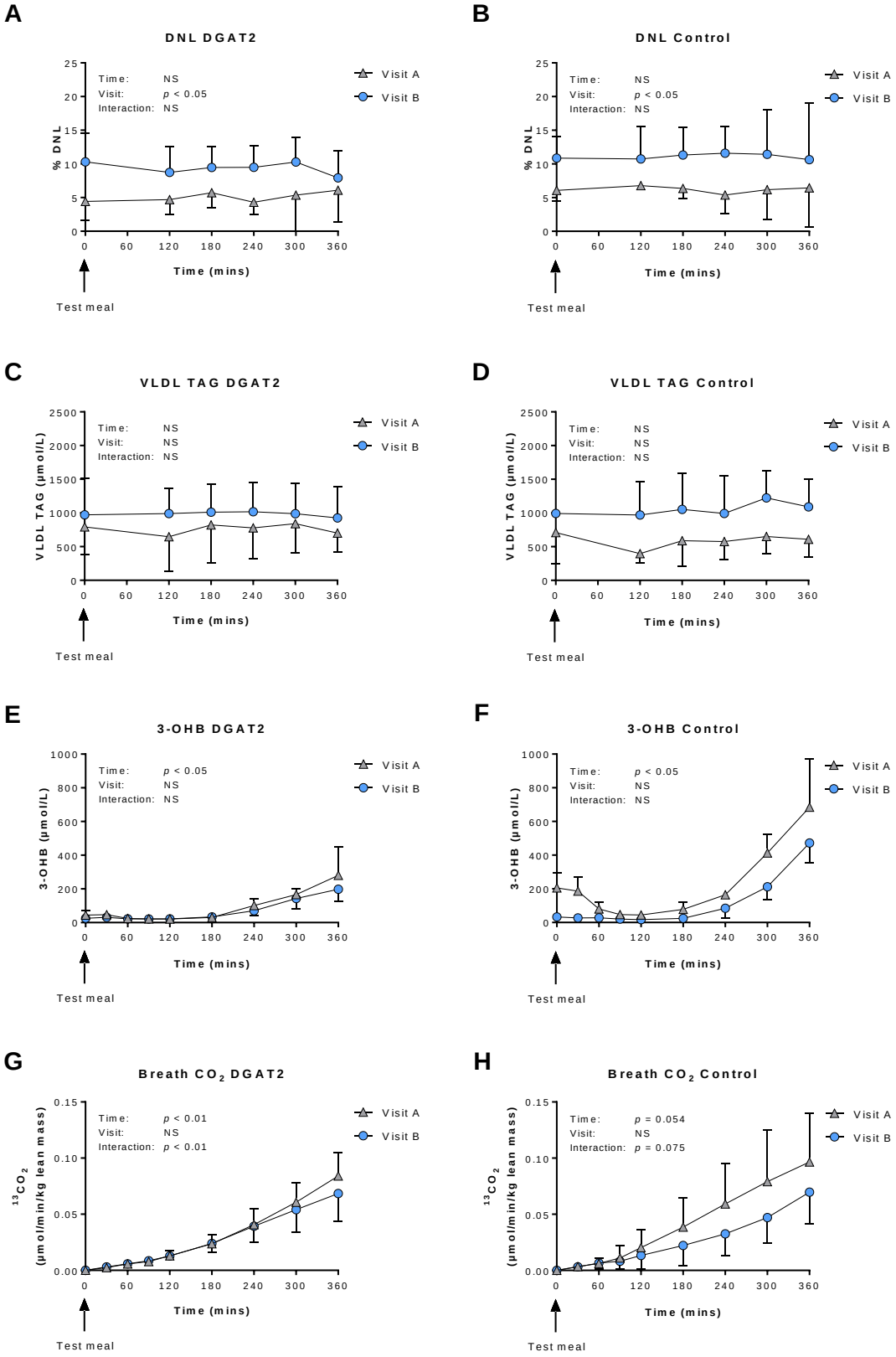


Figure 6.3.3-2. Figure legend can be found on previous page

Table 6.3.3-5. Postprandial measurements and area under the curve (AUC) values before and after a sugar overfeeding intervention in people carrying a *DGAT2* mutation and controls

	DGAT2 (*n* = 4)		Control (*n* = 3)	
	Visit A	**Visit B**	**Visit A**	**Visit B**
RQ	0.86 (0.78 - 0.96)	0.89 (0.8 - 0.98)	0.72 (0.71 - 0.75)	0.83 (0.76 - 0.84)*
CHO oxidation (mg/min)	178.7 (104.8 - 343.6)[a]	163.5 (97.8 - 279.4)	11.7 (3.61 - 35.8)[b]	38.0 (25.5 - 55.5)
Fat oxidation (mg/min)	54.3 (22.7 - 105.4)	33.6 (5.63 - 99.4)	94.9 (85.2 - 146.2)	87.7 (84.0 - 119.3)
HOMA-IR AUC (Mass units)	1.36 (1.01 - 3.14)	1.32 (1.23 - 4.02)	2.22 (0.45 - 6.99)	3.04 (0.34 - 6)
Glucose AUC (mmol/L)	5.37 (5.09 - 5.76)	5.22 (5.06 - 5.79)	5.13 (4.89 - 5.52)	5.34 (5.04 - 5.47)
Insulin AUC (mU/L)	22.2 (10.4 - 29.2)	22.8 (10.5 - 30.2)	19.9 (5.3 - 53.1)	24.3 (6.6 - 72.6)
NEFA AUC (µmol/L)	398 (295.3 - 624.2)	447.5 (354.9 - 514.2)	457.8 (327.4 - 549.8)	328.1 (289.6 - 514)
VLDL-TAG AUC (µmol/L)	704.1 (302.1 - 1322)	1157 (389.8 - 1255)	769.7 (102.1 - 1188)	598.1 (161.6 - 1211)
Chylomicron-TAG AUC (µmol/L)	271.6 (66 - 375.3)	369 (72 - 431.1)	187.2 (49.7 - 260.8)	299.9 (71.7 - 367.4)
3-OHB AUC (µmol/L)	84.4 (58.7 - 112.6)[a]	59.2 (50.5 - 101.3)	209.4 (144.3 - 263.3)[b]	92.8 (87.2 - 128.1)*
DNL AUC (%)	5.85 (1.97 - 6.27)	9.99 (5.53 - 12.23)*	5.94 (4.19 - 8.56)	11.0 (6.73 - 15.6)*
Breath AUC (µmol/min/kg lean mass)	0.03 (0.02 - 0.04)	0.03 (0.02 - 0.04)	0.04 (0.02 - 0.07)	0.02 (0.01 - 0.04)*

Participants with a mutation in the *DGAT2* gene (DGAT2) or matched controls (Control) were recruited and underwent postprandial study days before (visit A), and at the end of (visit B), a sugar overfeeding intervention that lasted 15-20 days. Participants were given a mixed meal at time point 0, and blood and breath was collected every 30 – 60 minutes for 6 hours. Data are presented as median (range). * $p < 0.05$ compared to pre-intervention within groups, different letters denote significant ($p < 0.05$) differences between groups; two-way ANOVA with Bonferroni's multiple comparisons tests. RQ, respiratory quotient; CHO, carbohydrate; HOMA-IR, homeostatic model assessment of insulin resistance; NEFA, non-esterified fatty acids; VLDL, very low-density lipoprotein; TAG, triacylglycerol; 3-OHB, 3-hydroxybutyrate; DNL, *de novo* lipogenesis.

6.4 DISCUSSION

The aims of this chapter were to investigate the effect of sugar overfeeding on DNL, liver fat and whole-body metabolism and the effect of mutations in *DGAT2* in these processes. Despite a small sample number, there were some interesting observations made. Overall, increasing sugar intake over a period of around two weeks approximately doubled rates of hepatic DNL among all participants recruited. This confirms the dietary analysis, which showed that there was good adherence to sugar overfeeding in participants. Although variable, habitual free sugar intakes were close to the recommended level of 5% of energy; as a result of the intervention, this increased to around 25% of total energy, which is equivalent to what is consumed by those in the 97.5th percentile for sugar intake in the UK population (NDNS, 2018). Although this level of consumption is only applicable to a small number of people, in the context of this study, sugar overfeeding was undertaken in order to stimulate DNL to augment and scrutinise any potential effects of DGAT2 activity on this process.

In both groups, increased sugar intake during the dietary intervention was associated with elevated caloric intake. In the control group, this was reflected in a tendency for weight gain and an increase in BMI, whereas the DGAT2 group displayed a consistent body weight, despite a larger increase in energy intake. In both the intervention study and the case-control cluster comparisons, there was a small but consistent trend for *DGAT2* mutation carriers to have higher lean body mass than controls. Although we did not measure resting energy expenditure, combined CO_2 production from fat and carbohydrate at 120 minutes in the DGAT2 group was approximately double that of the control group. In a mouse model, liver

and adipose-specific suppression of *Dgat2* expression resulted in increased energy expenditure and reduced fat mass (Choi *et al.*, 2007); the DGAT2 group maintained their fat mass during the intervention, whereas control participants gained approximately 1.5 kg. In addition, in a Chinese population, a rare nonsense, loss-of-function mutation in *DGAT2* was found to be associated with leanness (Ning *et al.*, 2017). Mutations in *DGAT2* therefore seemed to protect carriers from weight gain caused by sugar-mediated caloric excess, possibly *via* increased energy expenditure.

In terms of DNL itself, there was a very similar magnitude of response between groups, with an increase in contribution from around 6% of secreted palmitate in VLDL-TAG pre-intervention to 10% post-intervention; however, only in the control group was there a tendency for an increase in liver fat. These differences in response between control and *DGAT2* carriers is similar to what has previously been reported in response to a lifestyle intervention. Kantartzis *et al.* investigated the effect of the rs1944438 (C>T) SNP in *DGAT2* after a nine month weight loss programme (Kantartzis *et al.*, 2009). After adjustment for gender, age and body fat, there was a significant effect of genotype, with individuals who were heterozygous and homozygous for the minor allele demonstrating smaller reductions in liver fat compared to carriers of the wild type (C/C) allele (Kantartzis *et al.*, 2009). Similarly, in response to Niacin treatment, either homozygous or heterozygous carriers of the rs3060 (T>C) allele demonstrated smaller reductions in liver fat than wild type participants when adjusted for age, gender, and body weight (Hu *et al.*, 2012).

Although subtle, evidence from *DGAT2* mutation carriers suggests that DGAT2 may mediate a dissociation between either a liver fat-lowering environment (weight loss (Kantartzis *et al.*, 2009) and niacin treatment (Hu *et al.*, 2012)) or a liver fat-elevating environment (our results, due to increased DNL) and the expected change in liver fat. In both studies, this was not associated with any other differences in plasma biochemistry between genotypes. In addition, Katzartzis *et al.* found that *DGAT2* mutation carriers, although displaying smaller reductions in liver fat compared to controls, demonstrated similar improvements in insulin sensitivity; this suggests that the retained liver fat was not lipotoxic. In the DGAT2 KO model presented in Chapter 5, reductions in TAG content were associated with impaired insulin sensitivity. If the mutations previously studied resulted in increased DGAT2 activity, it would suggest that DGAT2-derived TAG protects from impaired insulin action through an undefined mechanism.

Unlike previous studies, the completion of postprandial study days in our protocol allowed observation of differences in metabolism that may be missed in the fasting state. Indeed, in the control group, there were a number of changes in postprandial response to an identical test meal before and after sugar overfeeding. Firstly, there was an augmented elevation in blood glucose after the test meal: this may be due to upregulated intestinal absorption of glucose in response to sugar overfeeding, an effect that has been reported previously (Ritze *et al.*, 2014). Higher glucose could also be accounted for by a decrease in clearance due to impaired insulin sensitivity; however there was no change in HOMA-IR after the intervention and insulin-stimulated suppression of NEFA was maintained, suggesting that individuals

were still insulin sensitive. A sustained increase in glucose availability also affected substrate oxidation, with an increase in carbohydrate oxidation in the control group after sugar overfeeding. In contrast, the DGAT2 group displayed very few changes in these parameters postprandially after sugar overfeeding.

In the control group, other responses to increased glucose availability were also observed in line with the existing literature: an approximate doubling of hepatic DNL appeared to inhibit hepatic fat oxidation and stimulate VLDL-TAG production in control participants (Chong *et al.*, 2007). In addition, a sharp peak in chylomicron-TAG appearance was noted around 300 minutes after the test meal post-intervention, which may be a result of increased VLDL production and clearance, thus delaying chylomicron release into the blood stream (Roberts *et al.*, 2008). Apart from DNL, although changes of the same direction were seen in the DGAT2 group, they appeared to be more blunted. Indeed, over 360 minutes, 3-OHB and breath CO_2 were already significantly lower than the control group at visit A and these levels were almost unchanged by sugar overfeeding. Likewise, the peak in chylomicron TAG seen during visit B for control participants was already evident during visit A in the DGAT2 group. Overall, it appears that the DGAT2 group were displaying postprandial characteristics at baseline that were evident in the control group after the dietary intervention.

The lack of response in the DGAT2 group to a high sugar diet may be indicative of a system that is already adapted to high glucose availability. Although not evident in the pilot study, there was a consistent trend in the case-control cluster analysis for slightly elevated fasting plasma glucose in *DGAT2* SNP carriers, which would support this theory. *DGAT2* carriers

also had a significantly higher RQ and carbohydrate oxidation rate compared to control participants at baseline, indicating a system adapted to the disposal of excess glucose. Interestingly, treatment with niacin, believed to be a DGAT2 inhibitor, has been found to significantly increase plasma glucose levels (Fabbrini *et al.*, 2010; Hu *et al.*, 2012); this is in line with the results from the DGAT2 KO model presented in Chapter 5. Although analysis of fasting plasma variables from the OBB cohort showed a reduction in plasma glucose in females with the rs140793537 SNP ($p = 0.061$), in the pilot study the female case had a fasting glucose level 1 mmol/L higher than the matched control pre and post-intervention.

Combined with the resistance to weight gain and liver fat accumulation, the present results indicate that the *DGAT2* variants we studied result in a loss-of-function. Although this may be counterintuitive, due to the lack of change in DNL, only hepatic levels was measured; if DNL in adipose tissue is lower in people with *DGAT2* mutations, it could explain the unchanged adiposity observed in this group after sugar overfeeding. Whether a loss-of-function mutation may affect metabolic health and NAFLD is unclear; certainly in the present cohort, there did not seem to be any detrimental effects. However, these were healthy individuals involved in a short-term dietary intervention. Similar to what was seen in the HFHS-treated KO cells in Chapter 5, it could be that this mutation predisposes to disease in combination with other factors. In line with this, in the ExTexT2D exome chip meta-analysis (Mahajan *et al.*, 2018) the rs140793537 SNP was significantly associated with type 2 diabetes (odds ratio: 1.10), which would support the role of DGAT2 activity of insulin signalling, as reported by Katzartzis *et al.* (Kantartzis *et al.*, 2009). It may therefore be that DGAT2-

associated TAG accumulation results in a benign, and possibly protective, metabolic phenotype.

There are however, some limitations to this work. The results presented in this chapter are preliminary and form part of a pilot study, meaning participant numbers are low; as a result, some statistical significance may have been over estimated where parametric tests were used and results in general should be interpreted with some caution. We also included people with two different DGAT2 SNPs in the DGAT2 group, as well as males and females, which may have added additional variation to results. Recruitment of more participants into the study would be required to confirm our findings, which given the interesting trends seen in this small group, has been undertaken. In addition, gene editing of Huh7 cells with the studies SNPs was unsuccessful: further pursuit of this method would allow confirmation of the loss-of-function hypothesis and further the understanding of how *DGAT2* mutations affect hepatocellular lipid accumulation and metabolism.

6.5 SUMMARY

- In people with DGAT2 mutations and controls, a pilot, two-week sugar overfeeding intervention, where sugars accounted for around 25% of total energy intake, resulted in elevated DNL during a postprandial study day
- In control participants, sugar overfeeding resulted in small increases in glucose and insulin, elevated blood lipids and a shift towards carbohydrate oxidation, with concurrent reductions in fat oxidation, in response to a test meal
- In participants with DGAT2 mutations, there were minimal changes in postprandial parameters due to sugar overfeeding, possibly as a result of adaption to a chronic elevation of blood glucose
- This, along with protection from weight gain and increased liver fat as seen in the control group, suggests that the rs151179593 and rs140793537 missense mutations result in DGAT2 loss-of-function, which may be detrimental to metabolic health; however, the present results and conclusions need to be confirmed in a larger dataset

Chapter 7

General discussion and future directions

7.1 GENERAL DISCUSSION AND FUTURE DIRECTIONS

Non-alcoholic fatty liver disease (NAFLD) is becoming an increasingly prevalent public health burden. The disease is characterised by excess hepatic triacylglycerol (TAG) accumulation and disturbances in hepatic, and whole-body, fatty acid (FA) metabolism. However, the exact pathogenesis of the disease remains to be elucidated, although it appears to encompass genetic and lifestyle factors, while investigation of hepatocellular FA metabolism is difficult due to the inaccessibility of the human liver. Therefore, the overarching aims of this thesis were to optimise a physiological cellular model of FA metabolism and fat accumulation and, by using this model and recruiting human participants with diacylglycerol acyltransferase (DGAT)2 mutations, to investigate the effect of nutritional substrates and altered activity of DGAT2 on FA metabolism and the potential impact of this on NAFLD.

7.1.1 Improving and developing *in vitro* hepatocyte models

Hepatoma-derived cell lines are commonly used in hepatocellular research, although there are several ways in which they do not represent normal hepatic function (*e.g.* rapid uptake and metabolism of glucose, poor mobilisation of stored FAs, low albumin secretion and minimal CYP enzyme function) (Amann *et al.*, 2009; Gibbons *et al.*, 1994; Green *et al.*, 2015b). In Chapters 3 and 4, I optimised a physiologically-relevant culture media for HepG2 and Huh7 cells, compared FA metabolism in these cell lines and developed a model of macrovesicular lipid droplet (LD) accumulation in Huh7 cells; this was done by altering glucose availability and culture serum and supplying exogenous FAs.

High glucose levels (22 mM) in Huh7 cells were found to promote proliferation, while low glucose levels (5.5 mM) caused ER stress in HepG2 and Huh7 cells (Chapter 3, section 3.3.2), resulting in 11 mM glucose being used for subsequent experiments. The use of human serum (HS) in culture media improved the metabolic profile of both Huh7 and HepG2 (Chapter 3, section 3.3.3), including a reduction in *de novo* lipogenesis (DNL) and evidence of improved insulin signalling as measured by Akt phosphorylation; previous studies have also reported an increase in albumin secretion and CYP expression (Pramfalk *et al.*, 2016; Steenbergen *et al.*, 2013). The effects of the *PNPLA3* I148M variant on HepG2 cell metabolism led to Huh7 cells being used for further experiments.

Since the liver is also exposed to dietary fat and non-esterified FAs (NEFAs) from adipose tissue, addition of FAs to the media was also investigated in Chapter 4. With HS alone, there was a reduction in DNL and increased expression of lipases, which led to higher levels of secretion and oxidation markers (Chapter 3, sections 3.3.3.1 and 3.3.3.3). In Chapter 4 (sections 4.3.2.2 and 4.3.2.4), the addition of exogenous FAs reduced DNL further, to levels seen in healthy individuals (5-10%), and the ability of Huh7 cells to secrete fully lipidated, very low-density lipoprotein (VLDL)-sized particles was demonstrated with the addition of 800 μM mixed FAs. The addition of fructose to the media, to mimic dietary sucrose intake, caused minimal effects on FA metabolism and storage in Huh7 cells.

In contrast, increasing exogenous FA supply caused large LDs to accumulate in cells, which were more characteristic of the macrovesicular pattern of steatosis seen in NAFLD: when compared to primary hepatocytes isolated from steatotic livers, the size distribution in high

fat-treated Huh7 cells was similar (Chapter 4, section 4.3.2.1). Although cells treated with high fat high sugar (HFHS) media accumulated more fat than the low fat-treated cells, measurement of metabolic and oxidative stress markers suggested that this mimicked a benign steatotic phenotype. This facilitates the use of this model for the investigation of factors that may cause benign steatosis to change to a progressive phenotype.

Overall, adjustment of glucose levels, provision of exogenous FAs and using HS for culturing cells proved to be a simple way to improve the function of cell lines and create a model for studying NAFLD pathogenesis, where primary cells or other models (*e.g.* 3D culture systems, HepaRG cells and inducible pluripotent stem cells) remain difficult to obtain or too expensive for many laboratories. Future work could include:

- Further investigation of the effects of HS in improving markers of differentiation and FA metabolism in cell lines, possibly through a transcriptomic approach
- Exploration of whether insulin signalling in Huh7 cells replicates what is seen *in vivo* and how altering insulin in culture media may better model a lean or obese phenotype
- Combining different cell types (*e.g.* Kupffer and stellate cells) in a 3D model could facilitate development of a progressive steatosis or NASH model, due to cell crosstalk, and larger LDs, as seen in liver tissue, which may be limited in a 2D system

7.1.2 Investigating the role of DGAT2 function in fatty acid metabolism

There are several genetic polymorphisms known to impact NAFLD development and progression (Sliz *et al.*, 2018). DGAT2, through its proposed role in regulating DNL and

VLDL secretion has previously been hypothesised to link hyperglycaemia and hyperlipidaemia (Zammit, 2013). Identification of changes in metabolic parameters in people carrying mutations in the *DGAT2* gene in the Oxford Biobank highlighted a potential role of this enzyme in metabolic disease. In Chapters 5 and 6 I investigated the interaction between DGAT2 function and substrate availability *in vitro*, in gene-edited Huh7 DGAT2 knockout (KO) cells, and in human participants with a *DGAT2* mutation, who underwent a sugar overfeeding intervention.

In the DGAT2 KO cell line, the most striking differences observed were a reduction in DNL, TAG secretion and glucose uptake (as determined by glucose remaining in the media; Chapter 5, sections 5.3.3.2, 5.3.3.6 and 5.3.3.9). This suggests that compared to DGAT1, DGAT2 has a specialised role in regulating DNL and contributing to TAG secretion. The effect of DGAT2 on DNL appeared to be largely mediated by carbohydrate responsive element binding protein (ChREBP; section 5.3.3.2), while insight from stable isotope enrichment showed a specific impairment of the addition of exogenous FA to VLDL particles (section 5.3.3.7), although the exact role of DGAT2 in this process was not clear.

In healthy people carrying a *DGAT2* mutation, there was a tendency for elevated plasma glucose compared to age, sex, height, weight and BMI-matched control clusters (Chapter 6, section 6.3.3.1), which was similar to the results seen in the DGAT2 KO cells. An elevation in carbohydrate oxidation and minimal changes in postprandial parameters after a sugar overfeeding intervention (sections 6.3.3.3-6.3.3.5) led to the hypothesis that these participants had adapted to elevated glucose levels and were able to cope with high sugar intake. Although

hepatic DNL didn't change, a resistance to adiposity gain (sections 6.3.3.3 and 6.3.3.5) could indicate a reduction in adipocyte DNL, potentially due to DGAT2 loss-of-function; however, results should be interpreted with some caution due to the preliminary nature of this study.

In terms of how a change in DGAT2 function might impact fat accumulation and NAFLD pathogenesis, the results suggest that DGAT2 may have a role. In KO cells, an increase in reactive oxygen species and interleukin-8 and a tendency for a reduction in insulin sensitivity (Chapter 5, sections 5.3.3.8-5.3.3.10), suggests that in some circumstances where a predisposition to NAFLD exists (*e.g.* a high fat diet, obesity, systemic insulin resistance) a loss of DGAT2 function could contribute towards the progression of NAFLD. Previous reports of a protective role of DGAT2 in dissociating liver fat accumulation and insulin resistance (Kantartzis *et al.*, 2009) further support a role for DGAT2 in NAFLD.

Overall, studying changes in DGAT2 function *in vitro* and *in vivo* indicate that it has an important role in glucose homeostasis, DNL and VLDL-TAG secretion, which in certain circumstances could contribute to NAFLD pathogenesis. Future work could include:

- Lipidomic analysis of Huh7 cells with altered DGAT2 function may identify changes in lipid species and elucidate the role of DGAT2 function on insulin signalling
- Assessing glucose uptake, DNL and gene expression in adipose biopsies from people carrying *DGAT2* mutations would help to determine whether there is a reduction in system glucose disposal, DNL and adiposity
- A high fat dietary intervention in *DGAT2* mutation carriers, to determine whether these people can be metabolically flexible in response to a high fat challenge

Appendices

Appendix A

Chapter 2 supplementary material

Table A.1. TaqMan® Assays used for gene expression analysis (continued next page)

Gene symbol	Gene name	ABI Assay ID
18S	*Eukaryotic 18S rRNA*	Hs99999901_s1
ACACA	*acetyl-CoA carboxylase alpha*	Hs01046047_m1
ACACB	*acetyl-CoA carboxylase beta*	Hs00153715_m1
AFP	*alpha-fetoprotein*	Hs00173490_m1
ALB	*albumin*	Hs00910225_m1
APOB	*apolipoprotein B*	Hs00181142_m1
B2M	*beta-2-microglobulin*	Hs00187842_m1
BSCL2	*seipin lipid droplet biogenesis associated*	Hs00949220_m1
CES1	*carboxylesterase 1*	Hs00275607_m1
CIDEB	*cell death inducing DFFA like effector b*	Hs00205339_m1
CIDEC	*cell death inducing DFFA like effector c*	Hs00535724_gH
CPT1A	*carnitine palmitoyltransferase 1A*	Hs00912671_m1
DGAT1	*diacylglycerol O-acyltransferase 1*	Hs01020362_g1
DGAT2	*diacylglycerol O-acyltransferase 2*	Hs01045913_m1
ELOVL2	*fatty acid elongase 2*	Hs00214936_m1
ELOVL5	*fatty acid elongase 5*	Hs01094711_m1
ELOVL6	*fatty acid elongase 6*	Hs00907564_m1
FADS1	*fatty acid desaturase 1*	Hs01096545_m1
FADS2	*fatty acid desaturase 2*	Hs00927433_m1
FASN	*fatty acid synthase*	Hs01005622_m1
GAPDH	*glyceraldehyde-3-phosphate dehydrogenase*	Hs02758991_g1
G6PC	*glucose-6-phosphatase, catalytic subunit*	Hs02560787_s1
HMBS	*hydroxymethylbilane synthase*	Hs00609296_g1
HNF4A	*hepatocyte nuclear factor 4, alpha*	Hs00230853_m1
HPRT1	*hypoxanthine phosphoribosyltransferase 1*	Hs02800695_m1
LIPC	*lipase C, hepatic type*	Hs00165106_m1
MKI67	*antigen identified by monoclonal antibody Ki-67*	Hs01032443_m1
MLXIPL	*MLX interacting protein like*	Hs00975714_m1
MTTP	*microsomal triglyceride transfer protein*	Hs00165177_m1
NR1H3	*nuclear receptor subfamily 1 group H member 3*	Hs00172885_m1
NR1H4	*nuclear receptor subfamily 1 group H member 4*	Hs01026590_m1
PDHA1	*pyruvate dehydrogenase (lipoamide) alpha 1*	Hs01049345_g1
PNPLA2	*patatin like phospholipase domain containing 2*	Hs00982042_m1
PNPLA3	*patatin like phospholipase domain containing 3*	Hs00228747_m1
PLIN1	*perilipin 1*	Hs00160173_m1
PLIN2	*perilipin 2*	Hs00605340_m1
PLIN3	*perilipin 3*	Hs00998416_m1
PLIN5	*perilipin 5*	Hs00965990_m1

Table A.1. TaqMan® Assays used for gene expression analysis (continued from previous page)

Gene symbol	Gene name	ABI Assay ID
PPARA	*peroxisome proliferator activated receptor alpha*	Hs00947536_m1
PPARG	*peroxisome proliferator activated receptor gamma*	Hs01115513_m1
PPARGC1A	*PPARG coactivator 1 alpha*	Hs00173304_m1
SCD	*stearoyl-CoA desaturase (delta-9-desaturase)*	Hs01682761_m1
SREBF1	*sterol regulatory element binding transcription factor 1*	Hs01088679_g1
TM6SF2	*transmembrane 6 superfamily member 2*	Hs00403495_m1
UBC	*ubiquitin C*	Hs01871556_s1
YWHAZ	*tyrosine 3-monooxygenase/tryptophan 5-monooxygenase activation protein, zeta polypeptide*	Hs03044281_g1

Table A.2. List of antibodies from Cell Signalling (MA, USA) used for immunoblotting

Protein	Secondary antibody	Catalogue number
β-Tubulin (9F3)	Goat anti-Rabbit	2128
CHOP	Goat anti-Rabbit	D46F1
IRE1-α	Goat anti-Rabbit	14C10
p-GSK3-α/β (Ser21/9)	Goat anti-Mouse	D17D2
Total GSK3-α/β	Goat anti-Mouse	D75D3
Akt (pan)	Goat anti-Mouse	4804
p-Akt (S473)	Goat anti-Rabbit	193H12
apoB*	Rabbit anti-Sheep	(S-18) sc-11795

*apoB was purchased from Santa Cruz Biotechnology (TX, USA)

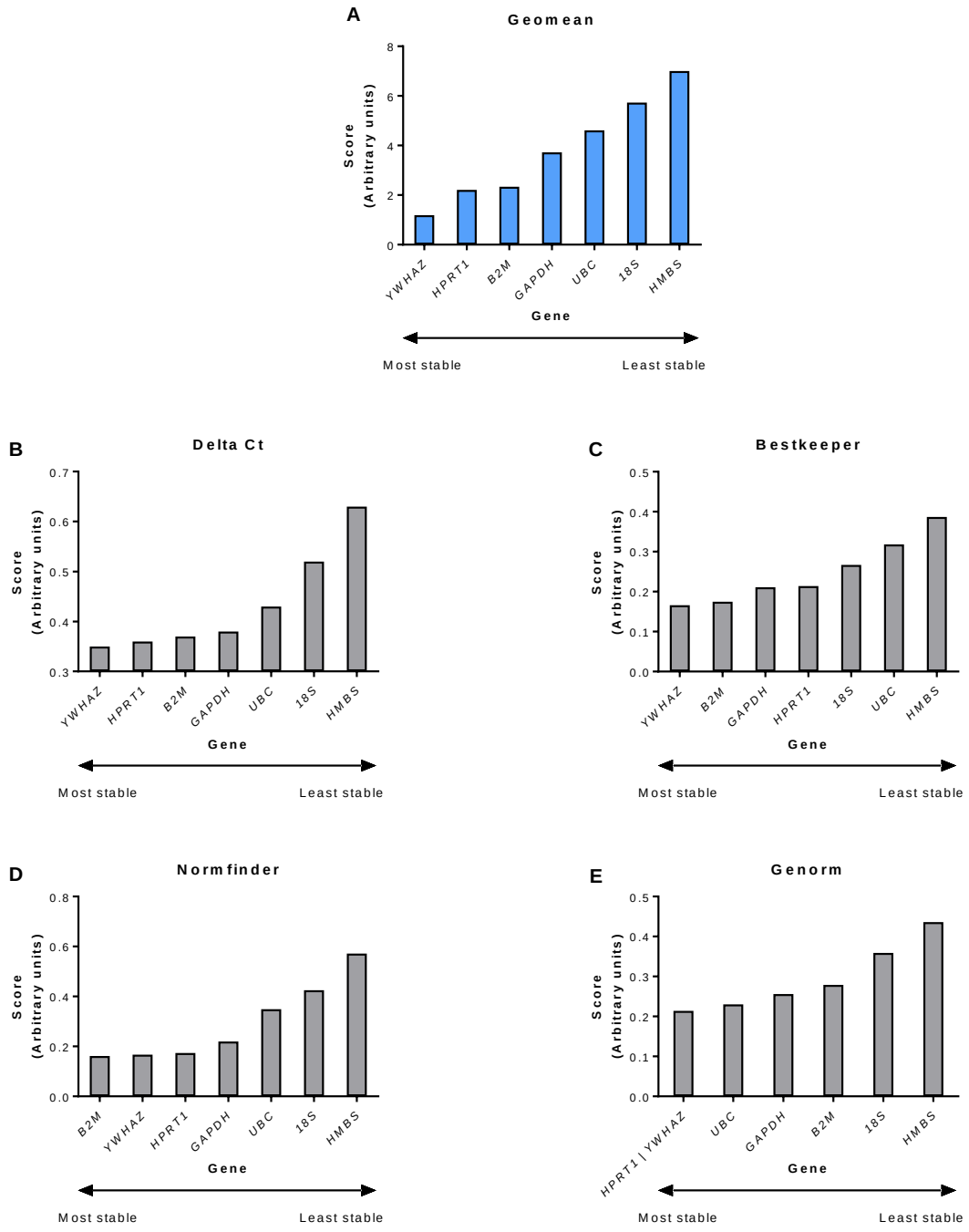


Figure A.1. The stability of reference genes in HepG2 cells grown for 2, 4, 7, 14 and 21 days in 1% dimethyl sulfoxide (DMSO), or a control condition grown to Day 2 without DMSO. Overall scores are presented in the Geomean figure (**A**), which combines scores from the Delta Ct (**B**), Bestkeeper (**C**), Normfinder (**D**) and Genorm (**E**) methods. Genes are ranked from most stable (left of x-axis) to least stable (right of x-axis). Scores are calculated from Ct values of three replicates and six conditions.

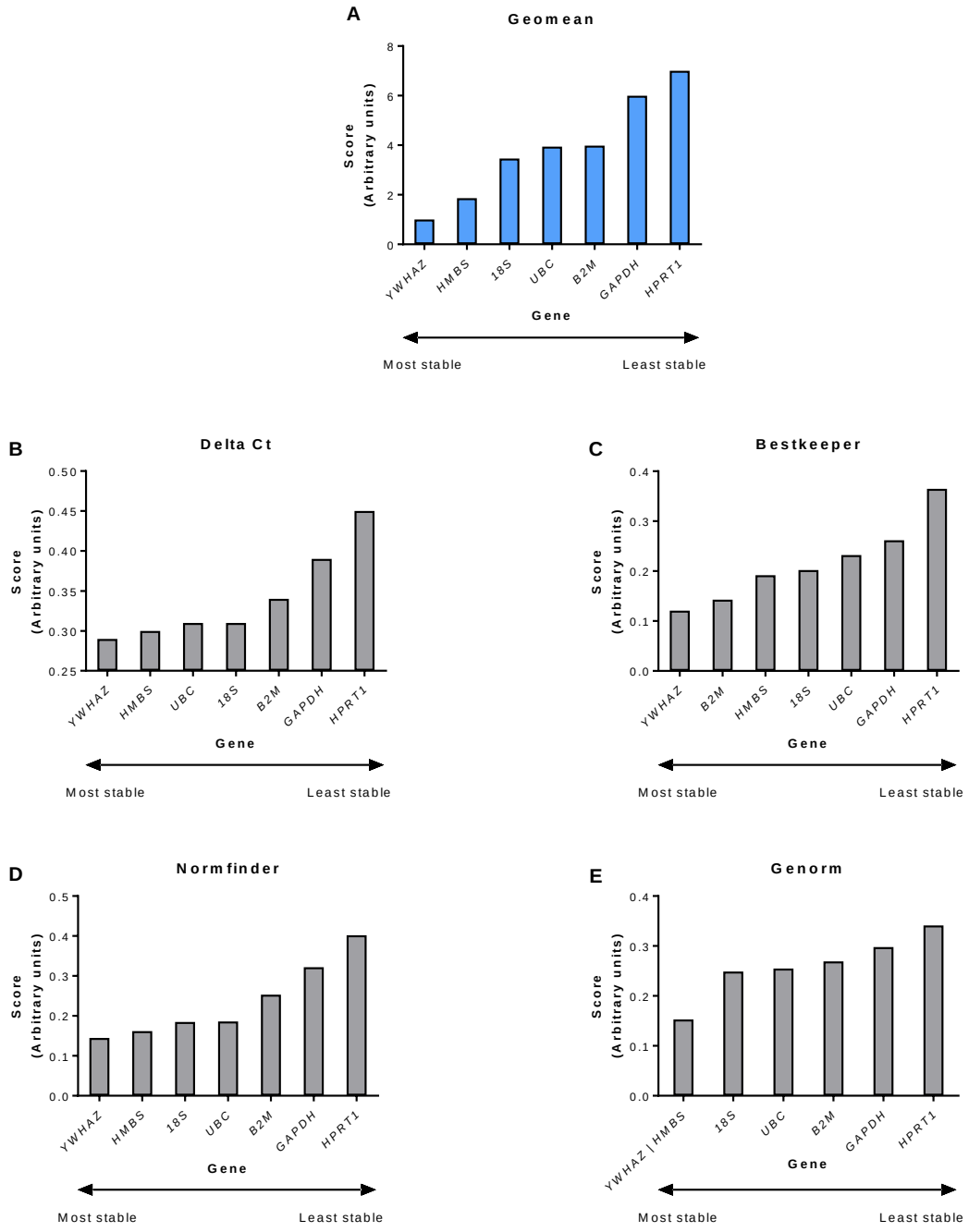


Figure A.2. The stability of reference genes in Huh7 cells grown for seven days only in human serum, or with an additional seven day of either low fat low sugar (LFLS; 11 mM glucose + 200 µM fatty acids), low fat high sugar (LFHS; 200 µM fatty acids + 11 mM glucose + 5.5 mM fructose) or high fat high sugar (HFHS; 800 µM fatty acids + 11 mM glucose + 5.5 mM fructose) treatment. Overall scores are presented in the Geomean figure (**A**), which combines scores from the Delta Ct (**B**), Bestkeeper (**C**), Normfinder (**D**) and Genorm (**E**) methods. Genes are ranked from most stable (left of x-axis) to least stable (right of x-axis). Scores are calculated from Ct values of three replicates and six conditions.

Appendix B

Chapter 3 supplementary material

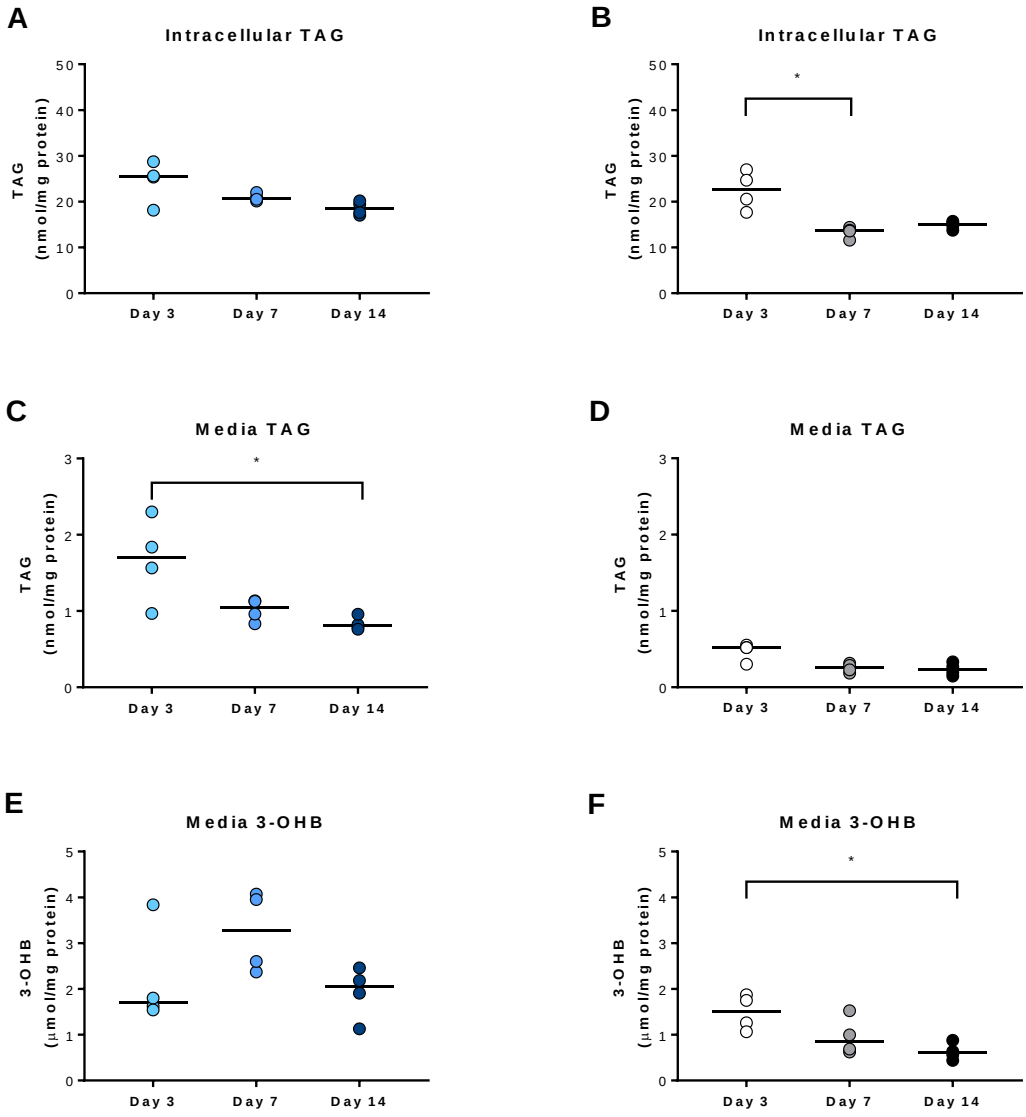


Figure B-1. Markers of FA metabolism in HepG2 cells when grown in human serum (**A, C, E**) and foetal bovine serum (**B, D, F**) cells for three, seven or 14 days. Intracellular triacylglycerol (TAG) content was measured (**A, B**), as were levels of media TAG (**C, D**) and 3-hydroxybutyrate (3-OHB; **E, F**), as markers of fatty acid secretion and oxidation, respectively. Media was added to cells 24 hours prior to collection and all results were corrected to protein content of cells. Data are presented as individual values and median, $n = 4$. * $p < 0.05$; Kruskal-Wallis test with Dunn's multiple comparisons test.

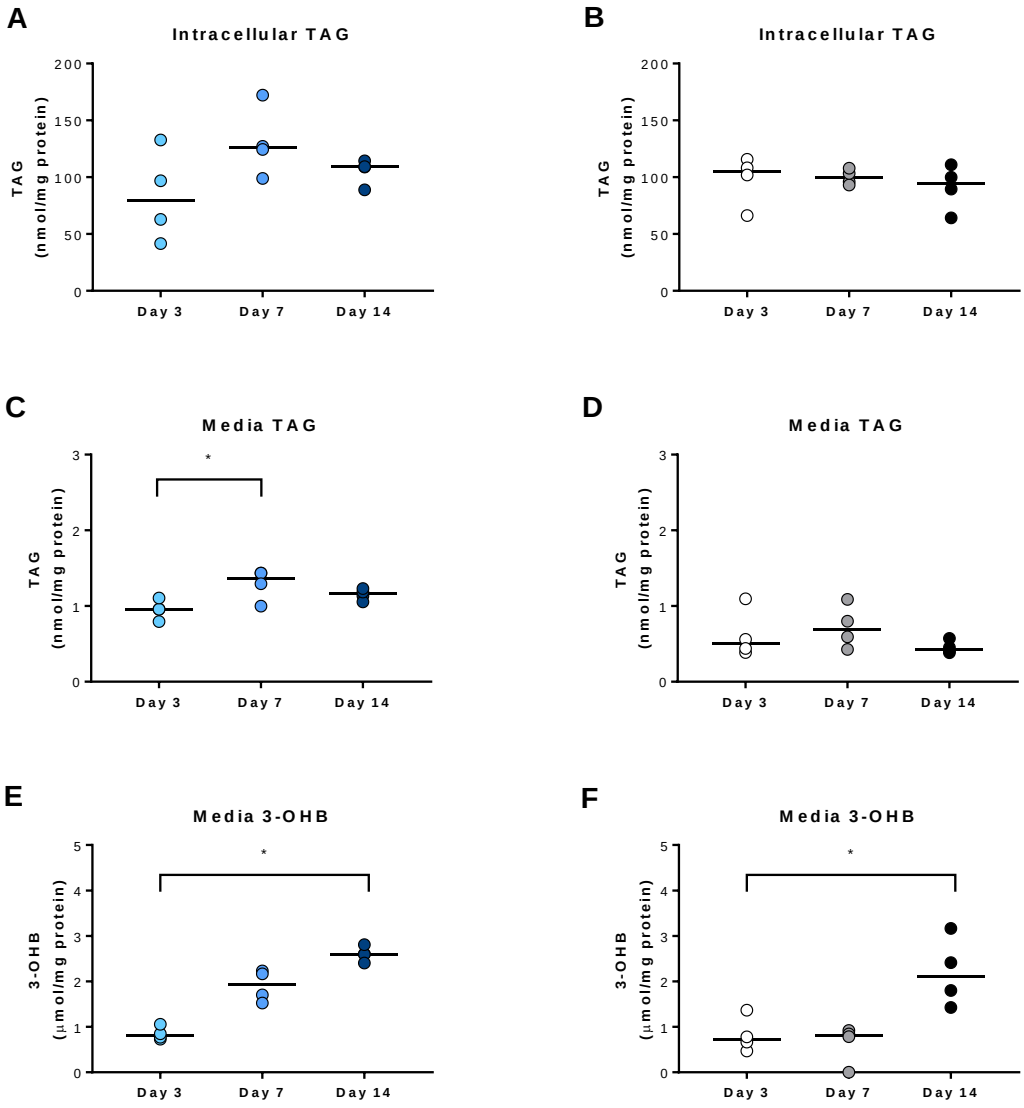


Figure B-2. Markers of FA metabolism in Huh7 cells when grown in human serum (**A, C, E**) and foetal bovine serum (**B, D, F**) cells for three, seven or 14 days. Intracellular triacylglycerol (TAG) content was measured (**A, B**), as were levels of media TAG (**C, D**) and 3-hydroxybutyrate (3-OHB; **E, F**), as markers of fatty acid secretion and oxidation, respectively. Media was added to cells 24 hours prior to collection and all results were corrected to protein content of cells. Data are presented as individual values and median, $n = 4$. * $p < 0.05$; Kruskal-Wallis test with Dunn's multiple comparisons test.

Table B-1. mRNA expression of FA metabolism genes in HepG2 cells when grown in human serum (HS) and foetal bovine serum (FBS) cells for three, seven or 14 days.

	HS			FBS		
	D3	**D7**	**D14**	**D3**	**D7**	**D14**
Hepatic nuclear receptors						
HNF4A	1.41 (1.28 - 1.44)*	1.16 (1.16 - 1.38)	0.97 (0.85 - 1.04)*	1.06 (0.96 - 1.10)†	0.95 (0.89 - 0.99)	0.78 (0.70 - 0.91)†
NR1H3	0.84 (0.78 - 1.19)	0.90 (0.83 - 1.25)*	0.57 (0.38 - 0.76)*	0.70 (0.52 - 0.87)	0.72 (0.42 - 0.96)	0.59 (0.47 - 0.73)
NR1H4	0.46 (0.43 - 0.71)	0.51 (0.51 - 0.62)*	0.25 (0.20 - 0.70)*	0.20 (0.15 - 0.24)	0.16 (0.14 - 0.32)	0.10 (0.06 - 0.19)
Transcription factors						
MLXIPL	2.87 (1.87 - 5.08)*	2.76 (1.66 - 3.60)	0.89 (0.63 - 1.98)*	1.88 (1.00 - 2.47)†	1.11 (0.95 - 1.29)	0.44 (0.33 - 0.74)†
PPARA	0.70 (0.61 - 0.96)*	0.77 (0.65 - 0.86)	0.55 (0.47 - 0.59)*	0.60 (0.54 - 0.64)	0.63 (0.55 - 0.76)	0.46 (0.36 - 0.79)
PPARG	0.28 (0.20 - 0.53)	0.47 (0.26 - 0.70)	0.43 (0.40 - 0.47)	0.29 (0.18 - 0.46)	0.28 (0.21 - 0.36)	0.42 (0.29 - 0.55)
PPARGC1A	1.79 (1.71 - 3.13)	2.90 (2.47 - 2.96)	2.44 (2.02 - 2.79)	1.59 (1.55 - 1.69)	2.53 (1.75 - 3.05)†	1.04 (0.91 - 2.02)†
SREBF1	0.91 (0.86 - 0.97)	0.62 (0.58 - 0.66)	0.62 (0.49 - 0.67)	0.77 (0.71 - 1.00)	0.76 (0.69 - 0.80)	0.57 (0.53 - 0.61)

mRNA expression is presented relative to a calibrator sample, all genes were corrected to two reference genes (*B2M* and *YWHAZ*). Data are presented as median (range), $n = 4$. * $p < 0.05$, matching symbols denote significant differences between means at different time points in HS (*) and FBS (†), $p < 0.05$; Kruskal-Wallis test with Dunn's multiple comparisons test.

Table B-2. mRNA expression of FA metabolism genes in Huh7 cells when grown in human serum (HS) and foetal bovine serum (FBS) cells for three, seven or 14 days.

	HS			FBS		
	D3	**D7**	**D14**	**D3**	**D7**	**D14**
Hepatic nuclear receptors						
HNF4A	1.02 (0.89 - 1.34)	1.26 (1.03 - 1.39)	1.00 (0.66 - 1.45)	1.19 (1.01 - 1.30)	1.26 (1.14 - 1.32)	0.95 (0.71 - 1.20)
NR1H3	1.38 (1.21 - 1.64)	1.35 (1.23 - 1.41)*	0.97 (0.91 - 1.10)*	1.39 (1.26 - 1.55)	1.17 (0.98 - 1.52)	0.91 (0.89 - 1.28)
NR1H4	1.32 (1.27 - 2.10)	1.34 (0.99 - 1.50)	1.51 (1.19 - 2.15)	1.36 (1.03 - 2.39)	1.35 (0.86 - 1.64)	1.40 (0.96 - 1.64)
Transcription factors						
MLXIPL	0.21 (0.10 - 0.51)	0.19 (0.13 - 0.26)	0.27 (0.10 - 0.34)	0.13 (0.12 - 0.66)	0.19 (0.15 - 0.23)	0.25 (0.13 - 0.43)
PPARA	1.45 (0.88 - 1.77)	1.14 (1.08 - 1.40)	1.37 (0.97 - 1.42)	1.36 (0.75 - 1.70)	1.05 (0.80 - 1.21)	1.09 (1.03 - 1.21)
PPARG	1.81 (1.07 - 3.05)	1.08 (0.77 - 1.39)	1.47 (1.29 - 2.05)	1.68 (1.36 - 2.89)	1.01 (0.78 - 1.31)	1.03 (0.94 - 1.64)
PPARGC1A	0.02 (0.02 - 0.03)	0.01 (0.01 - 0.03)*	0.04 (0.02 - 0.08)*	0.02 (0.01 - 0.03)	0.01 (0.01 - 0.02)	0.04 (0.02 - 0.04)
SREBF1	1.85 (1.51 - 2.12)*	0.94 (0.84 - 0.96)	0.84 (0.62 - 0.96)*	1.99 (1.60 - 2.38)†	0.79 (0.71 - 1.03)†	0.90 (0.69 - 1.02)

mRNA expression is presented relative to a calibrator sample, all genes were corrected to two reference genes (*B2M* and *YWHAZ*). Data are presented as median (range), $n = 4$. * $p < 0.05$, matching symbols denote significant differences between means at different time points in HS (*) and FBS (†), $p < 0.05$; Kruskal-Wallis test with Dunn's multiple comparisons test.

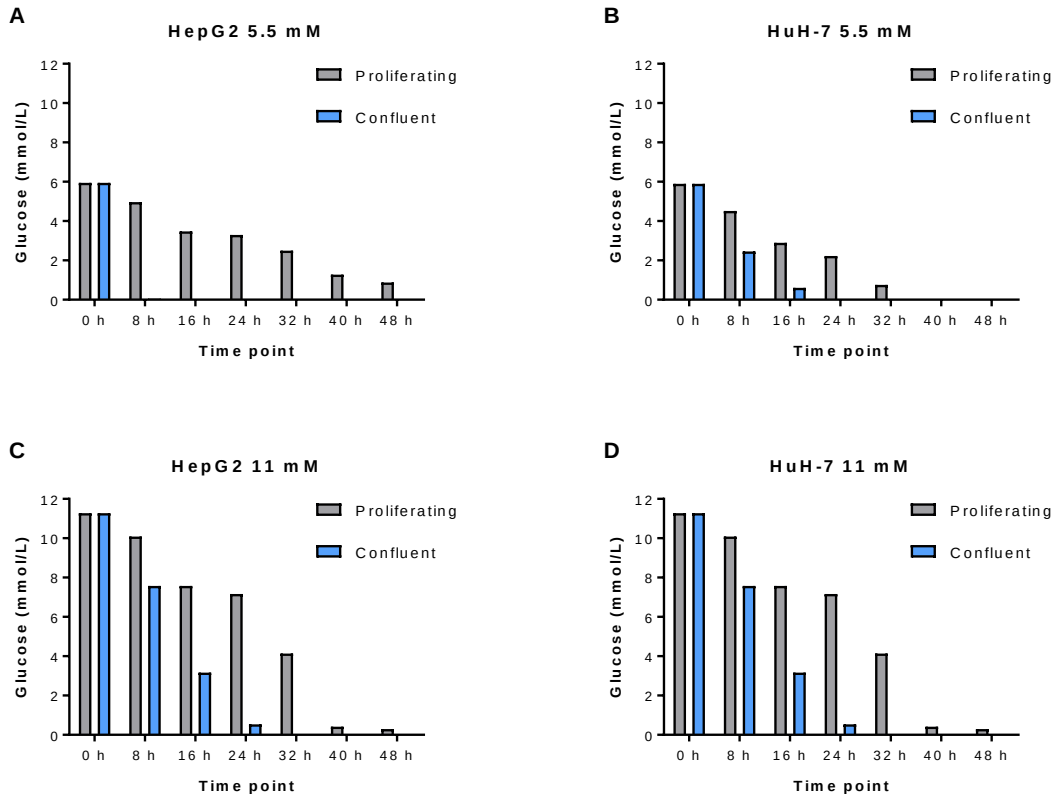


Figure B-3. A time course of glucose uptake in HepG2 and Huh7 cells. Cells were grown for four days (confluent) or one day (proliferating) in 5.5 mM glucose before having either 5.5 mM of 11 mM glucose added. Media was collected from independent wells at 8 hour intervals for the next 48 hours, $n = 1$.

Table B-3. Fatty acid composition in foetal bovine serum (FBS) and human serum (HS)

	FBS	HS
C14:0	1.26	1.80
C16:0	10.9	27.9
C18:0	2.27	4.55
SFA	**14.4**	**34.3**
C16:1*n*-7	2.13	3.77
C18:1*n*-9	10.2	35.1
C18:1*n*-7	2.79	0.37
C20:1*n*-9	0.00	0.31
MUFA	**15.1**	**39.6**
C18:2*n*-6	3.44	20.2
C18:3*n*-6	0.00	0.53
C18:3*n*-3	0.00	0.66
C20:3*n*-6	9.34	1.19
C20:3*n*-3	47.4	0.42
C20:4*n*-6	9.40	1.20
PUFA	**69.6**	**24.2**
Total FA in media (μM)	**7.78**	**13.0**

Foetal bovine serum and human serum underwent lipid extraction and gas chromatography in duplicate. Fatty acids are presented as mol%, unless otherwise stated.

Appendix C

Chapter 4 supplementary material

C.1 Isolation of primary hepatocytes

Primary hepatocytes were isolated following the method of Green *et al.* (Green *et al.*, 2017). Reagents are listed in Table 2.1-1 or were purchased from Sigma-Aldrich; Gillingham, UK, unless otherwise stated. Whole liver tissue was kept in cold HBSS until isolation and the isolation procedure was carried out on ice. First, liver tissue was minced using two scalpels and, once pieces were less than 3 mm in size, was washed with HBSS to remove excess blood. Tissue was then transferred to a container, covered with EGTA dissociation buffer (0.5% BSA and 0.5 mM EGTA in HBSS), placed in a water bath and shaken at 37°C for 10 mins. Tissue was again washed with HBSS, covered with digestion buffer (0.5% BSA, 0.05% collagenase IV and 10 mM calcium chloride in HBSS) and returned to the water bath for 30 minutes. The supernatant was filtered through 148 μm and 58 μm mesh and the remaining tissue was covered with fresh digestion buffer and returned to the water bath for a further 30 minutes before the second supernatant was filtered.

Each supernatant was then added to an equal volume of wash buffer (1% penicillin-streptomycin, 1% GlutaMAX™ and 0.5% BSA in William's E; Gibco™, Life Technologies; Paisley, UK) and centrifuged at room temperature for 5 minutes at 80 x g (700 rpm). After centrifuging, the majority of supernatant was removed with the pellet resuspended in any remaining supernatant. Ammonium-chloride-potassium (ACK) lysing buffer (Gibco™, Life Technologies; Paisley, UK) was then added for 3 minutes to lyse red blood cells before inactivation with an equal volume of PBS and centrifugation as previously. After centrifuging, the supernatant was poured off without dislodging the pellet, which was then gently

resuspended by rotation in the remaining supernatant. This washing step was repeated with the hepatocytes resuspended in a small amount of supernatant.

At this point, viability was checked using Trypan blue and cells were counted. For isolations with viability above 50%, the protocol continued with centrifugation, removal of supernatant and resuspension of the cell pellet to 1 x 10^6 cells per mL in plating media (2% human serum, 100 nM insulin, 100 nM dexamethasone, 1% penicillin-streptomycin, 1% GlutaMAX™ and 0.5% BSA in William's E). Cells were then seeded into collagen-coated plates at a density of 2 x 10^5 cells per cm^2 and incubated at 37°C for 3-4 hours. After this time, media was changed to the appropriate treatment media and cells were cultured for up to 48 hours.

Table C.1. The effect of media composition on fatty acid composition of triacylglycerol in Huh7 cells (nmol/mg protein)

	LFLS	LFHS	HFHS
C14:0	3.31 ± 0.22	3.28 ± 0.30	3.63 ± 0.22
C16:0	22.7 ± 1.10**	22.4 ± 1.85**	40.1 ± 1.72
C18:0	3.39 ± 0.24	3.39 ± 0.32	4.16 ± 0.28
SFA	**29.4 ± 1.54****	**29.1 ± 2.46****	**47.9 ± 2.20**
C16:1*n*-7	6.52 ± 0.28	6.50 ± 0.47	6.38 ± 0.26
C18:1*n*-9	33.0 ± 1.16**	32.7 ± 1.91**	76.3 ± 3.14
C18:1*n*-7	4.66 ± 0.20*	4.79 ± 0.37*	3.45 ± 0.25
C20:1*n*-9	0.44 ± 0.02**	0.43 ± 0.02**	0.82 ± 0.04
MUFA	**44.7 ± 1.57****	**44.4 ± 2.73****	**86.9 ± 3.51**
C18:2*n*-6	7.41 ± 0.26**	7.33 ± 0.42**	27.7 ± 1.00
C18:3*n*-6	3.10 ± 0.57*	2.33 ± 0.39	1.40 ± 0.26
C18:3*n*-3	0.06 ± 0.02**	0.05 ± 0.02**	1.25 ± 0.07
C20:4*n*-6	0 ± 0**	0 ± 0**	0.34 ± 0.02
C20:5*n*-3	0.14 ± 0.02	0.09 ± 0.02	0.15 ± 0.03
PUFA	**10.7 ± 0.63****	**9.81 ± 0.65****	**30.9 ± 1.32**

Once confluent, cells were treated with media containing 2% human serum and 11 mM glucose for seven days before treatment media was added. Treatments consisted of either low fat low sugar (LFLS; 11 mM glucose + 200 μM fatty acids), low fat high sugar (LFHS; 200 μM fatty acids + 11 mM glucose + 5.5 mM fructose) or high fat high sugar (HFHS; 800 μM fatty acids + 11 mM glucose + 5.5 mM fructose). Data are mean ± SEM, $n = 6$. * $p < 0.05$; ** $p < 0.001$ compared to HFHS-treated cells; two-way ANOVA with Bonferroni's multiple comparisons test.

Table C.2. The effect of media composition on fatty acid composition of phospholipids in Huh7 cells (nmol/mg protein)

	LFLS	LFHS	HFHS
C14:0	0.94 ± 0.06**	0.79 ± 0.07**	0.38 ± 0.05
C16:0	62.3 ± 2.31	54.8 ± 2.47	56.7 ± 3.53
C18:0	38.1 ± 1.38	34.4 ± 1.14	39.5 ± 1.80
SFA	**101.4 ± 3.54**	**90.0 ± 3.63**	**96.5 ± 5.28**
C16:1*n*-7	7.00 ± 0.62**	5.31 ± 0.30**	2.00 ± 0.24
C18:1*n*-9	45.4 ± 1.86	40.4 ± 1.69	35.7 ± 6.55
C18:1*n*-7	8.26 ± 0.38**	7.29 ± 0.27**	3.68 ± 0.21
C20:1*n*-9	0.67 ± 0.06	0.61 ± 0.04	0.76 ± 0.02
MUFA	**61.3 ± 2.39***	**53.6 ± 2.03**	**48.1 ± 2.82**
C18:2*n*-6	40.5 ± 1.78**	35.7 ± 1.16**	57.2 ± 2.54
C18:3*n*-6	1.56 ± 0.20*	1.10 ± 0.06	0.76 ± 0.02
C18:3*n*-3	0.45 ± 0.02*	0.43 ± 0.03*	0.60 ± 0.06
C20:4*n*-6	10.6 ± 0.50*	10.1 ± 0.37*	12.4 ± 0.32
C20:5*n*-3	1.04 ± 0.06	0.93 ± 0.04*	1.21 ± 0.08
C22:5*n*-3	2.81 ± 0.15*	2.54 ± 0.18*	1.91 ± 0.16
C22:6*n*-3	1.64 ± 0.07	1.53 ± 0.05*	1.84 ± 0.02
PUFA	**58.6 ± 2.34****	**52.3 ± 1.64****	**76.0 ± 2.87**

Once confluent, cells were treated with media containing 2% human serum and 11 mM glucose for seven days before treatment media was added. Treatments consisted of either low fat low sugar (LFLS; 11 mM glucose + 200 μM fatty acids), low fat high sugar (LFHS; 200 μM fatty acids + 11 mM glucose + 5.5 mM fructose) or high fat high sugar (HFHS; 800 μM fatty acids + 11 mM glucose + 5.5 mM fructose). Data are mean ± SEM, $n = 6$. * $p < 0.05$; ** $p < 0.001$ compared to HFHS-treated cells; two-way ANOVA with Bonferroni's multiple comparisons test.

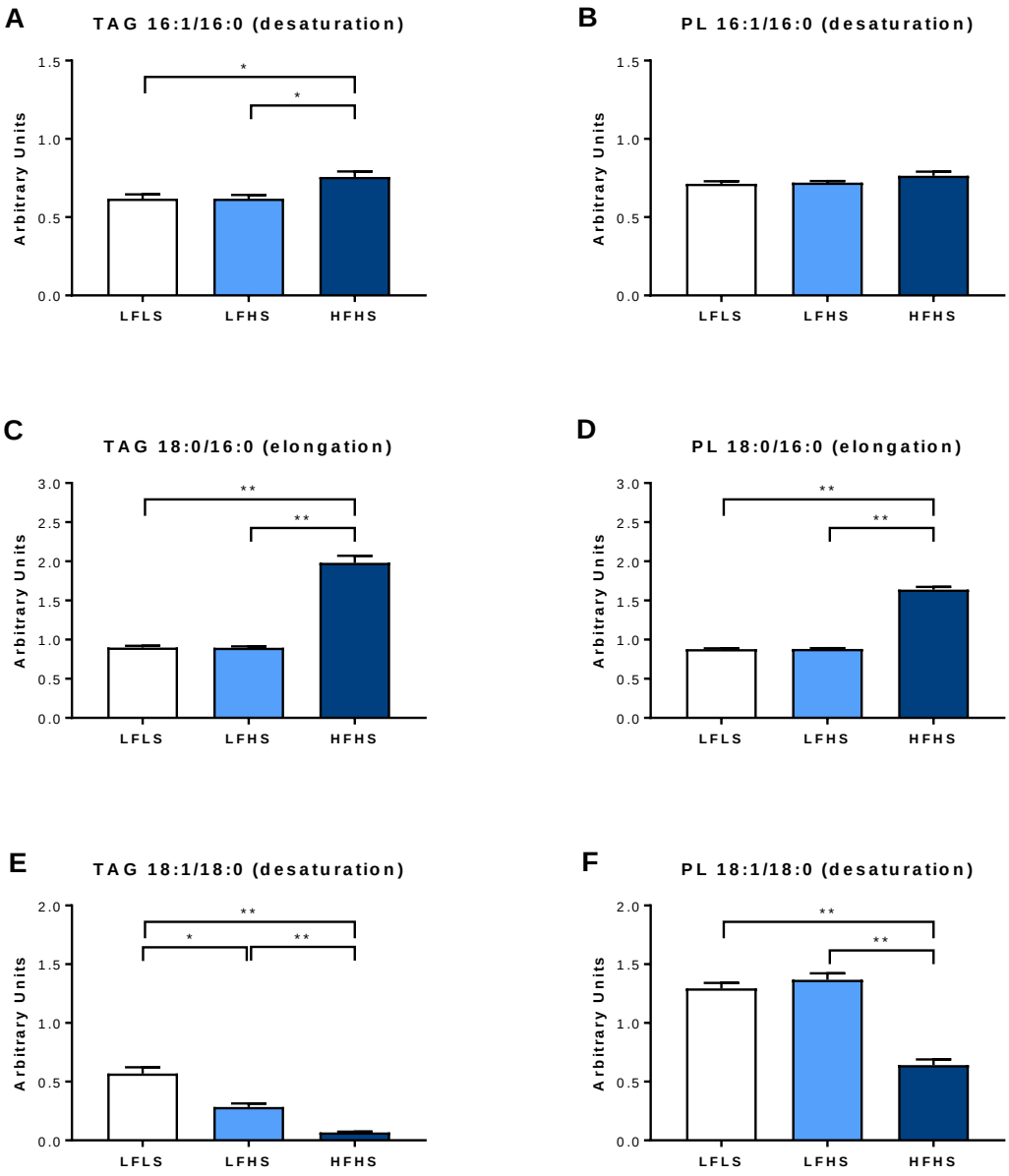


Figure C.1. The effect of media composition on fatty acid metabolism in triacylglycerol (TAG; **A, C, E**) and phospholipids (PLs; **B, D, F**) of Huh7 cells. Upon reaching confluence, cells were treated with media containing 2% human serum and 11 mM glucose for seven days before treatment media was added. Treatments consisted of either low fat low sugar (LFLS; 11 mM glucose + 200 μM fatty acids), low fat high sugar (LFHS; 200 μM fatty acids + 11 mM glucose + 5.5 mM fructose) or high fat high sugar (HFHS; 800 μM fatty acids + 11 mM glucose + 5.5 mM fructose). The contribution of *de novo* lipogenesis was calculated from deuterium appearance in C16:0, C16:1*n*-7, C18:0 and C18:1*n*-7 & 9 and indices of C16:0 desaturation (**A, B**) and elongation (**C, D**) and C18:0 desaturation (**E, F**) were calculated. Media was changed every 48 to 72 hours and 24 hours prior to collection. Data are mean ± SEM, $n = 6$. * $p < 0.05$, ** $p < 0.001$; two-way ANOVA with Bonferroni's multiple comparisons test.

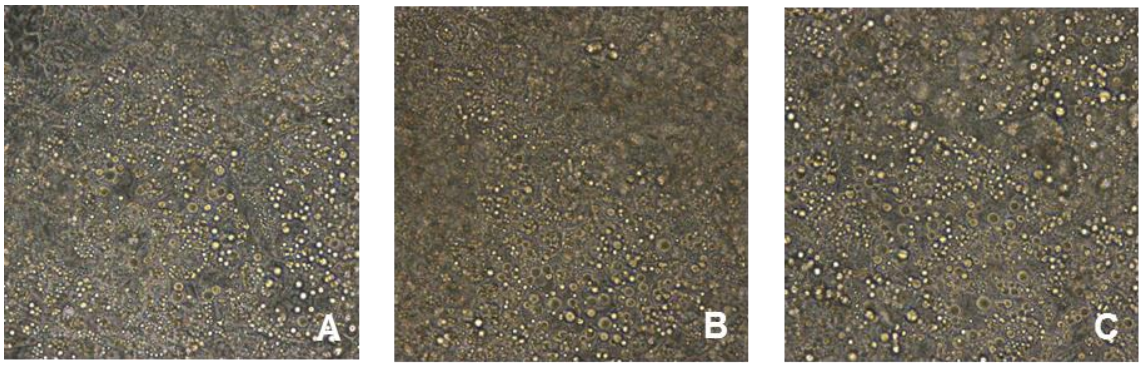


Figure C.2. The effect of culture time on lipid droplet accumulation in Huh7 cells. Once confluent, cells were treated with media containing 2% human serum and 11 mM glucose for seven days before treatment media was added. Treatment consisted of 800 μM fatty acids + 11 mM glucose + 5.5 mM fructose (high fat high sugar) and images were taken at 7 (**A**), 10 (**B**) and 14 (**C**) days. Images were taken via light microscopy (40X magnification) and media was changed every 48 hours.

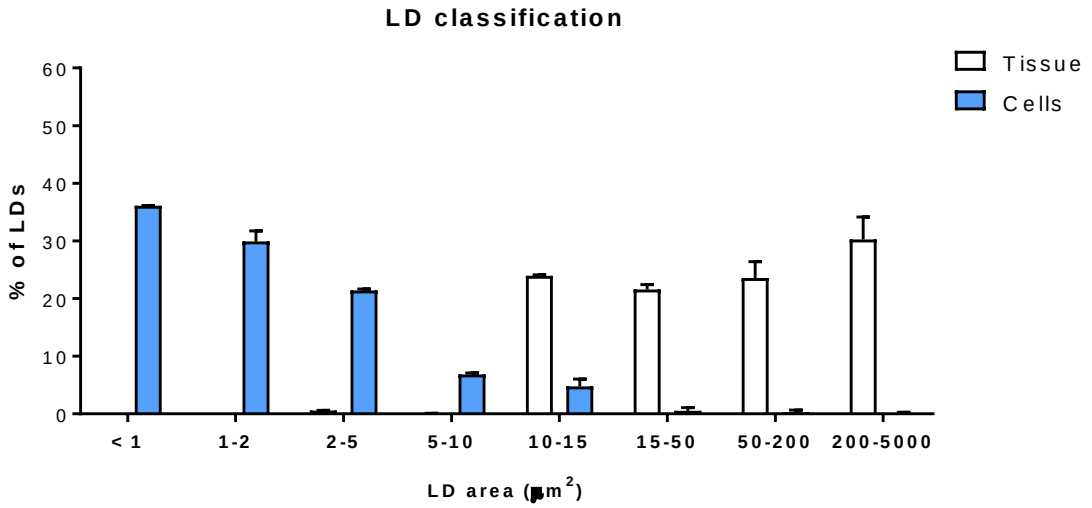


Figure C.3. Lipid droplet (LD) populations in whole liver tissue (white bars) and isolated hepatocytes (blue bars) from two steatotic (25% and 30% fat) livers. Tissue LDs were quantified by the IN Cell 6000 as shown in Figure C.4. Hepatocytes from the same livers were isolated and culted for 24 hours before being fixed and LDs identified and area quantified. Due to magnification differences (4X in tissue and 40X in cells) the smallest detectable LD in tissue is 2 μm^2. Data are mean ± SD, $n = 2$. This work was carried out by Dr. Charlotte Green.

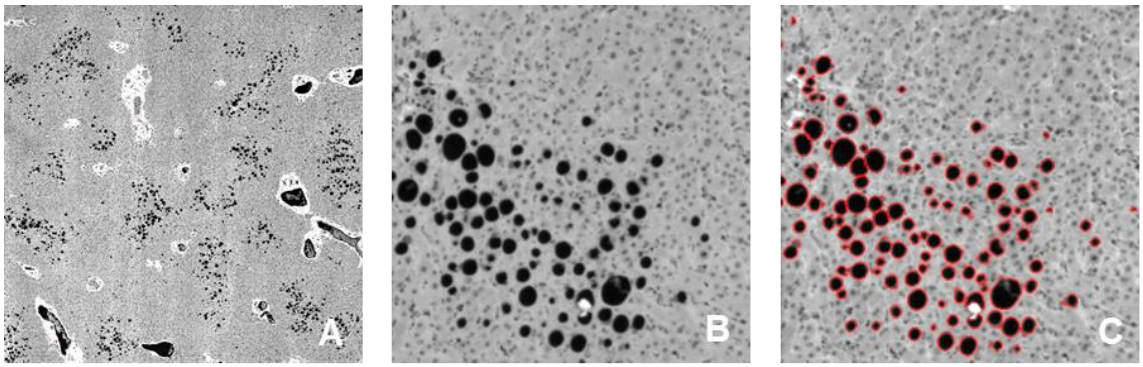


Figure C.4. Lipid droplet population and quantification in liver histology samples using the IN Cell Analyzer 6000. Representative liver tissue slide from FITC channel with 4x magnification, lipid droplets are shown in black clusters (**A**). Zoomed image of area of lipid droplets (**B**) and screen shot of analysis, with lipid droplets counted in analysis circled in red (**C**). This work was carried out by Dr. Charlotte Green.

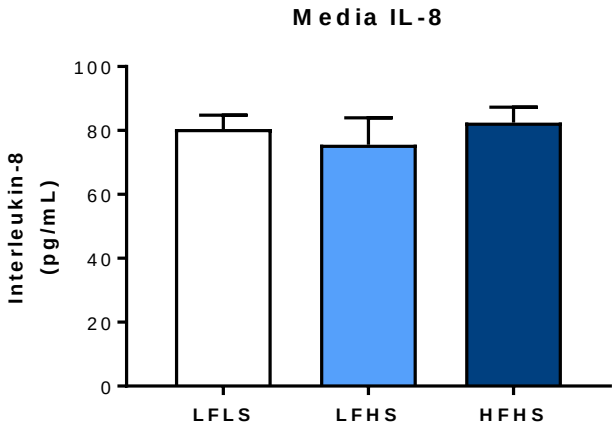


Figure C.5. Interleukin (IL)-8 levels in the media of Huh7 cells. Once confluent, cells were treated with media containing 2% human serum and 11 mM glucose for seven days before treatment media was added. Treatments consisted of either low fat low sugar (LFLS; 11 mM glucose + 200 μM fatty acids), low fat high sugar (LFHS; 200 μM fatty acids + 11 mM glucose + 5.5 mM fructose) or high fat high sugar (HFHS; 800 μM fatty acids + 11 mM glucose + 5.5 mM fructose). Data are mean ± SD, $n = 2$.

Appendix D

Chapter 5 supplementary material

Table D.1. Target sequences of the four DGAT2-targeting siRNA contained in Dharmafect ON-TARGET*plus* DGAT2 siRNA

siRNA ID	Target sequence	Molecular weight (g/mol)	Extension coefficient (L/mol.cm)
J-009333-05	GAACACACCCAAGAAAGGU	13,429.90	369,706
J-009333-06	GGAGGUAUCUGCCCUGUCA	13,459.90	362,141
J-009333-07	UCAUGGAGCUGACCUGGUU	13,444.80	364,900
J-009333-08	GAAUGCCUGUGUUGAGGGA	13,444.90	363,743

Table D.2. Target sequences of the four non-targeting siRNA contained in Dharmafect ON-TARGET*plus* Non-targeting Control Pool

siRNA ID	Target sequence	Molecular weight (g/mol)	Extension coefficient (L/mol.cm)
n/a	UGGUUUACAUGUCGACUAA	13,429.90	369,706
n/a	UGGUUUACAUGUUGUGUGA	13,459.90	362,141
n/a	UGGUUUACAUGUUUUCUGA	13,444.80	364,900
n/a	UGGUUUACAUGUUUUCCUA	13,444.90	363,743

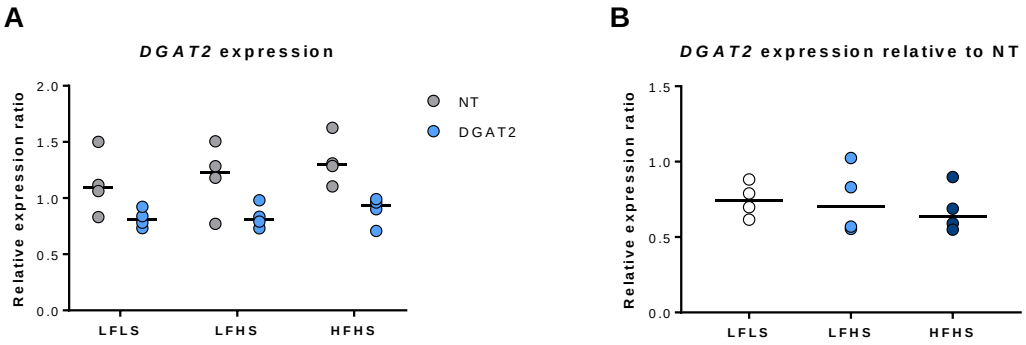


Figure D.1. Preliminary results investigating the efficiency of DGAT2 knockdown in Huh7 cells. After seeding, cells were cultured in maintenance media until confluence, before being cultured in human serum-containing media for seven days. After this, 100 nM siRNA either targeting DGAT2 or a non-targeting (NT) control was added to cells with 10 µL/mL Dharmafect 4 in antibiotic and serum-free media for 24 hours before treatment media was added. Treatments consisted of either low fat low sugar (LFLS; 11 mM glucose + 200 µM fatty acids), low fat high sugar (LFHS; 200 µM fatty acids + 11 mM glucose + 5.5 mM fructose) or high fat high sugar (HFHS; 800 µM fatty acids + 11 mM glucose + 5.5 mM fructose). To confirm knockdown, *DGAT2* mRNA expression was measured in cells treated with NT and DGAT2 siRNA and expressed relative to a pooled mRNA sample (**A**). Each DGAT2 replicate was also expressed relative to its NT control sample (**B**). Media was changed every 48 to 72 hours and 24 hours prior to collection and DGAT2 was corrected to three reference genes (*B2M*, *HMBS* and *YWHAZ*). Data are presented as individual values and median, $n = 4$.

Table D.3. The effect of media composition on fatty acid composition of triacylglycerol in Huh7 cells with wildtype (WT) or knockout (KO) of the *DGAT2* gene (nmol/mg protein)

	LFLS		LFHS		HFHS	
	WT	**KO**	**WT**	**KO**	**WT**	**KO**
C14:0	11.8 (10.3 - 14.3)**[a]	1.41 (1.10 - 2.49)**	11.1 (10.7 - 11.4)**[a]	1.34 (1.16 - 1.73)**	13.9 (12.8 - 17.1)**[b]	2.32 (1.70 - 2.97)**
C16:0	99.5 (92.0 - 121.8)**[a]	22.2 (17.1 - 38.3)**[a]	95.0 (92.2 - 103.7)**[a]	22.3 (18.7 - 26.1)**[a]	244.4 (232.6 - 305.0)**[b]	105.0 (83.9 - 123.6)**[b]
C18:0	17.3 (15.4 - 20.1)**[a]	3.14 (2.36 - 5.50)**	15.4 (15.1 - 17.3)**[a]	3.00 (2.48 - 3.57)**[a]	22.8 (20.0 - 26.6)**[b]	6.89 (5.06 - 8.55)**[b]
SFA	128.7 (117.7 - 156.1)**[a]	26.8 (20.6 - 46.3)**[a]	121.5 (118.0 - 132.4)**[a]	26.7 (22.3 - 31.4)**[a]	281.0 (265.3 - 348.6)**[b]	114.9 (90.6 - 133.7)**[b]
C16:1*n*-7	26.1 (23.2 - 31.4)**	2.79 (2.11 - 4.65)**	24.2 (23.8 - 27.4)**[a]	2.65 (2.28 - 3.10)**	29.0 (26.9 - 35.7)**[b]	4.31 (3.15 - 5.70)**
C18:1*n*-9	145.6 (134.2 - 182.1)**[a]	41.8 (33.9 - 74.6)**[a]	143.1 (137.4 - 154.7)*[a]	46.0 (37.1 - 50.1)*[a]	471.6 (447.0 - 581.5)**[b]	208.5 (171.6 - 250.5)**[b]
C18:1*n*-7	23.1 (20.7 - 27.2)**	4.50 (3.26 - 8.06)**	21.4 (20.6 - 23.5)**	4.31 (3.64 - 5.10)**	24.3 (22.4 - 29.6)**	7.98 (5.61 - 11.0)**
C20:1*n*-9	1.45 (1.28 - 1.67)**	0.57 (0.45 - 0.69)**[a]	1.35 (1.31 - 1.50)**	0.40 (0.28 - 0.49)**[a]	1.64 (1.46 - 1.93)*	1.15 (0.90 - 1.73)*[b]
MUFA	196.3 (179.5 - 242.4)**[a]	49.7 (39.7 - 88.0)**[a]	190.0 (183.3 - 207.0)**[a]	53.3 (43.3 - 58.8)**[a]	526.5 (497.7 - 648.7)**[b]	223.8 (181.3 - 265.2)**[b]
C18:2*n*-6	33.5 (31.9 - 40.8)*[a]	8.86 (7.54 - 16.5)*[a]	32.7 (32.3 - 35.8)*[a]	10.2 (8.11 - 11.0)*[a]	178.4 (169.0 - 219.3)**[b]	83.7 (65.3 - 99.1)**[b]
C18:3*n*-6	0.74 (0.68 - 1.07)[a]	0.14 (0.12 - 0.31)[a]	0.81 (0.69 - 0.86)[a]	0.21 (0.16 - 0.22)[a]	3.33 (2.88 - 4.54)**[b]	1.91 (1.37 - 2.45)**[b]
C18:3*n*-3	0.63 (0.59 - 0.84)[a]	0.23 (0.18 - 0.49)[a]	0.66 (0.62 - 0.69)[a]	0.23 (0.21 - 0.42)[a]	3.68 (3.36 - 4.27)**[b]	1.57 (1.16 - 1.89)**[b]
C20:4*n*-6	0.64 (0.50 - 0.77)[a]	0.22 (0.10 - 0.55)[a]	0.60 (0.55 - 0.62)[a]	0.28 (0.22 - 0.30)[a]	2.71 (2.47 - 3.42)**[b]	1.25 (1.02 - 1.67)**[b]
PUFA	35.6 (33.7 - 43.5)*[a]	9.41 (8.02 - 17.9)*[a]	34.8 (34.2 - 37.9)*[a]	11.0 (8.71 - 12.0)*[a]	188.0 (178.1 - 231.5)**[b]	87.8 (70.2 - 105.0)**[b]

Once confluent, cells were treated with media containing 2% human serum and 11 mM glucose for seven days before treatment media was added. Treatments consisted of either low fat low sugar (LFLS; 11 mM glucose + 200 µM fatty acids), low fat high sugar (LFHS; 200 µM fatty acids + 11 mM glucose + 5.5 mM fructose) or high fat high sugar (HFHS; 800 µM fatty acids + 11 mM glucose + 5.5 mM fructose). Data are presented as median (range), $n = 4$. * $p < 0.05$, ** $p < 0.001$; different letters denote significant differences between means within WT or KO cells, $p < 0.05$; two-way ANOVA with Bonferroni's multiple comparisons tests.

Table D.4. The effect of media composition on fatty acid composition of phospholipids in Huh7 cells with wildtype (WT) or knockout (KO) of the *DGAT2* gene (nmol/mg protein)

	LFLS		LFHS		HFHS	
	WT	**KO**	**WT**	**KO**	**WT**	**KO**
C14:0	0.59 (0.50 - 0.62)**[a]	0.28 (0.20 - 0.40)**[a]	0.58 (0.53 - 0.65)**[a]	0.34 (0.26 - 0.39)**[a]	0.30 (0.26 - 0.30)*[b]	0.12 (0.10 - 0.14)*[b]
C16:0	45.7 (41.7 - 50.6)	49.3 (32.2 - 62.5)	47.2 (40.7 - 50.2)	52.1 (41.8 - 60.5)	41.1 (34.2 - 54.8)	62.0 (44.3 - 76.8)
C18:0	24.1 (21.5 - 28.1)	19.9 (14.7 - 26.4)	23.8 (21.0 - 27.9)	20.7 (15.5 - 24.2)	19.1 (16.2 - 23.9)	15.9 (14.0 - 17.7)
SFA	70.4 (63.6 - 79.2)	69.4 (47.1 - 89.3)	71.6 (62.2 - 78.7)	74.6 (57.6 - 82.2)	59.2 (53.1 - 79.6)	78.1 (58.4 - 94.5)
C16:1*n*-7	3.97 (3.48 - 4.22)**[a]	1.33 (1.03 - 1.81)**	3.68 (3.52 - 4.09)**[a]	1.55 (1.14 - 2.43)**[a]	1.16 (0.84 - 1.67)[b]	0.44 (0.32 - 1.65)[b]
C18:1*n*-9	35.5 (32.2 - 42.8)	40.9 (21.2 - 51.9)	36.9 (31.3 - 40.8)	47.1 (34.1 - 48.4)	35.9 (26.5 - 42.3)*	50.0 (41.9 - 59.7)*
C18:1*n*-7	5.76 (5.13 - 6.91)	5.61 (2.00 - 7.37)	5.81 (5.01 - 9.57)[a]	6.65 (4.89 - 7.16)[a]	3.12 (2.18 - 4.40)[b]	2.84 (2.44 - 3.25)[b]
C20:1*n*-9	0.29 (0.25 - 0.44)	0.40 (0.31 - 0.45)[a]	0.31 (0.29 - 0.50)[a]	0.36 (0.31 - 0.38)	0.15 (0.15 - 0.30)[b]	0.22 (0.14 - 0.34)[b]
MUFA	45.6 (41.0 - 55.5)	48.3 (24.5 - 61.5)	47.4 (40.2 - 58.6)	56.4 (40.4 - 56.9)	40.7 (29.6 - 48.0)	54.0 (44.8 - 63.8)
C18:2*n*-6	27.4 (25.9 - 31.5)[a]	41.8 (28.0 - 51.5)	27.7 (24.4 - 32.1)*[a]	43.8 (32.1 - 46.9)*	43.8 (32.1 - 46.9)[b]	49.3 (41.5 - 57.3)
C18:3*n*-6	0.99 (0.90 - 1.12)	0.64 (0.38 - 0.67)	0.89 (0.45 - 1.24)	0.67 (0.47 - 1.17)	1.23 (0.86 - 1.35)	0.75 (0.50 - 0.97)
C18:3*n*-3	0.22 (0.17 - 0.31)*	0.10 (0.08 - 0.12)*	0.21 (0.17 - 0.29)	0.16 (0.08 - 0.26)	0.27 (0.20 - 0.34)	0.16 (0.10 - 0.23)
C20:4*n*-6	7.98 (7.11 - 9.45)	7.68 (6.46 - 11.5)[a]	8.29 (6.66 - 10.1)	11.1 (7.80 - 12.1)[a]	10.7 (8.28 - 14.2)	15.4 (11.2 - 19.1)[b]
C20:5*n*-3	0.48 (0.36 - 0.83)	0.40 (0.27 - 0.61)	0.39 (0.07 - 0.53)	0.42 (0.32 - 0.54)	0.62 (0.39 - 0.73)	0.31 (0.26 - 0.95)
C22:5*n*-3	2.14 (1.91 - 3.27)[a]	1.70 (0.97 - 2.45)	2.01 (1.82 - 2.62)	1.77 (1.22 - 2.27)	1.55 (1.07 - 1.68)[b]	1.76 (1.55 - 2.14)
C22:6*n*-3	2.14 (2.03 - 2.90)	3.27 (2.31 - 3.86)	2.38 (1.94 - 2.57)*	3.83 (2.77 - 4.22)*	1.69 (0.35 - 2.31)*	3.01 (2.53 - 3.51)*
PUFA	41.1 (39.2 - 49.2)	55.6 (38.9 - 70.4)	42.1 (36.6 - 47.9)	62.8 (46.9 - 65.0)	58.2 (47.9 - 73.4)	70.0 (60.8 - 84.1)

Once confluent, cells were treated with media containing 2% human serum and 11 mM glucose for seven days before treatment media was added. Treatments consisted of either low fat low sugar (LFLS; 11 mM glucose + 200 µM fatty acids), low fat high sugar (LFHS; 200 µM fatty acids + 11 mM glucose + 5.5 mM fructose) or high fat high sugar (HFHS; 800 µM fatty acids + 11 mM glucose + 5.5 mM fructose). Data are presented as median (range), $n = 4$. * $p < 0.05$, ** $p < 0.001$; different letters denote significant differences between means within WT or KO cells, $p < 0.05$; two-way ANOVA with Bonferroni's multiple comparisons tests.

Table D.5. The effect of media composition on fatty acid composition of triacylglycerol secreted in the media of Huh7 cells with wildtype (WT) or knockout (KO) of the *DGAT2* gene (nmol/mg protein)

	LFLS		LFHS		HFHS	
	WT	**KO**	**WT**	**KO**	**WT**	**KO**
C16:0	7.22 (7.06 - 7.48)[a]	5.91 (3.73 - 6.94)	6.90 (6.01 - 7.77)[a]	6.05 (4.24 - 6.63)	10.2 (7.83 - 12.1)*[b]	6.70 (4.51 - 7.55)*
C18:0	1.45 (1.23 - 2.03)	1.45 (0.83 - 2.09)	1.44 (1.15 - 1.65)	1.78 (0.84 - 1.91)	1.33 (0.95 - 1.81)	1.46 (1.02 - 1.96)
C16:1*n*-7	1.27 (1.13 - 1.55)**[a]	0.64 (0.41 - 0.93)**	1.31 (0.99 - 1.55)**[a]	0.70 (0.49 - 0.79)**	0.79 (0.59 - 0.94)[b]	0.54 (0.41 - 0.75)
C18:1*n*-9	10.8 (9.69 - 11.4)[a]	7.28 (4.72 - 9.63)	10.5 (8.87 - 12.6)[a]	7.49 (5.05 - 11.0)	17.8 (13.0 - 21.0)**[b]	9.05 (5.95 - 11.8)**
C18:1*n*-7	0.96 (0.94 - 1.33)*	0.51 (0.27 - 0.73)*	1.18 (0.93 - 1.30)**	0.51 (0.28 - 0.75)**	0.85 (0.63 - 1.08)	0.49 (0.26 - 0.80)
C18:2*n*-6	3.66 (3.30 - 4.14)[a]	3.42 (2.57 - 4.24)	3.69 (3.14 - 4.31)[a]	3.47 (2.38 - 5.53)	7.58 (5.71 - 8.74)**[b]	4.42 (3.20 - 5.26)**

Once confluent, cells were treated with media containing 2% human serum and 11 mM glucose for seven days before treatment media was added. Treatments consisted of either low fat low sugar (LFLS; 11 mM glucose + 200 μM fatty acids), low fat high sugar (LFHS; 200 μM fatty acids + 11 mM glucose + 5.5 mM fructose) or high fat high sugar (HFHS; 800 μM fatty acids + 11 mM glucose + 5.5 mM fructose). Data are presented as median (range), $n = 4$. * $p < 0.05$, ** $p < 0.001$; different letters denote significant differences between means within WT or KO cells, $p < 0.05$; two-way ANOVA with Bonferroni's multiple comparisons tests.

Table D.6. The effect of media composition on fatty acid composition of phospholipids secreted in the media of Huh7 cells with wildtype (WT) or knockout (KO) of the *DGAT2* gene (nmol/mg protein)

	LFLS		LFHS		HFHS	
	WT	**KO**	**WT**	**KO**	**WT**	**KO**
C16:0	12.5 (12.2 - 13.5)	11.5 (7.63 - 14.6)	11.1 (8.39 - 12.9)	11.2 (9.00 - 13.4)	11.4 (8.95 - 16.5)	13.2 (7.51 - 13.4)
C18:0	5.74 (5.02 - 6.22)	6.81 (4.88 - 7.82)	5.86 (5.27 - 6.03)	7.30 (4.79 - 8.43)	5.71 (5.11 - 6.72)	7.09 (6.20 - 8.85)
C18:1*n*-9	4.86 (4.31 - 5.37)*	3.50 (2.37 - 4.42)*	4.80 (4.26 - 5.64)	3.66 (3.02 - 4.01)	5.32 (4.63 - 5.95)	4.72 (2.95 - 5.16)
C18:1*n*-7	0.67 (0.60 - 0.93)	0.66 (0.38 - 0.81)	0.73 (0.68 - 0.94)	0.68 (0.36 - 0.91)	0.52 (0.37 - 0.71)	0.61 (0.59 - 0.79)
C18:2*n*-6	7.08 (6.29 - 7.67)[a]	7.34 (5.48 - 7.42)	7.37 (6.45 - 7.77)[a]	7.28 (5.90 - 7.74)	10.2 (9.22 - 11.8)*[b]	8.20 (6.78 - 10.2)*
C20:4*n*-6	2.06 (1.66 - 2.44)*	2.98 (2.26 - 3.11)*	2.29 (2.12 - 2.42)	2.58 (2.28 - 3.45)	2.49 (2.37 - 2.58)	2.88 (2.70 - 4.12)

Once confluent, cells were treated with media containing 2% human serum and 11 mM glucose for seven days before treatment media was added. Treatments consisted of either low fat low sugar (LFLS; 11 mM glucose + 200 μM fatty acids), low fat high sugar (LFHS; 200 μM fatty acids + 11 mM glucose + 5.5 mM fructose) or high fat high sugar (HFHS; 800 μM fatty acids + 11 mM glucose + 5.5 mM fructose). * $p < 0.05$; different letters denote significant differences between means within WT or KO cells, $p < 0.05$; two-way ANOVA with Bonferroni's multiple comparisons tests.

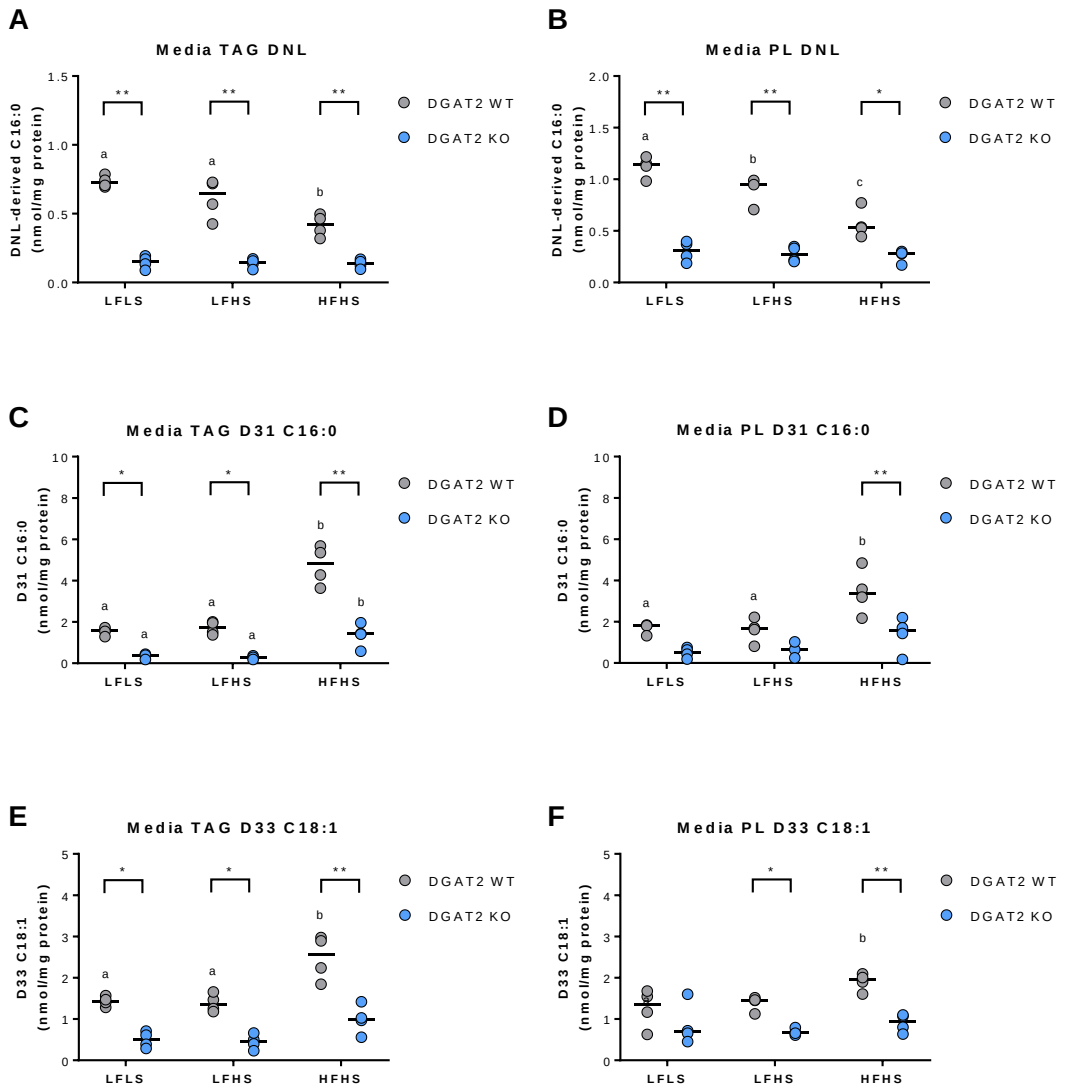


Figure D.3. The effect of media composition on exogenous fatty acid (FA) secretion in Huh7 cells with wildtype (WT) or knockout (KO) of the *DGAT2* gene. Once confluent, cells were treated with media containing 2% human serum and 11 mM glucose for seven days before treatment media was added. Treatments consisted of either low fat low sugar (LFLS; 11 mM glucose + 200 µM FAs), low fat high sugar (LFHS; 200 µM FAs + 11 mM glucose + 5.5 mM fructose) or high fat high sugar (HFHS; 800 µM FAs + 11 mM glucose + 5.5 mM fructose). Glucose and fructose consisted of 50% ^{12}C and 50% ^{13}C to allow tracing of carbon into *de novo* synthesised palmitate and absolute (nmol/mg protein) contribution of DNL to total TAG (**A**) and PLs (**B**) was calculated. The FA mix contained 100% labelling of [$^{2}H_{31}$]palmitate (D31) and [$^{2}H_{33}$]oleate (D33) to allow tracing of exogenous FAs into the media FA pool. Absolute (nmol/mg protein) enrichment of D31 palmitate in TAG (**C**) and PLs (**D**) was calculated as was enrichment of D33 oleate (TAG, **E**; PLs, **F**). Media was changed every 48 to 72 hours and 24 hours prior to collection. Data are presented as individual values and median, $n = 4$. * $p < 0.05$, ** $p < 0.001$; different letters denote significant differences between means within WT or KO cells, $p < 0.05$; two-way ANOVA with Bonferroni's multiple comparisons tests.

Appendix E

Chapter 6 supplementary material

Table E.1. Primers designed for amplification of exons 6 and 7 in the *DGAT2* gene

	Sequence (5'->3')	Template strand	Length	Start	Stop	Tm	GC%	SC	SC 3'
Exon 6 F1	GCAACCCTGACTGTTGCGTC	Plus	20	66	85	62.12	60	7	1
Exon 6 R1	TGGGGTCTGGGTCCTGTCTT	Minus	20	369	350	62.34	60	3	0
Product length	**304**								
Exon 6 R2	TACCTGACTGTGTGCCGGG	Plus	19	27	45	61.58	63.16	4	3
Exon 6 F2	GGGTCTGGGTCCTGTCTTCAG	Minus	21	367	347	61.78	61.9	3	2
Product length	**341**								
Exon 7 R2	AGGGCCTCTAGGCTGACATAG	Plus	21	53	73	60.48	57.14	6	3
Exon 7 F2	AGGTGGCCTGCATTGGAATC	Minus	20	421	402	60.69	55	4	3
Product length	**369**								
Exon 7 R1	AGGGCCTCTAGGCTGACATA	Plus	20	53	72	59.44	55	6	2
Exon 7 F1	CCTGCATTGGAATCCCGTCT	Minus	20	415	396	60.11	55	5	0
Product length	**363**								

SC, self-complementarity

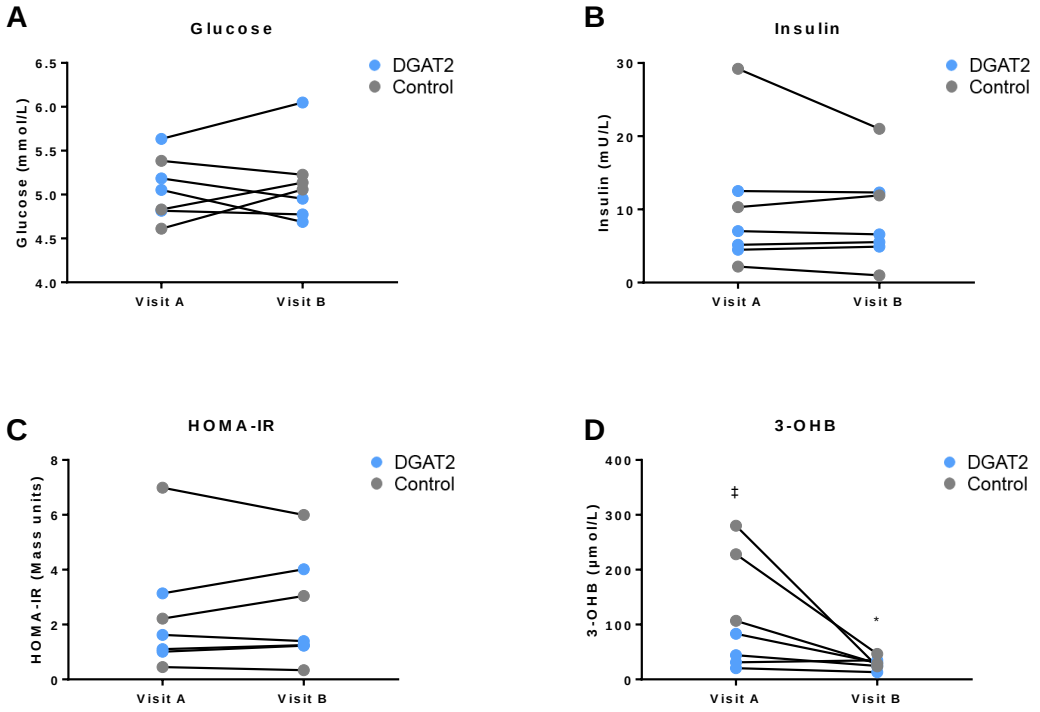


Figure E.1. The effect of sugar overfeeding on fasting plasma biochemistry in participants with a mutation in the *DGAT2* gene (DGAT2; blue dots) or matched controls (Control; grey dots). Participants had samples taken before (visit A), and at the end of (visit B), a sugar overfeeding intervention that lasted 15-20 days. Glucose (**A**) and insulin (**B**) were measured, and the homeostatic assessment model of insulin resistance (HOMA-IR) was calculated (**C**). As a marker of hepatic fatty acid oxidation, 3-hydroxybutyrate (3-OHB; **D**) was measured. Data are presented individual data points. * $p < 0.05$ compared to visit A for the control group, ‡ $p < 0.05$ between DGAT2 and control groups at visit A; two-way ANOVA with Bonferroni's multiple comparisons tests.

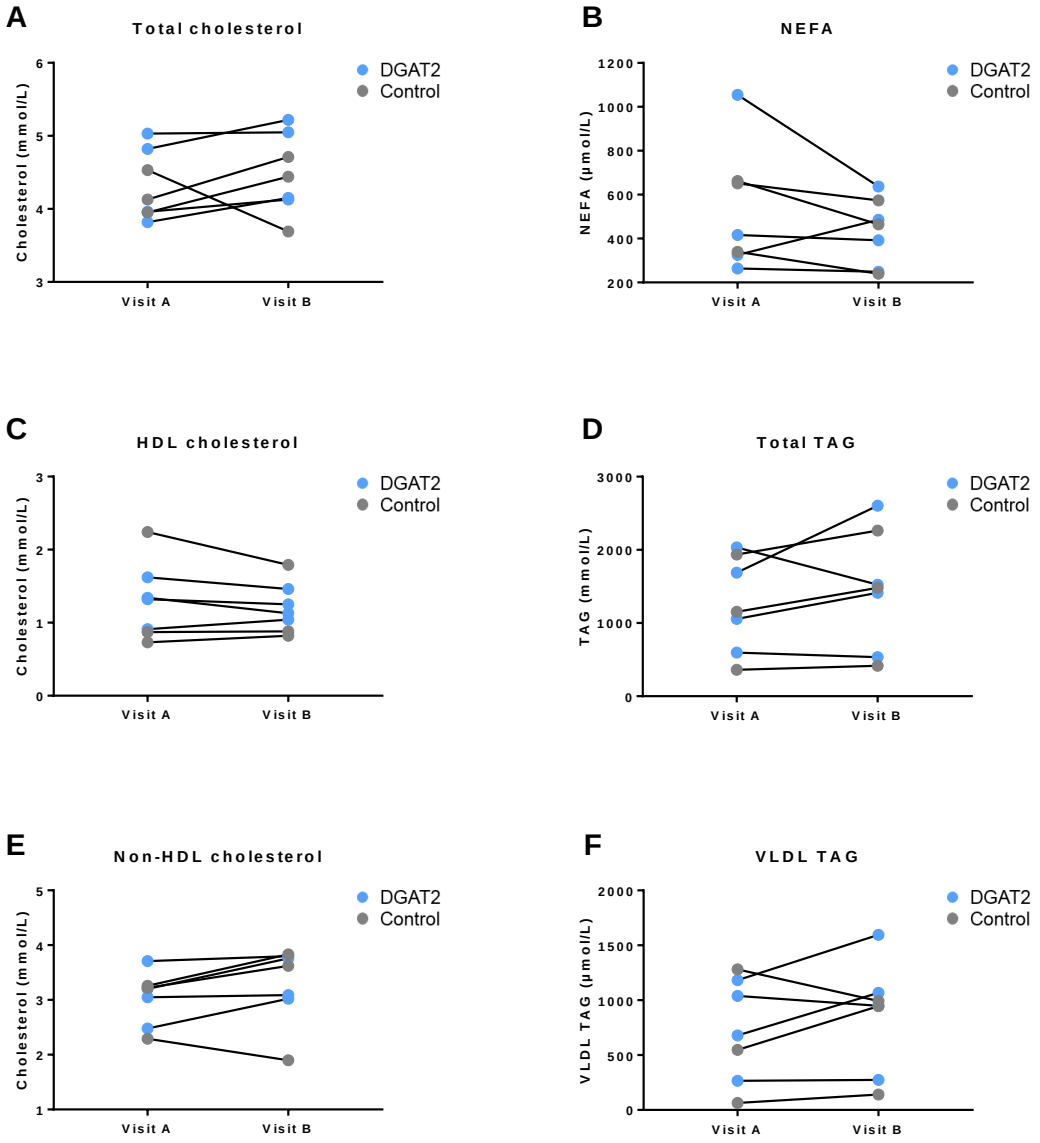


Figure E.2. The effect of sugar overfeeding on fasting plasma biochemistry in participants with a mutation in the *DGAT2* gene (DGAT2; blue dots) or matched controls (Control; grey dots). Participants had samples taken before (visit A), and at the end of (visit B), a sugar overfeeding intervention that lasted 15-20 days. Total cholesterol (**A**), high-density lipoprotein (HDL) cholesterol (**C**) and non-HDL cholesterol (**E**) were measured. Circulating non-esterified fatty acids (NEFA; **B**), total triacylglycerol (TAG; **D**) and very low-density lipoprotein (VLDL; **F**) levels were also determined. Data are presented individual data points.

Reference list

Abdelmalek, M. F., Suzuki, A., Guy, C., Unalp-Arida, A., Colvin, R., Johnson, R. J., Diehl, A. M., & Nonalcoholic Steatohepatitis Clinical Research, N. (2010). Increased fructose consumption is associated with fibrosis severity in patients with nonalcoholic fatty liver disease. *Hepatology, 51*(6), 1961-1971.

Adelman, R. C., Ballard, F. J., & Weinhouse, S. (1967). Purification and properties of rat liver fructokinase. *J Biol Chem, 242*(14), 3360-3365.

Aden, D. P., Fogel, A., Plotkin, S., Damjanov, I., & Knowles, B. B. (1979). Controlled synthesis of HBsAg in a differentiated human liver carcinoma-derived cell line. *Nature, 282*(5739), 615-616.

Allain, C. C., Poon, L. S., Chan, C. S., Richmond, W., & Fu, P. C. (1974). Enzymatic determination of total serum cholesterol. *Clin Chem, 20*(4), 470-475.

Allard, J. P., Aghdassi, E., Mohammed, S., Raman, M., Avand, G., Arendt, B. M., Jalali, P., Kandasamy, T., Prayitno, N., Sherman, M., *et al.* (2008). Nutritional assessment and hepatic fatty acid composition in non-alcoholic fatty liver disease (NAFLD): a cross-sectional study. *J Hepatol, 48*(2), 300-307.

Amann, T., Maegdefrau, U., Hartmann, A., Agaimy, A., Marienhagen, J., Weiss, T. S., Stoeltzing, O., Warnecke, C., Scholmerich, J., Oefner, P. J., *et al.* (2009). GLUT1 expression is increased in hepatocellular carcinoma and promotes tumorigenesis. *Am J Pathol, 174*(4), 1544-1552.

Andersen, C. L., Jensen, J. L., & Orntoft, T. F. (2004). Normalization of real-time quantitative reverse transcription-PCR data: a model-based variance estimation approach to identify genes suited for normalization, applied to bladder and colon cancer data sets. *Cancer Res, 64*(15), 5245-5250.

Andrieu-Abadie, N., Gouaze, V., Salvayre, R., & Levade, T. (2001). Ceramide in apoptosis signaling: relationship with oxidative stress. *Free Radic Biol Med, 31*(6), 717-728.

Anstee, Q. M., Targher, G., & Day, C. P. (2013). Progression of NAFLD to diabetes mellitus, cardiovascular disease or cirrhosis. *Nat Rev Gastroenterol Hepatol, 10*(6), 330-344.

Arab, J. P., Arrese, M., & Trauner, M. (2018). Recent Insights into the Pathogenesis of Nonalcoholic Fatty Liver Disease. *Annu Rev Pathol, 13*, 321-350.

Araya, J., Rodrigo, R., Videla, L. A., Thielemann, L., Orellana, M., Pettinelli, P., & Poniachik, J. (2004). Increase in long-chain polyunsaturated fatty acid n - 6/n - 3 ratio in relation to hepatic steatosis in patients with non-alcoholic fatty liver disease. *Clin Sci (Lond), 106*(6), 635-643.

Arendt, B. M., Comelli, E. M., Ma, D. W., Lou, W., Teterina, A., Kim, T., Fung, S. K., Wong, D. K., McGilvray, I., Fischer, S. E., *et al.* (2015). Altered hepatic gene expression in nonalcoholic fatty liver disease is associated with lower hepatic n-3 and n-6 polyunsaturated fatty acids. *Hepatology, 61*(5), 1565-1578.

Asgari-Taee, F., Zerafati-Shoae, N., Dehghani, M., Sadeghi, M., Baradaran, H. R., & Jazayeri, S. (2018). Association of sugar sweetened beverages consumption with non-alcoholic fatty liver disease: a systematic review and meta-analysis. *Eur J Nutr.*

Banerjee, R., Rial, B., Pavlides, M., Osuchukwu, C., Lewandowski, A. J., Collier, J. D., Schneider, J. E., Neubauer, S., & Barnes, E. (2014). Multiparametric Magnetic Resonance Shows That Obesity Is Strongly Associated with Hepatic Steatosis in Adults and Children and Can Differentiate Patients with Nash from Nafld. *Journal of Hepatology, 60*(1), S344-S345.

Barrangou, R., Fremaux, C., Deveau, H., Richards, M., Boyaval, P., Moineau, S., Romero, D. A., & Horvath, P. (2007). CRISPR provides acquired resistance against viruses in prokaryotes. *Science, 315*(5819), 1709-1712.

Bartenschlager, R., & Pietschmann, T. (2005). Efficient hepatitis C virus cell culture system: what a difference the host cell makes. *Proc Natl Acad Sci U S A, 102*(28), 9739-9740.

Bechmann, L. P., Gieseler, R. K., Sowa, J. P., Kahraman, A., Erhard, J., Wedemeyer, I., Emons, B., Jochum, C., Feldkamp, T., Gerken, G., *et al.* (2010). Apoptosis is associated with CD36/fatty acid translocase upregulation in non-alcoholic steatohepatitis. *Liver Int, 30*(6), 850-859.

Becuwe, M., Bond, L. M., Mejhert, N., Boland, S., Elliott, S. D., Cicconet, M., Liu, X. N., Graham, M. M., Walther, T. C., & Farese Jr., R. V. (2018). FIT2 is a lipid phosphate phosphatase crucial for endoplasmic reticulum homeostasis. *In press.*

Bell, C. C., Dankers, A. C. A., Lauschke, V. M., Sison-Young, R., Jenkins, R., Rowe, C., Goldring, C. E., Park, K., Regan, S. L., Walker, T., *et al.* (2018). Comparison of Hepatic 2D Sandwich Cultures and 3D Spheroids for Long-term Toxicity Applications: A Multicenter Study. *Toxicological Sciences, 162*(2), 655-666.

Bell, C. C., Hendriks, D. F. G., Moro, S. M. L., Ellis, E., Walsh, J., Renblom, A., Puigvert, L. F., Dankers, A. C. A., Jacobs, F., Snoeys, J., *et al.* (2016). Characterization of primary human hepatocyte spheroids as a model system for drug-induced liver injury, liver function and disease. *Scientific Reports, 6.*

Bell, C. C., Lauschke, V. M., Vorrink, S. U., Palmgren, H., Duffin, R., Andersson, T. B., & Ingelman-Sundberg, M. (2017). Transcriptional, Functional, and Mechanistic Comparisons of Stem Cell-Derived Hepatocytes, HepaRG Cells, and Three-Dimensional Human Hepatocyte Spheroids as Predictive In Vitro Systems for Drug-Induced Liver Injury. *Drug Metabolism and Disposition, 45*(4), 419-429.

Benhamed, F., Denechaud, P. D., Lemoine, M., Robichon, C., Moldes, M., Bertrand-Michel, J., Ratziu, V., Serfaty, L., Housset, C., Capeau, J., *et al.* (2012). The lipogenic transcription factor ChREBP dissociates hepatic steatosis from insulin resistance in mice and humans. *J Clin Invest, 122*(6), 2176-2194.

Bergen, W. G., & Mersmann, H. J. (2005). Comparative aspects of lipid metabolism: impact on contemporary research and use of animal models. *J Nutr, 135*(11), 2499-2502.

Berger, E., Vega, N., Weiss-Gayet, M., & Geloen, A. (2015). Gene Network Analysis of Glucose Linked Signaling Pathways and Their Role in Human Hepatocellular Carcinoma Cell Growth and Survival in HuH7 and HepG2 Cell Lines. *Biomed Research International.*

Berlanga, A., Guiu-Jurado, E., Porras, J. A., & Auguet, T. (2014). Molecular pathways in non-alcoholic fatty liver disease. *Clin Exp Gastroenterol, 7*, 221-239.

Bhatt-Wessel, B., Jordan, T. W., Miller, J. H., & Peng, L. (2018). Role of DGAT enzymes in triacylglycerol metabolism. *Arch Biochem Biophys, 655*, 1-11.

Bjermo, H., Iggman, D., Kullberg, J., Dahlman, I., Johansson, L., Persson, L., Berglund, J., Pulkki, K., Basu, S., Uusitupa, M., *et al.* (2012). Effects of n-6 PUFAs compared with SFAs on liver fat, lipoproteins, and inflammation in abdominal obesity: a randomized controlled trial. *Am J Clin Nutr, 95*(5), 1003-1012.

Blond, E., Rieusset, J., Alligier, M., Lambert-Porcheron, S., Bendridi, N., Gabert, L., Chetiveaux, M., Debard, C., Chauvin, M. A., Normand, S., *et al.* (2014). Nicotinic acid effects on

insulin sensitivity and hepatic lipid metabolism: an in vivo to in vitro study. *Horm Metab Res, 46*(6), 390-396.

Boberg, J., Carlson, L. A., & Freyschuss, U. (1972). Determination of splanchnic secretion rate of plasma triglycerides and of total and splanchnic turnover of plasma free fatty acids in man. *Eur J Clin Invest, 2*(3), 123-132.

Bortolotti, M., Maiolo, E., Corazza, M., Van Dijke, E., Schneiter, P., Boss, A., Carrel, G., Giusti, V., Le, K. A., Quo Chong, D. G., *et al.* (2011). Effects of a whey protein supplementation on intrahepatocellular lipids in obese female patients. *Clin Nutr, 30*(4), 494-498.

Boyraz, M., Pirgon, O., Dundar, B., Cekmez, F., & Hatipoglu, N. (2015). Long-Term Treatment with n-3 Polyunsaturated Fatty Acids as a Monotherapy in Children with Nonalcoholic Fatty Liver Disease. *J Clin Res Pediatr Endocrinol, 7*(2), 121-127.

Brandt, C., McFie, P. J., & Stone, S. J. (2016). Biochemical characterization of human acyl coenzyme A: 2-monoacylglycerol acyltransferase-3 (MGAT3). *Biochem Biophys Res Commun, 475*(3), 264-270.

Brito, A. F., Abrantes, A. M., Ribeiro, M., Oliveira, R., Casalta-Lopes, J., Goncalves, A. C., Sarmento-Ribeiro, A. B., Tralhao, J. G., & Botelho, M. F. (2015). Fluorine-18 Fluorodeoxyglucose Uptake in Hepatocellular Carcinoma: Correlation with Glucose Transporters and p53 Expression. *J Clin Exp Hepatol, 5*(3), 183-189.

Brunt, E. M., Wong, V. W., Nobili, V., Day, C. P., Sookoian, S., Maher, J. J., Bugianesi, E., Sirlin, C. B., Neuschwander-Tetri, B. A., & Rinella, M. E. (2015). Nonalcoholic fatty liver disease. *Nat Rev Dis Primers, 1*, 15080.

Bruschi, F. V., Tardelli, M., Claudel, T., & Trauner, M. (2017). PNPLA3 expression and its impact on the liver: current perspectives. *Hepat Med, 9*, 55-66.

Burdge, G. C., Wright, P., Jones, A. E., & Wootton, S. A. (2000). A method for separation of phosphatidylcholine, triacylglycerol, non-esterified fatty acids and cholesterol esters from plasma by solid-phase extraction. *Br J Nutr, 84*(5), 781-787.

Byrne, C. D., & Targher, G. (2015). NAFLD: a multisystem disease. *J Hepatol, 62*(1 Suppl), S47-64.

Cai, Y., McClinchie, E., Price, A., Nguyen, T. N., Gidda, S. K., Watt, S. C., Yurchenko, O., Park, S., Sturtevant, D., Mullen, R. T., *et al.* (2017). Mouse fat storage-inducing transmembrane protein 2 (FIT2) promotes lipid droplet accumulation in plants. *Plant Biotechnol J, 15*(7), 824-836.

Calzadilla Bertot, L., & Adams, L. A. (2016). The Natural Course of Non-Alcoholic Fatty Liver Disease. *Int J Mol Sci, 17*(5).

Carr, R. M., & Ahima, R. S. (2016). Pathophysiology of lipid droplet proteins in liver diseases. *Exp Cell Res, 340*(2), 187-192.

Carr, R. M., Dhir, R., Mahadev, K., Comerford, M., Chalasani, N. P., & Ahima, R. S. (2017). Perilipin Staining Distinguishes Between Steatosis and Nonalcoholic Steatohepatitis in Adults and Children. *Clin Gastroenterol Hepatol, 15*(1), 145-147.

Carrasco-Torres, G., Baltierrez-Hoyos, R., Andrade-Jorge, E., Villa-Trevino, S., Trujillo-Ferrara, J. G., & Vasquez-Garzon, V. R. (2017). Cytotoxicity, Oxidative Stress, Cell Cycle Arrest, and Mitochondrial Apoptosis after Combined Treatment of Hepatocarcinoma Cells with Maleic Anhydride Derivatives and Quercetin. *Oxid Med Cell Longev, 2017*, 2734976.

Cartwright, B. R., & Goodman, J. M. (2012). Seipin: from human disease to molecular mechanism. *J Lipid Res, 53*(6), 1042-1055.

Cases, S., Smith, S. J., Zheng, Y. W., Myers, H. M., Lear, S. R., Sande, E., Novak, S., Collins, C., Welch, C. B., Lusis, A. J., *et al.* (1998). Identification of a gene encoding an acyl CoA:diacylglycerol acyltransferase, a key enzyme in triacylglycerol synthesis. *Proc Natl Acad Sci U S A, 95*(22), 13018-13023.

Cases, S., Stone, S. J., Zhou, P., Yen, E., Tow, B., Lardizabal, K. D., Voelker, T., & Farese, R. V., Jr. (2001). Cloning of DGAT2, a second mammalian diacylglycerol acyltransferase, and related family members. *J Biol Chem, 276*(42), 38870-38876.

Chalasani, N., Younossi, Z., Lavine, J. E., Diehl, A. M., Brunt, E. M., Cusi, K., Charlton, M., & Sanyal, A. J. (2012). The diagnosis and management of non-alcoholic fatty liver disease: practice Guideline by the American Association for the Study of Liver Diseases, American College of Gastroenterology, and the American Gastroenterological Association. *Hepatology, 55*(6), 2005-2023.

Chan, D. C., Watts, G. F., Gan, S., Wong, A. T., Ooi, E. M., & Barrett, P. H. (2010). Nonalcoholic fatty liver disease as the transducer of hepatic oversecretion of very-low-density lipoprotein-apolipoprotein B-100 in obesity. *Arterioscler Thromb Vasc Biol, 30*(5), 1043-1050.

Chavez-Tapia, N. C., Rosso, N., & Tiribelli, C. (2012). Effect of intracellular lipid accumulation in a new model of non-alcoholic fatty liver disease. *BMC Gastroenterol, 12*, 20.

Chavez, J. A., & Summers, S. A. (2012). A ceramide-centric view of insulin resistance. *Cell Metab, 15*(5), 585-594.

Chen, H. C., Ladha, Z., Smith, S. J., & Farese, R. V., Jr. (2003). Analysis of energy expenditure at different ambient temperatures in mice lacking DGAT1. *Am J Physiol Endocrinol Metab, 284*(1), E213-218.

Chetty, S., Pagliuca, F. W., Honore, C., Kweudjeu, A., Rezania, A., & Melton, D. A. (2013). A simple tool to improve pluripotent stem cell differentiation. *Nat Methods, 10*(6), 553-556.

Chiappini, F., Coilly, A., Kadar, H., Gual, P., Tran, A., Desterke, C., Samuel, D., Duclos-Vallee, J. C., Touboul, D., Bertrand-Michel, J., *et al.* (2017). Metabolism dysregulation induces a specific lipid signature of nonalcoholic steatohepatitis in patients. *Sci Rep, 7*, 46658.

Chiavaroli, L., de Souza, R. J., Ha, V., Cozma, A. I., Mirrahimi, A., Wang, D. D., Yu, M., Carleton, A. J., Di Buono, M., Jenkins, A. L., *et al.* (2015). Effect of Fructose on Established Lipid Targets: A Systematic Review and Meta-Analysis of Controlled Feeding Trials. *J Am Heart Assoc, 4*(9), e001700.

Chitraju, C., Mejhert, N., Haas, J. T., Diaz-Ramirez, L. G., Grueter, C. A., Imbriglio, J. E., Pinto, S., Koliwad, S. K., Walther, T. C., & Farese, R. V., Jr. (2017). Triglyceride Synthesis by DGAT1 Protects Adipocytes from Lipid-Induced ER Stress during Lipolysis. *Cell Metab, 26*(2), 407-418 e403.

Chiu, S., Sievenpiper, J. L., de Souza, R. J., Cozma, A. I., Mirrahimi, A., Carleton, A. J., Ha, V., Di Buono, M., Jenkins, A. L., Leiter, L. A., *et al.* (2014). Effect of fructose on markers of non-alcoholic fatty liver disease (NAFLD): a systematic review and meta-analysis of controlled feeding trials. *Eur J Clin Nutr, 68*(4), 416-423.

Choi, C. S., Savage, D. B., Kulkarni, A., Yu, X. X., Liu, Z. X., Morino, K., Kim, S., Distefano, A., Samuel, V. T., Neschen, S., *et al.* (2007). Suppression of diacylglycerol acyltransferase-2

(DGAT2), but not DGAT1, with antisense oligonucleotides reverses diet-induced hepatic steatosis and insulin resistance. *J Biol Chem, 282*(31), 22678-22688.

Choi, S., Sainz, B., Jr., Corcoran, P., Uprichard, S., & Jeong, H. (2009). Characterization of increased drug metabolism activity in dimethyl sulfoxide (DMSO)-treated Huh7 hepatoma cells. *Xenobiotica, 39*(3), 205-217.

Chong, M. F., Fielding, B. A., & Frayn, K. N. (2007). Mechanisms for the acute effect of fructose on postprandial lipemia. *Am J Clin Nutr, 85*(6), 1511-1520.

Chong, M. F., Hodson, L., Bickerton, A. S., Roberts, R., Neville, M., Karpe, F., Frayn, K. N., & Fielding, B. A. (2008). Parallel activation of de novo lipogenesis and stearoyl-CoA desaturase activity after 3 d of high-carbohydrate feeding. *Am J Clin Nutr, 87*(4), 817-823.

Choudhary, V., Ojha, N., Golden, A., & Prinz, W. A. (2015). A conserved family of proteins facilitates nascent lipid droplet budding from the ER. *J Cell Biol, 211*(2), 261-271.

Chung, M., Ma, J., Patel, K., Berger, S., Lau, J., & Lichtenstein, A. H. (2014). Fructose, high-fructose corn syrup, sucrose, and nonalcoholic fatty liver disease or indexes of liver health: a systematic review and meta-analysis. *Am J Clin Nutr, 100*(3), 833-849.

Cicinnati, V. R., Shen, Q., Sotiropoulos, G. C., Radtke, A., Gerken, G., & Beckebaum, S. (2008). Validation of putative reference genes for gene expression studies in human hepatocellular carcinoma using real-time quantitative RT-PCR. *BMC Cancer, 8*, 350.

Clifton, P. M., & Keogh, J. B. (2017). A systematic review of the effect of dietary saturated and polyunsaturated fat on heart disease. *Nutr Metab Cardiovasc Dis, 27*(12), 1060-1080.

Coleman, R. A., & Lee, D. P. (2004). Enzymes of triacylglycerol synthesis and their regulation. *Prog Lipid Res, 43*(2), 134-176.

Collins, J. M., Neville, M. J., Pinnick, K. E., Hodson, L., Ruyter, B., van Dijk, T. H., Reijngoud, D. J., Fielding, M. D., & Frayn, K. N. (2011). De novo lipogenesis in the differentiating human adipocyte can provide all fatty acids necessary for maturation. *J Lipid Res, 52*(9), 1683-1692.

Cox, C. L., Stanhope, K. L., Schwarz, J. M., Graham, J. L., Hatcher, B., Griffen, S. C., Bremer, A. A., Berglund, L., McGahan, J. P., Havel, P. J., *et al.* (2012). Consumption of fructose-sweetened beverages for 10 weeks reduces net fat oxidation and energy expenditure in overweight/obese men and women. *Eur J Clin Nutr, 66*(2), 201-208.

Crow, J. P. (1997). Dichlorodihydrofluorescein and dihydrorhodamine 123 are sensitive indicators of peroxynitrite in vitro: implications for intracellular measurement of reactive nitrogen and oxygen species. *Nitric Oxide, 1*(2), 145-157.

Cui, W., Chen, S. L., & Hu, K. Q. (2010). Quantification and mechanisms of oleic acid-induced steatosis in HepG2 cells. *Am J Transl Res, 2*(1), 95-104.

Daniels, V. W., Smans, K., Royaux, I., Chypre, M., Swinnen, J. V., & Zaidi, N. (2014). Cancer cells differentially activate and thrive on de novo lipid synthesis pathways in a low-lipid environment. *PLoS One, 9*(9), e106913.

Dashti, N., Alaupovic, P., Knight-Gibson, C., & Koren, E. (1987). Identification and partial characterization of discrete apolipoprotein B containing lipoprotein particles produced by human hepatoma cell line HepG2. *Biochemistry, 26*(15), 4837-4846.

Dashti, N., & Wolfbauer, G. (1987). Secretion of lipids, apolipoproteins, and lipoproteins by human hepatoma cell line, HepG2: effects of oleic acid and insulin. *J Lipid Res, 28*(4), 423-436.

de Castro, G. S., & Calder, P. C. (2018). Non-alcoholic fatty liver disease and its treatment with n-3 polyunsaturated fatty acids. *Clin Nutr, 37*(1), 37-55.

de Souza, R. J., Mente, A., Maroleanu, A., Cozma, A. I., Ha, V., Kishibe, T., Uleryk, E., Budylowski, P., Schunemann, H., Beyene, J., *et al.* (2015). Intake of saturated and trans unsaturated fatty acids and risk of all cause mortality, cardiovascular disease, and type 2 diabetes: systematic review and meta-analysis of observational studies. *BMJ, 351*, h3978.

de Wit, N. J., Afman, L. A., Mensink, M., & Muller, M. (2012). Phenotyping the effect of diet on non-alcoholic fatty liver disease. *J Hepatol, 57*(6), 1370-1373.

Debosch, B. J., Chen, Z., Saben, J. L., Finck, B. N., & Moley, K. H. (2014). Glucose transporter 8 (GLUT8) mediates fructose-induced de novo lipogenesis and macrosteatosis. *J Biol Chem, 289*(16), 10989-10998.

Della Pepa, G., Vetrani, C., Lombardi, G., Bozzetto, L., Annuzzi, G., & Rivellese, A. A. (2017). Isocaloric Dietary Changes and Non-Alcoholic Fatty Liver Disease in High Cardiometabolic Risk Individuals. *Nutrients, 9*(10).

Denison, H., Nilsson, C., Lofgren, L., Himmelmann, A., Martensson, G., Knutsson, M., Al-Shurbaji, A., Tornqvist, H., & Eriksson, J. W. (2014). Diacylglycerol acyltransferase 1 inhibition with AZD7687 alters lipid handling and hormone secretion in the gut with intolerable side effects: a randomized clinical trial. *Diabetes Obes Metab, 16*(4), 334-343.

Dentin, R., Hedrick, S., Xie, J. X., Yates, J., & Montminy, M. (2008). Hepatic glucose sensing via the CREB coactivator CRTC2. *Science, 319*(5868), 1402-1405.

Diraison, F., Moulin, P., & Beylot, M. (2003). Contribution of hepatic de novo lipogenesis and reesterification of plasma non esterified fatty acids to plasma triglyceride synthesis during non-alcoholic fatty liver disease. *Diabetes Metab, 29*(5), 478-485.

Diraison, F., Pachiaudi, C., & Beylot, M. (1997). Measuring lipogenesis and cholesterol synthesis in humans with deuterated water: use of simple gas chromatographic/mass spectrometric techniques. *J Mass Spectrom, 32*(1), 81-86.

Donato, M. T., Lahoz, A., Castell, J. V., & Gomez-Lechon, M. J. (2008). Cell lines: a tool for in vitro drug metabolism studies. *Curr Drug Metab, 9*(1), 1-11.

Donnelly, K. L., Smith, C. I., Schwarzenberg, S. J., Jessurun, J., Boldt, M. D., & Parks, E. J. (2005). Sources of fatty acids stored in liver and secreted via lipoproteins in patients with nonalcoholic fatty liver disease. *J Clin Invest, 115*(5), 1343-1351.

Doudna, J. A., & Charpentier, E. (2014). Genome editing. The new frontier of genome engineering with CRISPR-Cas9. *Science, 346*(6213), 1258096.

Ekstedt, M., Franzen, L. E., Mathiesen, U. L., Thorelius, L., Holmqvist, M., Bodemar, G., & Kechagias, S. (2006). Long-term follow-up of patients with NAFLD and elevated liver enzymes. *Hepatology, 44*(4), 865-873.

Elizondo, A., Araya, J., Rodrigo, R., Poniachik, J., Csendes, A., Maluenda, F., Diaz, J. C., Signorini, C., Sgherri, C., Comporti, M., *et al.* (2007). Polyunsaturated fatty acid pattern in liver and erythrocyte phospholipids from obese patients. *Obesity (Silver Spring), 15*(1), 24-31.

Ellsworth, J. L., Erickson, S. K., & Cooper, A. D. (1986). Very low and low density lipoprotein synthesis and secretion by the human hepatoma cell line Hep-G2: effects of free fatty acid. *J Lipid Res, 27*(8), 858-874.

Fabbrini, E., & Magkos, F. (2015). Hepatic Steatosis as a Marker of Metabolic Dysfunction. *Nutrients, 7*(6), 4995-5019.

Fabbrini, E., Mohammed, B. S., Korenblat, K. M., Magkos, F., McCrea, J., Patterson, B. W., & Klein, S. (2010). Effect of fenofibrate and niacin on intrahepatic triglyceride content, very low-density lipoprotein kinetics, and insulin action in obese subjects with nonalcoholic fatty liver disease. *J Clin Endocrinol Metab, 95*(6), 2727-2735.

Fabbrini, E., Mohammed, B. S., Magkos, F., Korenblat, K. M., Patterson, B. W., & Klein, S. (2008). Alterations in adipose tissue and hepatic lipid kinetics in obese men and women with nonalcoholic fatty liver disease. *Gastroenterology, 134*(2), 424-431.

Fabbrini, E., Tiemann Luecking, C., Love-Gregory, L., Okunade, A. L., Yoshino, M., Fraterrigo, G., Patterson, B. W., & Klein, S. (2016). Physiological Mechanisms of Weight Gain-Induced Steatosis in People With Obesity. *Gastroenterology, 150*(1), 79-81 e72.

Feingold, K. R., & Grunfeld, C. (2000). Introduction to Lipids and Lipoproteins. In L. J. De Groot, G. Chrousos, K. Dungan, K. R. Feingold, A. Grossman, J. M. Hershman, C. Koch, M. Korbonits, R. McLachlan, M. New, J. Purnell, R. Rebar, F. Singer, & A. Vinik (Eds.), *Endotext*. South Dartmouth (MA).

Filhoulaud, G., Guilmeau, S., Dentin, R., Girard, J., & Postic, C. (2013). Novel insights into ChREBP regulation and function. *Trends Endocrinol Metab, 24*(5), 257-268.

Fisher, M., Levine, P. H., & Leaf, A. (1989). n-3 fatty acids and cellular aspects of atherosclerosis. *Arch Intern Med, 149*(8), 1726-1728.

Folch, J., Lees, M., & Sloane Stanley, G. H. (1957). A simple method for the isolation and purification of total lipides from animal tissues. *J Biol Chem, 226*(1), 497-509.

Foster, D. W. (2012). Malonyl-CoA: the regulator of fatty acid synthesis and oxidation. *J Clin Invest, 122*(6), 1958-1959.

Friedel, S., Reichwald, K., Scherag, A., Brumm, H., Wermter, A. K., Fries, H. R., Koberwitz, K., Wabitsch, M., Meitinger, T., Platzer, M., *et al.* (2007). Mutation screen and association studies in the diacylglycerol O-acyltransferase homolog 2 gene (DGAT2), a positional candidate gene for early onset obesity on chromosome 11q13. *BMC Genet, 8*, 17.

Fujii, H., Ikura, Y., Arimoto, J., Sugioka, K., Iezzoni, J. C., Park, S. H., Naruko, T., Itabe, H., Kawada, N., Caldwell, S. H., *et al.* (2009). Expression of perilipin and adipophilin in nonalcoholic fatty liver disease; relevance to oxidative injury and hepatocyte ballooning. *J Atheroscler Thromb, 16*(6), 893-901.

Furth, E. E., Sprecher, H., Fisher, E. A., Fleishman, H. D., & Laposata, M. (1992). An in vitro model for essential fatty acid deficiency: HepG2 cells permanently maintained in lipid-free medium. *J Lipid Res, 33*(11), 1719-1726.

Ganji, S. H., Tavintharan, S., Zhu, D., Xing, Y., Kamanna, V. S., & Kashyap, M. L. (2004). Niacin noncompetitively inhibits DGAT2 but not DGAT1 activity in HepG2 cells. *J Lipid Res, 45*(10), 1835-1845.

Gemmink, A., Goodpaster, B. H., Schrauwen, P., & Hesselink, M. K. C. (2017). Intramyocellular lipid droplets and insulin sensitivity, the human perspective. *Biochim Biophys Acta, 1862*(10 Pt B), 1242-1249.

Gibbons, G. F., Bartlett, S. M., Sparks, C. E., & Sparks, J. D. (1992). Extracellular fatty acids are not utilized directly for the synthesis of very-low-density lipoprotein in primary cultures of rat hepatocytes. *Biochem J, 287 (Pt 3)*, 749-753.

Gibbons, G. F., Islam, K., & Pease, R. J. (2000). Mobilisation of triacylglycerol stores. *Biochim Biophys Acta, 1483*(1), 37-57.

Gibbons, G. F., Khurana, R., Odwell, A., & Seelaender, M. C. (1994). Lipid balance in HepG2 cells: active synthesis and impaired mobilization. *J Lipid Res, 35*(10), 1801-1808.

Gluchowski, N. L., Becuwe, M., Walther, T. C., & Farese, R. V., Jr. (2017a). Lipid droplets and liver disease: from basic biology to clinical implications. *Nat Rev Gastroenterol Hepatol, 14*(6), 343-355.

Gluchowski, N. L., Chitraju, C., Picoraro, J. A., Mejhert, N., Pinto, S., Xin, W., Kamin, D. S., Winter, H. S., Chung, W. K., Walther, T. C., *et al.* (2017b). Identification and characterization of a novel DGAT1 missense mutation associated with congenital diarrhea. *J Lipid Res, 58*(6), 1230-1237.

Gnocchi, D., Massimi, M., Alisi, A., Incerpi, S., & Bruscalupi, G. (2014). Effect of fructose and 3,5-diiodothyronine (3,5-T(2)) on lipid accumulation and insulin signalling in non-alcoholic fatty liver disease (NAFLD)-like rat primary hepatocytes. *Horm Metab Res, 46*(5), 333-340.

Godoy, P., Hewitt, N. J., Albrecht, U., Andersen, M. E., Ansari, N., Bhattacharya, S., Bode, J. G., Bolleyn, J., Borner, C., Bottger, J., *et al.* (2013). Recent advances in 2D and 3D in vitro systems using primary hepatocytes, alternative hepatocyte sources and non-parenchymal liver cells and their use in investigating mechanisms of hepatotoxicity, cell signaling and ADME. *Arch Toxicol, 87*(8), 1315-1530.

Goh, V. J., & Silver, D. L. (2013). The lipid droplet as a potential therapeutic target in NAFLD. *Semin Liver Dis, 33*(4), 312-320.

Graffmann, N., Ring, S., Kawala, M. A., Wruck, W., Ncube, A., Trompeter, H. I., & Adjaye, J. (2016). Modeling Nonalcoholic Fatty Liver Disease with Human Pluripotent Stem Cell-Derived Immature Hepatocyte-Like Cells Reveals Activation of PLIN2 and Confirms Regulatory Functions of Peroxisome Proliferator-Activated Receptor Alpha. *Stem Cells Dev, 25*(15), 1119-1133.

Graham, A., & Russell, L. J. (1994). Stimulation of low-density lipoprotein uptake in HepG2 cells by epidermal growth factor via a tyrosine kinase-dependent, but protein kinase C-independent, mechanism. *Biochem J, 298 Pt 3*, 579-584.

Greco, D., Kotronen, A., Westerbacka, J., Puig, O., Arkkila, P., Kiviluoto, T., Laitinen, S., Kolak, M., Fisher, R. M., Hamsten, A., *et al.* (2008). Gene expression in human NAFLD. *Am J Physiol Gastrointest Liver Physiol, 294*(5), G1281-1287.

Green, C. J., Charlton, C. A., Wang, L. M., Silva, M., Morten, K. J., & Hodson, L. (2017). The isolation of primary hepatocytes from human tissue: optimising the use of small non-encapsulated liver resection surplus. *Cell Tissue Bank, 18*(4), 597-604.

Green, C. J., & Hodson, L. (2014). The influence of dietary fat on liver fat accumulation. *Nutrients, 6*(11), 5018-5033.

Green, C. J., Johnson, D., Amin, H. D., Sivathondan, P., Silva, M. A., Wang, L. M., Stevanato, L., McNeil, C. A., Miljan, E. A., Sinden, J. D., *et al.* (2015a). Characterization of lipid metabolism in a novel immortalized human hepatocyte cell line. *Am J Physiol Endocrinol Metab, 309*(6), E511-522.

Green, C. J., Parry, S. A., Gunn, P. J., Ceresa, C. D. L., Rosqvist, F., Piche, M. E., & Hodson, L. (2018). Studying non-alcoholic fatty liver disease: the ins and outs of in vivo, ex vivo and in vitro human models. *Horm Mol Biol Clin Investig.*

Green, C. J., Pramfalk, C., Morten, K. J., & Hodson, L. (2015b). From whole body to cellular models of hepatic triglyceride metabolism: man has got to know his limitations. *Am J Physiol Endocrinol Metab, 308*(1), E1-20.

Gstraunthaler, G., & Lindl, T. (2011). *Zell- und Gewebekultur* (7th ed.). Heidelberg: Spektrum Springer Verlag.

Gunn, P. J., Green, C. J., Pramfalk, C., & Hodson, L. (2017). In vitro cellular models of human hepatic fatty acid metabolism: differences between Huh7 and HepG2 cell lines in human and foetal bovine culturing serum. *Physiol Rep, 5*(24).

Haas, J. T., Winter, H. S., Lim, E., Kirby, A., Blumenstiel, B., DeFelice, M., Gabriel, S., Jalas, C., Branski, D., Grueter, C. A., *et al.* (2012). DGAT1 mutation is linked to a congenital diarrheal disorder. *J Clin Invest, 122*(12), 4680-4684.

Hagenfeldt, L., Wahren, J., Pernow, B., & Raf, L. (1972). Uptake of individual free fatty acids by skeletal muscle and liver in man. *J Clin Invest, 51*(9), 2324-2330.

Hannah, V. C., Ou, J., Luong, A., Goldstein, J. L., & Brown, M. S. (2001). Unsaturated fatty acids down-regulate srebp isoforms 1a and 1c by two mechanisms in HEK-293 cells. *J Biol Chem, 276*(6), 4365-4372.

Hara, S., McCall, M. R., & Forte, T. M. (1993). Re-uptake of nascent low-density lipoproteins by HepG2 cells. *Biochim Biophys Acta, 1168*(2), 199-204.

Higuchi, N., Kato, M., Shundo, Y., Tajiri, H., Tanaka, M., Yamashita, N., Kohjima, M., Kotoh, K., Nakamuta, M., Takayanagi, R., *et al.* (2008). Liver X receptor in cooperation with SREBP-1c is a major lipid synthesis regulator in nonalcoholic fatty liver disease. *Hepatol Res, 38*(11), 1122-1129.

Higuchi, N., Kato, M., Tanaka, M., Miyazaki, M., Takao, S., Kohjima, M., Kotoh, K., Enjoji, M., Nakamuta, M., & Takayanagi, R. (2011). Effects of insulin resistance and hepatic lipid accumulation on hepatic mRNA expression levels of apoB, MTP and L-FABP in non-alcoholic fatty liver disease. *Exp Ther Med, 2*(6), 1077-1081.

Hirahatake, K. M., Meissen, J. K., Fiehn, O., & Adams, S. H. (2011). Comparative effects of fructose and glucose on lipogenic gene expression and intermediary metabolism in HepG2 liver cells. *PLoS One, 6*(11), e26583.

Hiramine, Y., & Tanabe, T. (2011). Characterization of acyl-coenzyme A:diacylglycerol acyltransferase (DGAT) enzyme of human small intestine. *J Physiol Biochem, 67*(2), 259-264.

Hodson, L., Bickerton, A. S., McQuaid, S. E., Roberts, R., Karpe, F., Frayn, K. N., & Fielding, B. A. (2007). The contribution of splanchnic fat to VLDL triglyceride is greater in insulin-resistant than insulin-sensitive men and women: studies in the postprandial state. *Diabetes, 56*(10), 2433-2441.

Hodson, L., Skeaff, C. M., & Fielding, B. A. (2008). Fatty acid composition of adipose tissue and blood in humans and its use as a biomarker of dietary intake. *Prog Lipid Res, 47*(5), 348-380.

Hong, Y. B., Kang, J., Kim, J. H., Lee, J., Kwak, G., Hyun, Y. S., Nam, S. H., Hong, H. D., Choi, Y. R., Jung, S. C., *et al.* (2016). DGAT2 Mutation in a Family with Autosomal-Dominant Early-Onset Axonal Charcot-Marie-Tooth Disease. *Hum Mutat, 37*(5), 473-480.

Honka, M. J., Latva-Rasku, A., Bucci, M., Virtanen, K. A., Hannukainen, J. C., Kalliokoski, K. K., & Nuutila, P. (2018). Insulin-stimulated glucose uptake in skeletal muscle, adipose tissue and liver: a positron emission tomography study. *Eur J Endocrinol, 178*(5), 523-531.

Houten, S. M., Violante, S., Ventura, F. V., & Wanders, R. J. (2016). The Biochemistry and Physiology of Mitochondrial Fatty Acid beta-Oxidation and Its Genetic Disorders. *Annu Rev Physiol, 78*, 23-44.

Hu, M., Chu, W. C., Yamashita, S., Yeung, D. K., Shi, L., Wang, D., Masuda, D., Yang, Y., & Tomlinson, B. (2012). Liver fat reduction with niacin is influenced by DGAT-2 polymorphisms in hypertriglyceridemic patients. *J Lipid Res, 53*(4), 802-809.

Huang, D., Dhawan, T., Young, S., Yong, W. H., Boros, L. G., & Heaney, A. P. (2011). Fructose impairs glucose-induced hepatic triglyceride synthesis. *Lipids Health Dis, 10*, 20.

Huang, M. C., Chang, W. T., Chang, H. Y., Chung, H. F., Chen, F. P., Huang, Y. F., Hsu, C. C., & Hwang, S. J. (2017). FADS Gene Polymorphisms, Fatty Acid Desaturase Activities, and HDL-C in Type 2 Diabetes. *Int J Environ Res Public Health, 14*(6).

Hudgins, L. C., Parker, T. S., Levine, D. M., & Hellerstein, M. K. (2011). A dual sugar challenge test for lipogenic sensitivity to dietary fructose. *J Clin Endocrinol Metab, 96*(3), 861-868.

Huynh, F. K., Green, M. F., Koves, T. R., & Hirschey, M. D. (2014). Measurement of fatty acid oxidation rates in animal tissues and cell lines. *Methods Enzymol, 542*, 391-405.

Iizuka, K. (2017). The Role of Carbohydrate Response Element Binding Protein in Intestinal and Hepatic Fructose Metabolism. *Nutrients, 9*(2).

Iizuka, K., Bruick, R. K., Liang, G., Horton, J. D., & Uyeda, K. (2004). Deficiency of carbohydrate response element-binding protein (ChREBP) reduces lipogenesis as well as glycolysis. *Proc Natl Acad Sci U S A, 101*(19), 7281-7286.

Iizuka, K., & Horikawa, Y. (2008). ChREBP: a glucose-activated transcription factor involved in the development of metabolic syndrome. *Endocr J, 55*(4), 617-624.

Irimia, J. M., Meyer, C. M., Segvich, D. M., Surendran, S., DePaoli-Roach, A. A., Morral, N., & Roach, P. J. (2017). Lack of liver glycogen causes hepatic insulin resistance and steatosis in mice. *J Biol Chem, 292*(25), 10455-10464.

Itabe, H., Yamaguchi, T., Nimura, S., & Sasabe, N. (2017). Perilipins: a diversity of intracellular lipid droplet proteins. *Lipids Health Dis, 16*(1), 83.

Jackson, A. L., Burchard, J., Leake, D., Reynolds, A., Schelter, J., Guo, J., Johnson, J. M., Lim, L., Karpilow, J., Nichols, K., *et al.* (2006). Position-specific chemical modification of siRNAs reduces "off-target" transcript silencing. *RNA, 12*(7), 1197-1205.

Jahn, D., Kircher, S., Hermanns, H. M., & Geier, A. (2018). Animal models of NAFLD from a hepatologist's point of view. *Biochim Biophys Acta Mol Basis Dis.*

Jakobsson, A., Westerberg, R., & Jacobsson, A. (2006). Fatty acid elongases in mammals: their regulation and roles in metabolism. *Prog Lipid Res, 45*(3), 237-249.

Jakubowski, W., & Bartosz, G. (2000). 2,7-dichlorofluorescin oxidation and reactive oxygen species: what does it measure? *Cell Biol Int, 24*(10), 757-760.

Janevski, M., Ratnayake, S., Siljanovski, S., McGlynn, M. A., Cameron-Smith, D., & Lewandowski, P. (2012). Fructose containing sugars modulate mRNA of lipogenic genes ACC and FAS and protein levels of transcription factors ChREBP and SREBP1c with no effect on body weight or liver fat. *Food Funct, 3*(2), 141-149.

Javitt, N. B. (1990). Hep G2 cells as a resource for metabolic studies: lipoprotein, cholesterol, and bile acids. *FASEB J, 4*(2), 161-168.

Jensen, T., Abdelmalek, M. F., Sullivan, S., Nadeau, K. J., Green, M., Roncal, C., Nakagawa, T., Kuwabara, M., Sato, Y., Kang, D. H., *et al.* (2018). Fructose and sugar: A major mediator of non-alcoholic fatty liver disease. *J Hepatol, 68*(5), 1063-1075.

Jeon, Y. J., & Kim, Y. S. (2011). Cyclosporin a inhibits albumin synthesis in Huh7 cells. *Korean J Intern Med, 26*(3), 314-319.

Jinek, M., Chylinski, K., Fonfara, I., Hauer, M., Doudna, J. A., & Charpentier, E. (2012). A programmable dual-RNA-guided DNA endonuclease in adaptive bacterial immunity. *Science, 337*(6096), 816-821.

Jo, H., Choe, S. S., Shin, K. C., Jang, H., Lee, J. H., Seong, J. K., Back, S. H., & Kim, J. B. (2013). Endoplasmic reticulum stress induces hepatic steatosis via increased expression of the hepatic very low-density lipoprotein receptor. *Hepatology, 57*(4), 1366-1377.

Jois, T., Chen, W., Howard, V., Harvey, R., Youngs, K., Thalmann, C., Saha, P., Chan, L., Cowley, M. A., & Sleeman, M. W. (2017). Deletion of hepatic carbohydrate response element binding protein (ChREBP) impairs glucose homeostasis and hepatic insulin sensitivity in mice. *Mol Metab, 6*(11), 1381-1394.

Jornayvaz, F. R., Birkenfeld, A. L., Jurczak, M. J., Kanda, S., Guigni, B. A., Jiang, D. C., Zhang, D., Lee, H. Y., Samuel, V. T., & Shulman, G. I. (2011). Hepatic insulin resistance in mice with hepatic overexpression of diacylglycerol acyltransferase 2. *Proc Natl Acad Sci U S A, 108*(14), 5748-5752.

Kanerva, N., Sandboge, S., Kaartinen, N. E., Mannisto, S., & Eriksson, J. G. (2014). Higher fructose intake is inversely associated with risk of nonalcoholic fatty liver disease in older Finnish adults. *Am J Clin Nutr, 100*(4), 1133-1138.

Kantartzis, K., Machicao, F., Machann, J., Schick, F., Fritsche, A., Haring, H. U., & Stefan, N. (2009). The DGAT2 gene is a candidate for the dissociation between fatty liver and insulin resistance in humans. *Clin Sci (Lond), 116*(6), 531-537.

Karim, S., Adams, D. H., & Lalor, P. F. (2012). Hepatic expression and cellular distribution of the glucose transporter family. *World J Gastroenterol, 18*(46), 6771-6781.

Karpe, F., Vasan, S. K., Humphreys, S. M., Miller, J., Cheeseman, J., Dennis, A. L., & Neville, M. J. (2018). Cohort Profile: The Oxford Biobank. *Int J Epidemiol, 47*(1), 21-21g.

Kennedy, A., Martinez, K., Chuang, C. C., LaPoint, K., & McIntosh, M. (2009). Saturated fatty acid-mediated inflammation and insulin resistance in adipose tissue: mechanisms of action and implications. *J Nutr, 139*(1), 1-4.

Kihara, A. (2012). Very long-chain fatty acids: elongation, physiology and related disorders. *J Biochem, 152*(5), 387-395.

Kim, S., & Kim, T. (2003). Selection of optimal internal controls for gene expression profiling of liver disease. *Biotechniques, 35*(3), 456-458, 460.

Kimmel, A. R., & Sztalryd, C. (2016). The Perilipins: Major Cytosolic Lipid Droplet-Associated Proteins and Their Roles in Cellular Lipid Storage, Mobilization, and Systemic Homeostasis. *Annu Rev Nutr, 36*, 471-509.

Kirk, E., Reeds, D. N., Finck, B. N., Mayurranjan, S. M., Patterson, B. W., & Klein, S. (2009). Dietary fat and carbohydrates differentially alter insulin sensitivity during caloric restriction. *Gastroenterology, 136*(5), 1552-1560.

Kleiner, D. E., & Brunt, E. M. (2012). Nonalcoholic fatty liver disease: pathologic patterns and biopsy evaluation in clinical research. *Semin Liver Dis, 32*(1), 3-13.

Kmiec, Z. (2001). Cooperation of liver cells in health and disease. *Adv Anat Embryol Cell Biol, 161*, III-XIII, 1-151.

Knolle, P. A., & Gerken, G. (2000). Local control of the immune response in the liver. *Immunol Rev, 174*, 21-34.

Kohjima, M., Enjoji, M., Higuchi, N., Kato, M., Kotoh, K., Yoshimoto, T., Fujino, T., Yada, M., Yada, R., Harada, N., *et al.* (2007). Re-evaluation of fatty acid metabolism-related gene expression in nonalcoholic fatty liver disease. *Int J Mol Med, 20*(3), 351-358.

Kohjima, M., Higuchi, N., Kato, M., Kotoh, K., Yoshimoto, T., Fujino, T., Yada, M., Yada, R., Harada, N., Enjoji, M., *et al.* (2008). SREBP-1c, regulated by the insulin and AMPK signaling pathways, plays a role in nonalcoholic fatty liver disease. *Int J Mol Med, 21*(4), 507-511.

Koliaki, C., Szendroedi, J., Kaul, K., Jelenik, T., Nowotny, P., Jankowiak, F., Herder, C., Carstensen, M., Krausch, M., Knoefel, W. T., *et al.* (2015). Adaptation of hepatic mitochondrial function in humans with non-alcoholic fatty liver is lost in steatohepatitis. *Cell Metab, 21*(5), 739-746.

Koo, H. Y., Miyashita, M., Cho, B. H., & Nakamura, M. T. (2009). Replacing dietary glucose with fructose increases ChREBP activity and SREBP-1 protein in rat liver nucleus. *Biochem Biophys Res Commun, 390*(2), 285-289.

Kooy, N. W., Royall, J. A., & Ischiropoulos, H. (1997). Oxidation of 2',7'-dichlorofluorescin by peroxynitrite. *Free Radic Res, 27*(3), 245-254.

Kostrzewski, T., Cornforth, T., Snow, S. A., Ouro-Gnao, L., Rowe, C., Large, E. M., & Hughes, D. J. (2017). Three-dimensional perfused human in vitro model of non-alcoholic fatty liver disease. *World J Gastroenterol, 23*(2), 204-215.

Kotronen, A., Seppala-Lindroos, A., Vehkavaara, S., Bergholm, R., Frayn, K. N., Fielding, B. A., & Yki-Jarvinen, H. (2009). Liver fat and lipid oxidation in humans. *Liver Int, 29*(9), 1439-1446.

Kuerschner, L., Moessinger, C., & Thiele, C. (2008). Imaging of lipid biosynthesis: how a neutral lipid enters lipid droplets. *Traffic, 9*(3), 338-352.

Lai, M., Chandrasekera, P. C., & Barnard, N. D. (2014). You are what you eat, or are you? The challenges of translating high-fat-fed rodents to human obesity and diabetes. *Nutr Diabetes, 4*, e135.

Lambert, J. E., Ramos-Roman, M. A., Browning, J. D., & Parks, E. J. (2014). Increased de novo lipogenesis is a distinct characteristic of individuals with nonalcoholic fatty liver disease. *Gastroenterology, 146*(3), 726-735.

Lanaspa, M. A., Sanchez-Lozada, L. G., Choi, Y. J., Cicerchi, C., Kanbay, M., Roncal-Jimenez, C. A., Ishimoto, T., Li, N., Marek, G., Duranay, M., *et al.* (2012). Uric acid induces hepatic steatosis by generation of mitochondrial oxidative stress: potential role in fructose-dependent and -independent fatty liver. *J Biol Chem, 287*(48), 40732-40744.

Lardizabal, K. D., Mai, J. T., Wagner, N. W., Wyrick, A., Voelker, T., & Hawkins, D. J. (2001). DGAT2 is a new diacylglycerol acyltransferase gene family: purification, cloning, and expression in insect cells of two polypeptides from Mortierella ramanniana with diacylglycerol acyltransferase activity. *J Biol Chem, 276*(42), 38862-38869.

Lau, J. K., Zhang, X., & Yu, J. (2017). Animal models of non-alcoholic fatty liver disease: current perspectives and recent advances. *J Pathol, 241*(1), 36-44.

Le, K. A., Ith, M., Kreis, R., Faeh, D., Bortolotti, M., Tran, C., Boesch, C., & Tappy, L. (2009). Fructose overconsumption causes dyslipidemia and ectopic lipid deposition in healthy subjects with and without a family history of type 2 diabetes. *Am J Clin Nutr, 89*(6), 1760-1765.

Lee, W. N., Bassilian, S., Ajie, H. O., Schoeller, D. A., Edmond, J., Bergner, E. A., & Byerley, L. O. (1994a). In vivo measurement of fatty acids and cholesterol synthesis using D2O and mass isotopomer analysis. *Am J Physiol, 266*(5 Pt 1), E699-708.

Lee, W. N., Bassilian, S., Guo, Z., Schoeller, D., Edmond, J., Bergner, E. A., & Byerley, L. O. (1994b). Measurement of fractional lipid synthesis using deuterated water (2H2O) and mass isotopomer analysis. *Am J Physiol, 266*(3 Pt 1), E372-383.

Legrand, P., & Rioux, V. (2010). The complex and important cellular and metabolic functions of saturated fatty acids. *Lipids, 45*(10), 941-946.

Lehner, R., Cui, Z., & Vance, D. E. (1999). Subcellullar localization, developmental expression and characterization of a liver triacylglycerol hydrolase. *Biochem J, 338 (Pt 3)*, 761-768.

Lehner, R., Lian, J., & Quiroga, A. D. (2012). Lumenal lipid metabolism: implications for lipoprotein assembly. *Arterioscler Thromb Vasc Biol, 32*(5), 1087-1093.

Leighton, F., Bergseth, S., Rortveit, T., Christiansen, E. N., & Bremer, J. (1989). Free acetate production by rat hepatocytes during peroxisomal fatty acid and dicarboxylic acid oxidation. *J Biol Chem, 264*(18), 10347-10350.

Li, C., Li, L., Lian, J., Watts, R., Nelson, R., Goodwin, B., & Lehner, R. (2015a). Roles of Acyl-CoA:Diacylglycerol Acyltransferases 1 and 2 in Triacylglycerol Synthesis and Secretion in Primary Hepatocytes. *Arterioscler Thromb Vasc Biol, 35*(5), 1080-1091.

Li, X. B., Gu, J. D., & Zhou, Q. H. (2015b). Review of aerobic glycolysis and its key enzymes - new targets for lung cancer therapy. *Thorac Cancer, 6*(1), 17-24.

Liang, J. J., Oelkers, P., Guo, C., Chu, P. C., Dixon, J. L., Ginsberg, H. N., & Sturley, S. L. (2004). Overexpression of human diacylglycerol acyltransferase 1, acyl-coa:cholesterol acyltransferase 1, or acyl-CoA:cholesterol acyltransferase 2 stimulates secretion of apolipoprotein B-containing lipoproteins in McA-RH7777 cells. *J Biol Chem, 279*(43), 44938-44944.

Lim, J. S., Mietus-Snyder, M., Valente, A., Schwarz, J. M., & Lustig, R. H. (2010). The role of fructose in the pathogenesis of NAFLD and the metabolic syndrome. *Nat Rev Gastroenterol Hepatol, 7*(5), 251-264.

Lima-Cabello, E., Garcia-Mediavilla, M. V., Miquilena-Colina, M. E., Vargas-Castrillon, J., Lozano-Rodriguez, T., Fernandez-Bermejo, M., Olcoz, J. L., Gonzalez-Gallego, J., Garcia-Monzon, C., & Sanchez-Campos, S. (2011). Enhanced expression of pro-inflammatory mediators and liver X-receptor-regulated lipogenic genes in non-alcoholic fatty liver disease and hepatitis C. *Clin Sci (Lond), 120*(6), 239-250.

Lin, J., Yang, R., Tarr, P. T., Wu, P. H., Handschin, C., Li, S., Yang, W., Pei, L., Uldry, M., Tontonoz, P., *et al.* (2005). Hyperlipidemic effects of dietary saturated fats mediated through PGC-1beta coactivation of SREBP. *Cell, 120*(2), 261-273.

Liu, L., Shi, X., Bharadwaj, K. G., Ikeda, S., Yamashita, H., Yagyu, H., Schaffer, J. E., Yu, Y. H., & Goldberg, I. J. (2009). DGAT1 expression increases heart triglyceride content but ameliorates lipotoxicity. *J Biol Chem, 284*(52), 36312-36323.

Liu, Q., Siloto, R. M., Lehner, R., Stone, S. J., & Weselake, R. J. (2012). Acyl-CoA:diacylglycerol acyltransferase: molecular biology, biochemistry and biotechnology. *Prog Lipid Res, 51*(4), 350-377.

Liu, Y. L., Reeves, H. L., Burt, A. D., Tiniakos, D., McPherson, S., Leathart, J. B., Allison, M. E., Alexander, G. J., Piguet, A. C., Anty, R., *et al.* (2014). TM6SF2 rs58542926 influences hepatic fibrosis progression in patients with non-alcoholic fatty liver disease. *Nat Commun, 5*, 4309.

Lopez-Terrada, D., Cheung, S. W., Finegold, M. J., & Knowles, B. B. (2009). Hep G2 is a hepatoblastoma-derived cell line. *Hum Pathol, 40*(10), 1512-1515.

Lopez-Velazquez, J. A., Carrillo-Cordova, L. D., Chavez-Tapia, N. C., Uribe, M., & Mendez-Sanchez, N. (2012). Nuclear receptors in nonalcoholic Fatty liver disease. *J Lipids, 2012*, 139875.

Luckert, C., Schulz, C., Lehmann, N., Thomas, M., Hofmann, U., Hammad, S., Hengstler, J. G., Braeuning, A., Lampen, A., & Hessel, S. (2017). Comparative analysis of 3D culture methods on human HepG2 cells. *Arch Toxicol, 91*(1), 393-406.

Luukkonen, P. K., Sadevirta, S., Zhou, Y., Kayser, B., Ali, A., Ahonen, L., Lallukka, S., Pelloux, V., Gaggini, M., Jian, C., *et al.* (2018). Saturated Fat Is More Metabolically Harmful for the Human Liver Than Unsaturated Fat or Simple Sugars. *Diabetes Care, 41*(8), 1732-1739.

Luukkonen, P. K., Zhou, Y., Sadevirta, S., Leivonen, M., Arola, J., Oresic, M., Hyotylainen, T., & Yki-Jarvinen, H. (2016). Hepatic ceramides dissociate steatosis and insulin resistance in patients with non-alcoholic fatty liver disease. *J Hepatol, 64*(5), 1167-1175.

Ma, L., Robinson, L. N., & Towle, H. C. (2006). ChREBP*Mlx is the principal mediator of glucose-induced gene expression in the liver. *J Biol Chem, 281*(39), 28721-28730.

Madec, S., Cerec, V., Pleé-Gautier, E., Antoun, J., Glaise, D., Salaun, J.-P., Guguen-Guillouzo, C., & Corlu, A. (2011). CYP4F3B Expression Is Associated with Differentiation of HepaRG Human Hepatocytes and Unaffected by Fatty Acid Overload. *Drug Metab Dispos, 39*(10), 1987–1996.

Mahajan, A., Wessel, J., Willems, S. M., Zhao, W., Robertson, N. R., Chu, A. Y., Gan, W., Kitajima, H., Taliun, D., Rayner, N. W., *et al.* (2018). Refining the accuracy of validated target identification through coding variant fine-mapping in type 2 diabetes. *Nat Genet, 50*(4), 559-571.

Mahdessian, H., Taxiarchis, A., Popov, S., Silveira, A., Franco-Cereceda, A., Hamsten, A., Eriksson, P., & van't Hooft, F. (2014). TM6SF2 is a regulator of liver fat metabolism influencing triglyceride secretion and hepatic lipid droplet content. *Proc Natl Acad Sci U S A, 111*(24), 8913-8918.

Maldonado, E. M. (2016). *An investigation of the role of glucose and fructose in non-alcoholic fatty liver disease using systems approaches.* (Doctor of Philosophy), University of Surrey, Surrey, UK.

Man, W. C., Miyazaki, M., Chu, K., & Ntambi, J. (2006). Colocalization of SCD1 and DGAT2: implying preference for endogenous monounsaturated fatty acids in triglyceride synthesis. *J Lipid Res, 47*(9), 1928-1939.

Marchesini, G., Bugianesi, E., Forlani, G., Cerrelli, F., Lenzi, M., Manini, R., Natale, S., Vanni, E., Villanova, N., Melchionda, N., *et al.* (2003). Nonalcoholic fatty liver, steatohepatitis, and the metabolic syndrome. *Hepatology, 37*(4), 917-923.

Marques-Lopes, I., Ansorena, D., Astiasaran, I., Forga, L., & Martinez, J. A. (2001). Postprandial de novo lipogenesis and metabolic changes induced by a high-carbohydrate, low-fat meal in lean and overweight men. *Am J Clin Nutr, 73*(2), 253-261.

Maruyama, H., Takahashi, M., Sekimoto, T., Shimada, T., & Yokosuka, O. (2014). Linoleate appears to protect against palmitate-induced inflammation in Huh7 cells. *Lipids Health Dis, 13*, 78.

Marventano, S., Kolacz, P., Castellano, S., Galvano, F., Buscemi, S., Mistretta, A., & Grosso, G. (2015). A review of recent evidence in human studies of n-3 and n-6 PUFA intake on cardiovascular disease, cancer, and depressive disorders: does the ratio really matter? *Int J Food Sci Nutr, 66*(6), 611-622.

Mashek, D. G. (2013). Hepatic fatty acid trafficking: multiple forks in the road. *Adv Nutr, 4*(6), 697-710.

Mashek, D. G., Khan, S. A., Sathyanarayan, A., Ploeger, J. M., & Franklin, M. P. (2015). Hepatic lipid droplet biology: Getting to the root of fatty liver. *Hepatology, 62*(3), 964-967.

Masterton, G., Ngoh, L. Y. C., Lockman, A., Hayes, P. C., & Plevris, J. (2011). The significance of fat droplet size and the prognostic value of hyaluronic acid in non-alcoholic fatty liver disease (NAFLD): a biopsy based analysis. *Gut, 60*(Suppl 1), A239-A240.

Matthews, D. R., Hosker, J. P., Rudenski, A. S., Naylor, B. A., Treacher, D. F., & Turner, R. C. (1985). Homeostasis model assessment: insulin resistance and beta-cell function from fasting plasma glucose and insulin concentrations in man. *Diabetologia, 28*(7), 412-419.

McLaren, D. G., Han, S., Murphy, B. A., Wilsie, L., Stout, S. J., Zhou, H., Roddy, T. P., Gorski, J. N., Metzger, D. E., Shin, M. K., *et al.* (2018). DGAT2 Inhibition Alters Aspects of Triglyceride Metabolism in Rodents but Not in Non-human Primates. *Cell Metab, 27*(6), 1236-1248 e1236.

McManus, J. F. (1962). The effect of various solvents and other conditions on periodate oxidation of carbohydrates in the PAS reaction. *Ann Histochim, 7*, 57-59.

McPherson, S., Hardy, T., Henderson, E., Burt, A. D., Day, C. P., & Anstee, Q. M. (2015). Evidence of NAFLD progression from steatosis to fibrosing-steatohepatitis using paired biopsies: implications for prognosis and clinical management. *J Hepatol, 62*(5), 1148-1155.

Meegalla, R. L., Billheimer, J. T., & Cheng, D. (2002). Concerted elevation of acyl-coenzyme A:diacylglycerol acyltransferase (DGAT) activity through independent stimulation of mRNA expression of DGAT1 and DGAT2 by carbohydrate and insulin. *Biochem Biophys Res Commun, 298*(3), 317-323.

Meex, S. J., Andreo, U., Sparks, J. D., & Fisher, E. A. (2011). Huh-7 or HepG2 cells: which is the better model for studying human apolipoprotein-B100 assembly and secretion? *J Lipid Res, 52*(1), 152-158.

Millar, J. S., Stone, S. J., Tietge, U. J., Tow, B., Billheimer, J. T., Wong, J. S., Hamilton, R. L., Farese, R. V., Jr., & Rader, D. J. (2006). Short-term overexpression of DGAT1 or DGAT2 increases hepatic triglyceride but not VLDL triglyceride or apoB production. *J Lipid Res, 47*(10), 2297-2305.

Miura, Y. (2013). The biological significance of omega-oxidation of fatty acids. *Proc Jpn Acad Ser B Phys Biol Sci, 89*(8), 370-382.

Mojica, F. J., Juez, G., & Rodriguez-Valera, F. (1993). Transcription at different salinities of Haloferax mediterranei sequences adjacent to partially modified PstI sites. *Mol Microbiol, 9*(3), 613-621.

Monetti, M., Levin, M. C., Watt, M. J., Sajan, M. P., Marmor, S., Hubbard, B. K., Stevens, R. D., Bain, J. R., Newgard, C. B., Farese, R. V., Sr., *et al.* (2007). Dissociation of hepatic steatosis and insulin resistance in mice overexpressing DGAT in the liver. *Cell Metab, 6*(1), 69-78.

Moore, J. B., Gunn, P. J., & Fielding, B. A. (2014). The role of dietary sugars and de novo lipogenesis in non-alcoholic fatty liver disease. *Nutrients, 6*(12), 5679-5703.

Mosmann, T. (1983). Rapid colorimetric assay for cellular growth and survival: application to proliferation and cytotoxicity assays. *J Immunol Methods, 65*(1-2), 55-63.

Mowbray, C. A. (2011). *In vitro systems to predict hepatotoxicity: models based on hepatocarcinoma cell lines.* (Doctor of Philosophy), Newcastle University.

Mueckler, M., & Thorens, B. (2013). The SLC2 (GLUT) family of membrane transporters. *Mol Aspects Med, 34*(2-3), 121-138.

Musa-Veloso, K., Venditti, C., Lee, H. Y., Darch, M., Floyd, S., West, S., & Simon, R. (2018). Systematic review and meta-analysis of controlled intervention studies on the effectiveness of long-chain omega-3 fatty acids in patients with nonalcoholic fatty liver disease. *Nutr Rev, 76*(8), 581-602.

Nativ, N. I., Yarmush, G., Chen, A., Dong, D., Henry, S. D., Guarrera, J. V., Klein, K. M., Maguire, T., Schloss, R., Berthiaume, F., *et al.* (2013). Rat hepatocyte culture model of macrosteatosis: effect of macrosteatosis induction and reversal on viability and liver-specific function. *J Hepatol, 59*(6), 1307-1314.

NDNS. (2018). *National Diet and Nutrition Survey Years 1-8, 2008/09-2015/16.* London (UK).

Nguyen, P., Leray, V., Diez, M., Serisier, S., Le Bloc'h, J., Siliart, B., & Dumon, H. (2008). Liver lipid metabolism. *J Anim Physiol Anim Nutr (Berl), 92*(3), 272-283.

Nikolaou, N., Green, C. J., Gunn, P. J., Hodson, L., & Tomlinson, J. W. (2016). Optimizing human hepatocyte models for metabolic phenotype and function: effects of treatment with dimethyl sulfoxide (DMSO). *Physiol Rep, 4*(21).

Ning, T., Zou, Y., Yang, M., Lu, Q., Chen, M., Liu, W., Zhao, S., Sun, Y., Shi, J., Ma, Q., *et al.* (2017). Genetic interaction of DGAT2 and FAAH in the development of human obesity. *Endocrine, 56*(2), 366-378.

Nunes, P. M., Wright, A. J., Veltien, A., van Asten, J. J., Tack, C. J., Jones, J. G., & Heerschap, A. (2014). Dietary lipids do not contribute to the higher hepatic triglyceride levels of fructose- compared to glucose-fed mice. *FASEB J, 28*(5), 1988-1997.

Ohsaki, Y., Cheng, J., Suzuki, M., Fujita, A., & Fujimoto, T. (2008). Lipid droplets are arrested in the ER membrane by tight binding of lipidated apolipoprotein B-100. *J Cell Sci, 121*(Pt 14), 2415-2422.

Okumura, T. (2011). Role of lipid droplet proteins in liver steatosis. *J Physiol Biochem, 67*(4), 629-636.

Ontko, J. A. (1972). Metabolism of free fatty acids in isolated liver cells. Factors affecting the partition between esterification and oxidation. *J Biol Chem, 247*(6), 1788-1800.

Ota, T., Gayet, C., & Ginsberg, H. N. (2008). Inhibition of apolipoprotein B100 secretion by lipid-induced hepatic endoplasmic reticulum stress in rodents. *J Clin Invest, 118*(1), 316-332.

Pal, R., Mamidi, M. K., Das, A. K., & Bhonde, R. (2012). Diverse effects of dimethyl sulfoxide (DMSO) on the differentiation potential of human embryonic stem cells. *Arch Toxicol, 86*(4), 651-661.

Parini, P., Johansson, L., Broijersen, A., Angelin, B., & Rudling, M. (2006). Lipoprotein profiles in plasma and interstitial fluid analyzed with an automated gel-filtration system. *Eur J Clin Invest, 36*(2), 98-104.

Park, H. G., Kothapalli, K. S. D., Park, W. J., DeAllie, C., Liu, L., Liang, A., Lawrence, P., & Brenna, J. T. (2016). Palmitic acid (16:0) competes with omega-6 linoleic and omega-3 a-linolenic acids for FADS2 mediated Delta6-desaturation. *Biochim Biophys Acta, 1861*(2), 91-97.

Parry, S. A., & Hodson, L. (2017). Influence of dietary macronutrients on liver fat accumulation and metabolism. *J Investig Med, 65*(8), 1102-1115.

Pawella, L. M., Hashani, M., Eiteneuer, E., Renner, M., Bartenschlager, R., Schirmacher, P., & Straub, B. K. (2014). Perilipin discerns chronic from acute hepatocellular steatosis. *J Hepatol, 60*(3), 633-642.

Pawlak, M., Lefebvre, P., & Staels, B. (2015). Molecular mechanism of PPARalpha action and its impact on lipid metabolism, inflammation and fibrosis in non-alcoholic fatty liver disease. *J Hepatol, 62*(3), 720-733.

Peng, C., Chiappini, F., Kascakova, S., Danulot, M., Sandt, C., Samuel, D., Dumas, P., Guettier, C., & Le Naour, F. (2015). Vibrational signatures to discriminate liver steatosis grades. *Analyst, 140*(4), 1107-1118.

Peng, K. Y., Watt, M. J., Rensen, S., Greve, J. W., Huynh, K., Jayawardana, K. S., Meikle, P. J., & Meex, R. C. R. (2018). Mitochondrial dysfunction-related lipid changes occur in non-alcoholic fatty liver disease progression. *J Lipid Res.*

Perla, F. M., Prelati, M., Lavorato, M., Visicchio, D., & Anania, C. (2017). The Role of Lipid and Lipoprotein Metabolism in Non-Alcoholic Fatty Liver Disease. *Children (Basel), 4*(6).

Perumpail, B. J., Li, A. A., John, N., Sallam, S., Shah, N. D., Kwong, W., Cholankeril, G., Kim, D., & Ahmed, A. (2018). The Role of Vitamin E in the Treatment of NAFLD. *Diseases, 6*(4).

Peter, A., Kovarova, M., Nadalin, S., Cermak, T., Konigsrainer, A., Machicao, F., Stefan, N., Haring, H. U., & Schleicher, E. (2014). PNPLA3 variant I148M is associated with altered hepatic lipid composition in humans. *Diabetologia, 57*(10), 2103-2107.

Petersen, M. C., Vatner, D. F., & Shulman, G. I. (2017). Regulation of hepatic glucose metabolism in health and disease. *Nat Rev Endocrinol, 13*(10), 572-587.

Pfaffl, M. W. (2001). A new mathematical model for relative quantification in real-time RT-PCR. *Nucleic Acids Res, 29*(9), e45.

Pfaffl, M. W., Tichopad, A., Prgomet, C., & Neuvians, T. P. (2004). Determination of stable housekeeping genes, differentially regulated target genes and sample integrity: BestKeeper--Excel-based tool using pair-wise correlations. *Biotechnol Lett, 26*(6), 509-515.

Pirazzi, C., Adiels, M., Burza, M. A., Mancina, R. M., Levin, M., Stahlman, M., Taskinen, M. R., Orho-Melander, M., Perman, J., Pujia, A., *et al.* (2012). Patatin-like phospholipase domain-containing 3 (PNPLA3) I148M (rs738409) affects hepatic VLDL secretion in humans and in vitro. *J Hepatol, 57*(6), 1276-1282.

Poirier, Y., Antonenkov, V. D., Glumoff, T., & Hiltunen, J. K. (2006). Peroxisomal beta-oxidation--a metabolic pathway with multiple functions. *Biochim Biophys Acta, 1763*(12), 1413-1426.

Polimeni, L., Del Ben, M., Baratta, F., Perri, L., Albanese, F., Pastori, D., Violi, F., & Angelico, F. (2015). Oxidative stress: New insights on the association of non-alcoholic fatty liver disease and atherosclerosis. *World J Hepatol, 7*(10), 1325-1336.

Postic, C., Dentin, R., Denechaud, P. D., & Girard, J. (2007). ChREBP, a transcriptional regulator of glucose and lipid metabolism. *Annu Rev Nutr, 27*, 179-192.

Pramfalk, C., Larsson, L., Hardfeldt, J., Eriksson, M., & Parini, P. (2016). Culturing of HepG2 cells with human serum improve their functionality and suitability in studies of lipid metabolism. *Biochim Biophys Acta, 1861*(1), 51-59.

Purcell, S., Neale, B., Todd-Brown, K., Thomas, L., Ferreira, M. A., Bender, D., Maller, J., Sklar, P., de Bakker, P. I., Daly, M. J., *et al.* (2007). PLINK: a tool set for whole-genome association and population-based linkage analyses. *Am J Hum Genet, 81*(3), 559-575.

Puri, P., Baillie, R. A., Wiest, M. M., Mirshahi, F., Choudhury, J., Cheung, O., Sargeant, C., Contos, M. J., & Sanyal, A. J. (2007). A lipidomic analysis of nonalcoholic fatty liver disease. *Hepatology, 46*(4), 1081-1090.

Qi, J., Lang, W., Geisler, J. G., Wang, P., Petrounia, I., Mai, S., Smith, C., Askari, H., Struble, G. T., Williams, R., *et al.* (2012). The use of stable isotope-labeled glycerol and oleic acid to differentiate the hepatic functions of DGAT1 and -2. *J Lipid Res, 53*(6), 1106-1116.

Ran, F. A., Hsu, P. D., Lin, C. Y., Gootenberg, J. S., Konermann, S., Trevino, A. E., Scott, D. A., Inoue, A., Matoba, S., Zhang, Y., *et al.* (2013a). Double nicking by RNA-guided CRISPR Cas9 for enhanced genome editing specificity. *Cell, 154*(6), 1380-1389.

Ran, F. A., Hsu, P. D., Wright, J., Agarwala, V., Scott, D. A., & Zhang, F. (2013b). Genome engineering using the CRISPR-Cas9 system. *Nat Protoc, 8*(11), 2281-2308.

Rasmussen, A. L., Diamond, D. L., McDermott, J. E., Gao, X., Metz, T. O., Matzke, M. M., Carter, V. S., Belisle, S. E., Korth, M. J., Waters, K. M., *et al.* (2011). Systems virology identifies a mitochondrial fatty acid oxidation enzyme, dodecenoyl coenzyme A delta isomerase, required for hepatitis C virus replication and likely pathogenesis. *J Virol, 85*(22), 11646-11654.

Ricoult, S. J., Dibble, C. C., Asara, J. M., & Manning, B. D. (2016). Sterol Regulatory Element Binding Protein Regulates the Expression and Metabolic Functions of Wild-Type and Oncogenic IDH1. *Mol Cell Biol, 36*(18), 2384-2395.

Ritze, Y., Bardos, G., D'Haese, J. G., Ernst, B., Thurnheer, M., Schultes, B., & Bischoff, S. C. (2014). Effect of high sugar intake on glucose transporter and weight regulating hormones in mice and humans. *PLoS One, 9*(7), e101702.

Roberts, R., Bickerton, A. S., Fielding, B. A., Blaak, E. E., Wagenmakers, A. J., Chong, M. F., Gilbert, M., Karpe, F., & Frayn, K. N. (2008). Reduced oxidation of dietary fat after a short term high-carbohydrate diet. *Am J Clin Nutr, 87*(4), 824-831.

Romeo, S., Kozlitina, J., Xing, C., Pertsemlidis, A., Cox, D., Pennacchio, L. A., Boerwinkle, E., Cohen, J. C., & Hobbs, H. H. (2008). Genetic variation in PNPLA3 confers susceptibility to nonalcoholic fatty liver disease. *Nat Genet, 40*(12), 1461-1465.

Rosqvist, F., Iggman, D., Kullberg, J., Cedernaes, J., Johansson, H. E., Larsson, A., Johansson, L., Ahlstrom, H., Arner, P., Dahlman, I., *et al.* (2014). Overfeeding polyunsaturated and

saturated fat causes distinct effects on liver and visceral fat accumulation in humans. *Diabetes, 63*(7), 2356-2368.

Ruhanen, H., Perttila, J., Holtta-Vuori, M., Zhou, Y., Yki-Jarvinen, H., Ikonen, E., Kakela, R., & Olkkonen, V. M. (2014). PNPLA3 mediates hepatocyte triacylglycerol remodeling. *J Lipid Res, 55*(4), 739-746.

SACN. (2015). *SACN Carbohydrates and Health Report.* London (UK).

Sahini, N., & Borlak, J. (2014). Recent insights into the molecular pathophysiology of lipid droplet formation in hepatocytes. *Prog Lipid Res, 54*, 86-112.

Sahini, N., & Borlak, J. (2016). Genomics of human fatty liver disease reveal mechanistically linked lipid droplet-associated gene regulations in bland steatosis and nonalcoholic steatohepatitis. *Transl Res.*

Sainz, B., Jr., Barretto, N., & Uprichard, S. L. (2009). Hepatitis C virus infection in phenotypically distinct Huh7 cell lines. *PLoS One, 4*(8), e6561.

Samanez, C. H., Caron, S., Briand, O., Dehondt, H., Duplan, I., Kuipers, F., Hennuyer, N., Clavey, V., & Staels, B. (2012). The human hepatocyte cell lines IHH and HepaRG: models to study glucose, lipid and lipoprotein metabolism. *Arch Physiol Biochem, 118*(3), 102-111.

Sampson, E. J., Baird, M. A., Burtis, C. A., Smith, E. M., Witte, D. L., & Bayse, D. D. (1980). A Coupled-Enzyme Equilibrium Method for Measuring Urea in Serum - Optimization and Evaluation of the Aacc Study-Group on Urea Candidate Reference Method. *Clinical Chemistry, 26*(7), 816-826.

Samuel, V. T., & Shulman, G. I. (2016). The pathogenesis of insulin resistance: integrating signaling pathways and substrate flux. *J Clin Invest, 126*(1), 12-22.

Sandalio, L. M., Rodriguez-Serrano, M., Romero-Puertas, M. C., & del Rio, L. A. (2013). Role of peroxisomes as a source of reactive oxygen species (ROS) signaling molecules. *Subcell Biochem, 69*, 231-255.

Sanders, F. W., & Griffin, J. L. (2016). De novo lipogenesis in the liver in health and disease: more than just a shunting yard for glucose. *Biol Rev Camb Philos Soc, 91*(2), 452-468.

Sanyal, A. J., Campbell-Sargent, C., Mirshahi, F., Rizzo, W. B., Contos, M. J., Sterling, R. K., Luketic, V. A., Shiffman, M. L., & Clore, J. N. (2001). Nonalcoholic steatohepatitis: association of insulin resistance and mitochondrial abnormalities. *Gastroenterology, 120*(5), 1183-1192.

Sassa, T., & Kihara, A. (2014). Metabolism of very long-chain Fatty acids: genes and pathophysiology. *Biomol Ther (Seoul), 22*(2), 83-92.

Schrader, M., Costello, J., Godinho, L. F., & Islinger, M. (2015). Peroxisome-mitochondria interplay and disease. *J Inherit Metab Dis, 38*(4), 681-702.

Schwarz, J. M., Linfoot, P., Dare, D., & Aghajanian, K. (2003). Hepatic de novo lipogenesis in normoinsulinemic and hyperinsulinemic subjects consuming high-fat, low-carbohydrate and low-fat, high-carbohydrate isoenergetic diets. *Am J Clin Nutr, 77*(1), 43-50.

Semple, R. K., Sleigh, A., Murgatroyd, P. R., Adams, C. A., Bluck, L., Jackson, S., Vottero, A., Kanabar, D., Charlton-Menys, V., Durrington, P., *et al.* (2009). Postreceptor insulin resistance contributes to human dyslipidemia and hepatic steatosis. *J Clin Invest, 119*(2), 315-322.

Senkal, C. E., Salama, M. F., Snider, A. J., Allopenna, J. J., Rana, N. A., Koller, A., Hannun, Y. A., & Obeid, L. M. (2017). Ceramide Is Metabolized to Acylceramide and Stored in Lipid Droplets. *Cell Metab, 25*(3), 686-697.

Sevastianova, K., Santos, A., Kotronen, A., Hakkarainen, A., Makkonen, J., Silander, K., Peltonen, M., Romeo, S., Lundbom, J., Lundbom, N., *et al.* (2012). Effect of short-term carbohydrate overfeeding and long-term weight loss on liver fat in overweight humans. *Am J Clin Nutr, 96*(4), 727-734.

Shaikh, S. R., & Edidin, M. (2008). Polyunsaturated fatty acids and membrane organization: elucidating mechanisms to balance immunotherapy and susceptibility to infection. *Chem Phys Lipids, 153*(1), 24-33.

Shimano, H., & Sato, R. (2017). SREBP-regulated lipid metabolism: convergent physiology - divergent pathophysiology. *Nat Rev Endocrinol, 13*(12), 710-730.

Shulman, G. I. (2014). Ectopic fat in insulin resistance, dyslipidemia, and cardiometabolic disease. *N Engl J Med, 371*(12), 1131-1141.

Silver, N., Best, S., Jiang, J., & Thein, S. L. (2006). Selection of housekeeping genes for gene expression studies in human reticulocytes using real-time PCR. *BMC Mol Biol, 7*, 33.

Simopoulos, A. P. (2016). An Increase in the Omega-6/Omega-3 Fatty Acid Ratio Increases the Risk for Obesity. *Nutrients, 8*(3), 128.

Sirek, A. S., Liu, L., Naples, M., Adeli, K., Ng, D. S., & Jin, T. (2009). Insulin stimulates the expression of carbohydrate response element binding protein (ChREBP) by attenuating the repressive effect of Pit-1, Oct-1/Oct-2, and Unc-86 homeodomain protein octamer transcription factor-1. *Endocrinology, 150*(8), 3483-3492.

Sivertsson, L., Edebert, I., Palmertz, M. P., Ingelman-Sundberg, M., & Neve, E. P. (2013). Induced CYP3A4 expression in confluent Huh7 hepatoma cells as a result of decreased cell proliferation and subsequent pregnane X receptor activation. *Mol Pharmacol, 83*(3), 659-670.

Sivertsson, L., Ek, M., Darnell, M., Edebert, I., Ingelman-Sundberg, M., & Neve, E. P. (2010). CYP3A4 catalytic activity is induced in confluent Huh7 hepatoma cells. *Drug Metab Dispos, 38*(6), 995-1002.

Sliz, E., Sebert, S., Wurtz, P., Kangas, A. J., Soininen, P., Lehtimaki, T., Kahonen, M., Viikari, J., Mannikko, M., Ala-Korpela, M., *et al.* (2018). NAFLD risk alleles in PNPLA3, TM6SF2, GCKR and LYPLAL1 show divergent metabolic effects. *Hum Mol Genet, 27*(12), 2214-2223.

Smith, S. J., Cases, S., Jensen, D. R., Chen, H. C., Sande, E., Tow, B., Sanan, D. A., Raber, J., Eckel, R. H., & Farese, R. V., Jr. (2000). Obesity resistance and multiple mechanisms of triglyceride synthesis in mice lacking Dgat. *Nat Genet, 25*(1), 87-90.

Sobrecases, H., Le, K. A., Bortolotti, M., Schneiter, P., Ith, M., Kreis, R., Boesch, C., & Tappy, L. (2010). Effects of short-term overfeeding with fructose, fat and fructose plus fat on plasma and hepatic lipids in healthy men. *Diabetes Metab, 36*(3), 244-246.

Sommerfeld, A., Reinehr, R., & Haussinger, D. (2015). Free fatty acids shift insulin-induced hepatocyte proliferation towards CD95-dependent apoptosis. *J Biol Chem, 290*(7), 4398-4409.

Song, Y. M., Song, S. O., Jung, Y. K., Kang, E. S., Cha, B. S., Lee, H. C., & Lee, B. W. (2012). Dimethyl sulfoxide reduces hepatocellular lipid accumulation through autophagy induction. *Autophagy, 8*(7), 1085-1097.

Spadaro, L., Magliocco, O., Spampinato, D., Piro, S., Oliveri, C., Alagona, C., Papa, G., Rabuazzo, A. M., & Purrello, F. (2008). Effects of n-3 polyunsaturated fatty acids in subjects with nonalcoholic fatty liver disease. *Dig Liver Dis, 40*(3), 194-199.

Spahis, S., Delvin, E., Borys, J. M., & Levy, E. (2017). Oxidative Stress as a Critical Factor in Nonalcoholic Fatty Liver Disease Pathogenesis. *Antioxid Redox Signal, 26*(10), 519-541.

Staiger, K., Staiger, H., Weigert, C., Haas, C., Haring, H. U., & Kellerer, M. (2006). Saturated, but not unsaturated, fatty acids induce apoptosis of human coronary artery endothelial cells via nuclear factor-kappaB activation. *Diabetes, 55*(11), 3121-3126.

Stanhope, K. L., Schwarz, J. M., Keim, N. L., Griffen, S. C., Bremer, A. A., Graham, J. L., Hatcher, B., Cox, C. L., Dyachenko, A., Zhang, W., *et al.* (2009). Consuming fructose-sweetened, not glucose-sweetened, beverages increases visceral adiposity and lipids and decreases insulin sensitivity in overweight/obese humans. *J Clin Invest, 119*(5), 1322-1334.

Steenbergen, R. H., Joyce, M. A., Thomas, B. S., Jones, D., Law, J., Russell, R., Houghton, M., & Tyrrell, D. L. (2013). Human serum leads to differentiation of human hepatoma cells, restoration of very-low-density lipoprotein secretion, and a 1000-fold increase in HCV Japanese fulminant hepatitis type 1 titers. *Hepatology, 58*(6), 1907-1917.

Stephen, J., Vilboux, T., Haberman, Y., Pri-Chen, H., Pode-Shakked, B., Mazaheri, S., Marek-Yagel, D., Barel, O., Di Segni, A., Eyal, E., *et al.* (2016). Congenital protein losing enteropathy: an inborn error of lipid metabolism due to DGAT1 mutations. *Eur J Hum Genet, 24*(9), 1268-1273.

Stone, S. J., Levin, M. C., Zhou, P., Han, J., Walther, T. C., & Farese, R. V., Jr. (2009). The endoplasmic reticulum enzyme DGAT2 is found in mitochondria-associated membranes and has a mitochondrial targeting signal that promotes its association with mitochondria. *J Biol Chem, 284*(8), 5352-5361.

Stone, S. J., Myers, H. M., Watkins, S. M., Brown, B. E., Feingold, K. R., Elias, P. M., & Farese, R. V., Jr. (2004). Lipopenia and skin barrier abnormalities in DGAT2-deficient mice. *J Biol Chem, 279*(12), 11767-11776.

Straub, B. K., Stoeffel, P., Heid, H., Zimbelmann, R., & Schirmacher, P. (2008). Differential pattern of lipid droplet-associated proteins and de novo perilipin expression in hepatocyte steatogenesis. *Hepatology, 47*(6), 1936-1946.

Stubbs, C. D., & Smith, A. D. (1984). The modification of mammalian membrane polyunsaturated fatty acid composition in relation to membrane fluidity and function. *Biochim Biophys Acta, 779*(1), 89-137.

Su, H. M., Moser, A. B., Moser, H. W., & Watkins, P. A. (2001). Peroxisomal straight-chain Acyl-CoA oxidase and D-bifunctional protein are essential for the retroconversion step in docosahexaenoic acid synthesis. *J Biol Chem, 276*(41), 38115-38120.

Sun, S. Z., & Empie, M. W. (2012). Fructose metabolism in humans - what isotopic tracer studies tell us. *Nutr Metab (Lond), 9*(1), 89.

Sunny, N. E., Parks, E. J., Browning, J. D., & Burgess, S. C. (2011). Excessive hepatic mitochondrial TCA cycle and gluconeogenesis in humans with nonalcoholic fatty liver disease. *Cell Metab, 14*(6), 804-810.

Takahashi, Y., & Fukusato, T. (2014). Histopathology of nonalcoholic fatty liver disease/nonalcoholic steatohepatitis. *World J Gastroenterol, 20*(42), 15539-15548.

Tanaka, N., Sano, K., Horiuchi, A., Tanaka, E., Kiyosawa, K., & Aoyama, T. (2008). Highly purified eicosapentaenoic acid treatment improves nonalcoholic steatohepatitis. *J Clin Gastroenterol, 42*(4), 413-418.

Tandra, S., Yeh, M. M., Brunt, E. M., Vuppalanchi, R., Cummings, O. W., Unalp-Arida, A., Wilson, L. A., & Chalasani, N. (2011). Presence and significance of microvesicular steatosis in nonalcoholic fatty liver disease. *J Hepatol, 55*(3), 654-659.

Tantin, D., Schild-Poulter, C., Wang, V., Hache, R. J., & Sharp, P. A. (2005). The octamer binding transcription factor Oct-1 is a stress sensor. *Cancer Res, 65*(23), 10750-10758.

Tappy, L., & Le, K. A. (2010). Metabolic effects of fructose and the worldwide increase in obesity. *Physiol Rev, 90*(1), 23-46.

Tarling, E., Salter, A., & Bennett, A. (2004). Transcriptional regulation of human SREBP-1c (sterol-regulatory-element-binding protein-1c): a key regulator of lipogenesis. *Biochem Soc Trans, 32*(Pt 1), 107-109.

Tayek, J. A., & Katz, J. (1996). Glucose production, recycling, and gluconeogenesis in normals and diabetics: a mass isotopomer [U-13C]glucose study. *Am J Physiol, 270*(4 Pt 1), E709-717.

Ter Horst, K. W., & Serlie, M. J. (2017). Fructose Consumption, Lipogenesis, and Non-Alcoholic Fatty Liver Disease. *Nutrients, 9*(9).

Thrift, R. N., Forte, T. M., Cahoon, B. E., & Shore, V. G. (1986). Characterization of lipoproteins produced by the human liver cell line, Hep G2, under defined conditions. *J Lipid Res, 27*(3), 236-250.

Thuy, S., Ladurner, R., Volynets, V., Wagner, S., Strahl, S., Konigsrainer, A., Maier, K. P., Bischoff, S. C., & Bergheim, I. (2008). Nonalcoholic fatty liver disease in humans is associated with increased plasma endotoxin and plasminogen activator inhibitor 1 concentrations and with fructose intake. *J Nutr, 138*(8), 1452-1455.

Tiwari, S., & Siddiqi, S. A. (2012). Intracellular trafficking and secretion of VLDL. *Arterioscler Thromb Vasc Biol, 32*(5), 1079-1086.

Tong, X., Zhao, F., Mancuso, A., Gruber, J. J., & Thompson, C. B. (2009). The glucose-responsive transcription factor ChREBP contributes to glucose-dependent anabolic synthesis and cell proliferation. *Proc Natl Acad Sci U S A, 106*(51), 21660-21665.

Tsai, J., Qiu, W., Kohen-Avramoglu, R., & Adeli, K. (2007). MEK-ERK inhibition corrects the defect in VLDL assembly in HepG2 cells: potential role of ERK in VLDL-ApoB100 particle assembly. *Arterioscler Thromb Vasc Biol, 27*(1), 211-218.

Umpleby, A. M. (2015). HORMONE MEASUREMENT GUIDELINES: Tracing lipid metabolism: the value of stable isotopes. *J Endocrinol, 226*(3), G1-10.

Uyeda, K., & Repa, J. J. (2006). Carbohydrate response element binding protein, ChREBP, a transcription factor coupling hepatic glucose utilization and lipid synthesis. *Cell Metab, 4*(2), 107-110.

Van Herck, M. A., Vonghia, L., & Francque, S. M. (2017). Animal Models of Nonalcoholic Fatty Liver Disease-A Starter's Guide. *Nutrients, 9*(10).

van Herpen, N. A., Schrauwen-Hinderling, V. B., Schaart, G., Mensink, R. P., & Schrauwen, P. (2011). Three weeks on a high-fat diet increases intrahepatic lipid accumulation and

decreases metabolic flexibility in healthy overweight men. *J Clin Endocrinol Metab, 96*(4), E691-695.

Vandesompele, J., De Preter, K., Pattyn, F., Poppe, B., Van Roy, N., De Paepe, A., & Speleman, F. (2002). Accurate normalization of real-time quantitative RT-PCR data by geometric averaging of multiple internal control genes. *Genome Biol, 3*(7), RESEARCH0034.

Vila-Brau, A., De Sousa-Coelho, A. L., Mayordomo, C., Haro, D., & Marrero, P. F. (2011). Human HMGCS2 regulates mitochondrial fatty acid oxidation and FGF21 expression in HepG2 cell line. *J Biol Chem, 286*(23), 20423-20430.

Villanueva, C. J., Monetti, M., Shih, M., Zhou, P., Watkins, S. M., Bhanot, S., & Farese, R. V., Jr. (2009). Specific role for acyl CoA:Diacylglycerol acyltransferase 1 (Dgat1) in hepatic steatosis due to exogenous fatty acids. *Hepatology, 50*(2), 434-442.

Walther, T. C., Chung, J., & Farese, R. V., Jr. (2017). Lipid Droplet Biogenesis. *Annu Rev Cell Dev Biol, 33*, 491-510.

Wanders, R. J., Komen, J., & Kemp, S. (2011). Fatty acid omega-oxidation as a rescue pathway for fatty acid oxidation disorders in humans. *FEBS J, 278*(2), 182-194.

Wang, P., & Jin, T. (2010a). Hydrogen peroxide stimulates nuclear import of the POU homeodomain protein Oct-1 and its repressive effect on the expression of Cdx-2. *BMC Cell Biol, 11*, 56.

Wang, P., & Jin, T. (2010b). Oct-1 functions as a sensor for metabolic and stress signals. *Islets, 2*(1), 46-48.

Waraky, A., Aleem, E., & Larsson, O. (2016). Downregulation of IGF-1 receptor occurs after hepatic linage commitment during hepatocyte differentiation from human embryonic stem cells. *Biochem Biophys Res Commun, 478*(4), 1575-1581.

Watkins, P. A., Ferrell, E. V., Jr., Pedersen, J. I., & Hoefler, G. (1991). Peroxisomal fatty acid beta-oxidation in HepG2 cells. *Arch Biochem Biophys, 289*(2), 329-336.

Welsh, J. A., Sharma, A. J., Grellinger, L., & Vos, M. B. (2011). Consumption of added sugars is decreasing in the United States. *Am J Clin Nutr, 94*(3), 726-734.

Welte, M. A., & Gould, A. P. (2017). Lipid droplet functions beyond energy storage. *Biochim Biophys Acta, 1862*(10 Pt B), 1260-1272.

Westerbacka, J., Kolak, M., Kiviluoto, T., Arkkila, P., Siren, J., Hamsten, A., Fisher, R. M., & Yki-Jarvinen, H. (2007). Genes involved in fatty acid partitioning and binding, lipolysis, monocyte/macrophage recruitment, and inflammation are overexpressed in the human fatty liver of insulin-resistant subjects. *Diabetes, 56*(11), 2759-2765.

Westerbacka, J., Lammi, K., Hakkinen, A. M., Rissanen, A., Salminen, I., Aro, A., & Yki-Jarvinen, H. (2005). Dietary fat content modifies liver fat in overweight nondiabetic subjects. *J Clin Endocrinol Metab, 90*(5), 2804-2809.

WHO. (2015). *WHO Guideline: sugars intake for adults and children.* Geneva (Switzerland).

Wijarnpreecha, K., Thongprayoon, C., Edmonds, P. J., & Cheungpasitporn, W. (2016). Associations of sugar- and artificially sweetened soda with nonalcoholic fatty liver disease: a systematic review and meta-analysis. *QJM, 109*(7), 461-466.

Wilcox, G. (2005). Insulin and insulin resistance. *Clin Biochem Rev, 26*(2), 19-39.

Wilfling, F., Wang, H., Haas, J. T., Krahmer, N., Gould, T. J., Uchida, A., Cheng, J. X., Graham, M., Christiano, R., Frohlich, F., *et al.* (2013). Triacylglycerol synthesis enzymes mediate

lipid droplet growth by relocalizing from the ER to lipid droplets. *Dev Cell, 24*(4), 384-399.

Wilke, M. S., French, M. A., Goh, Y. K., Ryan, E. A., Jones, P. J., & Clandinin, M. T. (2009). Synthesis of specific fatty acids contributes to VLDL-triacylglycerol composition in humans with and without type 2 diabetes. *Diabetologia, 52*(8), 1628-1637.

Wu, M. T., Su, H. M., Cui, Y., Windust, A., Chou, H. N., & Huang, C. J. (2015). Fucoxanthin Enhances Chain Elongation and Desaturation of Alpha-Linolenic Acid in HepG2 Cells. *Lipids, 50*(10), 945-953.

Wu, X., Shang, A., Jiang, H., & Ginsberg, H. N. (1996). Low rates of apoB secretion from HepG2 cells result from reduced delivery of newly synthesized triglyceride to a "secretion-coupled" pool. *J Lipid Res, 37*(6), 1198-1206.

Wurie, H. R., Buckett, L., & Zammit, V. A. (2011). Evidence that diacylglycerol acyltransferase 1 (DGAT1) has dual membrane topology in the endoplasmic reticulum of HepG2 cells. *J Biol Chem, 286*(42), 36238-36247.

Wurie, H. R., Buckett, L., & Zammit, V. A. (2012). Diacylglycerol acyltransferase 2 acts upstream of diacylglycerol acyltransferase 1 and utilizes nascent diglycerides and de novo synthesized fatty acids in HepG2 cells. *FEBS J, 279*(17), 3033-3047.

Xie, F., Xiao, P., Chen, D., Xu, L., & Zhang, B. (2012). miRDeepFinder: a miRNA analysis tool for deep sequencing of plant small RNAs. *Plant Mol Biol.*

Yamazaki, T., Sasaki, E., Kakinuma, C., Yano, T., Miura, S., & Ezaki, O. (2005). Increased very low density lipoprotein secretion and gonadal fat mass in mice overexpressing liver DGAT1. *J Biol Chem, 280*(22), 21506-21514.

Yang, Q., Zhang, Z., Gregg, E. W., Flanders, W. D., Merritt, R., & Hu, F. B. (2014). Added sugar intake and cardiovascular diseases mortality among US adults. *JAMA Intern Med, 174*(4), 516-524.

Yarmush, G., Santos, L., Yarmush, J., Koundinyan, S., Saleem, M., Nativ, N. I., Schloss, R. S., Yarmush, M. L., Maguire, T. J., & Berthiaume, F. (2016). Metabolic Flux Distribution during Defatting of Steatotic Human Hepatoma (HepG2) Cells. *Metabolites, 6*(1).

Ye, J., & DeBose-Boyd, R. A. (2011). Regulation of cholesterol and fatty acid synthesis. *Cold Spring Harb Perspect Biol, 3*(7).

Yen, C. L., Nelson, D. W., & Yen, M. I. (2015). Intestinal triacylglycerol synthesis in fat absorption and systemic energy metabolism. *J Lipid Res, 56*(3), 489-501.

Yen, C. L., Stone, S. J., Koliwad, S., Harris, C., & Farese, R. V., Jr. (2008). Thematic review series: glycerolipids. DGAT enzymes and triacylglycerol biosynthesis. *J Lipid Res, 49*(11), 2283-2301.

Younossi, Z. M., Koenig, A. B., Abdelatif, D., Fazel, Y., Henry, L., & Wymer, M. (2016). Global epidemiology of nonalcoholic fatty liver disease-Meta-analytic assessment of prevalence, incidence, and outcomes. *Hepatology, 64*(1), 73-84.

Yu, X. X., Murray, S. F., Pandey, S. K., Booten, S. L., Bao, D., Song, X. Z., Kelly, S., Chen, S., McKay, R., Monia, B. P., *et al.* (2005). Antisense oligonucleotide reduction of DGAT2 expression improves hepatic steatosis and hyperlipidemia in obese mice. *Hepatology, 42*(2), 362-371.

Yu, Y., Maguire, T. G., & Alwine, J. C. (2014). ChREBP, a glucose-responsive transcriptional factor, enhances glucose metabolism to support biosynthesis in human cytomegalovirus-infected cells. *Proc Natl Acad Sci U S A, 111*(5), 1951-1956.

Zammit, V. A. (2013). Hepatic triacylglycerol synthesis and secretion: DGAT2 as the link between glycaemia and triglyceridaemia. *Biochem J, 451*(1), 1-12.

Zechner, R., Zimmermann, R., Eichmann, T. O., Kohlwein, S. D., Haemmerle, G., Lass, A., & Madeo, F. (2012). FAT SIGNALS--lipases and lipolysis in lipid metabolism and signaling. *Cell Metab, 15*(3), 279-291.

Zelman, S. (1952). The liver in obesity. *AMA Arch Intern Med, 90*(2), 141-156.

Zhao, L., Guo, X., Wang, O., Zhang, H., Wang, Y., Zhou, F., Liu, J., & Ji, B. (2016). Fructose and glucose combined with free fatty acids induce metabolic disorders in HepG2 cell: A new model to study the impacts of high-fructose/sucrose and high-fat diets in vitro. *Mol Nutr Food Res, 60*(4), 909-921.

Zhu, F. S., Liu, S., Chen, X. M., Huang, Z. G., & Zhang, D. W. (2008). Effects of n-3 polyunsaturated fatty acids from seal oils on nonalcoholic fatty liver disease associated with hyperlipidemia. *World J Gastroenterol, 14*(41), 6395-6400.